Visual Encoding in the Human Retina

Human ganglion cell physiology and comparison to other species

Dissertation

zur Erlangung des Grades eines

Doktors der Naturwissenschaften

der Mathematisch-Naturwissenschaftlichen Fakultät

und

der Medizinischen Fakultät

der Eberhard-Karls-Universität Tübingen

vorgelegt

von

Katja Reinhard

aus Kleindietwil, Schweiz

Oktober - 2015

Tag der mündlichen Prüfung: 26. Januar 2016

Dekan der Math.-Nat. Fakultät: Prof. Dr. W. Rosenstiel

Dekan der Medizinischen Fakultät: Prof. Dr. I. B. Autenrieth

1. Berichterstatter: Dr. Thomas Münch

2. Berichterstatter: Prof. Dr. Martin Spitzer

Prüfungskommission:

Dr. Thomas Münch

Prof. Dr. Martin Spitzer

Prof. Dr. Frank Schaeffel

Prof. Dr. Eberhart Zrenner

Erklärung:

Ich erkläre, dass ich die zur Promotion eingereichte Arbeit mit dem Titel:

„Visual Encoding in the Human Retina – Human ganglion cell physiology and comparison to other species“

selbständig verfasst, nur die angegebenen Quellen und Hilfsmittel benutzt und wörtlich oder inhaltlich übernommene Stellen als solche gekennzeichnet habe. Ich versichere an Eides statt, dass diese Angaben wahr sind und dass ich nichts verschwiegen habe. Mir ist bekannt, dass die falsche Abgabe einer Versicherung an Eides statt mit Freiheitsstrafe bis zu drei Jahren oder mit Geldstrafe bestraft wird.

Tübingen, den .....

Datum Unterschrift

Table of Contents

I. Abstract

Retinal information processing has been characterized in many animal models. Surprisingly, similar systematic measurements have never been performed in human retina. Non-human primate research often focuses on a few, most abundant ganglion cell types, which led to the impression that retinal image processing is less rich in primates than in other mammals.

I thus investigated the retinal computations in human retina, and compared it to retinal processing in mouse and pig, as well as to previous publications on non-human primate vision. Analysis of multi-electrode array recordings of mid-peripheral human retina revealed that visual processing is richer than suggested by current literature on primate retina. Human ganglion cells encoded a broad range of speeds, spatial periods, and temporal frequencies. For the first time, ON-OFF type responses have been described in the human retina. Further, I found potential candidates for a Y-like pathway in human retina. I characterized ganglion cells with distance-invariant encoding in both human and pig retina – a response behavior which so far has not been described.

I found that visual encoding in human and pig retina has many similarities while there were more differences between human and mouse visual processing. In general, human ganglion cells preferred higher speeds and were tuned to higher temporal frequencies than in mouse. For scientific questions related to very specific circuit behaviors, the porcine retina might thus be a better model than the mouse.

In this thesis I do not only discuss the measured retinal properties in humans and other species, but also elaborate on the availability of human retina and methodological possibilities to investigate this tissue. Further, I talk about difficulties with the analysis of high-throughput electrophysiological data and provide solutions. I conclude that donated human retina is a valuable tool for in-vitro physiology experiments. In the future, such tissue might be used for testing of short-term effects of pharmaceuticals and for the evaluation of novel treatment methods for visual impairment.

II. Synopsis

GENERAL INTRODUCTION

Vision is one of our most important senses. We rely on visual input for explorative, social, and self-maintenance behavior: we need high-acuity vision not only as predators, but also for social interactions, for example to read facial expressions. In addition, orientation, identification of edible food or recognition of friends and family members is, in humans, much more dependent on vision than on other senses.

The first stage of the neural visual pathway is the retina. The retina is far more than a camera recognizing pixel intensity and color – it pre-processes visual information before sending it to the brain. In many studies, researchers have shown the amazing computational capabilities of the retina in animal models. However, one of the big goals of natural science is to understand the human body and to interfere with pathologies of the human system. It is thus surprising how little is known about the detailed cell and circuit properties of the human retina. In non-human primate studies, researchers often focus only on a handful of retinal tasks, which led to the impression that the primate retina would not perform the complex computations found in other mammals. I therefore aimed to study the processing capability of the human retina.

Depending on the species, its habitat, behavior, and importance of visual input, the retina needs to process different kind of visual information. It is thus important to not only study the retina of animal models, but to investigate the human retina directly in order to better understand its detailed function. We will continue to rely on animal models for most of our research on neuronal circuit mechanisms, effects of diseases on cellular processes, and development of treatments. But knowledge about the human retina allows us to judge how well these results can be translated to the human situation. Finally, with this thesis I will show the possibilities for research with human retina and hope to promote future physiological studies with this precious tissue.

General retinal anatomy and physiology

The mammalian retina is a thin neuronal structure in the back of the eye. It is part of the central nervous system and forms the very first stage of the visual pathway (overview in **Fig. I**). Vision begins with two classes of photoreceptors, rods and cones, capturing photons. The photoreceptors form the outer-most part of the retina, the outer nuclear layer. Their most outstanding morphological feature is the elongated outer segment where the phototransduction takes place, i.e. the conversion of photons into electrical impulses (Rodieck, 1998).

The excitatory feedforward pathway in the retina consists of the photoreceptors, the bipolar cells, and the ganglion cells, which send their axons through the optic nerve to higher brain centers. One of the most basic functions of the retina is the distinction between light increments and decrements. This distinction starts already in the outer plexiform layer where photoreceptors and bipolar cells form the very first synapse of the visual system. Here the visual information is split into two general pathways. These pathways are formed by ON bipolar cells (responding to light increments) and OFF bipolar cells (encoding light decrements). Different glutamatergic receptors in the two classes of bipolar cells allow for this distinct behavior to identical input from rods and cones. The separation into information on light increment and decrement is passed onto the ganglion cells: ON bipolar cell axons terminate in the deepest layers of the inner plexiform layer, while OFF bipolar cells have shorter axons and terminate in the

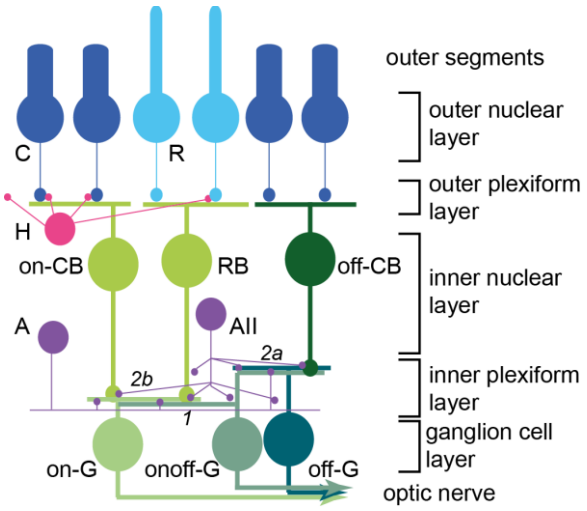

Fig. I: Retinal morphology. *C: cone; R: rod; on-CB: ON cone bipolar cell; off-CB: OFF cone bipolar cell; RB: rod bipolar cell; on-G: ON ganglion cell; onoff-G: ONOFF ganglion cell; off-G: OFF ganglion cell; H: horizontal cell; A / AII: amacrine cell. 1) RB to AII synapse; 2a) gap junctions from AII to on-CB, 2b) glycinergic synapse from AII to off-CB, off-G and onoff-G. Details are given in the text.*

outer layers. There they make synaptic contacts with the dendrites of ON, OFF, and ON-OFF ganglion cells (Rodieck, 1998).

The retina contains two classes of lateral inhibitory interneurons: in the outer retina, horizontal cells provide GABAergic inhibitory feedback to photoreceptors and lateral inhibition to bipolar cells. Amacrine cells are found in the inner retina where they are part of local feedforward and lateral inhibition as well as vertical inhibition to distant bipolar and ganglion cells. Finally, the retinal homeostasis and immune privilege are granted by the retinal glia – the Müller cells – and the pigment epithelium (Rodieck, 1998).

The specific properties of the phototransduction in rods and cones leads to different specialization of these photoreceptors. Rods are very sensitive and can detect single photons, which allows them to mediate visual information under very dim conditions. Cone responses are too noisy to reliably transmit information based on very few photoisomerizations, but they remain functional when exposed to arbitrarily high numbers of photons. While for cones the "photoreceptor → cone ON/OFF bipolar cells → ON/OFF/ON-OFF ganglion cells" is the main pathway, rods have at least three different possibilities to transmit light information. They have their dedicated rod ON bipolar cell contacting a specific amacrine cell, the AII cell (**Fig. I, *1***), which distributes this ON-signal into the cone ON-pathway (via gap junctions, ***2b***) and the cone OFF-pathway (via sign-inverting glycinergic synapses, ***2a***) (Rodieck, 1998). Alternatively, rods may form direct contacts to cone OFF bipolar cells (Mataruga et al, 2007) and can feed directly into the cone pathway via gap junctions between rods and cones (Devries & Baylor, 1997).

Pre-processing of visual information in the retina

Despite the importance of discriminating between dark and bright stimuli, the retina does not simply convert pixel intensities into electrical current. In addition to encoding changes in luminance, the retina also discriminates between different colors, contrasts, and sizes of stimuli. This leads to complex computations performed by the retina such as detection of movement and its direction (Barlow & Levick, 1965), encoding of the orientation of objects (Bloomfield, 1994), detection of local edges (Levick, 1967; Roska & Werblin, 2001; Zeck et al, 2005) or encoding of approaching objects (Munch et al, 2009). The retina pre-processes

visual information by extraction of over 30 such features from each given visual scene (Sanes & Masland, 2015). Many different mechanisms across the whole retina are responsible for this feature extraction. Part of this computation already happens in the outer retina: by activation of rods or cones or both photoreceptor types, different retinal circuits are used for visual encoding. In the outer plexiform layer, photoreceptor signals are distributed to at least 13 different types of bipolar cells. They not only split the visual information into ON and OFF, but they also incorporate chromatic processing (by getting input from different types of cones), they show transient or sustained response types (and thus different temporal processing), and might produce spikes instead of graded potential changes (Euler et al, 2014). Horizontal and amacrine cell further shape the visual signal by local inhibition or by widespread interaction across larger retinal areas. Amacrine cells come in many different shapes and sizes, and can use various combinations of neurotransmitters to shape the visual signal. Eventually, the processed signal cumulates in over 30 different ganglion cell types, each transmitting one specific feature of the visual input to the brain (Masland, 2001; Roska & Meister, 2014; Sanes & Masland, 2015). The axons of these ganglion cells constitute the optic nerve through which visual information is transmitted to two main retinal targets, the lateral geniculate nucleus (LGN) and the superior colliculus. The LGN is mostly involved in visual perception and further connects to the visual cortex (V1) (Burkhalter & Wang, 2008). The superior colliculus, on the other hand, is thought to mediate visually guided innate behavior (Bloomfield & Dacheux, 2001; May, 2006).

Species-specific vision

Almost every animal species possesses a visual sense mediated by a retina-like structure. Some anatomical differences between species are apparent, for example facetted eyes of insects or the inversed neuronal structure of squids with the photoreceptors in the inner-most part of the retina. Nevertheless, discrimination of bright and dark parts of the visual field or detection of movement and approach are retinal computations that are required in almost all mammals. However, there also many differences in the visual input or the ophthalmologic anatomy between species. For instance, the retinas of night- and day-active animals are specialized for very different luminance conditions. Further, the position and size of the eye as well as the body height of an animal strongly influence the visual field size and

proportions of viewed objects. Flying, under water, and land species observe the world from very different perspectives, are exposed to different colors and spatial scales. In some species such as humans, vision is one of the most important senses. In other species, different senses play a more important role and the retina is only needed for very basic visual guidance. Also color vision differs between species. Some animals are strongly guided by color when searching for example for food or mating partners, while for many other animals limited color differentiation is sufficient. It is conceivable that these very variable visual environments and dependences on visual input led to different specializations of the retina in different species. In order to judge how generalizable and translatable results are, it is thus necessary to study and compare the details of retinal processing in the different species.

AIM

The aim of my doctoral work has been the study of the functional properties of the human retina. Further, I have investigated the translatability of results gained with important animal models to the human situation. To answer these biological questions (described in Part 3 of this thesis), technical aspects had to be solved (Part 1), and analytical tools needed to be established (Part 2).

Part 1: Technical aspects. To my knowledge this is the first comprehensive study of human retinal ganglion cell physiology. Thus, several technical questions had to be answered. In part 1 I will discuss sources, availability, and quality of human retina and the methodological paradigms available to study this tissue.

Part 2: Analytical aspects. I have based my analysis of human retina physiology on a set of defined response parameters, measured from ganglion cells in the isolated retina in response to visual stimulation. In part 2, I will illustrate the necessary tools and difficulties when studying high-throughput electrophysiological data. Since human retina is rare, I have established many analytical aspects in a study with a mouse model for optic atrophy. These experiments with mouse used the identical paradigm as the human retina study and led to a comparable data-set. I will further elaborate on unexpected issues which I encountered here and their important impact on retinal research in general.

Part 3: Encoding in human retina and translatability between species. In part 3, I will discuss the properties of human retina which I have discovered, and the extent to which data obtained from animal models is translatable to the human retina. Then I will provide an overview of the open questions to be answered in follow-up experiments and I will discuss how my results might form a basis and guide for future research.

PART 1: TECHNICAL ASPECTS

Sources and availability of human retina

Human retina for scientific studies can be obtained from two sources: The first source is post-mortem tissue from cornea donors. During the donation process, the complete bulbus is removed from the donor. In addition to the cornea, the sclera is sometimes extracted as well to be used for implantation of artificial eye bulbs after enucleations. The rest of the eye, including the retina, is normally discarded. After obtaining the family's consent, the whole retina of cornea donors can thus be utilized for scientific studies.

The second source is ex-vivo donations from patients. These patients have to undergo enucleation, for example due to a uveal tumor with high risk for liver metastases. After ex-vivo enucleations, the eye bulb can be cut in two halves: the tumor-bearing tissue is analyzed by pathologists, but the half which is not needed for medical tests can be used for experimentation. A uveal melanoma is a tumor of the choroid and does not directly affect the retina, although while growing it can cause retinal detachment. However, the tissue further away from the tumor is often intact and patients may have comparatively good vision before enucleation.

During my doctoral thesis I was strongly involved in establishing collaborations with the local eye clinic as well as the local cornea bank. Within 23 months we obtained 16 ex-vivo and 6 post-mortem donations (for ex-vivo donations see Table 1 in Publication 1, for post-mortem donations Suppl. Table 1 in Publication 2). All publications are reproduced in the annex of this thesis.

Quality of human retina donations

Donation conditions

Many aspects and circumstances may interfere with the quality of both ex-vivo and post-mortem human retina tissue. First, these donations originate from patients with different life styles, medical histories, age, and ophthalmologic pathologies. In addition, the surgical procedure and subsequent treatment can further impact the quality of the retina. In particular in the case of post-mortem donations, the time span between the death of the donor and extraction of the retina can vary between approximately 6 and 48 hours. During this whole time, the retina is suffering from ischemia (Donnan & Davis, 2008), i.e. it lacks oxygen and nutrient supply. Ischemia also occurs in the case of ex-vivo retinas. Here, in

order to prevent extensive bleeding when the bulbus is removed, it is mandatory to clamp the optic nerve for 5 minutes before enucleation. In some of the donations, this time has been prolonged to up to 25 minutes due to unforeseen complications. In addition to reduced supply with oxygen and nutrients during the donation process, also the temperature in the eye goes down in both post-mortem and ex-vivo donations.

Effect of ischemia on retinal survival

To adequately plan, perform, analyze, and interpret experiments with tissue obtained under such variable conditions, it is essential to know the effects of these ischemic conditions and temperature changes on the retina. From stroke patients and related scientific studies in the brain it is known that only few minutes of ischemia lead to irreversible neuronal damage (Astrup et al, 1981); however, the retina appears to be more resistant (Hayreh & Jonas, 2000; Hayreh & Zimmerman, 2005; Osborne et al, 2004).

Together with Marion Mutter I systematically studied the effect of ischemia on pig retina (**Publication 2**). Pigs are in many aspects very similar to humans and are therefore often used as a model in medical research, also in ophthalmology (Lai & Lo, 2013; Middleton, 2010). We simulated the ischemic conditions that a human retina would experience during the donation process by storing pig eyes for various durations without any supply of oxygen and nutrients at body temperature, room temperature or in the fridge. Retinal pieces were then recorded on 60-electrode arrays as described in Publication 2 (detailed description of methods in Publication 3). As a simple read-out method, we counted the number of electrodes on which any spiking activity of ganglion cells could be detected (spontaneous and/or light-driven) as well as only the electrodes with light-modulated activity of ganglion cells. This allowed for a crude estimate of retinal survival during ischemia. The data resulted in two main conclusions: first, some retinal ganglion cells and also their underlying circuits can survive up to at least 50 hours (spontaneous activity) and 35 hours (light-modulated activity) of ischemia, (Publication 2, Fig. 2). Second, hypothermia strongly promotes survival of ischemic retina, with 4°C being the optimal temperature tested. In particular, the ischemic duration after which light-driven responses to standard, rather low contrast stimuli could be measured increased from 1 hour at 37°C to 2.5 hours at

21°C and 5 hours at 4°C. To high contrast stimuli, some cells even responded after 35 hours at 4°C. This is highly relevant because it indicates that not only the ganglion cells survived the ischemia, but that also at least some full retinal pathways from photoreceptors to bipolar cells and ganglion cells were still intact. Similarly, the presence of spontaneous activity was prolonged from 4 hours at 37°C to >50 hours at 4°C (Publication 2, Fig. 2). These data are consistent with previous studies in rats where ischemic durations of up to 1 hour at body temperature caused only little harm (Lafuente et al, 2002; Zhao et al, 2013) and with a report on prolonged retinal survival in rats when exposed to ischemia under hypothermic conditions (Faberowski et al, 1989).

Quality of obtained human retinas

These findings suggest that ganglion cells as well as at least parts of the retinal circuitry are functional in post-mortem retina for many hours after death. Such donations are stored at 4°C at least after enucleation, but potentially already earlier when the body is kept in a mortuary fridge. Indeed, 4 out of the 6 obtained post-mortem human retinas showed a high level of spontaneous activity after 12.5 to 27 hours of ischemia (Publication 2, Fig. 2). While this post-mortem human retina has not been light sensitive anymore, it can be used for studies where lack of responsivity could be an advantage, for example when testing the efficacy of optogenes as a treatment for visual impairment.

The ex-vivo donations, on the other hand, I intended to use to study the normal information processing in human retina. I thus needed tissue which was harmed as little as possible. Based on the high percentage of electrodes with light-evoked activity even after 1.5 hours of ischemia at room temperature, I predicted that ex-vivo retinas (which were exposed to only 7 to 25 minutes of ischemia) would be usable for physiological studies. In accordance with this prediction, I could record abundant light responses in 10 out of 16 ex-vivo retinas. One retina could not be recorded due to technical problems and five retinas showed no or only few light responses (Table 1 in Publication 1). While there are many possible reasons for the absence of light responses (e.g. medical history), prior radiation (for cancer treatment) and longer ischemia times (18 to 25 minutes) might explain the bad condition of the retinas with few or no light responses.

Methodology for studying human retina physiology

High-throughput electrophysiology

Physiology and information processing in the human retina has so far not been studied systematically on the level of single cells and detailed circuits. One possible reason may have been the lack of high-throughput techniques which would allow gaining a large dataset from a single retina. Such comprehensive datasets from individual retinas are desirable given the rare availability and the high variability of human retina. However, in the last 20 years, multi-electrode arrays (MEAs) with dozens to hundreds of electrodes have been developed which allow for largely unbiased recordings of big populations of cells (Meister et al, 1994). Since then, MEAs have been used in several studies to record the activity of many retinal ganglion cells in parallel (Chichilnisky & Kalmar, 2002; Fiscella et al, 2012; Frey et al, 2009; Segev et al, 2004; Zeck & Masland, 2007). The high sampling frequency of MEA recordings allows resolving also fast spike bursts which might reach frequencies of several hundred Hertz. This is one advantage over other high-throughput techniques such as calcium imaging. To study human and other retinas I have used MEAs with 59 recording electrodes as described in **Publication 3**. Briefly, in the case of human and pig retina, pieces of 3-4 x 3-4 mm^2 were put ganglion cell-side down onto the MEA electrodes. Whole mouse retinas were used in the same way. A set of various light stimuli was presented to the retina by a conventional projector and the ganglion cell responses were recorded by the MEAs. After the experiments, I performed spike sorting to extract the activity of individual ganglion cells (described in Publication 1).

Selection of retinal areas

The ganglion cell density varies between species. In mice we find a rather modest gradient of ganglion cell density changing with eccentricity from 8000 cells per mm^2 surrounding the optic disk to 2000 cells in the periphery (Drager & Olsen, 1981). In human retina, this gradient is much stronger from 35’000 ganglion cells per mm^2 in the fovea to 200-300 cells at the ora serrata (Curcio, 1990; Harman, 2000). Pigs do not have a fovea, but a band of higher acuity vision, the so-called visual streak. The ganglion cell density drops from >5000 cells per mm^2 in the densest parts of the visual streak to 500 cells in the outermost periphery (Hebel, 1976). For my experiments I have used the entire mouse retina. I estimated that the areas forming contact with the electrodes had ganglion cell densities of

approx. 3000-7000 ganglion cells per mm^2. In pig retinas, I chose regions within the visual streak, thus with 3000 to >5000 cells per mm^2. Recording from ganglion cells associated with the human fovea is very difficult due to the extremely high density of ganglion cells and because photoreceptors feeding into those ganglion cells are displaced towards the center of the fovea (Rodieck, 1998). Further, the foveal and para-foveal areas might be cut off after surgery if the tumor lies closely to the fovea. Therefore, I used mid-peripheral pieces of human retina which contain 2000-5000 ganglion cells per mm^2, depending on the source (Curcio, 1990; Harman, 2000).

Stability of retinal activity

MEA recordings over many hours have been performed in previous studies with retinas from different species. Also with human retina I could obtain stable responses during recording sessions lasting 5 hours (Publication 1, Fig. 2). Without pre-selection of good experiments, one can expect to cleanly extract around 40 ganglion cells from each mouse retina, and around 50 ganglion cells from human and pig retinal pieces (Publication 2). From the 10 ex-vivo human retinas with abundant light responses, I recorded 15 retinal pieces. The activity of almost 1000 ganglion cells was extracted from these recordings and one third responded to at least one of the presented light stimuli (Suppl. Table 1 in Publication 1).

Conclusion on feasibility of functional characterization of human retina

In summary, human retinas from enucleation patients normally survive the short ischemia times of around 10 minutes during the donation process very well. Moreover, the methodological paradigms established for recordings from other species' retinas can be applied to human retina. When using the whole mouse retina, pieces from the pig's visual streak and the mid-peripheral human retina, one is recording from retinal areas with similar cell density. This is of importance for comparisons across species and will be further discussed in Part 3.

PART 2: ANALYTICAL ASPECTS

Approaches to response characterization and classification

My approach to characterizing the function of human retina and to comparing it to the physiology of retinas from other species was as follows: First, I determined response parameters that characterize distinct properties of ganglion cell responses (e.g. response polarity, speed tuning, etc.). After extraction of those parameters for each individual recorded ganglion cell, they were used to describe the functional properties of ganglion cell populations. The parameters can be used to characterize retinal encoding in a given species, to compare the properties of transgenic and wild-type retinas, to compare visual processing in different species, and also to judge the repeatability of responses across experiments.

The analysis of hundreds of cells requires stable (semi-)automated algorithms to identify responses and to characterize their properties. Different such approaches to response characterization and subsequent classification exist in the literature. Zeck and Masland tackled this question by measuring inter-spike intervals of bursts in response to various stimuli (Zeck & Masland, 2007). Ganglion cells were then grouped based on their typical inter-spike interval distribution. They found that in rabbit retina, ganglion cells with similar inter-spike intervals had also similar responses to various stimuli (Zeck & Masland, 2007). Other studies focused on response characteristics to white-noise stimulation (Devries & Baylor, 1997; Segev et al, 2004). A third approach is the use of a set of stimuli where each stimulus is testing for one or few distinct response parameters such as temporal frequency tuning, polarity etc. (Carcieri et al, 2003; Farrow & Masland, 2011).

White-noise based classification is fundamentally different from characterization with a set of specific stimuli. The question is not “does the cell respond to a bright flash?” but “what was the stimulus leading to a response?” The advantage of white-noise is that the stimulus is well-defined and the result depends very little on the type and range of the shown stimulus. This analysis also allows for conclusions on specific response parameters such as polarity and latency, but it does not inform about complex computations like selectivity for movement direction (nevertheless, direction-selective cells might be identified as a coherent group based on their behavior in response to white-noise). Thus, if the goal is accurate grouping of cells of the same functional cell type, white-noise based

stimulation might be faster and less biased than other experimental paradigms. However, if one does not only want to classify cells, but also characterize their computational possibilities, stimuli which are testing directly for such parameters need to be applied.

Establishment of analysis with a mouse model for optic atrophy

The first step for a meaningful and stable assessment of ganglion cell physiology is the choice of a stimulus set that covers the expected range of responses. Next, one needs to define a set of parameters that characterize the recorded cell's responses. Ideally, the extracted parameters would allow distinguishing one cell type from another by identifying specific properties of cell types.

Human retina is a rarely available tissue, hence I have developed and established the analysis routine with mouse retina: I have studied changes in ganglion cell physiology in a mouse model for hereditary optic atrophy (**Publication 5**). This disease is caused by a mutation in the OPA1 gene and leads to slowly progressing ganglion cell death (Alavi et al, 2007). In this study, which I performed together with Irene González-Menéndez form the lab of Prof. Bernd Wissinger, we wondered if this was a general cell death or whether certain ganglion cell types were particularly vulnerable. To answer this question, I have recorded over 650 ganglion cells from wild-type and mutant mice at four different ages. Each cell was recorded under three light conditions (scotopic, mesopic, photopic). This dataset is very similar to the recordings performed with human retina: almost the same set of visual stimuli and identical MEAs have been used to record human ganglion cells. Also the goal is similar, namely characterization of ganglion cell responses and comparison between different types of retina (comparing species in one case, or health status in the Opa1 case).

Visual stimulation and response parameters

In my experiments, I chose to characterize and classify ganglion cells based on their responses to a set of defined visual stimuli. The goal has been to find a set of stimuli that allow a broad and comprehensive characterization of ganglion cell properties. This is not trivial (Masland & Martin, 2007). While ganglion cell types can be grouped into broad response categories based on their responses to light increments (ON stimuli), decrements (OFF stimuli) or both, they are also tuned to different temporal and spatial properties of the stimulus, show varying speed

preferences and contrast sensitivity, and they might have slow, sluggish or fast and sharp responses (Masland, 2001; Roska & Meister, 2014). These varying sensitivities can be determined for every ganglion cell (Carcieri et al, 2003; Farrow & Masland, 2011; Zeck & Masland, 2007), but only if the applied stimuli cover an appropriate range. For instance, if a certain ganglion cell exclusively responds to very high temporal frequencies, this property can only be detected if the stimulation paradigm covers the corresponding temporal frequencies. The different sensitivities, together with other specializations in the retinal circuitry presynaptic to different ganglion cell types, lead to different selectivity of ganglion cell types for distinct, complex features of the visual input. Some ganglion cells are for example selective for movement in certain directions (Barlow & Levick, 1965), selectively respond to approaching stimuli (Munch et al, 2009) or selectively encode luminance changes (Tien et al, 2015).

I have used a broad set of stimuli covering a wide range of parameters to characterize ganglion cell responses in my experiments. Such parameters should capture meaningful aspects of a cell's response. The set of parameters which I analyzed in my studies included:

Polarity: Response polarity (ON, OFF, ON-OFF) is one of the most striking difference between ganglion cell types and informs the visual system about positive and negative contrasts in a given stimulus.

Latency: Another aspect which has been analyzed in studies related to mine (Farrow & Masland, 2011; Lagali et al, 2008) is response latency, i.e. the time between stimulus onset and a cell's response. This is of importance because it influences the timing with which information reaches the brain.

Transiency/sustainedness: Similarly, transiency or sustainedness of a cells' response (i.e. its response duration) defines the duration of input from a given cell type to the brain (Lagali et al, 2008; Schiller & Malpeli, 1977).

Spatial tuning: In addition to contrast, another important aspect of the visual world is the size of objects and their movement. Size preferences can be investigated by receptive field measurements or calculation of spatial period tuning with sinusoidal gratings (Umino et al, 2008).

Speed preference: Objects might move across the visual field with very different speeds. Drifting sinusoidal gratings inform about the range of speeds a given ganglion cell encodes and about potential speed tuning (response to a specific speed, independently of spatial and temporal properties) (Umino et al, 2008). Alternatively, single bars moving with different speeds can be used to test for speed preference.

Temporal tuning: Speed preferences might be the result of a species' eye size since the same "real-world" speed causes higher retinal speeds in bigger eyes and lower retinal speeds in smaller eyes. Furthermore, a certain speed can be the result of various combinations of spatial periods and temporal frequencies. Temporal frequency tuning, on the other hand, is the result of the kinetics in the circuits from the photoreceptors to the ganglion cells. Encoding of temporal frequencies is often assessed by stimulation with drifting-grating stimuli (Crook et al, 2008; Demb et al, 1999; Umino et al, 2008).

Direction-selectivity: Not only the speed of an object may vary, but also the direction of movement. Bars, spots or gratings moving in eight or more directions are normally used to test for selectivity of ganglion cells for a certain direction (Farrow & Masland, 2011; Rivlin-Etzion et al, 2012).

Many additional response aspects may be measured, for instance detection of local edges, global motion, or chromatic tuning. However, physiological experiments are restricted in time, and a balance has to be found between the variety of stimuli that are presented and a high enough number of repetitions of a given stimulus. The choice of parameters is very crucial for the interpretation of MEA data.

Issues with parameter calculations

In this section, I will elaborate on some of the technical issues associated with the calculation of some of the response parameters and give potential solutions. For the interested reader, this section might therefore provide important background information that may help with robust and proper characterization of ganglion cell responses. Further details on the stimuli and their analysis can be found in the corresponding method sections in Publications 1, 2, 4, 5, and 6.

Latency parameter: Latency is a seemingly straightforward parameter and can be defined as time to response peak after onset of a negative or positive contrast steps (Farrow & Masland, 2011; Lagali et al, 2008). This is a good estimate of response latency for cells with sharp and crisp responses. However, in the case of sustained and sluggish responses, the calculated "latency" parameter is less robust, as illustrated in **Fig. IIa**. First, the timing of the peak strongly depends on how the firing rate is calculated. Further, in such cells it can be incorrect to call the maximal response the "time until the cell responds", i.e. latency. The cell in **Fig. IIa**, for example, starts responding to the stimulus at around 80 ms after stimulus onset. The peak of the mean firing rate at 1826 ms is rather due to a coincidental alignment of certain spike bursts and might vary strongly if including or excluding some of the 40 stimulus repetitions (see raster plot in **Fig. IIa$_2$**). I propose two solutions for this problem: 1) the first peak (defined by restrictions such as minimal height) can be taken as the response latency (used for Publication 5). This analysis requires manual inspection of all responses and some adjustment (in the example in **Fig. IIa**, this leads to a latency of 810 ms). 2) A more robust value, that lends itself to a more automated analysis, was used for Publication 1. I first detected the "first peak" (which may, in fact, be a later peak when doing the detection automatically). Then, I took 75% of the peak amplitude as a threshold and defined the cell's latency as the time when the response crosses this threshold. Manual inspection revealed that this approach yielded robust values, i.e. even when the detected peak was not the first peak, the time of threshold crossing ("latency") was hardly affected by those "mistakes". In **Fig. IIa$_1$**, this results in a latency of 413 ms. Note that it is important that latency is calculated in the same way for all cells that are used for analysis. It is not so critical which method is explicitely used, as long as the method itself yields robust results. With different methods, the absolute numbers may differ, but the relative properties between cells are preserved.

Response polarity parameter: Response polarity is often tested by flashing light and/or bright stimuli on the receptive field of a given cell. An OFF-cell responds only to the dark stimulus, an ON-cell to the bright one, and an ON-OFF cell to both. However, the extracted response polarity of a given cell can strongly depend on whether only responses directly after stimulus onset are considered or if long-latency responses are also taken into account (Publication 4, see also **Fig. IIb** for a

cell that has both short- and long-latency responses). It further depends on whether responses are considered only at the onset of a contrast steps (e.g. probing for ON responses at the beginning of a positive-contrast step) or also at the offset (probing for ON responses after the return to baseline of a negative contrast step). This can yield different results, as shown in Publication 4, Fig. 2a. In my analysis, I considered responses to both onset and offset of full-field negative and positive contrast steps. For the optic atrophy study I calculated a continuous polarity parameter ranging from -1 (pure OFF responses) to +1 (pure ON responses) for clustering purposes. For statistical analysis of polarities across different species, I applied "hard" classification into ON, OFF or ON-OFF cells.

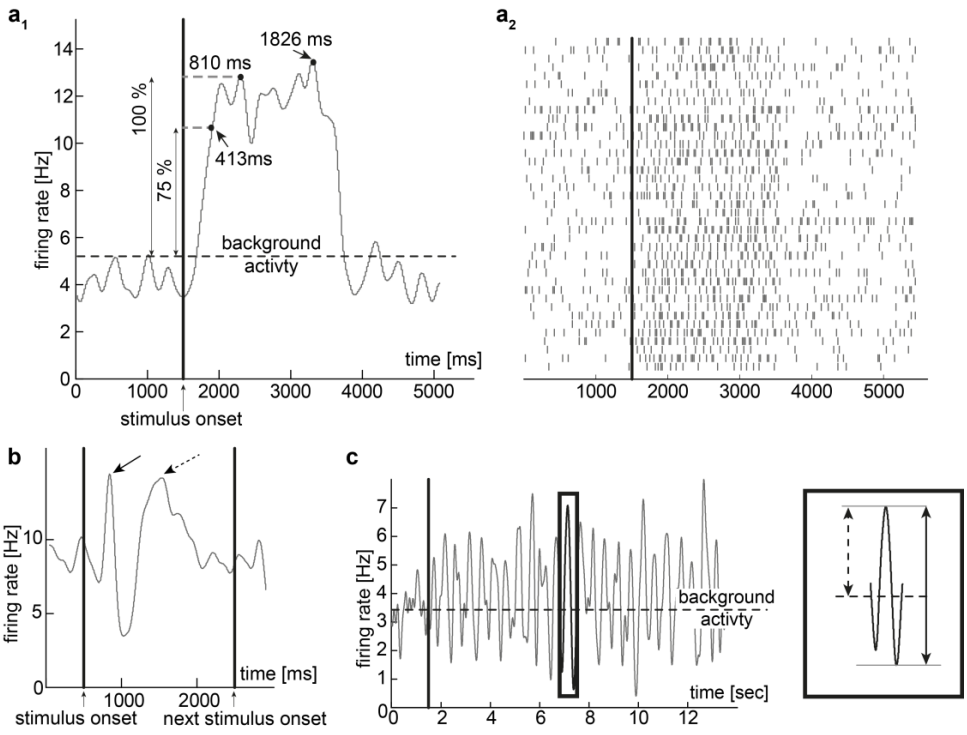

Fig. II: Response parameters. a) Different latency calculations. *Response of an example cell to a full-field contrast step (a_1) and the corresponding raster plot (a_2) showing all spikes produced during the 40 repetitions of the same stimulus. For sluggish and sustained responses, the maximal response does not represent the response latency well (right dot, 1826 ms). The peak at 810 ms was identified as the "first real peak" by an automated algorithm. Alternatively, the time at which 75% of the first real peak response is reached can be taken as a measurement for latency (left dot, 413 ms).* ***b) Issues with transiency/sustainedness calculations.*** *The primary response of this cell is transient. When calculating the percentage of early spikes (solid arrow) compared to the total number of spikes, delayed responses (dashed arrow) will strongly influence this transiency index.* ***c) Different calculations of response strength to drifting-grating stimuli.*** *The plot shows the response to a drifting-grating with 2000 µm spatial period and moving with 2 Hz. One approach to define response strength is to count the absolute number of spikes, usually normalized to background firing rate. However, the shown cell's response contains not only periods of increased firing rate, but is also modulated by inhibition. As shown in the inset on the right, counting spikes above background activity (dashed arrow) would underestimate the absolute response modulation (solid arrow).*

Sustainedness parameter: One possibility to calculate sustainedness (i.e. duration of a cell's response) is to compare the number of spikes in a window shortly after onset of a flash stimulus with a later reference time window or with the total number of spikes generated during several hundred of milliseconds after stimulus onset (Lagali et al, 2008; Schiller & Malpeli, 1977). The cell in **Fig. IIb** has a transient primary response (solid arrow). However, the delayed or rebound response (dashed arrow) will strongly increase the number in the later reference window and will thereby influence the calculated transiency index. This cell would thus be classified as rather sustained despite its initial transient response. Similar problems occur when calculating the area under the curve of poststimulus time histograms (Farrow & Masland, 2011). For the comparison of mutant and wild-type mice I was interested in distinguishing between very sustained and rather transient cells. I therefore defined sustainedness by the remaining activity at the end of the 2-second stimulus (Publication 5, Fig. $3A_1$). Due to the high background activity and often comparably weak response in human retinas, I did not determine sustainedness for this data.

Temporal frequency and spatial period tuning parameters: Temporal and spatial tuning is often tested by drifting sinusoidal grating stimuli. One way of analyzing the responses to such stimuli is to count the number of spikes produced in response to a drifting-grating stimulus (Lee et al, 1994). However, similarly to response sustainedness, this analysis can become unstable, e.g. for cells that get strongly inhibited (see example in **Fig. IIc**). In addition, ON-OFF cells will often obtain higher response strength scores since they respond with the double frequency compared to pure ON- or OFF-cells and thus produce more spikes in response to the same stimulus. Another approach is the calculation of the Fourier transform of the cells' response to drifting-grating stimuli (Crook et al, 2008; Demb et al, 1999). The amplitude at the stimulation frequency is then taken as response strength of this cell (see Publication 5, Fig. 2A). For my research I applied such Fourier transform calculations with high frequency resolution to binary firing rates (details in **Figs. IV and V**; I used this approach in Publication 1 and Publication 5). This analysis has the advantage that responses to another stimulus that tests for temporal frequency tuning, namely the chirp stimuli (i.e. full-field contrast modulation), can be analyzed similarly (see **Fig. VIII**). This

allows for easy comparison of tuning curves obtained with the two different stimulation paradigms.

Classification of response parameters

In order to group recorded ganglion cells into functional types, one can use clustering algorithms which group the extracted response parameters into functionally similar clusters of cells. Many different algorithms and validity indices (assessing the quality of the clustering result) exist. An overview of some of these algorithms applied to clustering of mouse ganglion cells recorded by MEAs can be found elsewhere (Farrow & Masland, 2011).

After optimization of the parameter extraction with the mouse model for optic atrophy, I applied many clustering algorithms to the data from mutant and wild-type mice. Here I have encountered a puzzling issue which I first took for a technical/mathematical problem of clustering, but which turned out to have an important biological background. Clustering of ganglion cells based on their response properties led to good separation when using data from one ambient light level (scotopic, mesopic, or photopic). However, the clusters obtained at different

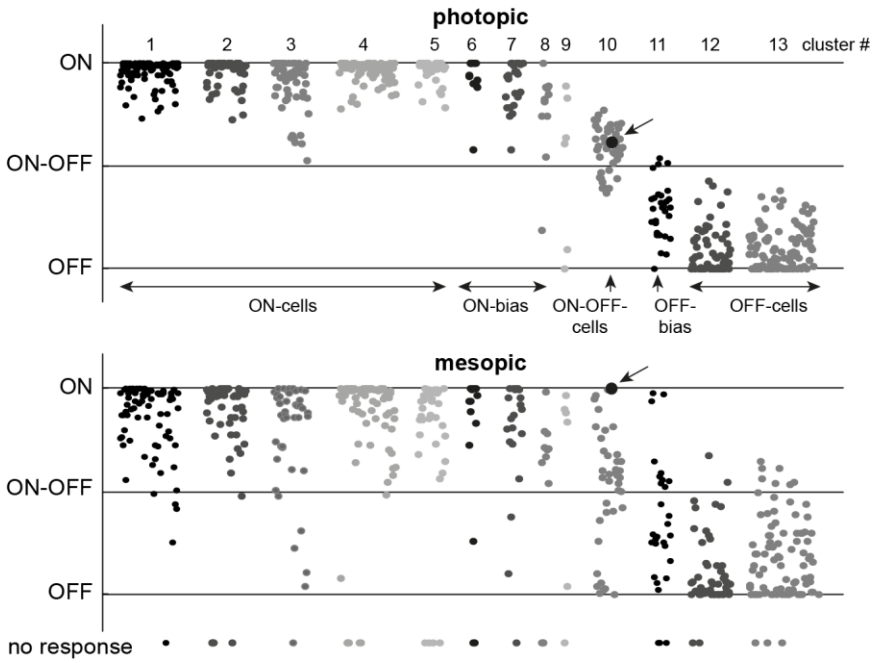

Fig. III: Clustering result for optic atrophy data. *k-means clustering of 654 ganglion cells based on 6 response parameters led to 13 ganglion cell groups (labelled 1-13). The plot shows the distribution of the "response polarity" parameter along the vertical axis; each dot corresponds to an individual ganglion cell. Clustering was performed with response parameters measured under photopic conditions (top). The bottom plot shows the response polarity of the same cells under mesopic conditions. The black circle and arrow indicate a cell that had equally strong ON and OFF responses under photopic conditions. It was therefore clustered into cluster 10. Under mesopic conditions, however, the cell is a pure ON-cell.*

light levels did not correspond to each other. In other words, ganglion cells that fell into a single group under photopic conditions could have very differing physiological properties at mesopic or scotopic light levels. Ironically, one of the most inconsistent parameters across different light levels was response polarity, which is exactly the parameter which is used most often for describing and even defining ganglion cells (e.g. "This is an ON cell"). For example, a clear ON-OFF-cell under photopic conditions might suddenly have pure ON-responses at mesopic light (**Fig. III**, the arrow highlights such a cell in cluster 10). This instable clustering across light levels complicated the classification of cell types and prompted me to further investigate this phenomenon.

Instability of functional properties

In a separate study I systematically analyzed the changing response polarity under different light conditions together with Alexandra Tikidji-Hamburyan (**Publication 4**). The visual system is exposed to many different sources of input variability on a daily basis. One of the biggest variations is introduced by changes in ambient illuminance. Day and night causes luminance changes of about 10^{10} fold, but even when viewing a single natural scene the ambient light may differ by up to 1000 fold or more, for example when a cloud passes by the sun. Systematic studies on how the retina adapts to these permanently changing conditions to allow stable and reliable visual processing across many log units of luminance have been missing. It was also not clear whether adaptation leads to identical encoding of a given stimulus feature under different light conditions. Previous reports (Allen et al, 2014; Dunn et al, 2007; Enroth-Cugell et al, 1975; Farrow et al, 2013; Grimes et al, 2014; Umino et al, 2008) and my data from the optic atrophy mouse model suggest changes in visual computations with luminance, which would result in luminance-specific processing of a given feature.

We thus systematically studied the response polarity of mouse and pig ganglion cells across 5 log units of luminance from scotopic (1 R* per rod per sec) to photopic conditions (10^4 R* per rod per sec). Our experiments revealed surprising response variability across transitions between different light levels: the majority of ganglion cells changed their response polarity at least at one light level transition (Publication 4, Fig. 3, Suppl. Fig. 5), e.g. from pure OFF to ON-OFF (Publication 4, Fig. 2a right, transition from ND7 to ND8). Importantly, while

response polarity may change at any luminance transition, it is stable at a given light level, i.e. when repeatedly testing a cell with the same stimulus at the same luminance it always showed the same response, even if there were intervening stimuli at other light levels (Publication 4, Fig. 5). We were worried that changing response polarities might be an artefact of in-vitro experimental conditions. However, they do occur also in-vivo, and they seem to be relevant for visual processing since they can be found in a retinal target, the LGN (Publication 4, Fig. 7). The mechanisms for such changing responses are diverse and include center-surround mechanisms (Publication 4, Fig. 8) and inhibitory interactions (Publication 4, Suppl. Fig. 2). Interestingly, luminance-dependent response changes could be found for all tested types of stimuli, such as full-field and localized contrast steps as well as with natural movies (Publication 4, Fig. 8 and Suppl. Fig. 3). We almost exclusively studied the impact of luminance on response polarity. In a recent publication, is has been shown that also contrast sensitivity is luminance-dependent while direction selectivity appears to be stable (Pearson & Kerschensteiner, 2015).

Conclusions and chosen analysis

What is a functional cell type?

The fact that the output of the retina changes qualitatively with changing illuminance has an impact on neuronal coding and one might even have to consider it when developing medical treatments, as discussed in Publication 4. Technically, it strongly affects the classification of retinal ganglion cells types based on their functional properties. The variety of response patterns across luminance levels which we observed is larger than one would expect from a population of approximately 30 different ganglion cell types. It is possible that one of the measured parameters – polarity of delayed responses – is not of importance for visual processing. However, if it is a meaningful aspect of a ganglion cell's output, it poses the question: how is a functional cell type defined if cells of the same type do not behave similarly across light levels?

Stable classification of ganglion cells into distinct types is still an unsolved issue. In addition to classification based on functional parameters, other classification schemes are commonly used. The oldest classification method – morphological characterization – has made use of parameters such as dendritic size and shape. Furthermore, the mosaic arrangement of ganglion cells can be taken into account.

Retinal cell types have been found to tile the whole retina so that they sample from every pixel but with little overlap (Wassle & Riemann, 1978). However, especially in species with very inhomogeneous retinas and cell densities, such as humans, the same cell type might look quite different in the central and peripheral retina. For example the midget cells in primates are very small in the foveal retina and form 1:1:1 contacts (1 cone, 1 bipolar cell, 1 midget cell), while up to 12 cones feed into the larger midget cells of the peripheral retina (Kolb & Marshak, 2003; Polyak, 1941; Watanabe & Rodieck, 1989). As another classification scheme, genetic identification of cell types might be the most objective and stable approach (Siegert et al, 2012). However, neither genetic nor morphological classifications necessarily correspond to functional identity.

All approaches eventually pose the same question: how similar is similar enough? Two cells which look similar and also behave similarly to all stimuli tested so far might respond differently to a visual stimulus which has not been used for the cell type identification. Do two cells "behave the same way" if they both respond to negative contrast? Or should they also have the same contrast sensitivity, the same transiency or even produce the same number of spikes? A simple example for this problem is the case of direction-selective cells. One can group cells according to whether they are selective for movement direction or not. However, direction-selective cells can be further separated according to the direction for which they are selective. This results in at least 7 different direction-selective cell types (Vaney et al, 2012).

One approach to tackle the question of functional cell types might be high-density MEA (hdMEA) recordings. hdMEA recordings allow recording almost every ganglion cell in the retinal patch covered by the electrode field, leading to a large, little biased dataset recorded under identical conditions. Further, the high density of electrodes provides spatial information so that mosaic formation can be used as a criterion and even some morphological features can be extracted based on the electrical footprint of cells. Further information could be obtained by recordings from genetically identified cell types by calcium imaging. Cell type identification might even be achieved in hdMEA recordings by expression of an optogene (i.e. a light-sensitive protein) in an identified subset of ganglion cells. Stimulation with strong light in the end of hdMEA recordings would activate these optogenes and

specific kinetics or chromatic sensitivities of the optogenes could allow physiological identification of marked cells. Eventually, by recording at different light levels, the stability of responses in a population of genetically identified cells can be assessed and used as an additional criterion for grouping or separating cells.

Population analysis

Given the unsolved issues of cell type identification and the phenomenon of response changes with luminance, I eventually decided against clustering of ganglion cells into different types, but instead I analyzed the effect of optic atrophy in mouse retina on a population level (**Publication 5**). Response parameters were determined separately for individual cells and the distribution of those parameters was then compared across genotype and age groups. This analysis revealed several significant changes in the functional properties of ganglion cells. Latency and sustainedness changed with age but there were no differences between wild-type and mutant retinas. Speed preference, temporal and spatial tuning, on the other hand, differed between mutant and wild-type animals, especially at the older age of 12 and 18 months, indicating an effect of the Opa1 mutation on these properties. We know from histological studies that around 50% of ganglion cells have died at that old age. Consequently, there are two possible mechanisms for these mutation-induced functional changes: a specific group of ganglion cells with certain response properties might have died in mutant retinas, leading to the observed shift in the population response properties in mutant retina. Alternatively, cells of all types died equally, but the surviving ganglion cells shifted to a different part in the parameter space. Both mechanisms as well as a combination of them could explain our data at a given light level. However, we found different, sometimes even opposing changes in the functional parameters under different light conditions (Publication 5, Fig. 2 and 3). These data suggest that not only the ganglion cells are affected by the Opa1 mutation, but also their underlying circuits. So far, only ganglion cells have been thought to be impaired in both mouse (Alavi et al, 2007; Heiduschka et al, 2010) and human retinas with optic atrophy (Schild et al, 2013).

I applied the experience from the optic atrophy study to the analysis of human data as well as to the comparison of human data with pig and mouse recordings. In addition to the unsolved questions on ganglion cell type classification and the naturally occurring changes in ganglion cell response properties across luminance, there is a further source for variability in the human data due to different genetic backgrounds, life style, age, and medical history. Further, many human ganglion cells only responded to a subset of the presented visual stimuli. While "no response" is also a meaningful attribute of a cell's function, clustering with such data is easily unstable. Already in the case of well-controlled sampling in a defined mouse line, a very high number of recorded cells is required for stable clustering. Assuming over 30 different ganglion cell types, one theoretically needs to record from at least 300 cells to have a significant sample of 10 cells per type. In reality, the resulting data set from MEA recordings is not unbiased. Statistically, the chance to record from cells with a smaller receptive field is higher due to their denser distribution. On the other hand, cells producing bigger action potentials are more easily extracted from the raw data. The size of the action potential depends on the distance of the cell to the electrode, but also on the cell's size and the depth of the cell body within the ganglion cell layer. All these aspects increase the required number of recorded, cleanly sorted, and responding cells. I will discuss in Conclusions & Outlook how this might be achieved with human retina data.

For the recordings performed during my thesis, I chose population analysis – similar to the optic atrophy mouse model – over cell type clustering. Only for the spatio-temporal tuning (measured in response to drifting-grating stimuli) I applied clustering algorithms. First, the number of cells responding to the drifting-grating stimulus was high in all three species. Second, the goal of the clustering in this case was not to identify different ganglion cell types across different light levels. Instead, I intended to analyze how the spatio-temporal space spanned by my stimuli was occupied by different cells within each species (i.e. to identify groups with similar spatial and temporal tuning, but not necessarily similar in other aspects) and to identify distinct groups of cells in a species, that are not present in other species.

PART 3: VISUAL PROCESSING IN HUMAN RETINA AND TRANSLATABILITY BETWEEN SPECIES

The human retina: current status

Short history of the science of human retina

Vision is one of the senses we rely on most for almost any behavior, and the eye is an easily accessible and manipulable organ. It is thus not surprising that we can find diagrams of the eye's structure and function originating from the ancient Arabs or even older (Kolb). However, only in the 16th and 17th century, the ancient drawings were corrected and the retina was identified as the photosensitive part of the eye. Techniques to stain neurons such as the Golgi method in combination with the extensive anatomical work by Santiago Ramón y Cajal in the late 19th century gave us first insights into the detailed structure of the retina on a cellular and subcellular level and allowed for assumptions about the function of its cells and circuits (Kolb). In parallel, academics investigated the visual perception. Goethe, for example, described in his "Farbenlehre" how the eye adapts to ambient light and colored patches (Goethe, 1808-1810). More recent publications described in detail the morphological types of neurons in the human retina (Kolb et al, 1992), their densities, and their distribution across the retina (Curcio, 1990; Harman, 2000; Hofer et al, 2005; Jonas et al, 1992; Roorda & Williams, 1999).

Functionally, the human retina has been studied mostly in-vivo in healthy subjects and as well as in patients by psychophysical methods and electoretinography. While the electroretinographic technique has seen great progress from full-field recordings of the complete population of photoreceptors and bipolar cells towards sophisticated assessment of subpopulations (Berninger & Arden, 1988; Kretschmann et al, 2000; Langrova et al, 2007), it has still a relatively low resolution and does not allow for single cell measurements.

Ganglion cells in the human and other primate retina

The mammalian retina sends information in at least 30 different "channels" to the brain and thus contains at least 30 distinct ganglion cell types (Sanes & Masland, 2015). Based on morphological classification, 17-22 different types of human and non-human primate ganglion cells have been identified (Dacey, 2004; Yamada et al, 2005). These include a group of three different "thorny cells": the broad thorny

cell with transient ON-OFF responses and two narrowly monostratified types (Dacey, 2004). Small and large "bistratified cells" have blue-ON/yellow-OFF properties (Dacey, 2004). The "recursive cells" show similar anatomy as direction selective cells in the rabbit retina; however, their responses have not yet been recorded (Dacey, 2004). "Giant monostratified cells" are the intrinsically photosensitive cells of the primate retina (Dacey et al, 2005). Two additional groups of monostratified cells comprise the "smooth cells" with similar anatomy to the cat Y-cell (Enroth-Cugell & Robson, 1966), and the "sparse monostratified cell" with blue-OFF responses (Dacey, 2004). Finally, ganglion cells with intraretinal axon collaterals have been described (Peterson & Dacey, 1998). Some of these cell types might be further separated (Yamada et al, 2005).

On a functional level, aspects of color vision (Calkins et al, 1994; Chatterjee & Callaway, 2003; Dacey et al, 2014), horizontal cell structure and function (Crook et al, 2011; Smith et al, 2001; Wassle et al, 2000), bipolar types and functions (Boycott & Wassle, 1991; Crook et al, 2014; Haverkamp et al, 2003; Joo et al, 2011; Puthussery et al, 2014; Wassle et al, 1994), amacrine cell function (Greschner et al, 2014; Yamada et al, 2003) and other aspects of primate retinal information processing have been characterized on a cell and circuit level. However, with respect to ganglion cells, non-human primate retina research has been dominated in the past 30 years by the detailed description of midget and parasol cells (Rodieck et al, 1985; Watanabe & Rodieck, 1989). It is still debated whether the small midget cells, which integrate spatial information across their receptive fields linearly, (Kaplan & Shapley, 1986) are responsible for high acuity vision (Reid & Shapley, 2002) or color opponency (Calkins & Sterling, 1999) or both (Lennie, 2000). The parasol cells, on the other hand, are larger and achromatic (Kaplan & Shapley, 1986) and have non-linear spatial integration. Both the midget and the parasol cells each have subtypes with ON- or OFF-responses, respectively. Especially midget (Dacey, 1993), but also parasol cells (Dacey & Petersen, 1992) form a dense mosaic and thus they constitute the majority of all ganglion cells in the primate retina (50-70%) (Dacey, 2004).

In the 1990s the focus in functional research of the primate retina has been extended to a fifth type, the "small bistratified" (or blue-ON/yellow-OFF) cell (Chichilnisky & Baylor, 1999; Dacey & Lee, 1994; Field et al, 2007) which

accounts for around 5% of the ganglion cell population (Dacey & Lee, 1994). Few publications describe the response behavior of additional cell types, e.g. the "large bistratified" cell (Dacey, 2004), the "giant sparse" cell (Dacey et al, 2005), and a ganglion cell with transient responses and highly non-linear spatial summation (Petrusca et al, 2007) similar to the Y-cell in the cat retina (Enroth-Cugell & Robson, 1966). Reports on direction-selective and approach-sensitive cells, local edge and global motion detectors – cell types known from the retina of other mammals (Barlow & Hill, 1963; Levick, 1967; Munch et al, 2009; Roska & Werblin, 2001; Roska & Werblin, 2003) – are anecdotal (De Monasterio & Gouras, 1975; Schiller & Malpeli, 1977) or do not exist.

Furthermore, there is almost no physiological data on human ganglion cells on the level of single cells and circuits. A literature search revealed only two publications where responses of individual ganglion cells were recorded directly: in 1971, Weinstein and colleagues performed extracellular recordings of ganglion cells in donated human retinas. They do not provide numbers of recorded cells or statistical analyses, but report on both ON- and OFF-cells, center-surround receptive fields in some units, and chromatic properties measured in two cells (Weinstein et al, 1971). The second set of recordings was obtained by Hashimoto and colleagues who found transient and sustained ON- and OFF-responses, but no ON-OFF fibers, in the optic nerve of Parkinson patients (Hashimoto et al, 2013).

The lack of data from human retinas together with the focus of primate research on only a few cell types created the general impression that the processing capability of the primate retina might be weaker than in other mammals. This focus on 5 cell types is mainly due to the fact that the probability to record from parasol and midget cells when blindly choosing cells is much higher than for other cell types due to their high density. Further, scientists might have been discouraged from studying human retina directly due to its rare availability and the limited control over subjects and tissue conditions.

Encoding of visual information in the human retina on cell and circuit level

Overview of findings

During my doctoral work I at least partially overcame these issues by establishing a collaboration with the big eye clinic in Tübingen and by the use of multi-electrode arrays. I aimed to characterize the pre-processing of visual stimuli in the human retina by recording from a large population of ganglion cells and to compare retinal processing in humans with the properties of pig and mouse retina. For the analysis I abstained from trying to identify and define cell types due to the general issues associated with the definition of ganglion cell types based on functional properties (discussed in Part 2). Instead, I analyzed and described the activity of 342 light-responsive human ganglion cells, recorded from 10 retinas, on the population level (**Publication 1**). The results suggest that image processing in the human retina is of similar complexity as in other mammals. I found both ON- and OFF-responses, which is consistent with the two previous publications (Hashimoto et al, 2013; Weinstein et al, 1971). In addition, for the first time, I described also ON-OFF responses. This ON-OFF behavior was very common as it occurred in almost 20% of ganglion cells responding to full-field contrast steps (Publication 1, Fig. 3D). Furthermore, I found a rich variety in response transiency ranging from sharp to very sustained responses (Publication 1, Fig. 3B). I also showed that human ganglion cells respond to a range of stimulus speeds. The average speed preference of individual cells could be anywhere between 2 and 10 mm/s (retinal speed; corresponds to approximately 7 to 33 °/s) and could occasionally be even lower or higher (Publication 1, Fig. 5). In addition, human ganglion cells responded to a broad range of temporal frequencies and spatial periods. I found both sharply tuned cells as well as ganglion cells covering a big part of the spatio-temporal space (Publication 1, Fig. 4).

Comparison to literature on primate retina

Y-like cells: The limited availability of physiological data from primate ganglion cells other than midget, parasol, and small bistratified ganglion cells, and the lack of spatial or morphological information in my own study make a direct comparison between published data from non-human primate retina and my human retina results difficult. Midget and parasol cells are usually identified by receptive field size and mosaic formation. With the chosen set of stimuli and the

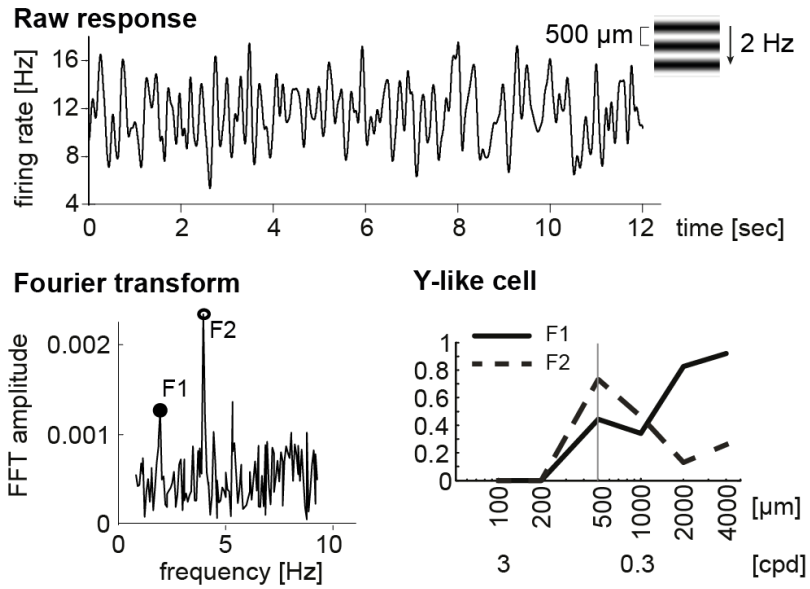

Fig. IV: Y-like cells. *Drifting-grating responses were used to test for non-linearity of ganglion cell responses (example response for a 500 µm grating moving with 2 Hz on top). I calculated the Fourier transform of these responses and took the amplitude at the stimulus frequency (F1) and at the second harmonic (F2) as response strengths of the cell (bottom left). All amplitudes were normalized to the maximal F1-response across all stimuli (24 gratings with different spatial and temporal properties). Candidates for a Y-like pathway were identified by F2-responses exceeding F1-responses, indicating strong non-linearity. On the bottom right, the F1- and F2- responses for this example cell are shown for the 6 different gratings (for each spatial period, the stimulus causing the highest F2-amplitude was taken). The gray line indicates the example stimulus shown on top and left. For details see Publication 1.*

wide spacing of electrodes in my MEAs, I did not obtain this information. However, after the discovery of the highly non-linear Y-cells in the cat retina (Enroth-Cugell & Robson, 1966), scientists set out to find homologue pathways in the primate retina. A recent publication described the functional properties of the so-called Upsilon-cell which has been proposed as one candidate for a Y-like ganglion cell (Petrusca et al, 2007). One of the characteristics of this cell is the strong second harmonic (F2[a]) response when stimulated with contrast-reversing sinusoidal gratings with spatial periods of approximately 500-2000 µm. Also the parasol cells have been suggested as an analog to Y-cells due to their strong F2-response to narrower gratings (Crook et al., 2008).

In my dataset, human ganglion cells rarely responded to drifting gratings of 200 µm or finer spatial period and did thus not show similar bevhavior to macaque parasol cells (Crook et al., 2008). However, 29 human ganglion cells had F2/F1-ratios bigger than 1 for at least one drifting-grating stimulus of 100-1000 µm

[a] When stimulated with a periodic stimulus, ganglion cells usually have a periodic response. F1 refers to the frequency of the cell's response that corresponds to the stimulus frequency; F2 refers to double this frequency. See also Fig. IV.

spatial period (example cells shown in **Fig. IV** and in Publication 1, Fig. 6). Most of these cells showed strong tuning to high spatial periods (= gratings with wide bars) based on their first harmonic response, similarly to the Upsilon-cells in primate retina (Petrusca et al, 2007). However, only few of these 29 cells showed a clear F2-tuning curve (for example the cell in **Fig. IV**) as it had been shown on a population level for the macaque Upsilon-cells (Petrusca et al, 2007). In other human ganglion cells the F2-curve exceeded the first harmonic curve only for one spatial period and temporal frequency or it remained stronger also for higher spatial periods than 2000 µm (Publication 1, Fig. B-D). Nevertheless, these cells are potential candidates for a human Y-like pathway.

Unfortunately, the majority of the human Y-like cells did not respond to full-field contrast steps and I could thus not use other criteria such as rapid and transient responses – the other known attributes of Upsilon-cells – to confirm their physiological identity. In addition, response sharpness and transiency is difficult to judge from high frequency drifting-gratings (to which Upsilon-cells preferentially respond) since the fast sinusoidal changes between negative and positive contrasts cause transient responses in almost all cells, also those that showed sustained responses to slower stimuli.

ON-OFF responses: Dacey described 3 (4 when including the melanopsin cells) bistratified cell types in the primate retina (Dacey, 2004). I found ON-OFF responses in 20% of cells; however, note that these are 20% of only those cells which responded to full-field contrast steps. Thus, direct comparison with the numbers of bistratified cells (~15%) is not possible. For instance, direction-selective cells do not respond well to full-field stimulation; thus, ON-OFF direction-selective cells might not be part of my ON-OFF cells. In addition, we have shown in mouse retina that also monostratified cells can respond to both light increment and decrement (Publication 4). Finally, I cannot exclude that some of the recorded ON-OFF responses might originate from spiking amacrine cells, which have also been recorded previously in MEA experiments with primate retina (Greschner et al, 2014). Future studies in both human and non-human primate retina, including morphological analysis and chromatic stimuli will be necessary to directly compare human ganglion cells with ON-OFF responses to human and other primate's bistratified cells.

Distance-invariant cells: I studied spatio-temporal properties of human ganglion cells by separation of their drifting-grating responses into 14 clusters using a k-means algorithm. These clusters could in turn be grouped into four categories of clusters with related properties (**Fig. V middle**): one group with temporal tuning properties, a spatially tuned group of clusters, a group of broadly tuned clusters, and a fourth group with two clusters containing cells with an "anti-speed" behavior (**Fig. V bottom** and Publication 1, Fig. 7F). "Anti-speed" conditions occur when an object is moving with a given real-world speed but at different distance from the observer. When the object is far away it appears smaller and its projected image on the retina moves relatively slowly. When the object is closer it appears bigger and the retinal speed is faster. Ganglion cells in these two last clusters showed corresponding spatio-temporal tuning: they responded well to wide stimuli when shown with high temporal frequency, but also to narrow stimuli with low temporal frequencies (**Fig. V bottom**). The role of these cells might thus be to detect objects of a given size and moving with a specific speed, independently of how far away this object is. I therefore named these cells "distance-invariant". A literature search did not reveal any similarly behaving cells in other species. However, this might be because similar stimuli and analyses have not been applied to retinas of other species. In my data I found distance-invariant cells also in pig, but not in mouse. In contrast to this "anti-speed" behavior, I did not detect any retinal cells with specificity for a certain speed. Speed-tuned cells have been described for example in the visual cortex of primates (Priebe et al, 2006).

Richness of visual encoding: Independently of direct comparison between non-human and human primate retina, based on spatio-temporal tuning alone human ganglion cells can be grouped into at least 10 clusters of cells with distinct response properties (**Fig. V**; Publication 1, Fig. 7). Why does the variety of ganglion cell responses appear to be higher in human retina than suggested by most of the literature on ganglion cells in primate retina? There may be multiple reasons:

Technical issues might artificially increase the variability in recorded responses. For example, I cannot fully exclude that during spike sorting, spikes of several cells may have been combined or that for some cells spikes have been missed. However, the signal-to-noise ratio was in general better in human recordings than in MEA recordings from mouse or pig retina, decreasing the likelihood of spike-sorting mistakes. Further, I restricted my analysis to very cleanly sortable units. Recording biases, for example for cells with high density and large action potentials, should rather decrease than increase the observed variability.

When recording from human retina, the correct identification of the recording location may be very difficult. For instance, the eccentricity is hard to define when the optic nerve and/or the fovea are not within the part of the eye bulb available for experiments. In addition, depending on the age of the donor, the

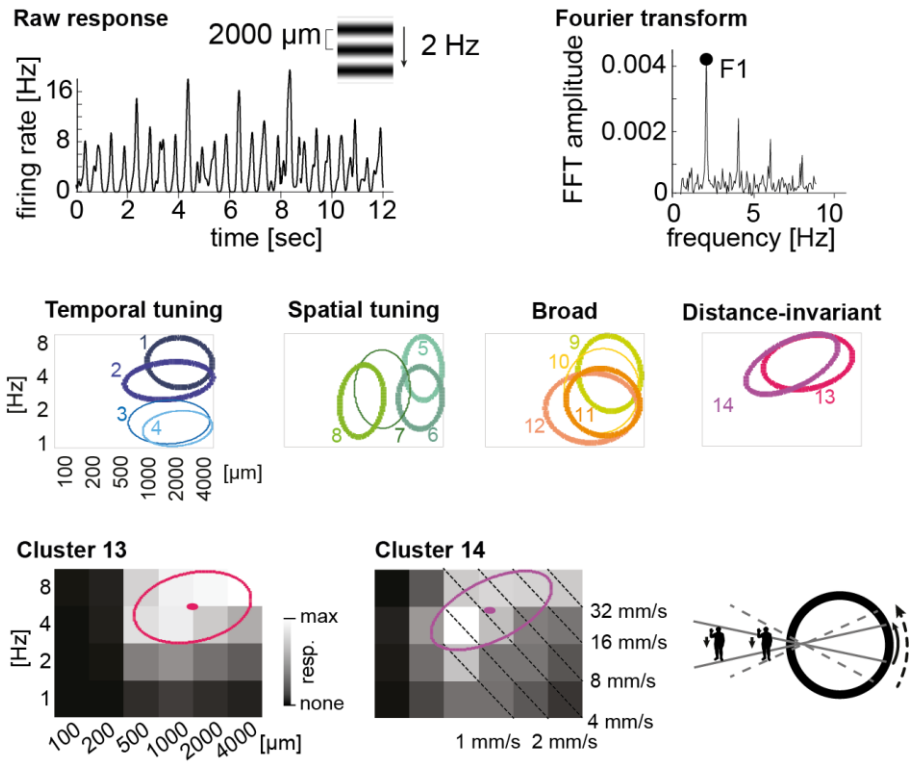

Fig. V: Distance-invariant cells. *Response strength to various spatial periods and temporal frequencies was extracted from drifting-grating stimuli as described in Fig. 4 and Publication 1 (top). The obtained F1-responses were normalized for each individual cell of human, pig, and mouse retina; cells of all three species were combined and clustered by a k-means algorithm. The Gaussian fits for the resulting 14 clusters can be grouped into four classes of related clusters (middle). To characterize each cluster, I fit a 2-dimensional Gaussians to the clusters' spatio-temporal heat-maps of F1-amplitudes as illustrated at the bottom for cluster 13 and 14. Thick Gaussian fits indicate clusters in which human retina was represented with at least 10 ganglion cells. Two resulting clusters (13 and 14) showed distance-invariant properties (bottom). The cells in these two clusters responded well to small and slow as well as big and fast stimuli, thus showed an "anti-speed" behavior with a tuning (Gaussian fits) perpendicular to the iso-speed lines (bottom middle).The purpose of such response behavior might be the encoding of an object moving with a given speed independently of whether it is far (and appears small and moving slowly) or close (big and fast) (bottom right).*

retina might detach when removing the vitreous, complicating the determination of retinal orientation. Since the ganglion cell density decreases with eccentricity, the receptive field size increases towards the periphery. Spatial tuning measurements with drifting-grating stimuli are influenced by receptive field size and could thus vary within a given cell type if recorded at different eccentricities. However, the influence of eccentricity on the functional receptive field size seems unclear: in one publication, parasol cells recorded at 10-40° eccentricity had receptive field diameters of 150-350 µm (Chichilnisky & Kalmar, 2002), while in a different study (Gauthier et al, 2009) they appeared rather similar in different retina pieces from 6-9 mm (approx. 20-30°) eccentricity. Then again, a third report showed that the receptive field diameter of parasol cells can vary between 100 and 170 µm at a given location 12 mm away from the fovea (Petrusca et al, 2007). Despite these disagreements, it is still possible that spatial tuning appears overly variable in my study due to mixing of cells from different eccentricity of the recorded retinal pieces. However, in addition to variety in spatial tuning, human ganglion cells also showed very distinct temporal tuning. Thus, even when excluding spatial variability, human ganglion cells can be grouped into at least 7 clusters solely based on their responses to drifting-gratings and without considering any other response properties.

It is worth noting that clustering based on responses to drifting gratings does not discriminate ON cells and OFF cells. If we assume that some ganglion cells with similar spatio-temporal properties come in functional ON/OFF pairs (like the midget and parasol cells), then we can conclude that functional diversity in the human retina is even more diverse than suggested by my clustering results.

Translatability of results from animal models

Species-specific retinal morphology

On one hand, the habitat, body size, and location of the eyes lead to a differently perceived visual world in different species. On the other hand, depending on whether an animal is diurnal or nocturnal, a predator or pray, moving rather slowly or quickly, and whether a species is more or less dependent on visual perception, the retina has to fulfill very different tasks. Since most retinal research is performed in animal models it is important to investigate how well results from these models can be translated to the human situation. I have thus compared the visual encoding in human, pig, and mouse retina.

Mouse: The mouse is an important model in retina research mostly due to the possibilities to apply powerful genetic tools. The mouse is preferentially active during the night and has a rod-dominated retina (Huberman & Niell, 2011). In addition, the mouse retina shows a dorso-ventral gradient of blue and green cones (Baden et al, 2013) and does not contain a region of highest acuity such as the human fovea, but has a more even and smoothly changing cell density profile (Drager & Olsen, 1981). Morphological analysis identified 22 different ganglion cell types (Sumbul et al, 2014). Functionally, there are at least 18 but most probably more different types (Sanes & Masland, 2015).

Pig: In medical research, pig and cow eyes are used for studies on ophthalmologic pathologies (Garcia et al, 2002; Komaromy et al, 2003; Lee et al, 2008), in pharmacological investigations (Iandiev et al, 2011; Januschowski et al, 2015; Januschowski et al, 2014; Luke et al, 2005; Tseng et al, 1990; Walter et al, 1999) or for the development of novel surgical procedures (Kamei et al, 2001; Lopez-Guajardo et al, 2011; Sorensen et al, 2011). Even some genetically modified pig models exist (Li et al, 1998; Petters et al, 1997; Ross et al, 2012). It has been shown that the pig eye and retina are in many aspects similar to the human, for example in terms of retinal vasculature, size, cone photoreceptor density or scleral thickness (Gerke Jr et al, 1995; Middleton, 2010). Differences can be observed in color vision (pigs are dichromats) (Hendrickson & Hicks, 2002) and visual acuity since pigs do not have a fovea but a band of higher acuity, a so-called visual streak (Garcia et al, 2005; Hebel, 1976). Veiga-Crespo and colleagues identified 18 morphological ganglion cell types in the porcine retina (Veiga-Crespo et al, 2013). Systematic functional characterization has not been performed previously.

Retinal encoding of visual stimuli in human, pig, and mouse

I found similarities as well as differences between the three species in the measured response parameters. In general, human ganglion cells were functionally more similar to pig ganglion cells than to mouse. In the following paragraphs, I will compare the various parameters across species.

Speed preference: I assessed speed preference with two different stimuli and two alternative analysis methods. Both methods and stimuli revealed similar species differences: mouse ganglion cells preferred lower speeds than human and pig cells (**Fig. VIa**; Publication 1, Fig. 9). Depending on the stimulus and analysis, human

ganglion cells also preferred slightly faster speeds than pig ganglion cells. The differences in speed preference might be related to the eye size of the three species (**Fig. VIb**). A stimulus of the size of 1° visual angle covers 33 µm on the mouse retina (Schmucker & Schaeffel, 2004). In the human retina, the same stimulus covers 288 µm (Drasdo & Fowler, 1974). Thus, a given stimulus moving at a certain speed in real world (e.g. 1°/s) exposes human ganglion cells to much higher retinal speeds than mouse ganglion cells. Pig eyes are of similar size as human eyes. The observed speed differences do not account for the complete size difference, but at least they make the range of encoded "real-world" speeds more similar.

Interestingly, both pig and mouse ganglion cells respond stronger to a single, fast white bar than to a single fast black bar (human ganglion cells responded well only to black bars, so comparison of response strength to black and white bars was not possible there). In fact, the speed response strength curve of mouse ganglion cells responding to a white bar (dashed blue curve in **Fig. VIa**) was similar to the pig response curve to a black bar (solid green curve in **Fig. VIa**).

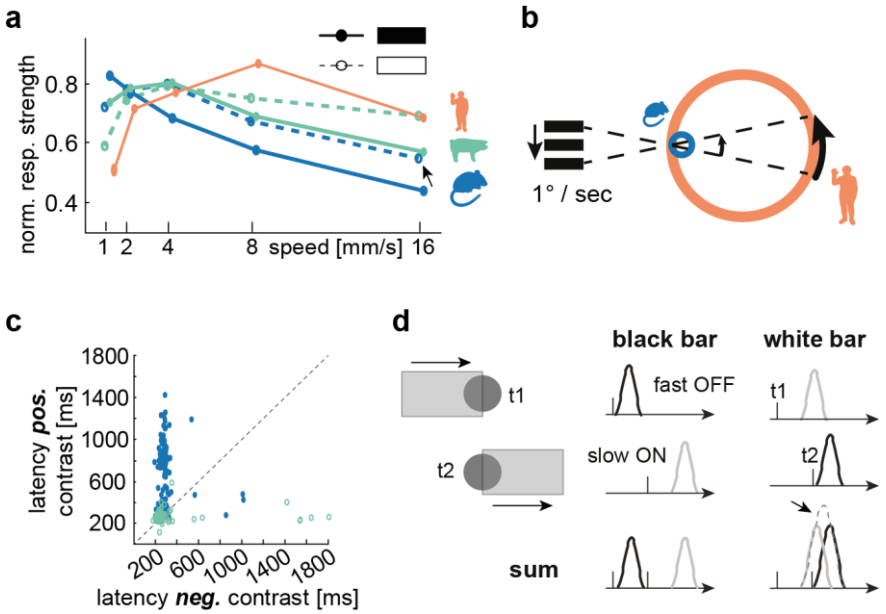

Fig. VI: Speed preference. *a) Speed preference in mouse, human, and pig in response to back bars (solid lines) and white bars (dashed lines). b) Different speed preferences between mouse and human might be an evolutionary adjustment to the different eye size. The same real-world speed causes a faster retinal speed in the big human eye than in the small mouse eye. c) Distribution of latencies to positive (y-axis) and negative (x-axis) contrast stimuli. Especially in mouse, latency to positive contrast is much higher in most ON-OFF cells. d) Resulting overlap of responses to fast white bars. The slow ON-response to the leading bright edge and the fast OFF-response to the trailing dark edge overlap and cause a higher peak response to fast white stimuli (bottom right). For a black bar, the situation is reversed (bottom left).This explains the different response strength to faster white and black bars in mouse and pig retina (see a).*

Analyzing the response latency of mouse ganglion cells to contrast steps, I found that they tended to respond more slowly (longer latency) to positive contrast steps than to negative contrast steps (**Fig. VIc**). Thus, when a bright bar is moving across the cells, the slow ON-response to the first edge and the fast OFF-response to the second edge are so close to each other that they form a single, higher peak during spike rate calculations for fast stimuli, but not for slow stimuli. Thereby, the relative peak amplitude is higher for fast than slow speeds, shifting the calculated speed preference towards higher values (**Fig. VId**). In pig ganglion cells, a small similar tendency could be observed.

Spatio-temporal tuning: Clustering of the responses to drifting-grating stimuli of the combined population of ganglion cells in human, pig, and mouse retina revealed several species-specific spatio-temporal tuning aspects. An overview of the clusters and the distribution of ganglion cells in those clusters for each species can be found in **Fig. VII** and Publication 1, Fig. 7B.

The majority of mouse ganglion cells did not have a sharp tuning to specific spatial and temporal frequencies, but responded well to a broad range of parameters (clusters 10 to 12), and the few strongly tuned cells in the mouse encoded low temporal frequencies (clusters 3 and 4). Almost no mouse ganglion cells exhibited spatial tuning properties (few or no cells in cluster 5-8). Very broadly tuned cells were also found in pig and human retina; however, even human ganglion cells responding to a broader set of drifting gratings were more

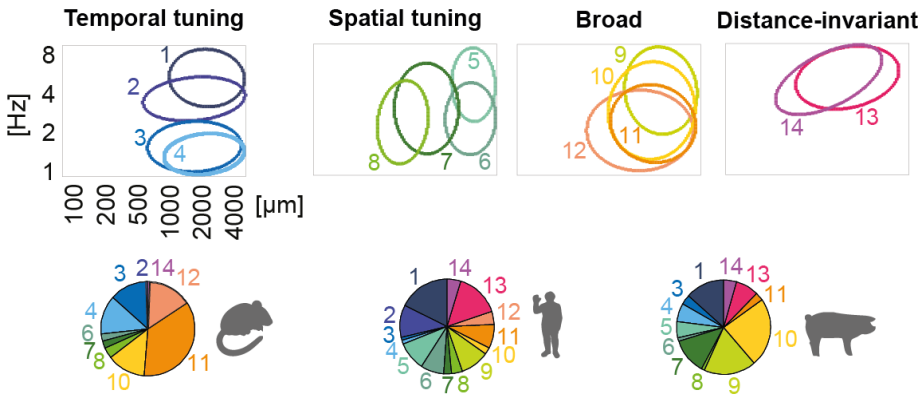

Fig. VII: Spatio-temporal clusters. *Responses to drifting-grating stimuli were grouped into 14 distinct clusters. Clusters 1-4 show temporal tuning (blue), cells in clusters 5-8 are spatially tuned (green), clusters 9-12 contain cells with responses to a broader range of periods and frequencies (orange), and distance-invariant cells are in cluster 13-14 (purple; see also Fig. 5). The pie charts show the percentage of ganglion cells belonging to the 14 spatio-temporal clusters in mouse, human, and pig retina.*

stringently tuned in terms of temporal frequencies (cluster 9 and 11) than pig and mouse cells. Further, human ganglion cells were rather grouped into clusters with tuning to very wide gratings while cells from pig retinas tended to occupy clusters with middle spatial periods (cluster 5 and 6 for human vs. cluster 7 for pig). Interestingly, cells tuned specifically to 4 Hz stimuli (cluster 2) were found exclusively in the human retina (except for a single mouse ganglion cell). Finally, the above described "distance-invariant" cells (cluster 13 and 14) could only be recorded in human and pig, but not mouse retina.

In summary, human and pig ganglion cells were often found in similar clusters with cells encoding preferentially high spatial periods and high temporal frequencies. Further, pig and human cells were generally tuned to a small subset of spatio-temporal features, i.e. they showed for example narrow spatial tuning (clusters 5 through 8), while most mouse ganglion cells responded well to a broad set of drifting-grating stimuli (clusters 10 to 12).

Temporal tuning: While differences in speed preference might be an evolutionary adjustment to differences in eye bulb size, temporal tuning can potentially be attributed to specific local circuit kinetics. In addition to the analysis of responses to drifting-gratings stimuli discussed above, I assessed temporal tuning also with a full-field chirp stimulus (full-field sinusoidal changes in contrast with increasing temporal frequency, shown at the bottom of **Fig. VIII**). This analysis reinforced the observed differences between species: on average, mouse ganglion cells preferred low frequency stimuli (maximal response strength around 1-3 Hz). Human ganglion cells, on the other hand responded only weakly to 1-3 Hz and maximal response strength was measured from 4 Hz to the maximal tested frequency of 7.5 Hz. This is consistent with primate studies where ganglion cells have been found to follow even 80 Hz stimulation (Lee et al, 1994). In contrast to mouse and human retina, pig ganglion cells had on average a flatter tuning curve which was very similar to human temporal tuning at higher frequencies. The similarities between temporal tuning curves calculated from chirp and wide drifting-gratings indicate that the species-specific temporal frequency preferences are a general and robust feature.

For mouse ganglion cells, previous publications found similar maximal temporal tuning as in my study, peaking around 2-5 Hz (Grubb & Thompson, 2005;

Pandarinath et al, 2010; Porciatti et al, 1999). However, Wang and colleagues showed that tuning to low temporal frequencies can be due to insufficient activation of blue cones and that stimulation with UV-light changes the temporal tuning of mouse ganglion cells towards higher frequencies (Wang et al, 2011). The projector used in my study produces only little UV light which might be a reason for the much lower temporal tuning in mouse than pig and human. Further, we showed that rod photoreceptors contribute to visual encoding also under photopic light levels (**Publication 6**). Since rods are slower than cones, rod activation could decrease the temporal frequency tuning under the tested photopic light conditions.

In order to directly compare visual encoding between species I reason that the exact same stimulus conditions should be applied. On the other hand, if one wants to study information channels for high temporal frequencies and has to use a mouse model, the study could be performed with stimulation that includes the UV-green spectral range.

Polarity: In all three species, approximately half of the cells (43-56%) responded exclusively to light increments (ON-responses) (**Fig. IX top**) when considering only responses within 550 ms after onset of positive or negative full-field contrast steps. Both mouse and human retinas had 16-19% of ON-OFF cells. In pig retinas, on the other hand, I found ON-OFF responses in 47% of all responding ganglion cells, reducing the pure OFF-responses to 10%. Previously, morphological analysis identified two bistratified cell types in the porcine retina (Veiga-Crespo

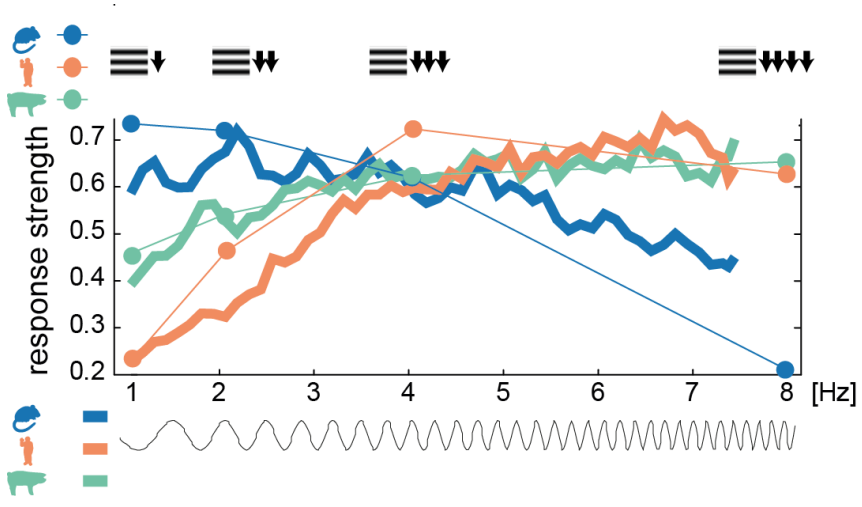

Fig. VIII: Temporal tuning. *Temporal tuning has been calculated from responses to a full-field chirp stimulus (bottom, thick lines) and from wide drifting-grating stimuli (top, dots connected by thin lines).*

et al, 2013). Both of these cells have small dendritic fields and probably form a dense mosaic. Similarly to midget and parasol cells in the primate retina, this might have led to an oversampling of these cell types in my experiments, increasing the percentage of observed ON-OFF responses. However, the actual correspondence between physiological ON-OFF responses and bistratified cell morphology remains to be investigated.

In addition to full-field contrast step analysis, the dominant response polarity can also be measured by spike-triggered average (STA) calculations from white-noise stimuli (**Fig. IX bottom**). Comparing these results with the polarity obtained from full-field contrast steps, I showed that in mouse retina, ON-OFF cells predominantly had OFF-STAs, suggesting that the stronger excitatory drive comes from the OFF system. In contrast, human and pig ON-OFF cells predominantly had ON-STAs. However, for many ON-OFF cells the STA was flat in these two species.

Direction-selectivity: Several direction-selective cell types have been found in the mouse retina (Vaney et al, 2012). I described for the first time direction-selectivity also in the pig retina. On average, 11 % of all responsive pig ganglion cells were selective for a certain movement direction. Half of those were ON-OFF cells based on full-field contrast steps, most others did not respond to the step stimulus. As mentioned above, direction-selectivity has not yet been observed robustly in primate retina. Also in the human retina I did not record any direction-selective responses (Publication 1). However, an adapted stimulus paradigm might reveal direction-selective cells. My stimulus to probe for direction-selective responses

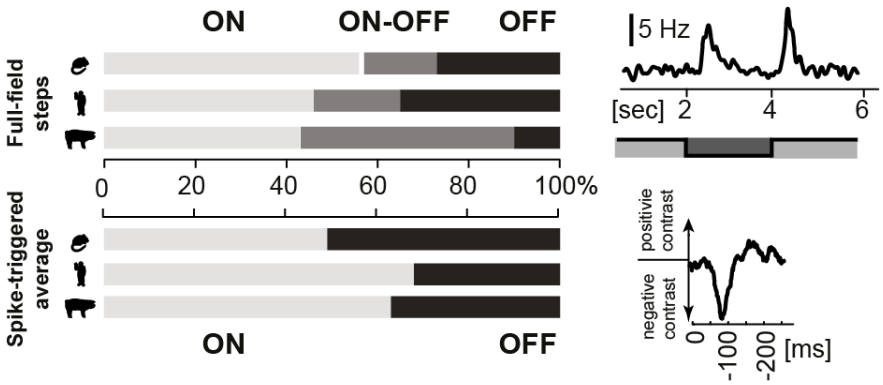

Fig. IX: Polarity. *Polarity determined from responses to full-field contrast steps (top) and by spike-triggered average (STA) from white noise stimulation (bottom). 100% correspond to all cells responding to the respective stimulus in a given species. The right panels show an example for an ON-OFF-response to a full-field contrast step (top) and for an OFF-STA (bottom).*

consisted of a single bar moving with 1 mm/s in eight different directions. Based on the preference of human ganglion cells for higher speeds revealed by my experiments (**Fig. VIa**), increased stimulus speed in future studies might reveal direction-selective cells also in the human or other primate retina.

Why not use primates?

Primates used in research differ from humans in size and habitat, especially in the case of marmosets, which might also have led to some adaptation of their visual system. Small differences have been found for example in cone density (Hendrickson, 2005), distribution of midget cells (Dacey, 1993) or dendritic fields of parasol cells (Dacey & Brace, 1992). Further, primate retina is usually obtained after killing of the animal in the course of another study. Depending on the study, the animal may have been exposed to medication, physically exhausting or harmful tests, and other treatments. The variability in terms of medical history and "life style" might thus not be much lower than in the case of human donations. Finally, research with primates poses ethical questions and issues far beyond the general concerns about animal testing. On the other hand, monkeys are certainly the closest to the human situation (Solomon & Rosa, 2014) and the choice between different animal models or ex-vivo human tissue depends on the scientific question (see Conclusions & Outlook).

Limitations of the study

To my knowledge this is the first comprehensive characterization of human retinal physiology on the level of single ganglion cells. It has its limitations and follow-up studies will be required to obtain a more complete picture of human retinal physiology. The main limitations include variability in the data, biased assessment of certain cell types and response properties, and the high percentage of non-responding cells. These issues are discussed below.

Variability within a given species

In addition to differences between species, I analyzed the variability in the physiological parameters between retinas or retinal pieces within the same species. Data of individual experiments in all three species can be found in the appendix (**Fig. X**: mouse, **Fig. XI**: human, **Fig. XII**: pig). Rather high variability at least in some parameters could be found in the human data-set. The relative number of ON, OFF, and ON-OFF cells, but also preferred speeds or the

distribution of ganglion cells in the spatio-temporal clusters varied between different retinal pieces.

One possible reason for this variability is the relative small number of cells per human retina that showed light responses, and the many cells that only responded to a few stimuli. Of the cells that responded to at least one type of stimulus, 86% responded to drifting-gratings, 40% responded to contrast steps, white-noise flicker or chirp , and only 11% responded to moving bars. Thus, only a subset of the recorded ganglion cell (types) responded in each retinal piece. Different compositions of this subset in each experiment can explain at least part of the observed variability between experiments.

Furthermore, part of the variability could have arisen from the insufficiently controlled eccentricity of the retinal pieces (see “Richness of visual encoding” on p. 36). Also physiological changes due to the tumor or the donation process cannot be excluded. However, the ischemia study (Publication 2) suggests that human retina does not suffer from few minutes without oxygen during the enucleation process and I found at least some light response in most tested human retinas.

Surprisingly, also the results from rather well-controlled pig experiments varied more between different retinas than in mouse. The pigs were exposed to medication during anesthesia and killing, which could have affected the conditions for the retina shortly before and during the enucleation. Further, the visual streak, from which I cut pieces for recordings, is relatively narrow and the ganglion cell density drops off sharply. Ganglion cell density might therefore have differed between experiments. This would likely affect spatial tuning the most, and possibly also speed preference. However, note that while experiment-wise comparison of e.g. speed preference did not necessarily confirm species differences, significant differences remained after classical bootstrapping (Publication 1). Nevertheless, I suggest for future studies to cut pieces from the dorsal part of the pig retina which provides a relatively large surface with constant ganglion cell density (Hebel, 1976).

Biased assessment of cell types and response properties

MEA recordings are a high-throughput technique and thus enhance the chance to record from all cell types in a tissue. However, a certain bias cannot be excluded. The number of cells extracted from a human retina piece with the 59-electrode MEAs applied here was around 50 (Publication 3). Thus, cells which account only for 1-2 % of all ganglion cells might have been missed. Further, cells which produce smaller action potentials or are located deeper in the ganglion cell layer might not be extractable during spike-sorting. Due to the rather strict criteria which I applied to identify responding cells, ganglion cell types with generally sluggish and weaker responses might have been missed as well.

Non-responding cells

Another striking difference between mouse, pig, and human experiments has been the number of non-responding ganglion cells. In mouse, 95% of all sorted cells showed light responses to at least one of the shown stimuli, and for each stimulus between 69-88% off all cells responded. (Note that "sorted cell" means that there were action potential waveforms present in the raw electrode trace that were sufficiently different from other such waveforms, so that they were sorted into a single unit. The sorting process does not take into account if those spikes arose spontaneously or from light stimulation.) Similarly, 90% of the sorted pig ganglion cells had light responses and 48-70% responded to each particular stimulus. In the human retina, only 37% of the sortable cells showed light responses at all (Publication 1, Suppl. Tables 2-4).

The reasons for this low number can be technical: in some isolated patches of the retina, photoreceptors or ganglion cells might have been harmed before or during the surgery or while removing the very sticky vitreous during preparation of the retina. However, responding and non-responding cells were often recorded by the same electrode. One would expect that mechanical or tumor-mediated injuries harmed a whole retinal patch rather than single ganglion cells or photoreceptors. Since many human ganglion cells are chromatic (Crook et al, 2011; Dacey et al, 2014; Dacey & Lee, 1994; Dacey & Packer, 2003), selective death of one photoreceptor type could lead to neighboring responding and non-responding ganglion cells if only one of them is selectively targeted by the lost photoreceptor type. It has been shown that blue cones are more susceptible to hypoxic insult than other photoreceptors (Connolly et al, 2008). In future studies one could use

colored stimuli to test for selective sensitivity reduction or death of blue cones. Alternatively, the strong surgery light or the dim red light during preparation might have altered the adaptive state of some photoreceptors and thereby reduced their sensitivity. In addition, small responses may have been missed due to the high spontaneous activity in human retina and the relatively strict inclusion criteria during analysis.

Finally, the reasons for non-responding cells could also be of more biological nature: it is possible that the applied stimulus set was not optimal for many of the ganglion cell types in the human retina. When working with fresh tissue, a scientist has to choose a stimulus set that allows gaining as much information as possible in a short time. In addition, MEA recordings, in contrast to single-cell recordings, make local stimulation difficult. Testing for local edge detection or center-surround properties is thus limited. Another important aspect of retinal pre-processing is encoding of color. Here again, local stimulation might be more appropriate than full-field stimulation since chromatic cells often code for opponent colors in their receptive fields' center and surround (Dacey & Packer, 2003). Most of these issues could be reduced by using high-density MEAs. With such arrays, almost all cells in a small retinal patch can be recorded. Therefore, a single local stimulus will stimulate the center of many recordable cells in parallel. Local and colored stimulation during hdMEA recordings might thus reveal more responding cells and response types in future experiments.

Another set of stimuli which I have not used in my study were flickering checker-board stimuli since they are time consuming and drive responses rather weakly. However, one might exclude some stimuli in favor of incorporating a checker-board stimulus in future studies. Checker-board stimuli would reveal spatial and temporal aspects of the cells' receptive fields, which might help to identify at least some of the cell types within a given tissue, and which could facilitate comparison with other studies. In combination with hdMEAs, the mosaics of ganglion cells of the same type can be revealed, which would further improve localization and identification of cells. Finally, the number of non-responding cells is usually not stated in publications, it is therefore not possible to compare the obtained percentages of responding ganglion cells with previous studies.

CONCLUSIONS & OUTLOOK

In summary, I found that visual processing in human retina is richer than suggested by current primate retina literature. Human ganglion cells encode a broad range of speeds, spatial periods, and temporal frequencies. For the first time, I described ON-OFF type responses in the human retina. Further, the human retina might contain Y-like ganglion cells. In addition, I characterized in both human and pig retina, ganglion cells with distance-invariant encoding – a response behavior which so far has not been described.

In future studies, the stimulation paradigm should be adapted according to the results presented here and might include local, colored, and checker-board stimuli. Further, the inter-experimental variability might be reduced when using high-density MEAs. Recently, important advances in the handling and analysis of data from hdMEAs have been made. Such MEAs would increase the number of recorded cells while decreasing a bias for bigger or denser cells. Bulk electroporation of ganglion cells with calcium sensors and subsequent imaging of their responses could complement experiments with hdMEAs. With these techniques, additional response patterns might be revealed, especially encoding of local and complex stimuli. I present here almost exclusively population results. In particular by a dense MEA layout, one would record from more cells in a retinal patch and increase the chances to record from at least one representative of each ganglion cell type. Thus, individual cell types could be identified in follow-up studies.

When comparing human and mouse retinas, I found that visual processing differs between these two species in several aspects: human ganglion cells prefer higher speeds, are tuned to higher temporal frequencies, and occupy a different part of the spatio-temporal stimulus space. Another example is that ON-OFF responses in human retinas are dominated by their ON-input while in mouse the OFF-input is stronger. In general, these findings suggest that one should be careful when interpreting results from mouse models. The porcine retina might be a better model to study circuit details with the goal to translate the results to the peripheral human retina. For instance, “distance-invariant” cells and ganglion cells tuned to high temporal frequencies and wide spatial periods were only observed in human

and pig retina, but not in mouse retina. Also speed tuning properties were more similar between pig and human retina.

In the end, the scientific question will have to determine which model is the most appropriate. Identification of defined functional cell types in the human retina will benefit the direct comparison of human visual encoding capabilities with those of other animals. For future retinal studies, such knowledge will also facilitate the decision on the appropriate human or non-human model system for a given scientific question. If the goal is to characterize the impact of an amacrine cell type on retinal processing, a mouse or zebrafish model might be the best choice since genetic tools allow manipulating single cell types. However, if a disease affects very specific aspects of vision, one would want to study the involved ganglion cell types. Detailed knowledge on the human retinal encoding would allow not only to identify candidates among the ganglion cell types, but also to assess in which animal model this type can be further investigated.

For certain tasks, monkeys are the best model, for instance when researching foveal vision. However, the pig retina appears to share many similarities with the peripheral human retina. In addition, it is one of the favored models in medical research. The characterization of both the human and the pig retina would improve the ability to interpret and translate findings from ophthalmologic research in pigs and therefore strengthen the results. Some examples of this synergistic approach have been given in my own work (e.g. Publication 2). Effects of diseases and treatments in the pig model are often tested with rather global, low-resolution techniques. My own and future data on retinal processing in pigs will enable researchers to complement such studies with single cells analysis. For example, it would be desirable to measure the beneficial as well as side-effects of neuroprotectiva and other drugs not only by in-vitro electroretinograms, but also on the level of single ganglion cell types.

Finally, I have shown that ex-vivo human retina survives the donations conditions and can be used for in-vitro physiological studies. Besides a deeper knowledge on the retinal processes in humans, ex-vivo as well as post-mortem human retina is suitable for a variety of studies. This may include testing of short-term effects of pharmaceutical agents, or development, evaluation, and improvement of treatments against visual impairment such as optogenetics. Optogenes are used to

render any cell light-sensitive. It can thereby potentially restore vision in patients with photoreceptor degeneration. These tests can even be performed with post-mortem retinas since retinas which are not light sensitive are even advantageous for the evaluation of such optogenetic approaches. In general, working with human retina allows direct experimentation with the tissue of interest, is inexpensive, and could partially replace animal experiments. I hope that in the future more scientists and clinicians will collaborate to make use of this precious tissue which is otherwise normally discarded in clinical practice.

ABBREVIATIONS

F1, F2	–	first (F1) or second (F2) harmonic of Fourier transform
LGN, dLGN	–	(dorsal) lateral geniculate nucleus
MEA, hdMEA	–	multi-electrode array, (high-density)
Opa1	–	optic atrophy 1 (refers to heterozygote mouse model)
PC	–	principal component
R*	–	rod isomerizations

REFERENCES

Alavi MV, Bette S, Schimpf S, Schuettauf F, Schraermeyer U et al (2007) A splice site mutation in the murine Opa1 gene features pathology of autosomal dominant optic atrophy. Brain : a journal of neurology 130**:** 1029-1042

Allen AE, Storchi R, Martial FP, Petersen RS, Montemurro MA et al (2014) Melanopsin-driven light adaptation in mouse vision. Curr Biol 24**:** 2481-2490

Astrup J, Siesjo BK, Symon L (1981) Thresholds in cerebral ischemia - the ischemic penumbra. Stroke; a journal of cerebral circulation 12**:** 723-725

Baden T, Schubert T, Chang L, Wei T, Zaichuk M et al (2013) A tale of two retinal domains: near-optimal sampling of achromatic contrasts in natural scenes through asymmetric photoreceptor distribution. Neuron 80**:** 1206-1217

Barlow HB & Hill RM (1963) Selective sensitivity to direction of movement in ganglion cells of the rabbit retina. Science 139**:** 412-414

Barlow HB & Levick WR (1965) The mechanism of directionally selective units in rabbit's retina. J Physiol 178**:** 477-504

Berninger TA & Arden GB (1988) The pattern electroretinogram. Eye (Lond) 2 Suppl**:** S257-283

Bloomfield SA (1994) Orientation-sensitive amacrine and ganglion cells in the rabbit retina. J Neurophysiol 71**:** 1672-1691

Bloomfield SA & Dacheux RF (2001) Rod vision: pathways and processing in the mammalian retina. Prog Retin Eye Res 20**:** 351-384

Boycott BB & Wassle H (1991) Morphological Classification of Bipolar Cells of the Primate Retina. Eur J Neurosci 3**:** 1069-1088

Burkhalter A & Wang Q (2008) Interconnections of Visual Cortical Areas in the Mouse. In Eye, retina, and visual system of the mouse, Chalupa LM, Williams RW (eds). MIT Press

Calkins DJ, Schein SJ, Tsukamoto Y, Sterling P (1994) M and L cones in macaque fovea connect to midget ganglion cells by different numbers of excitatory synapses. Nature 371**:** 70-72

Calkins DJ & Sterling P (1999) Evidence that circuits for spatial and color vision segregate at the first retinal synapse. Neuron 24**:** 313-321

Carcieri SM, Jacobs AL, Nirenberg S (2003) Classification of retinal ganglion cells: a statistical approach. J Neurophysiol 90**:** 1704-1713

Chatterjee S & Callaway EM (2003) Parallel colour-opponent pathways to primary visual cortex. Nature 426**:** 668-671

Chichilnisky EJ & Baylor DA (1999) Receptive-field microstructure of blue-yellow ganglion cells in primate retina. Nat Neurosci 2**:** 889-893

Chichilnisky EJ & Kalmar RS (2002) Functional asymmetries in ON and OFF ganglion cells of primate retina. J Neurosci 22**:** 2737-2747

Connolly DM, Barbur JL, Hosking SL, Moorhead IR (2008) Mild hypoxia impairs chromatic sensitivity in the mesopic range. Invest Ophthalmol Vis Sci 49**:** 820-827

Crook JD, Manookin MB, Packer OS, Dacey DM (2011) Horizontal cell feedback without cone type-selective inhibition mediates "red-green" color opponency in midget ganglion cells of the primate retina. J Neurosci 31**:** 1762-1772

Crook JD, Packer OS, Dacey DM (2014) A synaptic signature for ON- and OFF-center parasol ganglion cells of the primate retina. Vis Neurosci 31**:** 57-84

Crook JD, Peterson BB, Packer OS, Robinson FR, Troy JB et al (2008) Y-cell receptive field and collicular projection of parasol ganglion cells in macaque monkey retina. J Neurosci 28**:** 11277-11291

Curcio CA (1990) Topography of ganglion cells in human retina. J Comp Neurol

Dacey DM (1993) The mosaic of midget ganglion cells in the human retina. J Neurosc

Dacey DM (2004) Origins of Perception: Retinal Ganglion Cell Diversity and the Creation of Paralle Visual Pathways. In The Cognitive Neurosicences, Gazzaniga MS (ed), pp 281-301. Cambridge, MA: MIT Press

Dacey DM & Brace S (1992) A coupled network for parasol but not midget ganglion cells in the primate retina. Vis Neurosci 9**:** 279-290

Dacey DM, Crook JD, Packer OS (2014) Distinct synaptic mechanisms create parallel S-ON and S-OFF color opponent pathways in the primate retina. Vis Neurosci 31**:** 139-151

Dacey DM & Lee BB (1994) The 'blue-on' opponent pathway in primate retina originates from a distinct bistratified ganglion cell type. Nature 367**:** 731-735

Dacey DM, Liao HW, Peterson BB, Robinson FR, Smith VC et al (2005) Melanopsin-expressing ganglion cells in primate retina signal colour and irradiance and project to the LGN. Nature 433**:** 749-754

Dacey DM & Packer OS (2003) Colour coding in the primate retina: diverse cell types and cone-specific circuitry. Curr Opin Neurobiol 13**:** 421-427

Dacey DM & Petersen MR (1992) Dendritic field size and morphology of midget and parasol ganglion cells of the human retina. Proc Natl Acad Sci U S A 89**:** 9666-9670

De Monasterio FM & Gouras P (1975) Functional properties of ganglion cells of the rhesus monkey retina. J Physiol 251**:** 167-195

Demb JB, Haarsma L, Freed MA, Sterling P (1999) Functional circuitry of the retinal ganglion cell's nonlinear receptive field. J Neurosci 19**:** 9756-9767

Devries SH & Baylor DA (1997) Mosaic arrangement of ganglion cell receptive fields in rabbit retina. J Neurophysiol 78**:** 2048-2060

Donnan GA & Davis SM (2008) Breaking the 3 h barrier for treatment of acute ischaemic stroke. The Lancet Neurology 7**:** 981-982

Drager UC & Olsen JF (1981) Ganglion cell distribution in the retina of the mouse. Invest Ophthalmol Vis Sci 20**:** 285-293

Drasdo N & Fowler CW (1974) Non-linear projection of the retinal image in a wide-angle schematic eye. Br J Ophthalmol 58**:** 709-714

Dunn FA, Lankheet MJ, Rieke F (2007) Light adaptation in cone vision involves switching between receptor and post-receptor sites. Nature 449**:** 603-606

Enroth-Cugell C, Lennie P, Shapley RM (1975) Surround contribution to light adaptation in cat retinal ganglion cells. J Physiol 247**:** 579-588

Enroth-Cugell C & Robson JG (1966) The contrast sensitivity of retinal ganglion cells of the cat. J Physiol 187**:** 517-552

Euler T, Haverkamp S, Schubert T, Baden T (2014) Retinal bipolar cells: elementary building blocks of vision. Nature reviews Neuroscience 15**:** 507-519

Faberowski N, Stefansson E, Davidson RC (1989) Local hypothermia protects the retina from ischemia. A quantitative study in the rat. Invest Ophthalmol Vis Sci 30**:** 2309-2313

Farrow K & Masland RH (2011) Physiological clustering of visual channels in the mouse retina. J Neurophysiol 105**:** 1516-1530

Farrow K, Teixeira M, Szikra T, Viney TJ, Balint K et al (2013) Ambient illumination toggles a neuronal circuit switch in the retina and visual perception at cone threshold. Neuron 78**:** 325-338

Field GD, Sher A, Gauthier JL, Greschner M, Shlens J et al (2007) Spatial properties and functional organization of small bistratified ganglion cells in primate retina. J Neurosci 27**:** 13261-13272

Fiscella M, Farrow K, Jones IL, Jackel D, Muller J et al (2012) Recording from defined populations of retinal ganglion cells using a high-density CMOS-integrated microelectrode array with real-time switchable electrode selection. J Neurosci Methods 211**:** 103-113

Frey U, Egert U, Heer F, Hafizovic S, Hierlemann A (2009) Microelectronic system for high-resolution mapping of extracellular electric fields applied to brain slices. Biosens Bioelectron 24**:** 2191-2198

Garcia M, Forster V, Hicks D, Vecino E (2002) Effects of muller glia on cell survival and neuritogenesis in adult porcine retina in vitro. Invest Ophthalmol Vis Sci 43**:** 3735-3743

Garcia M, Ruiz-Ederra J, Hernandez-Barbachano H, Vecino E (2005) Topography of pig retinal ganglion cells. J Comp Neurol 486**:** 361-372

Gauthier JL, Field GD, Sher A, Shlens J, Greschner M et al (2009) Uniform signal redundancy of parasol and midget ganglion cells in primate retina. J Neurosci 29**:** 4675-4680

Gerke Jr C, Hao Y, Wong F (1995) Topography of rods and cones in the retina of the domestic pig. HKMJ**:** 302-308

Goethe JW (1808-1810) Zur Farbenlehre.

Greschner M, Field GD, Li PH, Schiff ML, Gauthier JL et al (2014) A polyaxonal amacrine cell population in the primate retina. J Neurosci 34**:** 3597-3606

Grimes WN, Schwartz GW, Rieke F (2014) The synaptic and circuit mechanisms underlying a change in spatial encoding in the retina. Neuron 82**:** 460-473

Grubb MS & Thompson ID (2005) Visual response properties of burst and tonic firing in the mouse dorsal lateral geniculate nucleus. J Neurophysiol 93**:** 3224-3247

Harman A (2000) Neuronal density in the human retinal ganglion cell layer from 16-77 years. Anat Rec

Hashimoto T, Katai S, Saito Y, Kobayashi F, Goto T (2013) ON and OFF channels in human retinal ganglion cells. J Physiol 591**:** 327-337

Haverkamp S, Haeseleer F, Hendrickson A (2003) A comparison of immunocytochemical markers to identify bipolar cell types in human and monkey retina. Vis Neurosci 20**:** 589-600

Hayreh SS & Jonas JB (2000) Appearance of the optic disk and retinal nerve fiber layer in atherosclerosis and arterial hypertension: an experimental study in rhesus monkeys. Am J Ophthalmol 130**:** 91-96

Hayreh SS & Zimmerman MB (2005) Central retinal artery occlusion: visual outcome. Am J Ophthalmol 140**:** 376-391

Hebel R (1976) Distribution of retinal ganglion cells in five mammalian species (pig, sheep, ox, horse, dog). Anatomy and embryology 150**:** 45-51

Heiduschka P, Schnichels S, Fuhrmann N, Hofmeister S, Schraermeyer U et al (2010) Electrophysiological and histologic assessment of retinal ganglion cell fate in a mouse model for OPA1-associated autosomal dominant optic atrophy. Invest Ophthalmol Vis Sci 51**:** 1424-1431

Hendrickson A (2005) Organization of the Adult Primate Fovea. Macular Degeneration

Hendrickson A & Hicks D (2002) Distribution and density of medium- and short-wavelength selective cones in the domestic pig retina. Exp Eye Res 74**:** 435-444

Hofer H, Carroll J, Neitz J, Neitz M, Williams DR (2005) Organization of the human trichromatic cone mosaic. J Neurosci 25**:** 9669-9679

Huberman AD & Niell CM (2011) What can mice tell us about how vision works? Trends in neurosciences 34**:** 464-473

Iandiev I, Francke M, Makarov F, Hollborn M, Uhlmann S et al (2011) Effects of intravitreal bevacizumab (Avastin) on the porcine retina. Graefes Arch Clin Exp Ophthalmol

Januschowski K, Krupp C, Mueller S, Hofmann K, Schnichels S et al (2015) Investigating short-term toxicity of melphalan in a model of an isolated and superfused bovine retina. Graefes Arch Clin Exp Ophthalmol

Januschowski K, Mueller S, Dollinger R, Schnichels S, Hofmann J et al (2014) Investigating retinal toxicity of tempol in a model of isolated and perfused bovine retina. Graefes Arch Clin Exp Ophthalmol 252**:** 935-941

Jonas JB, Schneider U, Naumann GO (1992) Count and density of human retinal photoreceptors. Graefes Arch Clin Exp Ophthalmol 230**:** 505-510

Joo HR, Peterson BB, Haun TJ, Dacey DM (2011) Characterization of a novel large-field cone bipolar cell type in the primate retina: evidence for selective cone connections. Vis Neurosci 28**:** 29-37

Kamei M, Roth DB, Lewis H (2001) Macular translocation with chorioscleral outfolding: an experimental study. Am J Ophthalmol 132**:** 149-155

Kaplan E & Shapley RM (1986) The primate retina contains two types of ganglion cells, with high and low contrast sensitivity. Proc Natl Acad Sci U S A 83**:** 2755-2757

Kolb H http://webvision.med.utah.edu (31 August 2015)

Kolb H, Linberg KA, Fisher SK (1992) Neurons of the human retina: a Golgi study. J Comp Neurol 318**:** 147-187

Kolb H & Marshak D (2003) The midget pathways of the primate retina. Doc Ophthalmol 106**:** 67-81

Komaromy AM, Brooks DE, Kallberg ME, Dawson WW, Szel A et al (2003) Long-term effect of retinal ganglion cell axotomy on the histomorphometry of other cells in the porcine retina. Journal of glaucoma 12**:** 307-315

Kretschmann U, Bock M, Gockeln R, Zrenner E (2000) Clinical applications of multifocal electroretinography. Doc Ophthalmol 100**:** 99-113

Lafuente MP, Villegas-Perez MP, Selles-Navarro I, Mayor-Torroglosa S, Miralles de Imperial J et al (2002) Retinal ganglion cell death after acute retinal ischemia is an ongoing process whose severity and duration depends on the duration of the insult. Neuroscience 109**:** 157-168

Lagali PS, Balya D, Awatramani GB, Munch TA, Kim DS et al (2008) Light-activated channels targeted to ON bipolar cells restore visual function in retinal degeneration. Nat Neurosci 11**:** 667-675

Lai AK & Lo AC (2013) Animal models of diabetic retinopathy: summary and comparison. Journal of diabetes research 2013**:** 106594

Langrova H, Jagle H, Zrenner E, Kurtenbach A (2007) The multifocal pattern electroretinogram (mfPERG) and cone-isolating stimuli. Vis Neurosci 24**:** 805-816

Lee BB, Pokorny J, Smith VC, Kremers J (1994) Responses to pulses and sinusoids in macaque ganglion cells. Vision Res 34**:** 3081-3096

Lee LA, Deem S, Glenny RW, Townsend I, Moulding J et al (2008) Effects of anemia and hypotension on porcine optic nerve blood flow and oxygen delivery. Anesthesiology 108**:** 864-872

Lennie P (2000) Color vision: putting it together. Curr Biol 10**:** R589-591

Levick WR (1967) Receptive fields and trigger features of ganglion cells in the visual streak of the rabbits retina. J Physiol 188**:** 285-307

Li ZY, Wong F, Chang JH, Possin DE, Hao Y et al (1998) Rhodopsin transgenic pigs as a model for human retinitis pigmentosa. Invest Ophthalmol Vis Sci 39**:** 808-819

Lopez-Guajardo L, Benitez-Herreros J, Silva-Mato A (2011) Experimental model to evaluate mechanical closure resistance of sutureless vitrectomy sclerotomies using pig eyes. Invest Ophthalmol Vis Sci 52**:** 4080-4084

Luke M, Weiergraber M, Brand C, Siapich SA, Banat M et al (2005) The isolated perfused bovine retina--a sensitive tool for pharmacological research on retinal function. Brain research Brain research protocols 16**:** 27-36

Masland RH (2001) The fundamental plan of the retina. Nat Neurosci 4**:** 877-886

Masland RH & Martin PR (2007) The unsolved mystery of vision. Curr Biol 17**:** R577-582

Mataruga A, Kremmer E, Muller F (2007) Type 3a and type 3b OFF cone bipolar cells provide for the alternative rod pathway in the mouse retina. J Comp Neurol 502**:** 1123-1137

May PJ (2006) The mammalian superior colliculus: laminar structure and connections. Prog Brain Res 151**:** 321-378

Meister M, Pine J, Baylor DA (1994) Multi-neuronal signals from the retina: acquisition and analysis. J Neurosci Methods 51**:** 95-106

Middleton S (2010) Porcine ophthalmology. The Veterinary clinics of North America Food animal practice 26**:** 557-572

Munch TA, da Silveira RA, Siegert S, Viney TJ, Awatramani GB et al (2009) Approach sensitivity in the retina processed by a multifunctional neural circuit. Nat Neurosci 12**:** 1308-1316

Osborne NN, Casson RJ, Wood JP, Chidlow G, Graham M et al (2004) Retinal ischemia: mechanisms of damage and potential therapeutic strategies. Prog Retin Eye Res 23**:** 91-147

Pandarinath C, Victor JD, Nirenberg S (2010) Symmetry breakdown in the ON and OFF pathways of the retina at night: functional implications. J Neurosci 30**:** 10006-10014

Pearson JT & Kerschensteiner D (2015) Ambient illumination switches contrast preference of specific retinal processing streams. J Neurophysiol 114**:** 540-550

Peterson BB & Dacey DM (1998) Morphology of human retinal ganglion cells with intraretinal axon collaterals. Vis Neurosci 15**:** 377-387

Petrusca D, Grivich MI, Sher A, Field GD, Gauthier JL et al (2007) Identification and characterization of a Y-like primate retinal ganglion cell type. J Neurosci 27**:** 11019-11027

Petters RM, Alexander CA, Wells KD, Collins EB, Sommer JR et al (1997) Genetically engineered large animal model for studying cone photoreceptor survival and degeneration in retinitis pigmentosa. Nature biotechnology 15**:** 965-970

Polyak SL (1941) The Retina, Illinois: The University of Chicago.

Porciatti V, Pizzorusso T, Maffei L (1999) The visual physiology of the wild type mouse determined with pattern VEPs. Vision Res 39**:** 3071-3081

Priebe NJ, Lisberger SG, Movshon JA (2006) Tuning for spatiotemporal frequency and speed in directionally selective neurons of macaque striate cortex. J Neurosci 26**:** 2941-2950

Puthussery T, Percival KA, Venkataramani S, Gayet-Primo J, Grunert U et al (2014) Kainate receptors mediate synaptic input to transient and sustained OFF visual pathways in primate retina. J Neurosci 34**:** 7611-7621

Reid RC & Shapley RM (2002) Space and time maps of cone photoreceptor signals in macaque lateral geniculate nucleus. J Neurosci 22**:** 6158-6175

Rivlin-Etzion M, Wei W, Feller MB (2012) Visual stimulation reverses the directional preference of direction-selective retinal ganglion cells. Neuron 76**:** 518-525

Rodieck RW (1998) The First Steps in Seeing: Sinauer Assn.

Rodieck RW, Binmoeller KF, Dineen J (1985) Parasol and midget ganglion cells of the human retina. J Comp Neurol 233**:** 115-132

Roorda A & Williams DR (1999) The arrangement of the three cone classes in the living human eye. Nature 397**:** 520-522

Roska B & Meister M (2014) The Retina Dissects the Visual Scene into Distinct Features. In The New Visual Neurosciences, Werner JS, Chalupa LM (eds). Cambridge MA: MIT Press

Roska B & Werblin F (2001) Vertical interactions across ten parallel, stacked representations in the mammalian retina. Nature 410**:** 583-587

Roska B & Werblin F (2003) Rapid global shifts in natural scenes block spiking in specific ganglion cell types. Nat Neurosci 6**:** 600-608

Ross JW, Fernandez de Castro JP, Zhao J, Samuel M, Walters E et al (2012) Generation of an inbred miniature pig model of retinitis pigmentosa. Invest Ophthalmol Vis Sci 53**:** 501-507

Sanes JR & Masland RH (2015) The Types of Retinal Ganglion Cells: Current Status and Implications for Neuronal Classification. Annu Rev Neurosci 38**:** 221-246

Schild AM, Ristau T, Fricke J, Neugebauer A, Kirchhof B et al (2013) SDOCT thickness measurements of various retinal layers in patients with autosomal dominant optic atrophy due to OPA1 mutations. BioMed research international 2013**:** 121398

Schiller PH & Malpeli JG (1977) Properties and tectal projections of monkey retinal ganglion cells. J Neurophysiol 40**:** 428-445

Schmucker C & Schaeffel F (2004) In vivo biometry in the mouse eye with low coherence interferometry. Vision Res 44**:** 2445-2456

Segev R, Goodhouse J, Puchalla J, Berry MJ, 2nd (2004) Recording spikes from a large fraction of the ganglion cells in a retinal patch. Nat Neurosci 7**:** 1154-1161

Siegert S, Cabuy E, Scherf BG, Kohler H, Panda S et al (2012) Transcriptional code and disease map for adult retinal cell types. Nat Neurosci 15**:** 487-495, S481-482

Smith VC, Pokorny J, Lee BB, Dacey DM (2001) Primate horizontal cell dynamics: an analysis of sensitivity regulation in the outer retina. J Neurophysiol 85**:** 545-558

Solomon SG & Rosa MG (2014) A simpler primate brain: the visual system of the marmoset monkey. Frontiers in neural circuits 8**:** 96

Sorensen NF, Ejstrup R, Svahn TF, Sander B, Kiilgaard J et al (2011) The effect of subretinal viscoelastics on the porcine retinal function. Graefes Arch Clin Exp Ophthalmol

Sumbul U, Song S, McCulloch K, Becker M, Lin B et al (2014) A genetic and computational approach to structurally classify neuronal types. Nature communications 5**:** 3512

Tien NW, Pearson JT, Heller CR, Demas J, Kerschensteiner D (2015) Genetically Identified Suppressed-by-Contrast Retinal Ganglion Cells Reliably Signal Self-Generated Visual Stimuli. J Neurosci 35**:** 10815-10820

Tseng MT, Liu KN, Radtke NR (1990) Facilitated ERG recovery in taurine-treated bovine eyes, an ex vivo study. Brain research 509**:** 153-155

Umino Y, Solessio E, Barlow RB (2008) Speed, spatial, and temporal tuning of rod and cone vision in mouse. J Neurosci 28**:** 189-198

Vaney DI, Sivyer B, Taylor WR (2012) Direction selectivity in the retina: symmetry and asymmetry in structure and function. Nature reviews Neuroscience 13**:** 194-208

Veiga-Crespo P, del Rio P, Blindert M, Ueffing M, Hauck SM et al (2013) Phenotypic map of porcine retinal ganglion cells. Molecular vision 19**:** 904-916

Walter P, Luke C, Sickel W (1999) Antibiotics and light responses in superfused bovine retina. Cellular and molecular neurobiology 19**:** 87-92

Wang YV, Weick M, Demb JB (2011) Spectral and temporal sensitivity of cone-mediated responses in mouse retinal ganglion cells. J Neurosci 31**:** 7670-7681

Wassle H, Dacey DM, Haun T, Haverkamp S, Grunert U et al (2000) The mosaic of horizontal cells in the macaque monkey retina: with a comment on biplexiform ganglion cells. Vis Neurosci 17**:** 591-608

Wassle H, Grunert U, Martin PR, Boycott BB (1994) Immunocytochemical characterization and spatial distribution of midget bipolar cells in the macaque monkey retina. Vision Res 34**:** 561-579

Wassle H & Riemann HJ (1978) The mosaic of nerve cells in the mammalian retina. Proc R Soc Lond B Biol Sci 200**:** 441-461

Watanabe M & Rodieck RW (1989) Parasol and midget ganglion cells of the primate retina. J Comp Neurol 289**:** 434-454

Weinstein GW, Hobson RR, Baker FH (1971) Extracellular recordings from human retinal ganglion cells. Science 171**:** 1021-1022

Yamada ES, Bordt AS, Marshak DW (2005) Wide-field ganglion cells in macaque retinas. Vis Neurosci 22**:** 383-393

Yamada ES, Dmitrieva N, Keyser KT, Lindstrom JM, Hersh LB et al (2003) Synaptic connections of starburst amacrine cells and localization of acetylcholine receptors in primate retinas. J Comp Neurol 461**:** 76-90

Zeck GM & Masland RH (2007) Spike train signatures of retinal ganglion cell types. Eur J Neurosci 26**:** 367-380

Zeck GM, Xiao Q, Masland RH (2005) The spatial filtering properties of local edge detectors and brisk-sustained retinal ganglion cells. Eur J Neurosci 22**:** 2016-2026

Zhao Y, Yu B, Xiang YH, Han XJ, Xu Y et al (2013) Changes in retinal morphology, electroretinogram and visual behavior after transient global ischemia in adult rats. PLoS One 8**:** e65555

APPENDIX

Here I provide the *mean, median or percentages* for various parameters for each experiment in a given species (tables). The parameter *distribution* can be found for each retina or retinal piece from mouse (**Fig. X**), human (**Fig. XI**), and pig (**Fig. XII**). The figures contain the following information: Spatio-temporal tuning: number of cells for each obtained cluster (see Publication 1, Fig. 7). Drifting-grating and bar: average speed preference obtained from these two stimuli (see Publication 1, Fig. 9). Chirp: temporal tuning curves as in Publication 1, Fig. 8. Latency: mean latency calculated from contrast steps (see Publication 1, Fig. 10).

Overview mouse data

MOUSE	Polarity (contrast steps)				Polarity (white-noise)			Latency		Speed pref. (bar)		Speed pref. (DG)	
retina (animal)	# *cells*	ON (%)	OFF (%)	ON-OFF (%)	#	ON (%)	OFF (%)	#	ms	#	mm/s	#	mm/s
1 (1)	*37*	62	19	16	*29*	41	59	*37*	367	*32*	2.00	*24*	2.79
2 (2)	*13*	54	38	8	*14*	50	50	*13*	317	*14*	2.50	*9*	2.80
3 (3)	*25*	72	12	16	*24*	71	29	*25*	305	*24*	1.81	*24*	2.67
4 (4)	*30*	30	33	37	*32*	38	63	*30*	323	*38*	2.00	*27*	2.85
5 (5)	*27*	44	37	15	*22*	41	59	*27*	281	*26*	3.14	*21*	3.11
6 (6)	*40*	65	28	8	*35*	54	46	*40*	308	*39*	2.88	*38*	2.60
7 (6)	*26*	62	31	8	*17*	53	47	*26*	320	*22*	3.04	*21*	3.60
Total / Average	***198***	***56***	***27***	***16***	***173***	***49***	***51***	***198***	***319***	***195***	***2.27***	***164***	***2.98***

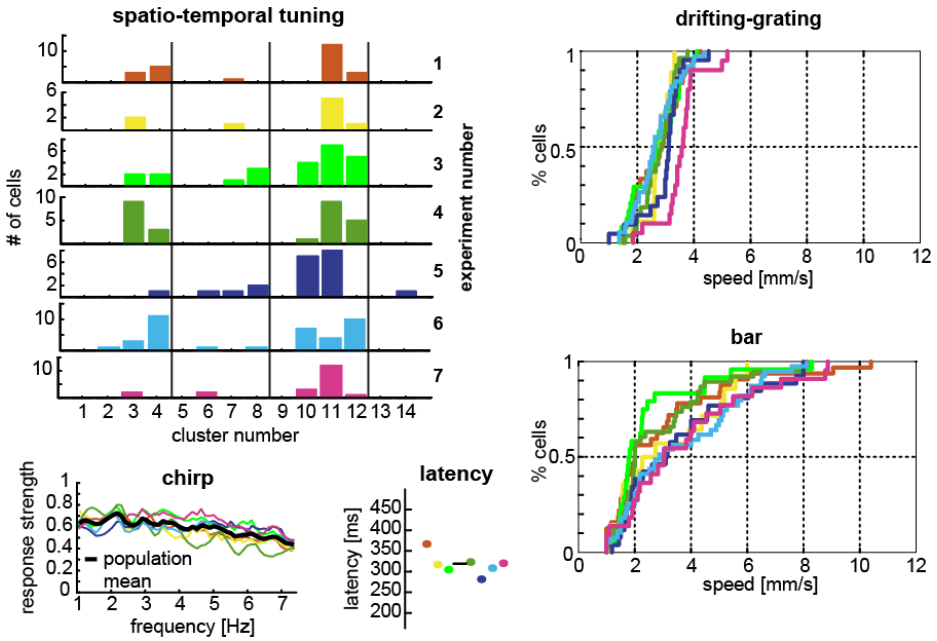

Fig. X: Overview single experiments with mouse retina. *Details in text.*

Overview human data

HUMAN	Polarity (contrast steps)				Polarity (white-noise)			Latency		Speed pref. (bar)		Speed pref. (DG)	
piece (retina)	# *cells*	ON (%)	OFF (%)	ON-OFF (%)	#	ON (%)	OFF (%)	#	ms	#	mm/s	#	mm/s
1 (1)	*15*	33	47	20	*5*	80	10	*15*	269	*2*	2.18	*18*	3.97
2 (2)	*15*	60	33	7	*26*	54	46	*15*	199	*4*	4.06	*29*	3.56
3 (3)	*0*				*0*			*0*		*0*		*5*	3.48
4 (4)	*1*	0	100	0	*5*	80	20	*1*	221			*15*	3.31
5 (5)	*8*	0	38	63	*24*	42	58	*8*	277	*9*	3.41	*22*	7.03
6 (6)	*1*	0	100	0	*3*	33	67	*1*	318			*20*	2.73
7 (6)	*2*	0	100	0	*3*	33	67	*2*	429	*1*	4.90	*18*	3.47
8 (6)	*0*				*0*			*0*		*0*		*15*	5.51
9 (7)	*22*	73	14	14	*17*	94	6	*22*	230	*5*	5.37	*39*	5.32
10 (7)	*15*	60	0	40	*28*	100		*15*	227	*6*	6.62	*29*	6.04
11 (7)	*5*	100	0	0	*5*	100		*5*	254			*18*	7.19
12 (8)	*20*	40	60	0	*4*	50	50	*20*	262			*20*	3.69
13 (8)	*6*	33	50	17	*1*	100	0	*6*	201			*3*	3.78
14 (9)	*8*	0	50	50	*11*	36	54	*8*	288	*10*	3.35	*13*	4.03
15 (10)	*3*	67	33	0	*0*			*3*	287			*29*	3.09
Total / Average	***121***	**46**	**35**	**19**	***132***	***68***	***32***	***121***	**242**	***37***	**3.78**	***293***	**3.99**

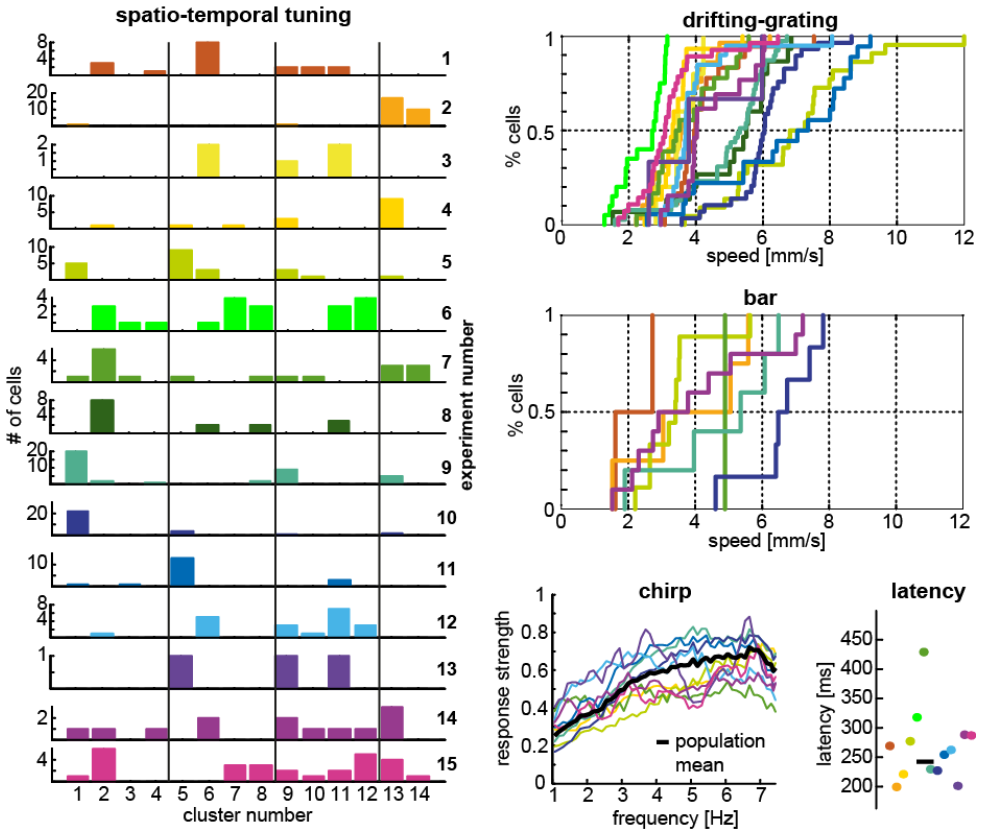

Fig. XI: Overview single experiments with human retina. *Details on page 59.*

Overview pig data

PIG	Polarity (contrast steps)				Polarity (white-noise)			Latency		Speed pref. (bar)		Speed pref. (DG)	
piece (retina, animal)	# *cells*	ON (%)	OFF (%)	ON-OFF (%)	#	ON (%)	OFF (%)	#	ms	#	mm/s	#	mm/s
1 (1, 1)	*17*	47	24	29	*20*	65	35	*17*	239	*8*	3.80	*16*	4.36
2 (2, 2)	*2*	100	0	0	*30*	40	60	*2*	198	*0*		*14*	6.07
3 (3, 2)	*4*	50	25	25	*33*	62	38	*4*	416	*0*		*22*	3.24
4 (4, 3)	*42*	38	10	52	*26*	85	15	*42*	205	*40*	1.85	*43*	3.67
5 (5, 4)	*8*	75	13	13	*21*	71	29	*8*	208	*15*	4.28	*27*	3.21
6 (6, 5)	*14*	57	7	36	*5*	80	20	*14*	232	*11*	6.20	*0*	
7 (7, 5)	*11*	82	0	18	*13*	38	62	*11*	229	*15*	2.63		
8 (6, 5)	*60*	28	8	63	*43*	67	33	*60*	228	*58*	4.14	*56*	3.47
Total / Average	***158***	**43**	**10**	**47**	***191***	**63**	**37**	***158***	**225**	***147***	**3.16**	***178***	**3.57**

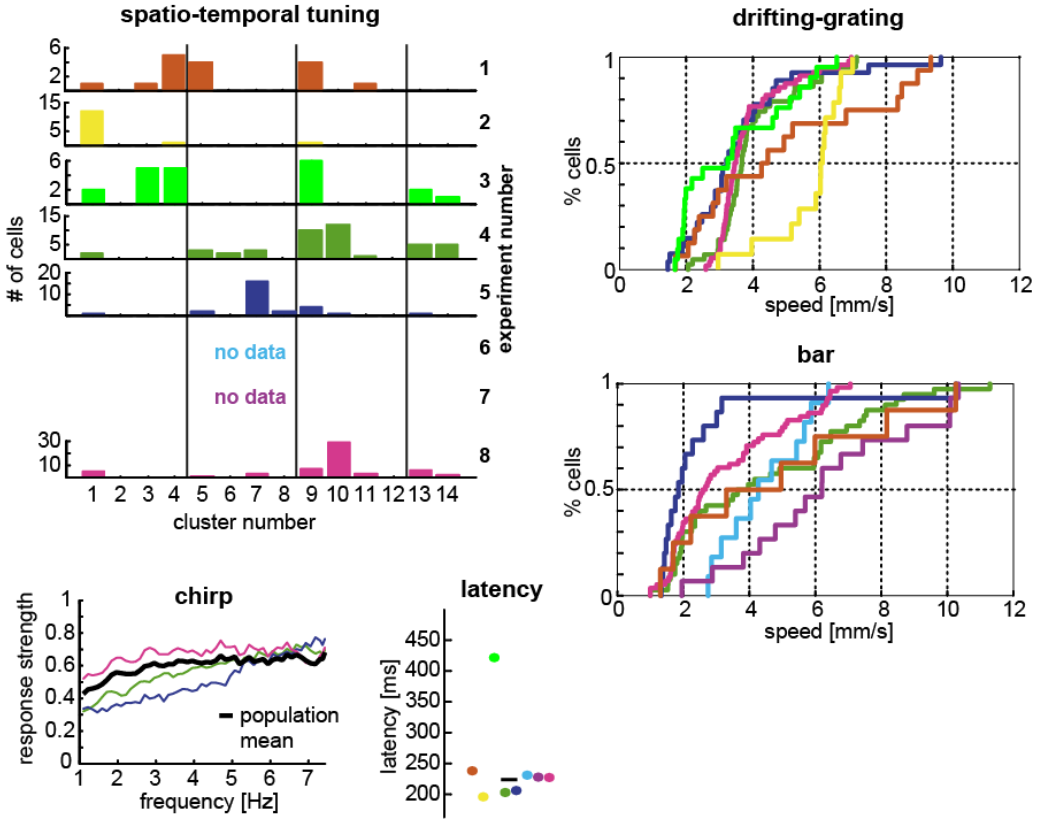

Fig. XII: Overview single experiments with pig retina. *Details on page 59.*

III. Publications and Statement of Contribution

Publication 1

Katja Reinhard & Thomas A Münch (submitted) Visual signal processing in human retina in comparison with pig and mouse retina.

Framework: This original research paper describes the functional properties of large populations of ganglion cells in the human retina. Further, visual encoding in human, pig, and mouse retina is compared.

My contribution: I established the collaboration with the Experimental Surgery Department in Tübingen to obtain pig eyes and was strongly involved in establishing human retina donations from the University Clinics Tübingen. I planned, performed, and analyzed the experiments with all three species. I wrote the manuscript and produced the figures.

Other contributions: TAM established collaborations for the donation process. He helped with planning of experiments, data analysis, and the manuscript.

Visual signal processing in human retina in comparison with pig and mouse retina

Katja Reinhard[1,2] *& Thomas A. Münch*[1,3]

[1]Retinal Circuits and Optogenetics, Centre for Integrative Neuroscience and Bernstein Center for Computational Neuroscience, University Tübingen, Germany

[2]Neuroscience Graduate School, University Tübingen, Germany

[3]Institute for Ophthalmic Research, University Tübingen, Germany

Abstract

Visual information processing in the retina has been characterized in many animal models. Surprisingly, similar systematic measurements in human retina have never been performed. Non-human primate research often focuses on a few most abundant ganglion cell types, which led to the impression that retinal image processing is less rich in primates than in other mammals. We studied visual information processing in human retina in-vitro and to compare it to data from two important animal models, mouse and pig.

We used multi-electrode arrays to record human ganglion cell responses in ex-vivo retinas from patients undergoing tumor-indicated enucleation. Out of 15 donations, 10 human retinas showed abundant light responses. Characterization of these light responses in 342 cells revealed ganglion cells of all three polarities (ON, OFF, and ON-OFF), of different transiency and with a diversity in spatio-temporal tuning. This indicates that retinal processing in humans is of similar richness as in other species. In general, ganglion cell responses in human and pig retina were similar, for instance in terms of spatial preferences or temporal frequency and speed tuning. Larger differences were found between human and mouse retinal light responses.

Our study provides a first systematic analysis of human retina function on the level of individual ganglion cells. Comparison to other species suggests that for the mid-peripheral human retina the pig might be a better model than mouse for certain scientific questions. We show that donated human retina is a valuable tool for in-vitro physiology experiments. Despite the less controlled conditions than in classical animal models, such tissue might be used to test short-term effects of neuroprotectiva, to improve the specificity of genetic tools, and for physiological evaluation of novel treatment methods for visual impairment, e.g. optogenetics.

Introduction

Vision is our most precious sense, experienced most vividly in everyday life. More than one third of the brain participates in the analysis of the visual input. Not a small part of visual processing is already performed at the very first stage of the visual system, in the retina. The retina is a highly structured part of the central nervous system, with the axons of the retinal ganglion cells forming the optic nerve. The retina transforms the incoming images into at least 30 parallel information channels which are embodied by the ganglion cells of a given type[1-3]: an information channel about color content[4], one about movement of small objects in a certain direction[5], one about approaching shadows[6], and so on.

Many different retinal ganglion cell types have been described and characterized in detail in animal models such as mouse[7], rabbit[8], rat[9], salamander[10], and also non-human primate[11,12]. In the primate retina we know at least 17 different ganglion cell types from morphological studies[12]. Nevertheless, scientists focus often on a few, most abundant functional ganglion cell types[13-19]. This led to the impression that on the level of the retina primate image processing may be less rich than in other mammals. These most abundant ganglion cell types comprise parasol and midget cells with each an ON-subtype (responding to light increment) and an OFF-subtype (responding to light decrement)[20,21]. Further, the color-opponent small bistratified ganglion cell is regularly found in electrophysiological recordings[12,15]. In contrast to the retinas of other species, one hardly finds descriptions of other ganglion cell types such as direction-selective cells, approach sensitive cells, or edge detectors.

Surprisingly, similar systematic measurements in human retina have never been performed. Functional examination of the human retina is mostly restricted to non-invasive in-patient measurements such as electroretinography (ERG), which has a relative low resolution. Literature search revealed only two electrophysiological studies on a cellular level with recordings of only few single cells in the human retina[22,23]. We thus aimed to study visual processing in the human retina on the level of individual cells and circuits.

Knowledge about the detailed functioning of the human retina would be desirable also in the context of retinal diseases. Retinal diseases, in particular blindness, have a big impact on individuals and the society. In recent years, research yielded some promising approaches to potentially healing blindness, including the application of neuroprotective substances to conserve as much of leftover visual capabilities as possible, and vision restoring methods, such as electrical retinal implants[24,25], optogenetics[26,27], and stem cell therapy[28]. What is common to all these approaches is the ultimate goal: to come as close as possible to full vision capabilities by interfering appropriately with the retina of the patient. These treatment options are mostly developed and tested in animal models. The lack of knowledge about the processing being performed by the human retina may impede further and faster progress in that field.

Human retina is difficult to obtain and in the past the available experimental methodology has limited the knowledge that could be gained from this rare tissue. In recent years, high-throughput

electrophysiological methods to record from many cells in parallel have been developed, and these multi-electrode arrays (MEAs) have been successfully applied in studies of various animal models[13,29-32]. In the present study, we have applied such MEA recordings to characterize ganglion cell function in human retina. We used retinas from patients which had to undergo enucleation of one eye due to a uveal melanoma. We characterized a variety of response parameters of several hundred ganglion cells, which is to our knowledge the first systematic recording of light responses from a large population of ganglion cells in human retina.

We compared the light responses from human retina ganglion cells also to retinal processing in two animal models, the mouse and the pig. The mouse is an important model in basic research, while porcine and bovine models are often used in medical research. Our characterization of mouse, pig, and human ganglion cell responses in identical settings and to the same stimulation paradigm revealed various similarities as well as differences between these three species, which have to be taken into consideration when translating findings from one species to another.

Material and Methods

Human retina donations

In order to characterize information processing in the retina**,** very fresh human tissue is necessary. We obtained such retina from patients of the University Eye Hospital in Tübingen, who had to undergo enucleation of one eye, usually to remove a tumor, and who provided informed consent to the use of the removed retina for scientific research purposes. The retina was protected from light during surgery if possible. An ischemia time of five minutes during the surgery (clamping of the optic nerve) was mandatory in order to prevent strong bleeding. The bulbous was cut in halves directly after enucleation, and the hemisphere without tumor was put immediately into CO_2-independent culture medium (Gibco), kept in darkness and transported to our lab. Under dim red light, we removed the vitreous and cut small mid-peripheral retinal pieces (~ 3x3 mm²). Within 23 months we obtained 15 ex-vivo donations (Table 1). 15 pieces from 10 retinas were used for experiments. All procedures were reviewed and approved by the Ethics Committee of the University Clinic Tübingen.

Pig retina

Pig retinas were obtained from five domestic pigs sacrificed during independent scientific studies at the Department of Experimental Surgery, University of Tübingen. Pigs were sedated and anesthetized by injection of atropine, azaperone, benzodiazepine (midazolam), and ketamine, and sacrificed with embutramide (T61). Before administration of embutramide, heparin was injected. After death was confirmed by a veterinarian, the eyes were enucleated immediately, the cornea, lens and vitreous removed, and the eyecup kept in CO_2-independent culture medium (Gibco) and protected from light. After transportation to the laboratory, pieces of ~ 3x3 mm² were cut from the visual streak. In total, 8 retinal pieces from 7 retinas were analyzed.

Mouse retina

Wild-type mice (C3H) were used for comparison with human and pig data.

Seven retinas from four mice of either sex were analyzed. For recordings, the whole retina was fixed on a filter paper with a central hole. Experiments were started under scotopic conditions and ambient luminance was increased in a step-wise fashion. Only data acquired after approximately half an hour at photopic light were used for analysis. Animal use was in accordance with German regulations and approved by the Regierungspräsidium Tübingen.

MEA recordings

To maximize the amount of information gained from the rare experiments with fresh human retina, we employed multi-electrode array (MEA) recordings that allow for measuring the activity of many neurons in parallel[33]. MEAs include a square or rectangular electrode arrangement that is brought in contact with the ganglion cells. This enables to measure the retinal output in response to light stimulation. MEA experiments have been described in detail elsewhere[34]. Briefly, the retinal pieces (pig and human) or whole retinas (mouse) were placed ganglion cell side-down on a MEA. We used perforated 60-electrode MEAs with 200 µm distance between the electrodes (60pMEA200/30iR-Ti-gr, Multichannel Systems, Reutlingen, Germany). Then, various light stimuli were focused onto the photoreceptors with a Digital Light Processing projector (Sharp PG-F212X-L, Sharp Corporation, Osaka, Japan or Acer K11, Acer, Taipeh, Taiwan), and we recorded the output of the retina (i.e. the action potentials of ganglion cells in response to the stimuli) at 25 kHz with a USB-MEA-system (USB-MEA1060, Multichannel Systems) or an MC-Card based MEA-system (MEA1060, Multichannel Systems). During the experiments, the retina was kept at 25°C and continuously superfused with Ringer solution (in mM: 110 NaCl, 2.5 KCl, 1 $CaCl_2$, 1.6 $MgCl_2$, 10 D-Glucose, and 22 $NaHCO_3$; ~270 mosm) or modified Ringer solution (in mM: 115 NaCl, 2.5 KCl, 2 $CaCl_2$, 1 $MgCl_2$, 15 D-Glucose, 1.3 $NaH_2PO_4*H_2O$, 0.5 L-Glutamine, and 25 $NaHCO_3$; ~285 mosm), both equilibrated with carbogen (95% O_2, 5% CO_2). All experiments were conducted with the retinal pigment epithelium removed.

Light stimulation

The stimulation intensity provided by our projectors spanned 3 log units of brightness between a black ('0') and white ('255') stimulus. The projector output was linearized, so that the grey ('128') background was midway between black and white, and the contrast step between black and grey and between grey and white had equal amplitude. Recordings were performed at photopic intensity levels (light intensity for day vision) with a mean illuminance of $8*10^4$ – $8*10^5$ rod isomerizations per rod per second. Each stimulus was repeated several times during recording sessions of two to six hours. A broad set of light stimuli was used and various parameters were calculated from the ganglion cells' responses (see below). We will discuss in this article nine parameters extracted from responses to the following six stimuli (see also Fig. 1):

Full-field contrast steps: Full-field contrast steps were applied for measurements of response polarity and latency (Fig. 1A). A single stimulus consisted of four transitions (grey → black → grey → white → grey) spanning the full projector intensity of 3 log units of brightness. Each contrast step lasted for 2 seconds.

White-noise flicker: We showed a full-field white-noise flicker stimulus with values between '0' (black) and '255' (white) drawn from a Gaussian distribution (Fig. 1B). Intervals of 20s high contrast (σ = 38.4) and 20s low contrast (σ = 7.68) were interleaved (each 5 times). The stimulus was updated every frame (60 Hz).

Sinusoidal drifting-gratings: Drifting sinusoidal grating stimuli with 24 different combinations of spatial periods and temporal frequencies (1, 2, 4, 8 Hz; 100, 200, 500, 1000, 2000, 4000 µm spatial period on the retina) were used for spatio-temporal analysis (Fig. 1C). The gratings were shown at full contrast ('0' to '255') and moved in one direction for 12 seconds.

Single bars at various velocities: We used single bars moving with different speed to test for speed preferences. A bar with 1000 µm extension in the movement direction (either black or white) was moved in front of a gray background in one direction with different speeds (1, 2, 4, 8, 16 mm/s) with a gap of 3 seconds before the next higher speed (Fig. 1D).

Chirp: Temporal tuning was also tested with a homogeneous chirp stimulus, i.e. full-field frequency modulation between black ('0) and white ('0'), according to: intensity = 128 + 128 sin (π (t^2 + t/10)), t is

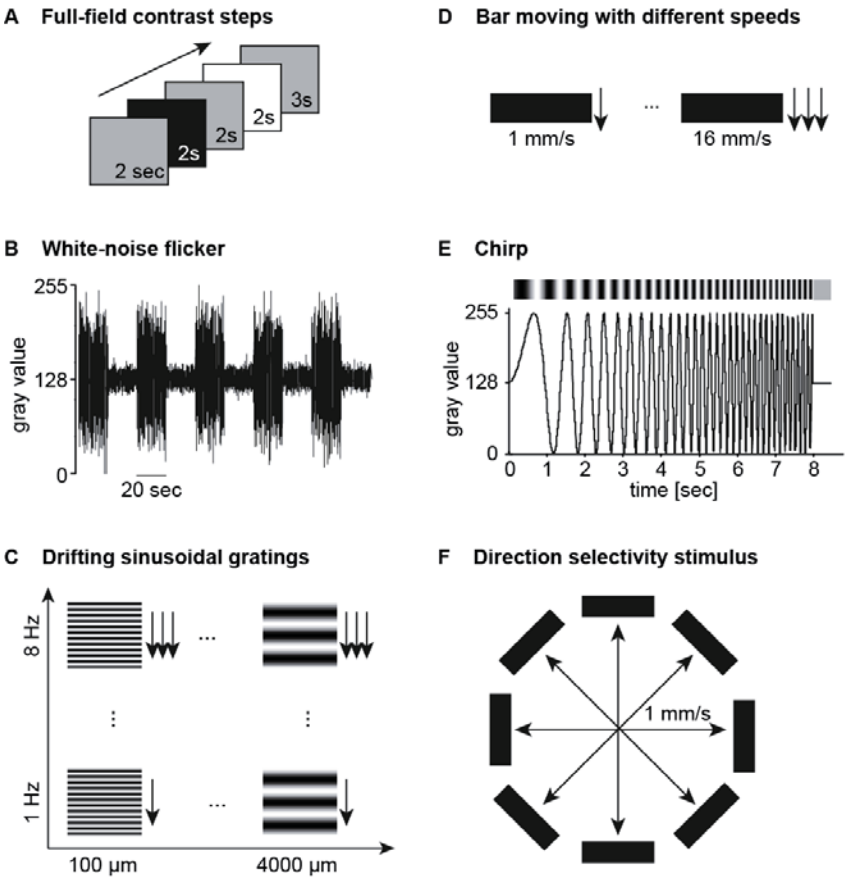

Figure 1: Light stimuli. *6 different light stimuli were applied. Details in text.*

given in seconds. The temporal frequency increased from 0.5 to 8 Hz over a time course of approximately 8 seconds (Fig. 1E).

Direction-selectivity: We used a single bar (black or white) moving in 8 directions to test for direction-selectivity. The bar of 1000 µm width was moved with 1 mm/s across the retina (Fig. 1F).

Spike extraction

Spike sorting (assignment of single action potentials to defined cells) was performed with an in-house Matlab (MathWorks, Massachusetts, USA) routine written by Alexandra Tikidji-Hamburyan. Different features of the action potentials, such as amplitude, width, or principal components, were calculated and projected onto 2-dimensional space in order to separate action potentials of different cells from each other and from noise. We determined light-responding cells by visual inspection of the activity to all stimuli. To calculate the firing rate, the spike train was convolved with a Gaussian and plotted against time. The sigma of the Gaussian varied for different analysis purposes; the value applied in each case is given in the description below. Only cells which could be sorted confidently were used for analysis (the same person performed spike sorting for all experiments and applied the identical quality judgement system). We applied cross-correlation analysis to detect recordings from the same cell on different electrodes (e.g. from cell body and axon). In this case, only one of the recorded units was used for the analysis.

Response parameter calculation

Illustrations for response parameter calculations are integrated in the corresponding figures in the Results section.

Latency: Full-field contrast steps were each presented for 2 seconds (Figs. 1A and 3B). A simple definition of the latency of a cell's response would be the time-to-peak of the response after stimulus onset. However, this can lead to very misleading latency values, for example in a sustained cell where the response rises quickly, but may reach the peak value very late. We instead used a more complex algorithm for determining the latency. First, the "first real response peak" was found automatically in the spike rate (sigma = 60 ms), defined as the maximum after stimulus onset, but only if it was bigger than the mean background firing rate (before the first contrast step) plus two standard deviations. If several local maxima fulfilled this condition, "real" peaks were identified by local minima between these peaks: these local minima had to drop below 75% of the higher peak (corrected for background firing). We manually excluded e.g. peaks resulting from very sustained responses to the previous contrast step. The first peak after stimulus onset which met all conditions was considered for further analysis. Second, latency was then defined as the time from stimulus onset to the time point when the firing rate reached 75% of the first real peak (see also Fig. 3A). For each cell, up to four latency values were obtained (one for each contrast step).

Polarity: Polarity was defined based on the results from latency calculations. Cells with non-zero latency values only for positive contrast steps were considered as ON-cells; OFF-cells had only detectable responses to negative contrasts, and for ON-OFF-cells latency values had been

obtained after both types of contrast steps (Figs. 1A and 3B).
As a second method, polarity was also determined with white-noise stimuli (Fig. 1B). We calculated the spike triggered average (STA) in response to full-field Gaussian white noise. The initial deflection of the STA indicates the dominant polarity of the cell (positive deflection → ON-polarity, negative deflection → OFF-polarity)[35]. The STAs of ON-OFF-cells are either flat in case of balanced ON and OFF drive or biased towards the stronger polarity. The obtained STAs were inspected manually and the initial deflection was taken as the cell's polarity (Fig. 3C).

Spatio-temporal tuning: Drifting sinusoidal grating stimuli were used for spatio-temporal analyses (Fig. 1C). Cells responding to at least one of the drifting-gratings were identified manually. For each cell and stimulus, the Fourier transform of the mean binary spike rate was calculated (Fig. 5A). The Fourier transform peak at the stimulus frequency (f) was then taken as the cell's response strength when it fulfilled 2 criteria: First, it had to be higher than the mean + 3 s.d. of the background Fourier amplitude (background was defined as the Fourier transform from 0.35 to f*3.5 Hz, excluding windows from -0.625 to +0.625 Hz around the frequencies f/2, f, 2f and 3f), and second, it had to be the highest peak in the range of f-f/2 to f+f/2. The F1 as well as F2 amplitudes (at frequencies f and 2*f, respectively) were then normalized for each cell for its maximal F1 amplitude across all 24 gratings and plotted as a heat-map (Fig. 4B).

Clustering based on spatio-temporal tuning. For clustering of ganglion cells into functional groups based on such grating-responses, we combined those "heat-maps" (normalized 24-vector of F1-values) of all cells and calculated the first five principle components. In addition, we determined the 2-dimenional center of mass of the heat map, yielding a total of 7 parameters for each cell. Based on those 7 parameters, a k-means-algorithm (Matlab routine; 10'000 replicates, 1000 iterations) was used for clustering of all responding cells from human, pig, and mouse retina. 14 clusters were identified as the optimal number based on silhouette calculations and comparison with other clustering algorithms (see Suppl. Fig. 1 and Suppl. Table 5). The silhouette of each data point is defined by the following formula: SI = (b-a) / max(a,b) with a = mean Euclidean distance to points within the same cluster, b = minimal Euclidean distance to points in all other clusters. Hence, the bigger the silhouette, the more similar a data point is to points in the same cluster and the more different to points in other clusters. The silhouette becomes negative if the data point is more similar to data points of other clusters.

Temporal tuning: Temporal tuning was tested with a chirp stimulus, i.e. frequency-modulated sinusoidal full-field change of contrast (Fig. 1E). We calculated the Fourier transform (FFT) of both, the stimulus and the response (mean binary spike train, frequency resolution of 0.125 Hz). Response strength was defined as: response = $\mathrm{norm}(FFT_{response})/FFT_{stimulus}$. Fluctuations which appear especially at low temporal frequencies due to the timing of ON- and OFF-responses were smoothed. Smoothing was achieved by averaging of the response strength with a moving average across a 3-datapoint-window (0.375 Hz) in steps of 1 data-point

(0.125 Hz). Population data is presented as median response strength across all responding cells of a given species (Fig. 8). We compared the temporal tuning of ganglion cells in different species by applying Wilcoxon ranksum tests to the response strength of all cells within a sliding 5-datapoint-window (0.625 Hz).
As a second method, temporal tuning was also calculated from the Fourier transform amplitudes obtained from the responses to drifting-grating stimuli (Fig. 1C). In order to directly compare these results to the results from the full-field chirp analysis, only drifting-gratings with the widest spatial periods (4000 µm) were considered. Data is presented as median response strength across all cells of a given species for each of the four tested temporal frequencies. For each frequency, statistical difference between species was assessed by Wilcoxon ranksum tests.

Speed preference: The data obtained from drifting gratings was also used for speed preference calculations. Note that the same speed can result from different gratings which combine different temporal frequency and spatial period (see iso-speed lines in Fig. $5A_1$). For speeds that can be realized in such different ways, we only took the value leading to the maximal response. Two types of analysis were used: first, the F1 amplitude of the Fourier transform was taken as response strength for each speed. We normalized the obtained values for each individual cell and plotted them as a speed tuning curve (Fig. $9A_1$). Second, to express this tuning curve as a single value, we took the center of mass of this tuning curve for each cell, which we call "average speed preference". Computationally, this was achieved by calculating the cumulative sum of the normalized Fourier transform amplitudes (starting from the slowest speed). The speed value for which 50% of the cumulative sum was reached was taken as the cells' average speed preference (see Fig. $9A_2$). For better comparison, we considered only speeds for analysis which were also tested with a single moving bar (see below, 1, 2, 4, 8, 16 mm/s); the maximal speed tested (32 mm/s) was excluded.
The same two analysis paradigms (tuning curve, average speed preference) were applied to peak response values obtained from responses to single, black or white, moving bars (Fig. 9B). A black or white bar was moved across the retina in one direction with various speeds. Similarly to the FFT amplitudes, the cumulative sum of peak responses for each speed (firing rate calculated with sigma 40) was computed. For each cell that responded to both, white and black bars, the higher preferred speed was taken for population analysis. Statistical significance was tested for all conditions with Wilcoxon ranksum tests.

Direction-selectivity: A single black or white bar moving in eight directions was presented to test for direction-selectivity. Peak responses for each direction (firing rate calculated with sigma 40) were extracted for each cell and their vector sum was calculated. We defined the direction-selectivity index (DSI) as the length of this vector. A cell was identified as direction-selective if the DSI exceeded 0.3 for both white and black bars (cells with and DSI > 0.3 for only one bar were counted if the response to the other bar was absent).

Results

Experimental paradigm

We extracted retinas from wild-type mice, domestic pigs, and human eyes from tumor patients. Ganglion cell responses were recorded in whole mouse retinas or pieces of pig and human retinas in response to various light stimuli. Due to the bright light conditions during human surgery, experiments were performed only under photopic conditions. Individual stimuli consisted of gray-scale images or movies spanning at most 3 log units of brightness. Most stimuli were shown during all experiments and were identical for all three species.

We obtained 15 human retina donations of variable quality, but included in the analysis only retinal pieces from which we could record light responses from at least 10 units. Several aspects can damage the tissue and prevent light responses: Depending on the surgery conditions, the ligated eye bulb might be exposed to longer times without blood flow or physiological solution. In this study we excluded all retinas exposed to >17 minutes of ischemia (see Table 1 for an overview of the donated tissue). Further, in tissue from elderly patients, the separation of vitreous, retina, and pigment epithelium can be difficult. While attached pigment epithelium did not influence our recordings, the remaining vitreous impaired the contact of the recording electrodes to the ganglion cells. Finally, in the case of very big tumors, the retina might have been detached from the pigment epithelium for a longer period of time prior to the enucleation, which harms

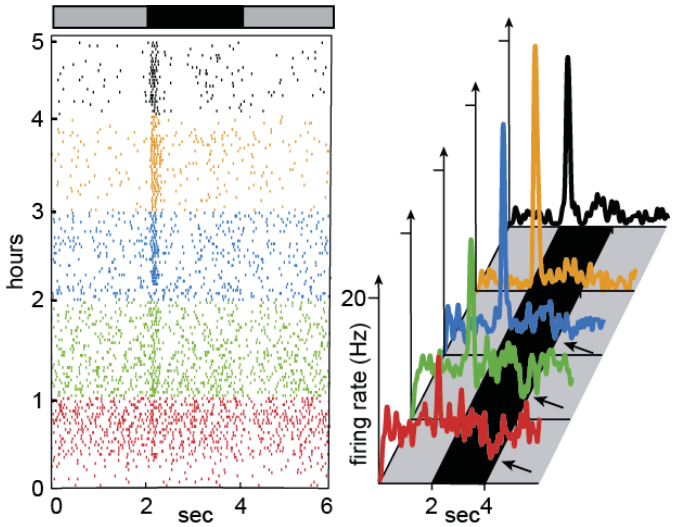

Figure 2: Stable responses in human retinas. *Human ganglion cell responses could be recorded stably for the maximally tested time of 5 hours. Raster plot (left, each tick represents a spike) and average spike rate (right) of one example ganglion cell. Different colors represent consecutive 1-hour-segments of the experiment. The transient OFF-response is visible throughout the experiment and also the ON-inhibition (arrows) can be detected whenever there is sufficient background firing rate.*

especially the light sensitive photoreceptors. Overall, we analyzed 920 cells from n=15 pieces cut from 10 human retinas, 306 cells from n=8 pieces cut from 6 pig retinas, and 224 cells from n=7 mouse retinas. 342 out of 920 human ganglion cells, 273 out of 306 pig cells, and 213 out of 224 mouse ganglion cells responded to at least one of the tested light stimuli (see Suppl. Table 1 for overview). MEA recordings were stable for many hours, and we were able to record stable light responses also in human retina (Fig. 2).

Table 1: Human retinas used for this study. *15 ex-vivo donations were obtained. The table gives information about the donated retina (left/right eye, part of the retina without tumor), sex, age, known medical history of the donors, surgery conditions (the ischemia time, i.e. time without oxygen and nutrient supply, and whether a dark lens was put on the donors eye during surgery). During preparation, the retina would sometimes roll up immediately after vitrectomy (rolling) or the vitreous was sticking strongly to the retina (sticky). The last two columns indicate whether any light responses were detected in our recordings and how many retinal pieces were used per donation for the final analysis. Light gray rows: retinas with some light responses but not used for analysis. Dark gray rows: no detectable light responses. In bold we give potential reasons for low quality. Ventr. = ventral, dors. = dorsal, temp. = temporal, m = male, f = female, radiation = radiation of the tumor-bearing eye, detachment = retinal detachment, n = no, y = yes. *preparation had been performed by another group in the course of a different study.*

donor	right/ left	ventr. dors. temp. nasal	sex	age (y)	notes	surgery conditions		prep.	any light resp.	# analyzed pieces
						ischemia (min)	dark lens			
1	r	vt	m	72	diabetic	7	n	easy	y	1
2	r	dn	f	49	***radiation***	7	n		n	-
3	l	dn	f	72	diabetic	7	n	rolling	y	1
4	l	n	f	69	detachment	17	n	easy	y	1
5	l	t	m	53		7	n	sticky	y	1
6*			m	75	sinus tumor	***18***	n		n	-
7	r	dn	m	89		***25***	n	sticky	y	-
8	l	vt	f	42		***20***	n	sticky	n	-
9	r	t	f	83		10	n	sticky	y	1
10	l	t	f	49		10	n	sticky	y	3
11	l	vn	f	60		7	y	sticky	y	3
12	l	dt	f	74	macula edema	7	y	easy	y	2
13	l	v	m	74		7	y	***very sticky***	y	-
14	l	n	f	79	radiation 10y ago	8	n	easy	y	1
15	l	n	m	67	detachment	10	n	easy	y	1

Visual processing in human retina is rich

The responses of 342 human ganglion cells were characterized with a set of light stimuli to obtain response parameters such as response polarity, latency, spatio-temporal preferences, temporal tuning, speed preferences, and direction-selectivity. For details on analysis see Methods and the corresponding paragraphs below. Ganglion cell characterization in human retina revealed a rich variety of response properties. The diversity of response properties suggests that processing in the human retina is of similar complexity as in other species. In the following paragraphs, we will discuss the diverse responses to visual stimulation found in the human retina.

ON, OFF, and ON-OFF responses in the human retina

In most species studied so far, ganglion cells with three types of response polarities have been found: ON-responses (responses to light increments), OFF-responses (to light decrements), and ON-OFF-responses (to both light increments and decrements). We used two definitions for response polarity: first, response polarity was defined based on the occurrence of a response within 550 ms after a full-field contrast step (Fig. 3A). Based on these analyses, we found all three types of responses in human retina as well (Fig. 3B). Around 46% of all responding cells had ON-responses (Fig. $3B_{1\text{-}2}$, 3D), 30% had OFF-responses (Fig. $3B_{3\text{-}4}$, 3D), and around 20% showed ON-OFF responses (Fig. $3B_5$, 3D). To date, ganglion cells with ON-OFF responses have not been explicitly shown to exist in human retina. On a morphological level, four bistratified ganglion cell types have been described in the primate retina, which account for approximately 15% of all ganglion cells[36]. Whether our ON-OFF cells correspond to such bistratified cells remains to be determined. Also note that we have demonstrated previously that short-latency ON-OFF responses also occur in monostratified ganglion cells[37].

As a second definition for polarity we used the first deflection in the spike-triggered average (STA) calculated from responses to full-field Gaussian white-noise flicker. Analysis based on STA calculation only allows separation into ON- or OFF-dominated responses. Cells with ON-OFF responses have, depending on the relative strengths of the two inputs, an ON-STA, an OFF-STA or a flat average. Similarly to the full-field contrast step responses, 32% of all ganglion cells with a non-flat STA showed a negative first deflection, thus were classified as OFF-cells (Fig. 3D, for an example see Fig. 3C). In human retina, the majority of cells with ON-OFF responses to contrast steps had an ON-dominated STA. Thus, the 68% of cells with ON-STAs comprise cells with pure short-latency (< 550 ms, Fig. $3A_3$) ON- as well as ON-OFF-responses to contrast steps (Fig 3D).

Response transiency

Another aspect which can be determined from full-field contrast steps is response transiency. Human ganglion cells tended to have a high background firing rate and comparably small responses (e.g. Fig. $3B_1$, B_3, B_5). This makes calculation of transiency properties unreliable and unstable. Thus, we did not analyze response transiency systematically. However, as shown in Fig. 3B, we found ganglion human ganglion cells with very sharp transient responses (Fig. $3B_3$) as well

as cells with sustained responses lasting for the whole 2 seconds of stimulation (Fig. 3B$_4$).

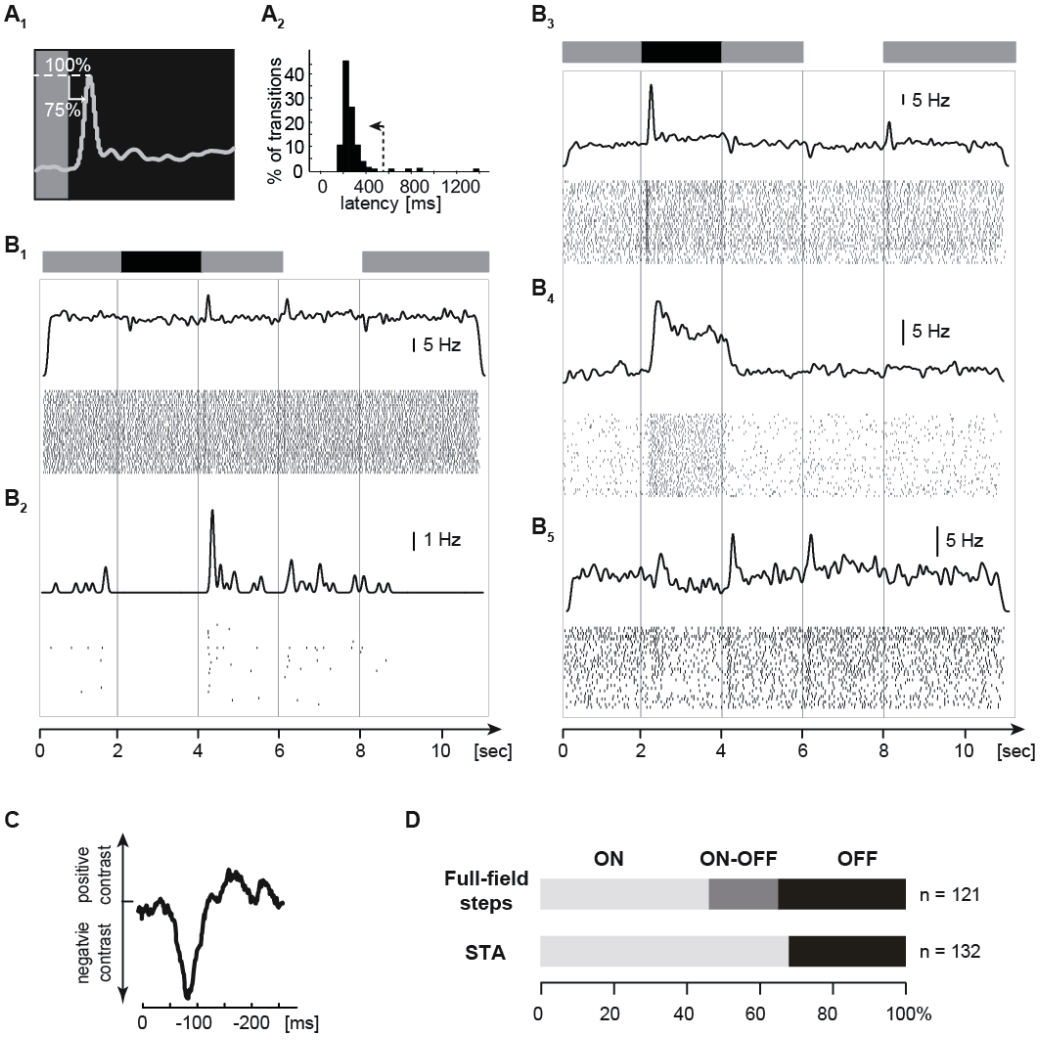

Figure 3: Human ganglion cells respond with all polarities and a broad range of response transiency. *A$_1$) Latency was defined as the time when 75% of the peak response was reached. A$_2$) Distribution of latencies in human ganglion cells. Responses with latencies ≤ 550 ms (arrow) were used for polarity calculation. B) Five example responses to full-field contrast steps (stimulus shown on top). These examples include: ON-cells (B$_{1-2}$), OFF-cells (B$_{3-4}$), ON-OFF-cells (B$_5$), cells with high background activity (B$_1$, B$_3$) and sparse activity (B$_2$), very transient cells (B$_3$) and cells with sustained responses (B$_4$). C) Example OFF-STA calculated from responses to white noise. D) Distribution ON, ON-OFF and OFF cells based on classification of their responses to full-field contrast steps (top) or STAs (bottom).*

Variety of spatio-temporal tuning in human retina

We used 24 different sinusoidal drifting gratings with various spatial periods (100, 200, 500, 1000, 2000, 4000 µm on the retina; 1 mm on the human retina corresponds to 3.47° visual angle[38]) and with different temporal frequencies (1, 2, 4, 8 Hz) to test for spatio-temporal tuning (Fig. 4). Temporal frequency tuning can arise from specificities at almost any step of retinal processing from horizontal feedback in the outer retina to neurotransmitter release in the inner retina. It is thus informative about the specific kinetics in a given circuit. Spatial tuning allows for an approximation of the receptive field size of ganglion cells.

In our analysis, cells which responded to at least one of the drifting-grating stimuli were identified manually and the Fourier transform of their response was calculated for each grating stimulus. The amplitude of the Fourier transform at the stimulus frequency was taken as the cell's response strength (Fig. 4A). For each cell we normalized its Fourier amplitudes to its

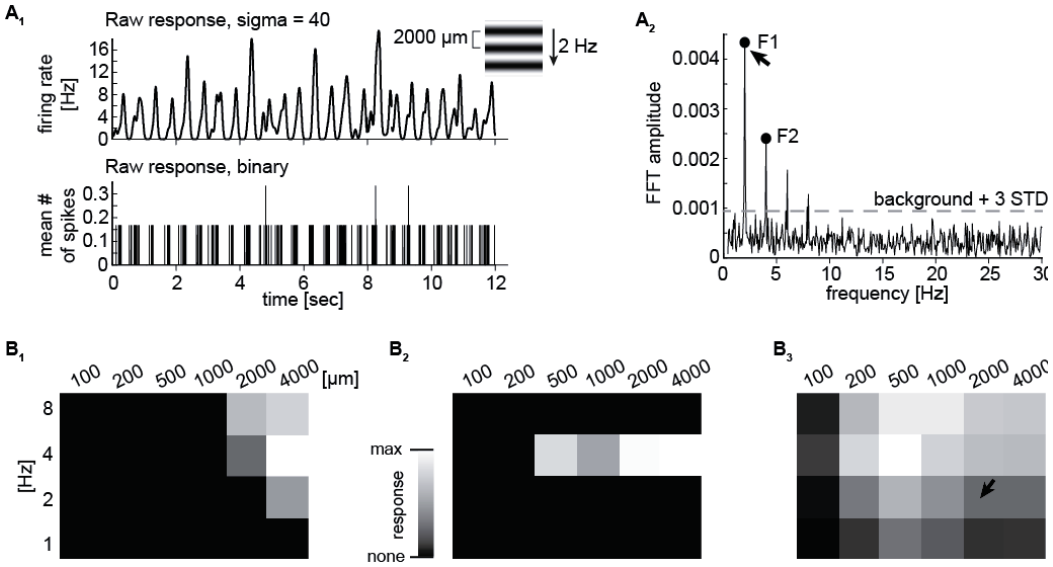

Figure 4: A variety of spatio-temporal tuning properties could be detected in human retina. *A_1) Spatio-temporal tuning was tested with sinusoidal drifting gratings. An example response to one of the grating stimuli is shown. For better visibility, the response was calculated by convolving a Gaussian (sigma = 40 ms) to the spike train (top). For analysis, the mean binary spike train has been used (bottom). A_2) Fourier transform (FFT) of the response in A_1. The amplitude of the Fourier transform at the stimulation frequency (F1) was defined as the cell's response strength. Second harmonic responses (F2) have been used for identification of Y-like cells. B) Heat-maps of normalized Fourier amplitudes of 3 example cells. For each drifting-grating stimulus the F1 response (arrow in A_2) was taken and normalized to the maximal amplitude for each cell. The three example cells showed spatial tuning (B_1), temporal tuning (B_2), or responded to a broad range of frequencies and spatial periods (B_3). Arrow in B_3: Example response from A.*

maximal response across all 24 grating stimuli. We found a variety of spatio-temporal tunings in human retina: some ganglion cells were tuned to specific spatial periods (e.g. Fig. $4B_1$) or temporal frequencies (e.g. Fig. $4B_2$). Other cells showed broader tuning to a range of spatial and temporal frequencies (e.g. Fig. $4B_3$). More systematic analysis is provided below when human data is compared to mouse and pig retina.

Variety of speed preference in human retina

Some of the 24 drifting-grating stimuli moved at the same retinal speed (iso-speed lines in Fig. $5A_1$). We took the maximal response to equal-speed drifting-gratings and plotted a response strength curve. The obtained curve was then normalized to its maximum for each cell (Fig. $5A_1$ "normalized peak"). In order to visualize the variety of speed encoding in human retina, we expressed these curves in a single "average speed preference" value which was defined as the center of mass of

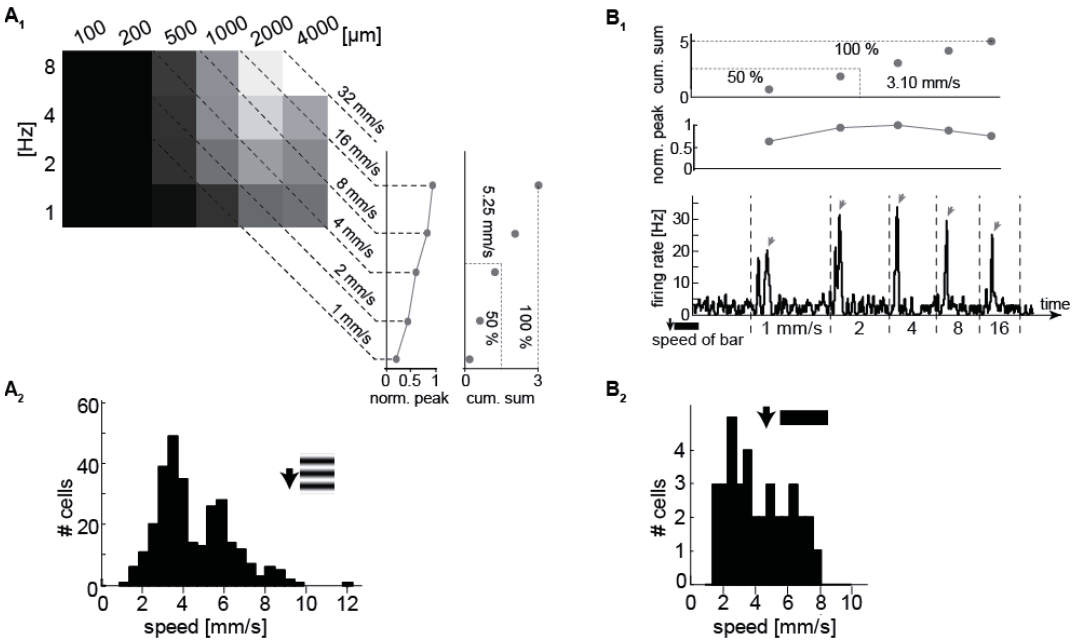

Figure 5: Diversity in average speed preference of human ganglion cells. *A_1) We calculated a speed tuning curve from responses to drifting gratings (normalized FFT amplitudes). The maximal value for each speed (lines indicate iso-speed) was taken for analysis. This curve was expressed in a single value, the "average preferred speed", which was defined as the speed for which 50% of the cumulative response (starting from the slowest) was reached (right). A_2) Distribution of average preferred speeds based on drifting-grating stimuli across all responding cells. B_1) Identical analysis was performed with peak responses to a single bar moving with different speeds (same cell as in A_1). B_2) Average preferred speeds tested with single moving bar.*

the curve (Fig. $5A_1$ "cum. sum"). This average speed preference covered a range from 2 to 12 mm/s in different cells (Fig. $5A_2$).

In addition, we tested speed encoding with a single black or white moving bar. The peak response to each speed was extracted (Fig. $5B_1$). After the same analysis as for drifting-gratings, the average speed preference in response to single bars varied between 2 and 8 mm/s (Fig. $5B_2$). For cells that responded to both black and white bars, we selected the higher average speed for population analysis. On average, speed preference was higher in response to drifting-grating (median: 3.99 mm/s) than to moving bars (median: 3.78 mm/s). The extended range towards higher speeds and the higher mean preferred speed might be due to more robust responses in the case of a repetitive drifting-grating compared to a single bar stimulus.

Highly non-linear cells

In addition to characterization of the midget, parasol and small bistratified cells, previous studies have set out to find analogs to the cat Y-cell[39]. The Y-cell is characterized by its very non-linear behavior. For instance, when stimulated with sinusoidal gratings, the second harmonic response (F2) of these cells can be higher than the first harmonic (F1) for a range of spatial periods.

29 cells (8.5 % of responding cells) in our human recordings had similar non-linear properties with F2/F1-ratios > 1 for drifting-grating stimuli of 500-2000 µm width (e.g. a response to a 500 µm grating in Fig. $6A_1$) and with spatial tuning (F1) to high spatial periods. These Y-like cells had various non-linear properties. A few cells, like the example in Fig. 6A, showed a similar F2-tuning curve as it had been shown on a population level for some macaque Y-like cells, termed Upsilon cells[40], namely with high F2-amplitudes only for a certain range of spatial periods but strong F1-responses for very wide stimuli (compare responses in Fig. $6A_1$ and A_2 and the tuning curve in Fig. $6A_3$). In other human ganglion cells in our data set the F2-curve exceeded the first harmonic curve only for one specific drifting-grating (Fig. 6B). We further found cells where the second harmonic response remained strong also for higher spatial periods than 2000 µm (Fig. 6C) and ganglion cells where the F2-response was even stronger than the F1-response for drifting-gratings with 4000 µm spatial period (Fig. 6D).

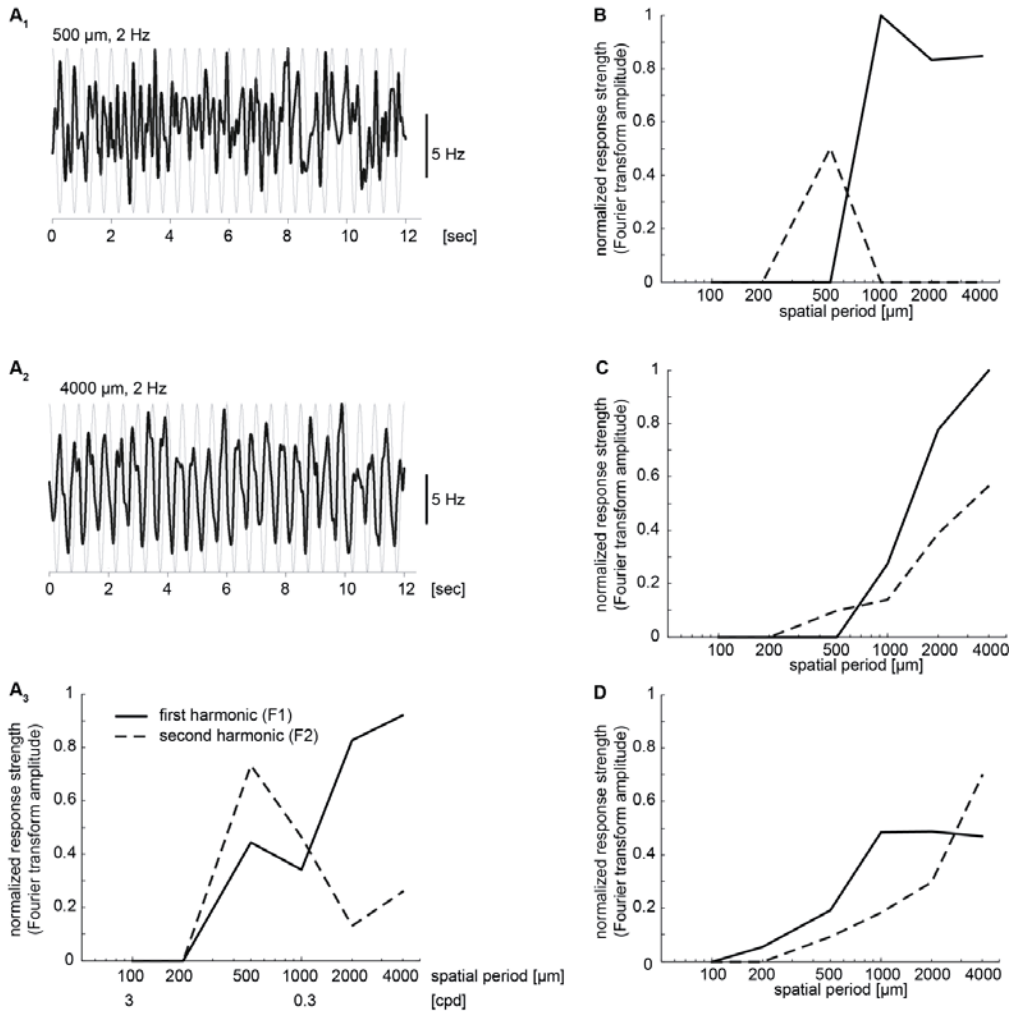

Figure 6: Candidates for Y-like ganglion cells in human retina. *A) Example cell with similar response profile as Y-like cells described in macaque retina[40]. A_1) Firing rate in response to 500 µm grating with 2 Hz temporal frequency (stimulus in gray). A strong second harmonic (F2) component is visible. A_2) The same cell responding with an almost pure F1 response to a 4000 µm grating with the same 2 Hz temporal frequency. A_3) F1 and F2 response of the same cell across spatial periods, normalized to the strongest observed F1 response. Each spatial period has been presented with four different temporal frequencies (1, 2, 4, 8 Hz). For each spatial period we plotted the maximal second harmonics (across temporal frequencies) and the corresponding first harmonic amplitudes at the same frequency. B) Cell with F2-responses only for 500 µm gratings. C) Cell with continuously increasing F2-response for wide stimuli. D) Cell with strongest F2-response for very wide stimuli.*

Similarities and differences in retinal encoding in human, pig, and mouse

Given the lack of human retinal data so far, it is unclear how results from retinal research with animal models can be translated to the human retina. To start approaching this question, we have characterized ganglion cell responses in pig and mouse retina with the same parameters as used for human retina. In general, the properties of pig and human ganglion cells tended to be more similar, while we found more differences between human and mouse ganglion cells.

Spatio-temporal tuning differs between species

Striking differences become apparent already when comparing the average spatio-temporal tuning taken across all responding ganglion cells in a given species (Fig. 7A): human ganglion cells are tuned to higher temporal frequencies than mouse ganglion cells, with overall maximal response strength for stimuli with temporal frequencies around 4 Hz (human) and 1 Hz (mouse). Similar to human retina, pig ganglion cells preferred higher temporal frequencies, but the tuning was broader than in human.

We further characterized the differences between the three species by grouping ganglion cells into functionally similar clusters. Clustering was performed based on 7 response parameters, namely five principal components of the 24 response amplitudes obtained from drifting-grating stimuli (see also Fig. 4) as well as the two coordinates of their center of mass. These 7 parameters characterizing the spatio-temporal tuning of each cell were clustered in Matlab by the k-means algorithm as described in the Methods section. Silhouette measurements were used to select the optimal number of clusters. The mean silhouette crossed the 0.75-border for 14 clusters (see Methods and Suppl. Fig. 1). The choice of 14 clusters was confirmed with 3 additional clustering algorithms and several quality indices (Suppl. Fig. 1 and Suppl. Table 5).

Clustering was performed with all ganglion cells of all species in our data set combined. The rational for this approach is that unique properties of ganglion cells in a species would result in a cluster that only contains cells of that species. Alternatively, properties that are shared by the species would result in mixed clusters. Fig. 7B summarizes the resulting cluster distribution for each species. Overall, in 10 of the 14 clusters we found at least 10 human ganglion cells (exceptions: clusters 3, 4, 7, 10). Pig ganglion cells were grouped into 8, and mouse cells only into 5 clusters. Remarkably, the clusters can be grouped into four categories with related properties: a group of 4 temporally tuned clusters (Fig. 7C), a group of 4 spatially tuned clusters (Fig. 7D), 4 broadly tuned clusters (Fig. 7E), and 2 clusters with "anti-speed" behavior (Fig. 7F). These are discussed in more detail below.

Almost two thirds of mouse ganglion cells were found in clusters 10 to 12 containing cells that respond well to a broader range of temporal frequencies and spatial periods (Fig. 7E). Cells that responded to a broad range of spatio-temporal stimuli could also be found in human and pig retina; however, in different clusters. Pig ganglion cells were grouped into cluster 9 and 10 (Fig. 7E) since they responded better to higher temporal frequencies. Human ganglion cells were in general more stringently tuned and could thus be found

in clusters 9 and 11 within the broad group (Fig. 7E).

Surprisingly, spatially tuned cells were almost absent in mouse retina, but abundant in human and pig retina (Fig. 7D). Human ganglion cells preferred wider stimuli (cluster 5 and 6), while pig ganglion cells were predominantly grouped into cluster 7 which contains cells with tuning to narrower spatial periods (Fig. 7D).

The remaining mouse ganglion cells were tuned to slow temporal frequencies (cluster 3 and 4, Fig. 7C). In contrast to mouse retina, we found human and pig ganglion cells mostly in cluster 1 which contains cells with tuning to high temporal frequencies. Interestingly, ganglion cells with very specific tuning to stimulation at 4 Hz could be detected only in human retina (cluster 2 in Fig. 7C).

Finally, we detected an "anti-speed" behavior in a significant number of ganglion cells in human and pig, but not in mouse (clusters 13 and 14 in Fig. 7F. Note that the orientation of the Gaussian fits of these "anti-speed" clusters is orthogonal to the iso-speed lines in Fig. $5A_1$). Cells tuned to specific speeds independently of spatial periods and temporal frequencies have been described e.g. in the visual cortex of primates[41]. The cells in cluster 13 and 14 showed an opposing tendency: they responded well to both, high spatial period shown with high temporal frequency and narrow stimuli with low temporal frequencies. We called these ganglion cells "distance-invariant" cells: Imagine a zebra running past an observer, producing a "drifting grating" on the observer's retina. When the observer is close to the zebra, it would appear large (high spatial period) and would move past the observer with an apparent high speed (high temporal frequency). When the observer is far away, the zebra would appear smaller and slower. The distance-invariant cells are tuned to respond well in both conditions.

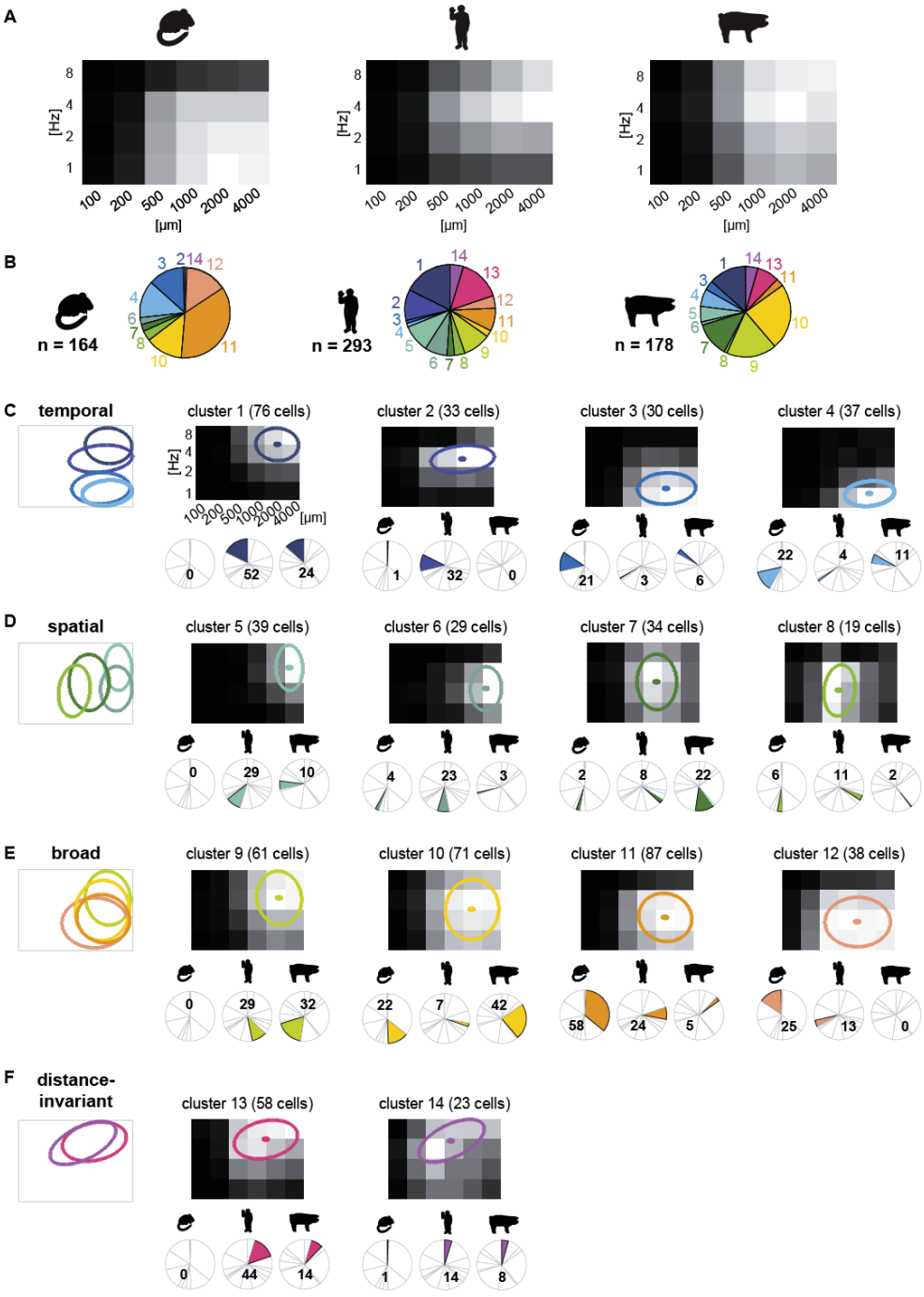

Figure 7: Spatio-temporal tuning of human, pig, and mouse ganglion cells. *A) Average normalized Fourier amplitude calculated from responses to drifting-grating stimuli. B) Distribution of mouse, human, and pig ganglion cells in 14 clusters resulting from k-means clustering of principal components and center of mass, based on the spatio-temporal response parameters of 634 ganglion cells. C-F) Heat-maps display mean response strength of all cells in a given cluster for each of the 24 drifting-grating stimuli. Pie charts indicate the percentage of cells in each cluster per species; numbers indicate absolute number of cells.*

Contours show the 1.5-sigma Gaussians fits to each mean heat-map. C) Clusters 1-4 contain cells with temporal tuning from high (cluster 1) to low frequencies (cluster 4). D) Clusters 5-8 contain cells with spatial tuning from wide (cluster 5) to narrow stimuli (cluster 8). E) Clusters 9-12 contain cells responding to a broad range of spatial periods and temporal frequencies. F) Distance-invariant cells with "anti-speed" tuning are contained in cluster 13 and 14.

Temporal tuning is more similar between human and pig ganglion cells

In addition to clustering of spatio-temporal properties, we analyzed temporal frequency tuning based on two different stimulation paradigms. First, we determined the response strength to a full-field sinusoidal stimulus with continuously increasing temporal frequency – a so-called frequency-modulated chirp stimulus (Fig. 1E). Response strength was defined as the smoothed ratio of the Fourier transform of the response and the Fourier transform of the stimulus. The resulting median tuning curves for the whole population of mouse (blue), human (orange), and pig (green) ganglion cells are shown as thick lines in Fig. 8.

Second, we measured temporal frequency tuning from responses to the widest drifting-grating stimuli (4000 µm), which are the most similar grating stimuli to the chirp in terms of spatial parameters. However, the drifting-grating stimuli were continuously shown for 12 seconds at each of the tested temporal frequencies and additionally contained a directed motion component. The population data extracted from drifting-grating stimuli is shown as open dots with connecting thin lines in Fig. 8.

Both stimuli led to similar conclusions: based on the chirp stimulus, human ganglion cells responded only weakly to low temporal frequencies and their responses reached a plateau from approx. 4 Hz up to the highest tested frequency of 7.5 Hz. Mouse ganglion cells showed the opposite behavior with strong responses to low temporal frequencies and decreasing response strength for higher frequencies. Interestingly, data from pig retina revealed a relatively flat tuning curve which resembled the human situation for higher temporal frequencies. Accordingly, all three species were significantly different from each other for frequencies of 1 Hz to approx. 2.5 Hz ($p < 0.05$ for mouse vs. pig) or almost 4 Hz ($p < 0.05$ for mouse vs. human and pig vs. human). Most tuning curves crossed at 4 Hz (except for the human curve obtained from drifting-gratings). For higher temporal frequencies, mouse ganglion cell tuning differed significantly from human and pig, while the two latter species behaved similarly.

As stated above, the tuning curves obtained from chirp and drifting-grating stimuli were very similar, even though they have been obtained at least partially from a different subset of cells (not all cells responded to both chirp and drifting-gratings). Similar differences between human, pig, and mouse retinas were found for both stimulation paradigms. Taken together, species-differences in temporal frequency tuning seem to be a general and robust feature.

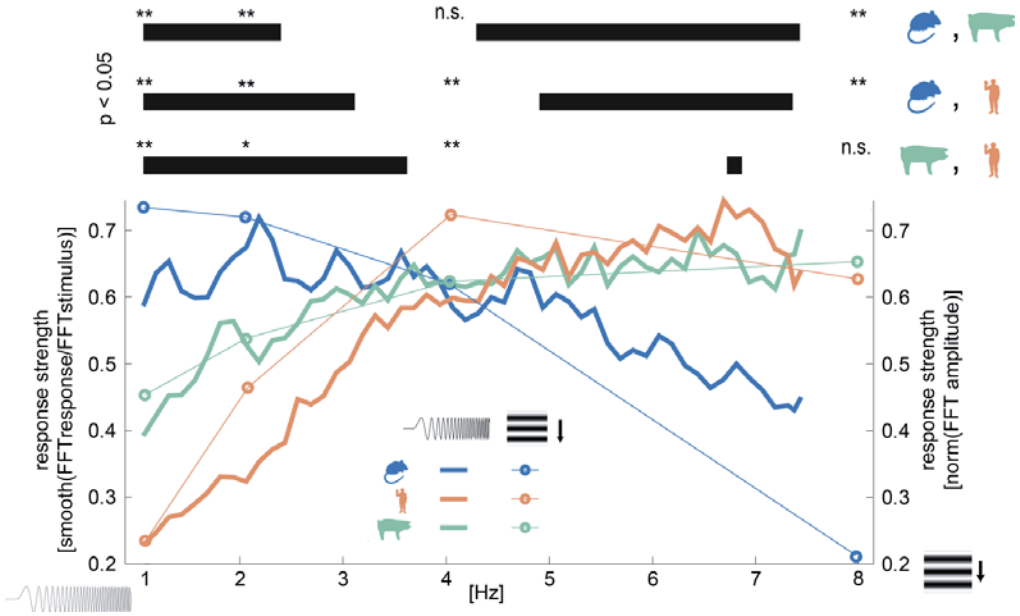

Figure 8: Temporal frequency tuning in mouse, human, and pig retina. *Temporal frequency tuning was calculated in response to a chirp stimulus (left axis; thick lines) and for responses obtained with drifting-grating stimuli (right axis; circles and thin lines). Human ganglion cells (orange; n = 139 for chirp, n = 293 for drifting-gratings) preferred high temporal frequencies, while mouse ganglion cells (blue; n = 155 for chirp, n = 164 for drifting-gratings) encoded lower frequencies better. Pig temporal tuning curves were rather flat (green; n = 114 for chirp, n = 221 for drifting-gratings). We compared tuning from chirp stimuli in 0.625-Hz-bins between different species; the thick lines on top indicate phases with significant differences below the 0.05 level (Wilcoxon ranksum test). Statistical analysis of the four drifting-grating stimuli is indicated above the black bars: * p < 0.05, ** p < 0.01, Wilcoxon ranksum test.*

Human and pig ganglion cells prefer higher speeds than mouse ganglion cells

A speed tuning curve was calculated from both single moving bars and drifting-gratings. For moving bars, the peak response for each presented speed (1, 2, 4, 8, 16 mm/s) was taken and normalized for each cell. For drifting-gratings, the first harmonic responses were treated identically. We found that the response strength of human ganglion cells increased with speed, independently of the stimulus (Fig. $9A_1$ and $9B_1$). In addition, responses of mouse ganglion cells dropped for higher speeds while speed tuning was flatter in pigs, resembling the mouse curve for slow speeds and the human data for higher speeds. The crossing point of the three species was higher for drifting-grating (8 mm/s) than for bars (4 mm/s), but the overall tendencies were the same, independently of the stimulus.

To capture the speed tuning curve in a single value, we calculated an “average speed preference” which corresponds to

the center of mass of the tuning curve (see Methods and Fig. 5). The distribution of the average speed preference is shown in the histograms in Fig. $9A_2$ and $9B_2$. In response to drifting-gratings, the average preferred speed was 2.98 ± 0.77 mm/s (mean ± STD; n = 164) in mouse ganglion cells, while pig (3.57 ± 1.60 mm/s; n = 178) and human ganglion cells (3.99 ± 1.77 mm/s; n = 293) preferred higher speeds. All species were significantly different from each other at the 0.001 level (Wilcoxon Ranksum Tests).

In response to single bars, we observed the same tendencies with all values slightly lower than for drifting-grating stimuli (mouse: 2.27 ± 2.05 mm/s, n = 195; pig: 3.16 ± 2.46 mm/s, n = 147; human: 3.78 ± 1.88 mm/s, n = 37). Significant differences remained between human and mouse ($p < 0.001$) as well as pig and mouse ($p < 0.01$). Pig and human ganglion cells appeared more similar ($p = 0.18$), probably also due to the much lower number of human ganglion cells with responses to moving bars compared to drifting-gratings (37 vs. 293). Significance between mouse and human ($p = 0.047$), but not between mouse and pig ($p = 0.27$) remained after bootstrapping.

Next, we looked at differences between speed tuning to black and white bars. Only two human ganglion cells responded to the white bar, so we did not further consider human ganglion cells for this analysis. In mouse and pig retina, speed tuning differed between black and white bars: we found tuning to higher speed for white than black bars (mouse: 2.16 ± 1.80 mm/s (white) vs 1.63 ± 1.71 mm/s (black); pig: 3.10 ± 2.27 mm/s (white) vs 2.02 ± 2.14 mm/s (black)). In fact, the mouse speed curve for white bars (dashed blue line in Fig. $9C_1$) almost overlapped with the pig curve for black bars (solid green line in Fig. $9C_1$). Response latencies to negative and positive contrast steps in ON-OFF cells revealed a potential mechanism for the different speed tuning. We found that in mouse, the response latencies for positive contrasts were higher than for negative contrast steps (Fig. $9C_2$), leading to more delayed ON-responses than OFF-responses in ON-OFF cells (median[$latency_{OFF}$/$lantecy_{ON}$] = 0.36*)*. In pig retina, there was a similar tendency, but much less pronounced (ratio = 0.97). When showing a black moving bar to such ganglion cells, they respond with two clearly distinct peaks: a fast response when the first, black edge enters the receptive field, and a delayed response to the second edge of positive contrast when the bar leaves the receptive field (Fig. $9C_3$ left). In the case of a white bar, the timing of the first, slow ON-response and the second, fast OFF-response is much closer to each other, which can lead to a single summed response in the case of fast bars (Fig. $9C_3$ right). Thus, when analyzing the response peak for each bar speed, they might be higher for fast, white bars due to overlapping ON- and OFF-responses than for slow, white bars. In response to black bars, this phenomenon does not appear due to the inverse timing of the first and second response.

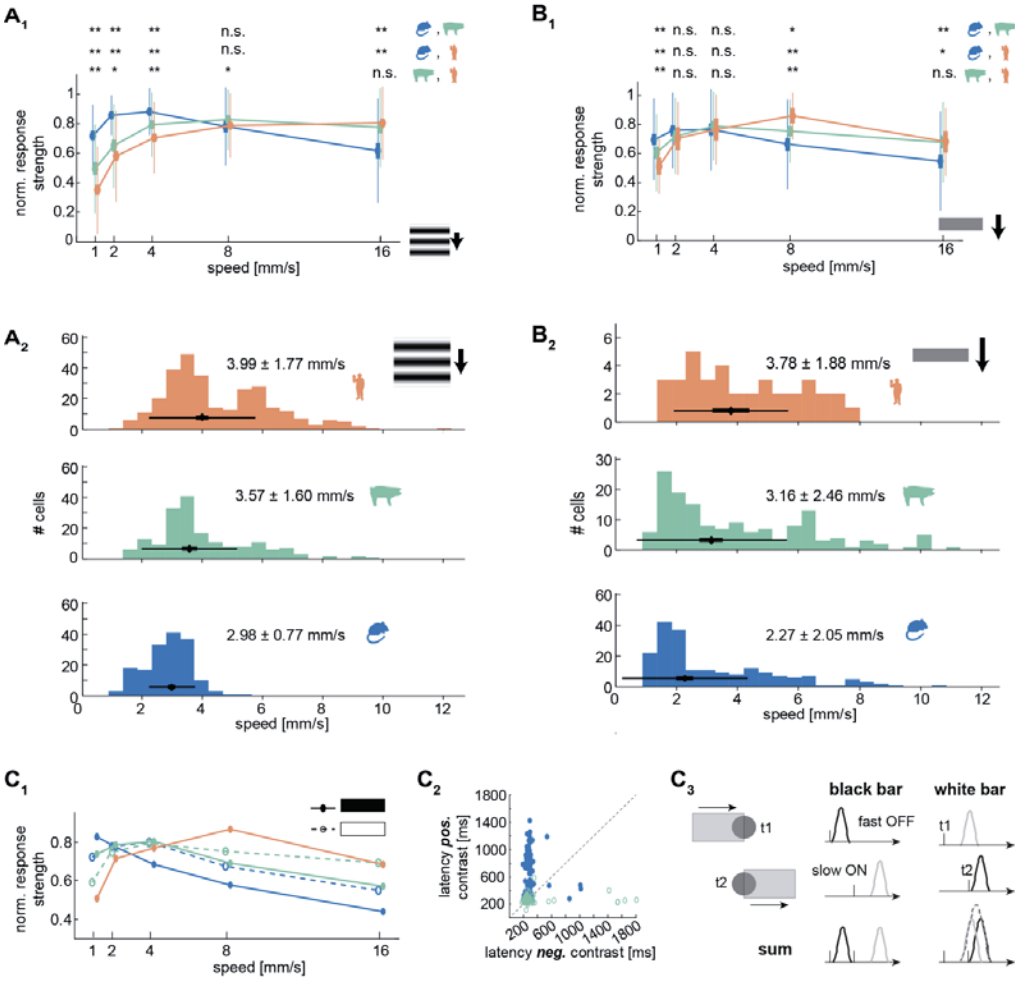

Figure 9: Speed preferences in human, pig, and mouse retina. A) Speed tuning obtained from drifting-gratings. *A_1) Mean response strength averaged across all responding cells. Thin error bars: standard deviation; thick error bars: 95% confidence interval of the mean. Mouse = blue, human = orange, pig = green. * $p<0.05$, ** $p<0.01$, Wilcoxon ranksum test. A_2) Distribution of average preferred speed (defined by 50% of the cumulative sum of F1 amplitudes, see Fig. 5A_1). Numbers indicate median ± standard deviation. Diamonds: median speed; thin error bars: standard deviation; thick error bars: 95% confidence interval.* ***B) Speed tuning obtained from single moving bars.*** *B_1) Tuning curves averaged across all responding cells. If a cell responded to both, black and white bars, the tuning with the higher speed preference was taken for the population mean. B_2) Histograms of average preferred speed.* ***C) Differences between white and black bar responses.*** *C_1) Speed tuning calculated separately for black (solid) and white (dashed) bars. C_2) Distribution of latencies to negative and positive contrast steps for mouse and pig ganglion cells. C_3) Schematic to explain the tuning to higher speeds for white bars, based on the longer latency to positive contrast steps.*

Species-specific response latency and polarity distribution

We found that in all three species about half of all responding ganglion cells were ON-cells (Fig. 10A). In mouse and human, 16-19 % of ganglion cells were ON-OFF cells, while in pig retinas 47% of all cells were ON-OFF. Therefore, the percentage of pure OFF-cells was reduced to 10% in the pig retina compared to 27-35% in the other two species. Note that the total number of cells responding to this stimulus (not the total number of recorded cells) was considered as 100%.

Response polarity was also calculated from the spike-triggered average (STA) obtained from responses to white-noise stimuli (Fig. 10B). STAs provide information on the polarity of the dominant excitatory drive to the ganglion cell. Although the data for polarity extraction from full-field steps and white-noise originated partially from different cells (not every cell responded to both contrast steps and white-noise), they corresponded well. For instance, the higher percentage of OFF-responses from STAs compared to step response in mouse retina (51% vs 27%) correlates with the fact that most cells with ON-OFF responses had an OFF-dominated STA (84%, data not shown). In human retina, on the other hand, more cells with ON-OFF responses had an ON-STA (48% ON vs. 26% OFF), matching the higher percentage of ON-STAs in human retina compared to ON step-responses. Based on the ON/OFF distributions for pig ganglion cells, the numbers of ON- and OFF-dominated linear filters of ON-OFF cells is expected to be balanced. Instead, we found a similar distribution as in human retina with 42% of ON-OFF cells having ON-STAs and 19% having OFF-STAs. However, note that in human and pig retinas, for many ganglion cells with ON-OFF responses the STA was flat (26% and 39%).

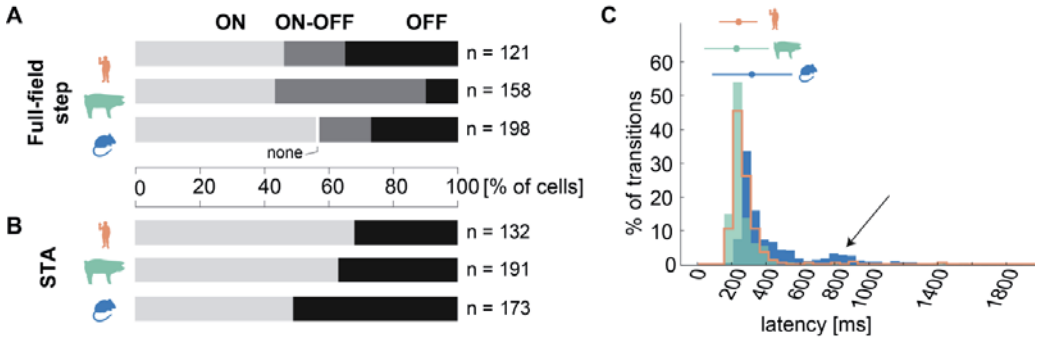

Figure 10: Polarity and latency distribution in human, pig, and mouse retina. *A) Polarity distribution based on full-field contrast step responses; only considering early responses (≤ 550 ms). One mouse ganglion cell responded to full-field contrast steps, but did not have any short-latency responses (= none). B) Polarity extracted from spike-triggered average (STA). C) Latency distribution of all primary responses to full-field contrast steps (i.e. the first response to all four contrast steps gray → black → gray → white → gray). Above the histogram, the mean latency ± standard deviation is indicated. Arrow points at delayed responses in mouse ganglion cells. Mouse (blue), human (orange), pig (green).*

We used the responses to full-field contrast steps also to calculate response latency. As mentioned above, each full-field stimulus consisted of two negative and two positive steps (Fig. 1A), thus four potential response latencies could be calculated per cell. Latency was defined as the time from stimulus onset to the time when 75% of the "first real" peak was reached (for details on response identification and latency calculations see Methods and Fig. 3). Fig. 10C shows the latency distribution of all primary responses (i.e. the first response to each contrast step) in mouse (blue), human (orange), and pig (green) retinas. The distribution of fast latencies was similar in all three species with slightly slower responses in mouse ganglion cells (median = 319 ms for mouse, 242 ms for human, and 225 ms for pig retina). Only very few human and pig ganglion cells had delayed (> 550 ms) primary responses, whereas they could be detected in a substantial fraction of mouse ganglion cells (Fig. 10C, arrow).

Direction-selective cells were observed in pig and mouse, but not human retina

The retina does not only separate information on light increment and decrement or detect the speed and size of an object, but also more complex computations are performed already in the retina before the visual information reaches the brain. For instance, movement direction is encoded by so called direction-selective ganglion cells which respond best to stimuli moving into one of the four cardinal directions[42]. We tested for direction-selectivity with black and white bars (width: 1mm, speed: 1mm/s) moving in eight different directions. The peak responses to each direction were taken for each cell and their vector sum was calculated. The direction-selectivity index was defined as the length of this vector. Cells were counted as selective if their direction-selectivity index (DSI) exceeded 0.3 for both white and black bars (cells with and DSI > 0.3 for only one bar were counted if the response to the other bar was absent). Direction-selective cells in mouse retina have been described previously[42] and accordingly we found such ganglion cells in our mouse recordings as well (3.8% of 213 responding cells). In pig retina we found that 10.6% of 273 responding ganglion cells were direction-selective, while none of the 342 human ganglion cells with light responses showed selectivity. 51.7% of direction-selective cells in pig retina had ON-OFF responses to full-field contrast steps, 3.4% hat ON- and 6.9% had OFF-responses, while the rest of the direction-selective cells (37.9%) did not respond to full-field flashes.

Discussion

Information processing is rich in human retina

By recording directly from a large population of human retinal ganglion cells we have shown variety in the retinal processing in humans. For the first time we have demonstrated the presence of ON-OFF responses in a substantial fraction of human ganglion cells. Furthermore, clustering of responses to drifting-gratings revealed at least 10 groups of distinct spatio-temporal preferences in the human retina. We found that certain ganglion cells were narrowly tuned to specific temporal frequencies, others preferred certain spatial periods, while a third group consisted of more broadly responding cells. In addition, speed preference varied between different human ganglion cells and ranged from 2 to

10 mm/s. Taken together, processing of visual stimuli appears to be of similar complexity in human retina as described previously in other species.

Y-like cells in the human retina

In the cat retina, ganglion cells have been separated into two big classes, the linearly behaving X-cells and the strongly non-linear Y-cells[39]. This led to an extensive search for a counterpart of the Y-cells in the primate retina. Crook and colleagues found that the second harmonic response in parasol cells is larger than the first harmonic for contrast-reversing gratings of approximately 30 to 300 µm periods and thus suggested parasol cells as a homolog pathway to the cat Y-cells[43]. In our human data set, only few cells responded at all to such narrow drifting gratings. However, an additional ganglion cell type in the macaque retina has been proposed as a Y-like pathway, the so-called Upsilon-cells, which are tuned to large spatial periods with an F1-tuning curve rising steeply from narrow to wide stimuli. Those cells have strong F2 response in the range of 500-2000 µm[40].

More than 8% of the human ganglion cells had a stronger F2 than F1 response for drifting-grating stimuli in the same range of spatial periods as the Upsilon-cells. Further, these cells were also tuned to wide stimuli. Other attributes of Y-like cells are rapid and transient responses. Since most of the human ganglion cells with strong second harmonic responses did not respond to full-field contrast steps or other simple and slow stimuli, the homology to the macaque Upsilon-cells by comparison of these parameters could not be confirmed. The only stimulus to which all those cells responded well was in fact the set of drifting-gratings. They also had common response properties with respect to their temporal tuning: they all encoded preferentially high temporal frequencies. Such fast sinusoidal changes between negative and positive contrast cause transient responses in most cell types (also in cells with more sustained responses to contrast steps), thus sharpness and transiency could not be judged from these responses. Nevertheless, the similarity in spatial tuning and mainly the strong non-linearity make these 29 human ganglion cells potential candidates for a Y-like cell type.

Distance-invariant cells

We found a ganglion cell behavior in response to drifting-grating stimuli which so far has not been described. Human (n=58) and pig ganglion cells (n=24) in two of the 14 spatio-temporal clusters encoded large stimuli drifting with high temporal frequencies as well as narrow stimuli drifting with low frequencies. Such "anti-speed" conditions occur in a natural situation when a specific object is moving with a given speed either close to the observer (big and fast on the retina) or further away (small and slow). The role of these cells might thus be to detect objects of a given size and moving with a specific speed independently of how far this object is away. We therefore named these cells "distance-invariant". A literature search did not reveal any similarly behaving cells in other species. However, this might be because similar stimuli and analyses have not been applied to retinas of other species. No such cells were detected in the mouse retina, but they appeared in the pig retina.

Pig retina as a model for human mid-peripheral vision

In medical research, porcine and bovine models are often used to test for

pathological conditions[44-46], effects and side-effects of medications[47-52] or to evaluate surgical methods[53-55]. Here we present the very first description of pig retinal function on the level of individual ganglion cells. Previous morphological classification revealed 18 different ganglion cell types[56]. In the present study, we found pig ganglion cell responses of all three polarities (ON, OFF, and ON-OFF) and they encoded a variety of speeds and spatio-temporal parameters. Further, we found direction-selective and distance-invariant ganglion cells. Our functional characterization thus supports rich information processing in pig retina.

The pig retina appears in many aspects to be a better model for mid-peripheral human retina than the mouse retina. Not only general parameters such as latency were similar in pig and human retina, but also speed preferences and spatio-temporal tuning. Especially when it comes to faster speeds as well as higher temporal frequencies, pig and human ganglion cells responded similarly while mouse ganglion cells in general preferred slower stimuli and lower temporal frequencies. We found that similarly to human ganglion cells, the pig retina was specifically tuned to high temporal frequencies (cluster 1 in Fig. 7), but did not show a temporal tuning to lower frequencies (few pig ganglion cells in cluster 2-4). In mouse retina, cells specifically tuned to specific spatial periods could not be detected, whereas pig and human retina contained spatially tuned ganglion cells. Finally, the distance-invariant ganglion cells appeared in human and pig, but not in mouse retina. Thus, when investigating specific circuit properties, especially when temporal kinetics and spatial preferences are of importance, data from the pig visual streak might be better translatable to the human situation.

Besides the similarities of human and pig ganglion cells, there were also some differences between these two species. For instance, while speed preference was similar to the one of human ganglion cells, pig ganglion cells still preferred slightly slower speeds. In addition, ganglion cells with exclusive tuning to 4 Hz stimulation, which were rather abundant in human retina, did not exist in pig retina. Also spatial tuning and the specific parameters of broadly tuned cells differed between these two species. Future studies with MEAs with more and denser electrodes, calcium imaging experiments or single cell recordings are needed to further clarify the homology of individual ganglion cell types in pig and human retina.

Eventually, the choice of the appropriate model depends strongly on the scientific question. Despite the availability of some genetically modified pigs[57-59], the advantages of a huge palette of genetic tools and the relatively low costs for mouse models will not be reached with pig models. Non-human primates are certainly the closest to the human situation, although several differences have been found between the retinas of macaque, marmoset, and humans[14,60,61]. However, primate research poses ethical questions far beyond the ones met with other animal models. We thus believe that pig retina, which can be obtained in the course of medical studies, can serve as a good model for studies on retinal circuits.

Limitations

While our data-set can be used as a basis for human retina studies as well as comparative questions, additional experiments are certainly needed to further

characterize visual processing in human retina. Our data-set has sources for variability in addition to differences between donors. For instance, the location of retinal pieces can be difficult to control because the eccentricity is less clearly definable if the optic nerve and/or the fovea are not within the obtained part of the eye bulb. In addition, depending on the age of the donor, the retina might detach when removing the vitreous and thereby complicate the orientation. Since the ganglion cell density decreases with eccentricity, the receptive field size increases toward the periphery. Spatial tuning measurements with drifting-grating stimuli are an indirect assessment of receptive field and could thus vary within a given cell type if recorded at different eccentricities. However, the degree of changes in functional receptive fields seems unclear[13,17,40]. Furthermore, temporal tuning, latency, response polarity, as well as spatio-temporal tuning width (narrow or broad) might be less affected by eccentricity.

Retinal pieces from pig retina were cut in the region of the visual streak. The visual streak is relatively narrow, thus some variability might arise if the cut pieces are shifted towards the dorsal or ventral part. For instance, while species differences in average speed preference to single bars remained significant after classical bootstrapping, experiment-wise comparison between species was not significant (data not shown). For future studies, it might be easier to use retinal pieces from the dorsal half of the pig retina which provides a large surface with relatively homogeneous ganglion cell densities[62].

Another striking difference between mouse, pig, and human experiments has been the number of ganglion cells without light responses. In mouse, 95% of all sorted cells showed light responses to at least one of the shown stimuli. Similarly, 90% of the sorted pig ganglion cells had light responses. In the human retina, only 37% of the sortable cells showed any light responses (Suppl. Table 2-4). The reasons for this low number can be technical: some ganglion cells or photoreceptors might have been harmed before or during the surgery or while removing the very sticky vitreous. However, responding and non-responding cells were often recorded by the same electrode which does not fit with mechanical or tumor-mediated injury of photoreceptors or ganglion cells in a restricted retinal patch. Alternatively, selective death of one photoreceptor type could result in neighboring responding and non-responding ganglion cells if only one of them is selectively targeted by the lost photoreceptor type. In future studies one could use colored stimuli to test for selective sensitivity reduction or death of blue cone, which have been shown to be most vulnerable[63]. Alternatively, the strong surgery light might have altered the adaptive state of some photoreceptors and thereby reduced the transmitted visual information, and small responses might have been missed due to strict inclusion criteria during analysis.

Outlook

The presented detailed data set on human retina physiology provides a basis for future research on visual encoding in humans. Based on our data, the stimulus paradigm can be adapted in future studies to detect additional ganglion cell behavior (suboptimal stimulation might have been an additional reason for non-responding

cells). For instance, given the preference for higher speeds, stimuli testing for direction-selectivity could be adjusted to bars moving at higher speeds than 1 mm/s. Further, by the use of high-density MEAs almost every cell in a given patch can be recorded[29], and local stimulation would be possible to test for center-surround mechanisms, local edge detection or approach sensitivity. It has been shown that each ganglion cell type tiles the retina with little overlap in order to encode every visual feature at each point in the visual field[64]. Such mosaic formation can as well be revealed with high-density MEA recordings[17,18,40] and can then be used for cell type identification.

Ex-vivo human retinas are a largely unused source of tissue for scientific studies. In addition to basic research on visual circuits, studying the human retina directly allows us judging how well animal model data can be translated to the human situation. For example, medical studies with pig retina might be expanded from rather low-resolution read-out methods like ERG to single cell (type) based analysis of medication effects, pathological conditions or surgical procedures. Finally, (side-)effects of drugs such as neuroproteciva could be tested directly on human retina instead of using porcine, bovine or other animal models. We also see a big advantage of using human retina for the further development of treatments against blindness. For instance, optogenes (light sensitive ion channels/pumps) are a promising tool to render degenerated photoreceptors or bipolar cells light sensitive[26,27,65,66]. Cell type specificity of the viral vector and the correct expression of the genetic construct containing the optogenes could be developed using ex-vivo human retina. Moreover, by subsequent comparison of the optogene-driven light responses with the natural responses presented in this study, one can evaluate the efficacy of the treatment. We thus hope that more research will make use of ex-vivo human retina in the future.

Acknowledgements

We thank Karl Ulrich Bartz-Schmidt, University Clinics Tübingen, and his operating team for the support during the human retina donation process as well as Martin Schenk and the team of the Experimental Surgery Tübingen for providing pig eyes and assistance during enucleations. We further thank Hartwig Seitter, Boris Benkner, Marion Mutter, and Natalia Swietek for technical support, and Alexandra Tikidji-Hamburyan for the spike-sorting code.

References

1 Dhande, O. S. & Huberman, A. D. Retinal ganglion cell maps in the brain: implications for visual processing. *Curr Opin Neurobiol* 24, 133-142, doi:10.1016/j.conb.2013.08.006 (2014).

2 Masland, R. H. The fundamental plan of the retina. *Nat Neurosci* 4, 877-886, doi:10.1038/nn0901-877 (2001).

3 Sanes, J. R. & Masland, R. H. The Types of Retinal Ganglion Cells: Current Status and Implications for Neuronal Classification. *Annu Rev Neurosci* 38, 221-246, doi:10.1146/annurev-neuro-071714-034120 (2015).

4 Rister, J. & Desplan, C. The retinal mosaics of opsin expression in invertebrates and vertebrates. *Dev Neurobiol* 71, 1212-1226, doi:10.1002/dneu.20905 (2011).

5 Barlow, H. B. & Levick, W. R. The mechanism of directionally selective units in rabbit's retina. *J Physiol* 178, 477-504 (1965).

6 Munch, T. A. *et al.* Approach sensitivity in the retina processed by a multifunctional neural circuit. *Nat Neurosci* 12, 1308-1316, doi:10.1038/nn.2389 (2009).

7 Farrow, K. & Masland, R. H. Physiological clustering of visual channels in the mouse retina. *J Neurophysiol* 105, 1516-1530, doi:10.1152/jn.00331.2010 (2011).

8 Devries, S. H. & Baylor, D. A. Mosaic arrangement of ganglion cell receptive fields in rabbit retina. *J Neurophysiol* 78, 2048-2060 (1997).

9 Wong, R. C., Cloherty, S. L., Ibbotson, M. R. & O'Brien, B. J. Intrinsic physiological properties of rat retinal ganglion cells with a comparative analysis. *J Neurophysiol* 108, 2008-2023, doi:10.1152/jn.01091.2011 (2012).

10 Marre, O. *et al.* Mapping a complete neural population in the retina. *J Neurosci* 32, 14859-14873, doi:10.1523/JNEUROSCI.0723-12.2012 (2012).

11 Doi, E. *et al.* Efficient coding of spatial information in the primate retina. *J Neurosci* 32, 16256-16264, doi:10.1523/JNEUROSCI.4036-12.2012 (2012).

12 Field, G. D. & Chichilnisky, E. J. Information processing in the primate retina: circuitry and coding. *Annu Rev Neurosci* 30, 1-30, doi:10.1146/annurev.neuro.30.051606.094252 (2007).

13 Chichilnisky, E. J. & Kalmar, R. S. Functional asymmetries in ON and OFF ganglion cells of primate retina. *J Neurosci* 22, 2737-2747, doi:20026215 (2002).

14 Dacey, D. M. & Brace, S. A coupled network for parasol but not midget ganglion cells in the primate retina. *Vis Neurosci* 9, 279-290 (1992).

15 Dacey, D. M. & Lee, B. B. The 'blue-on' opponent pathway in primate retina originates from a distinct bistratified ganglion cell type. *Nature* 367, 731-735, doi:10.1038/367731a0 (1994).

16 Field, G. D. *et al.* Spatial properties and functional organization of small bistratified ganglion cells in primate retina. *J Neurosci* 27, 13261-13272, doi:10.1523/JNEUROSCI.3437-07.2007 (2007).

17 Gauthier, J. L. *et al.* Uniform signal redundancy of parasol and midget ganglion cells in primate retina. *J Neurosci* 29, 4675-4680, doi:10.1523/JNEUROSCI.5294-08.2009 (2009).

18 Greschner, M. *et al.* Correlated firing among major ganglion cell types in primate retina. *J Physiol* 589, 75-86, doi:10.1113/jphysiol.2010.193888 (2011).

19 Shlens, J., Rieke, F. & Chichilnisky, E. Synchronized firing in the retina. *Curr Opin Neurobiol* 18, 396-402, doi:10.1016/j.conb.2008.09.010 (2008).

20 Rodieck, R. W., Binmoeller, K. F. & Dineen, J. Parasol and midget ganglion cells of the human retina. *J Comp Neurol* 233, 115-132, doi:10.1002/cne.902330107 (1985).

21 Watanabe, M. & Rodieck, R. W. Parasol and midget ganglion cells of the primate retina. *J Comp Neurol* 289, 434-454, doi:10.1002/cne.902890308 (1989).

22 Hashimoto, T., Katai, S., Saito, Y., Kobayashi, F. & Goto, T. ON and OFF channels in human retinal ganglion cells. *J Physiol* 591, 327-337, doi:10.1113/jphysiol.2012.243683 (2013).

23 Weinstein, G. W., Hobson, R. R. & Baker, F. H. Extracellular recordings from human retinal ganglion cells. *Science* 171, 1021-1022 (1971).

24 Dorn, J. D. *et al.* The Detection of Motion by Blind Subjects With the Epiretinal 60-Electrode (Argus II) Retinal Prosthesis. *JAMA Ophthalmol* 131, 183-189, doi:10.1001/2013.jamaophthalmol.221 (2013).

25 Zrenner, E. *et al.* Subretinal electronic chips allow blind patients to read letters and combine them to words. *Proc Biol Sci* 278, 1489-1497, doi:10.1098/rspb.2010.1747 (2011).

26 Busskamp, V., Picaud, S., Sahel, J. A. & Roska, B. Optogenetic therapy for retinitis

pigmentosa. *Gene Therapy* 19, 169-175, doi:10.1038/gt.2011.155 (2011).

27 Lagali, P. S. *et al.* Light-activated channels targeted to ON bipolar cells restore visual function in retinal degeneration. *Nat Neurosci* 11, 667-675, doi:10.1038/nn.2117 (2008).

28 Tibbetts, M. D., Samuel, M. A., Chang, T. S. & Ho, A. C. Stem cell therapy for retinal disease. *Curr Opin Ophthalmol* 23, 226-234, doi:10.1097/ICU.0b013e328352407d (2012).

29 Fiscella, M. *et al.* Recording from defined populations of retinal ganglion cells using a high-density CMOS-integrated microelectrode array with real-time switchable electrode selection. *J Neurosci Methods* 211, 103-113, doi:10.1016/j.jneumeth.2012.08.017 (2012).

30 Frey, U., Egert, U., Heer, F., Hafizovic, S. & Hierlemann, A. Microelectronic system for high-resolution mapping of extracellular electric fields applied to brain slices. *Biosens Bioelectron* 24, 2191-2198, doi:10.1016/j.bios.2008.11.028 (2009).

31 Segev, R., Goodhouse, J., Puchalla, J. & Berry, M. J., 2nd. Recording spikes from a large fraction of the ganglion cells in a retinal patch. *Nat Neurosci* 7, 1154-1161, doi:10.1038/nn1323 (2004).

32 Zeck, G. M. & Masland, R. H. Spike train signatures of retinal ganglion cell types. *Eur J Neurosci* 26, 367-380, doi:10.1111/j.1460-9568.2007.05670.x (2007).

33 Meister, M., Pine, J. & Baylor, D. A. Multi-neuronal signals from the retina: acquisition and analysis. *J Neurosci Methods* 51, 95-106 (1994).

34 Reinhard, K. *et al.* Step-by-step instructions for retina recordings with perforated multi electrode arrays. *PLoS One* 9, e106148, doi:10.1371/journal.pone.0106148 (2014).

35 Chichilnisky, E. J. A simple white noise analysis of neuronal light responses. *Network* 12, 199-213 (2001).

36 Dacey, D. M. in *The Cognitive Neurosicences* (ed M. S. Gazzaniga) 281-301 (MIT Press, 2004).

37 Tikidji-Hamburyan, A. *et al.* Retinal output changes qualitatively with every change in ambient illuminance. *Nat Neurosci* 18, 66-74, doi:10.1038/nn.3891 (2015).

38 Drasdo, N. & Fowler, C. W. Non-linear projection of the retinal image in a wide-angle schematic eye. *Br J Ophthalmol* 58, 709-714 (1974).

39 Enroth-Cugell, C. & Robson, J. G. The contrast sensitivity of retinal ganglion cells of the cat. *J Physiol* 187, 517-552 (1966).

40 Petrusca, D. *et al.* Identification and characterization of a Y-like primate retinal ganglion cell type. *J Neurosci* 27, 11019-11027, doi:10.1523/JNEUROSCI.2836-07.2007 (2007).

41 Priebe, N. J., Lisberger, S. G. & Movshon, J. A. Tuning for spatiotemporal frequency and speed in directionally selective neurons of macaque striate cortex. *J Neurosci* 26, 2941-2950, doi:10.1523/JNEUROSCI.3936-05.2006 (2006).

42 Vaney, D. I., Sivyer, B. & Taylor, W. R. Direction selectivity in the retina: symmetry and asymmetry in structure and function. *Nature reviews. Neuroscience* 13, 194-208, doi:10.1038/nrn3165 (2012).

43 Crook, J. D. *et al.* Y-cell receptive field and collicular projection of parasol ganglion cells in macaque monkey retina. *J Neurosci* 28, 11277-11291, doi:10.1523/JNEUROSCI.2982-08.2008 (2008).

44 Garcia, M., Forster, V., Hicks, D. & Vecino, E. Effects of muller glia on cell survival and neuritogenesis in adult porcine retina in vitro. *Invest Ophthalmol Vis Sci* 43, 3735-3743 (2002).

45 Komaromy, A. M. *et al.* Long-term effect of retinal ganglion cell axotomy on the histomorphometry of other cells in the porcine retina. *Journal of glaucoma* 12, 307-315 (2003).

46 Lee, L. A. *et al.* Effects of anemia and hypotension on porcine optic nerve blood flow and oxygen delivery. *Anesthesiology* 108, 864-872, doi:10.1097/ALN.0b013e31816c8a30 (2008).

47 Iandiev, I. *et al.* Effects of intravitreal bevacizumab (Avastin) on the porcine retina.

Graefes Arch Clin Exp Ophthalmol, doi:10.1007/s00417-011-1773-y (2011).

48 Januschowski, K. *et al.* Investigating short-term toxicity of melphalan in a model of an isolated and superfused bovine retina. *Graefes Arch Clin Exp Ophthalmol*, doi:10.1007/s00417-015-3149-1 (2015).

49 Januschowski, K. *et al.* Investigating retinal toxicity of tempol in a model of isolated and perfused bovine retina. *Graefes Arch Clin Exp Ophthalmol* 252, 935-941, doi:10.1007/s00417-014-2632-4 (2014).

50 Luke, M. *et al.* The isolated perfused bovine retina--a sensitive tool for pharmacological research on retinal function. *Brain research. Brain research protocols* 16, 27-36, doi:10.1016/j.brainresprot.2005.09.001 (2005).

51 Tseng, M. T., Liu, K. N. & Radtke, N. R. Facilitated ERG recovery in taurine-treated bovine eyes, an ex vivo study. *Brain research* 509, 153-155 (1990).

52 Walter, P., Luke, C. & Sickel, W. Antibiotics and light responses in superfused bovine retina. *Cellular and molecular neurobiology* 19, 87-92 (1999).

53 Kamei, M., Roth, D. B. & Lewis, H. Macular translocation with chorioscleral outfolding: an experimental study. *Am J Ophthalmol* 132, 149-155 (2001).

54 Lopez-Guajardo, L., Benitez-Herreros, J. & Silva-Mato, A. Experimental model to evaluate mechanical closure resistance of sutureless vitrectomy sclerotomies using pig eyes. *Invest Ophthalmol Vis Sci* 52, 4080-4084, doi:10.1167/iovs.10-6812 (2011).

55 Sorensen, N. F. *et al.* The effect of subretinal viscoelastics on the porcine retinal function. *Graefes Arch Clin Exp Ophthalmol*, doi:10.1007/s00417-011-1782-x (2011).

56 Veiga-Crespo, P. *et al.* Phenotypic map of porcine retinal ganglion cells. *Molecular vision* 19, 904-916 (2013).

57 Li, Z. Y. *et al.* Rhodopsin transgenic pigs as a model for human retinitis pigmentosa. *Invest Ophthalmol Vis Sci* 39, 808-819 (1998).

58 Petters, R. M. *et al.* Genetically engineered large animal model for studying cone photoreceptor survival and degeneration in retinitis pigmentosa. *Nature biotechnology* 15, 965-970, doi:10.1038/nbt1097-965 (1997).

59 Ross, J. W. *et al.* Generation of an inbred miniature pig model of retinitis pigmentosa. *Invest Ophthalmol Vis Sci* 53, 501-507, doi:10.1167/iovs.11-8784 (2012).

60 Dacey. The mosaic of midget ganglion cells in the human retina. *J Neurosc* (1993).

61 Hendrickson. Organization of the Adult Primate Fovea. *Macular Degeneration* (2005).

62 Hebel, R. Distribution of retinal ganglion cells in five mammalian species (pig, sheep, ox, horse, dog). *Anatomy and embryology* 150, 45-51 (1976).

63 Connolly, D. M., Barbur, J. L., Hosking, S. L. & Moorhead, I. R. Mild hypoxia impairs chromatic sensitivity in the mesopic range. *Invest Ophthalmol Vis Sci* 49, 820-827, doi:10.1167/iovs.07-1004 (2008).

64 Wassle, H. & Riemann, H. J. The mosaic of nerve cells in the mammalian retina. *Proc R Soc Lond B Biol Sci* 200, 441-461 (1978).

65 Bi, A. *et al.* Ectopic expression of a microbial-type rhodopsin restores visual responses in mice with photoreceptor degeneration. *Neuron* 50, 23-33, doi:10.1016/j.neuron.2006.02.026 (2006).

66 Mutter, M. & Munch, T. A. Strategies for expanding the operational range of channelrhodopsin in optogenetic vision. *PLoS One* 8, e81278, doi:10.1371/journal.pone.0081278 (2013).

Supplementary Data

Supplementary Table 1: Number of retinal pieces and extracted responses.

	Mouse	**Human**	**Pig**
# subjects, **# retinas,** **# retinal pieces**	4 7	10 10 15	5 7 8
# sortable cells	224	920	306
# cells with light responses to at least 1 stimulus	213	342	273
Cells with full-field flash responses	198 (111 ON, 53 OFF, 32 ON-OFF)	121 (56 ON, 42 OFF, 23 ON-OFF)	158 (68 ON, 16 OFF, 74 ON-OFF)
Cells with linear-filters	173 (85 ON, 88 OFF)	132 (90 ON, 42 OFF)	191 (120 ON, 71 OFF)
Cells with drifting-grating responses	164	293 (from 14 pieces)	221 (from 8 pieces)
Cells with chirp responses	155	139 (from 11 pieces)	114 (from 3 pieces)
Cells with responses to speed stimulus	195 (188 black, 170 white)	37 (37 black, 2 white)	147 (from 8 pieces) (136 black, 124 white)
Direction-selective cells	8	0	29

Supplemental table 2: Overview responses in human retina. *For each recorded retinal piece, the number of responding cells for each stimulus is given. The second last column contains the total number of considered cells (responsive and non-responsive), while the number of cells responding to at least one stimulus is given in the last column. x = this stimulus has been applied.*

HUMAN	**full-field steps**		**white-noise flicker**		**moving bar**		**drifting-grating**		**chirp**		**direction selectivity**		**total cells**	**resp. cells**
piece	tested	resp.	tested	resp.	tested	resp.	tested	resp.	tested	resp.	tested	sel.		
1	x	15	x	5	x	2	x	18			x		47	19
2	x	15	x	26	x	4	x	29			x		38	30
3	x		x		x		x	5			x		41	5
4	x	1	x	5	x		x	15	x	9	x		86	20
5	x	8	x	24	x	9	x	22	x	21	x		56	35
6	x	1	x	3	x		x	20	x		x		90	22
7	x	2	x	3	x	1	x	18	x	8	x		92	24
8	x		x		x		x	15	x		x		50	15
9	x	22	x	17	x	5	x	39	x	27	x		105	39
10	x	15	x	28	x	6	x	29	x	30	x		54	33
11	x	5	x	5	x		x	18	x	11	x		43	18
12	x	20	x	4	x		x	20	x	10	x		64	26
13	x	6	x	1	x		x	3	x	5	x		42	9
14	x	8	x	11	x	10	x	13	x	12	x		34	17
15	x	3	x		x		x	29	x	6	x		78	30
Total													920	342
Total resp.per stim.		121		132		37		293		139				
% of resp. cells		35		39		11		86		41		0		
% of total		13		14		4		32		15		0	37	

Supplementary Table 3: Overview responses in pig retina. *Conventions as for suppl. table 2.*

PIG	full-field steps		white-noise flicker		moving bar		drifting-grating		chirp		direction selectivity		total cells	resp. cells
piece	tested	resp.	tested	resp.	tested	resp.	tested	resp.	tested	resp.	tested	sel.		
1	x	17	x	20	x	8	x	16			x	2	23	46
2	x	2	x	30	x		x	14			x	1	30	33
3	x	4	x	33	x		x	22			x		55	18
4	x	42	x	26	x	40	x	43	x	45	x	14	46	22
5	x	8	x	21	x	15	x	27	x	10	x	8	36	57
6	x	14	x	5	x	11	x		x		x	1	21	23
7	x	11	x	13	x	15					x		35	30
8	x	60	x	43	x	58	x	56	x	59	x	3	60	44
Total													306	273
Total resp.per stim		158		191		147		178		114		29		
% of resp. cells		58		70		54		65		42		11		
% of total		52		62		48		58		37		9	90	

Supplementary Table 4: Overview responses in mouse retina. *Conventions as for suppl. table 2.*

MOUSE	full-field steps		white-noise flicker		moving bar		drifting-grating		chirp		direction selectivity		total cells	resp. cells
retina	tested	resp.	tested	resp.	tested	resp.	tested	resp.	tested	resp.	tested	sel.		
1	x	37	x	29	x	32	x	24	x	25	x	2	38	38
2	x	13	x	14	x	14	x	9	x	8	x		16	16
3	x	25	x	24	x	24	x	24	x	18	x	1	25	25
4	x	30	x	32	x	38	x	27	x	27	x	4	38	38
5	x	27	x	22	x	26	x	21	x	23	x	1	31	28
6	x	40	x	35	x	39	x	38	x	32	x		46	42
7	x	26	x	17	x	22	x	21	x	22	x		30	26
Total													224	213
Total resp. per stim		198		173		195		164		155		8		
% of resp. cells		93		81		92		77		73		4		
% of total		88		77		87		73		69		4	95	

Supplemental table 5: Comparison between different clustering algorithms. *Rand Index, adjusted Rand Index, Hubert Index, and Mirkin Index are shown for the result of 14 clusters obtained by the different clustering algorithms (k-means, c-means, mixture of Gaussians (MixGau), fuzzy Gustafson-Kessel (fuzzyGK); see Suppl. Fig. 1). Randomly assignment of numbers between 1 and 14 to each data-point was used as a control (random). Rand Index and Adjusted Rand Index measure the probability of agreement of two distinct clustering algorithms. The Adjusted Rand Index corrects for chance; in both cases 1 indicates perfect agreement. The Hubert Index assesses the difference between the probability for agreement and disagreement between two algorithms. An index of 1 indicates perfect agreement. The Mirkin Index measures the probability for disagreement, thus 0 indicates perfect agreement.*

Rand Index (Rand 1971)

	k-means	c-means	MixGau	fuzzyGK	random
k-means	1.00	0.84	0.93	0.90	*0.86*
c-means	0.84	1.00	0.91	0.90	*0.86*
MixGau	0.93	0.91	1.00	0.88	*0.86*
fuzzyGK	0.90	0.90	0.88	1.00	*0.85*
random	*0.86*	*0.86*	*0.86*	*0.85*	1.00

Adjusted Rand Index (Hubert & Arabie 1985)

	k-means	c-means	MixGau	fuzzyGK	random
kmeans	1.00	0.45	0.55	0.33	*0.00*
c-means	0.45	1.00	0.38	0.37	*0.00*
MixGau	0.55	0.38	1.00	0.27	*0.01*
fuzzyGK	0.33	0.37	0.27	1.00	*0.00*
random	*0.00*	*0.00*	*0.01*	*0.00*	1.00

HI (Hubert 1977)

	k-means	c-means	MixGau	fuzzyGK	random
k-means	1.00	0.84	0.87	0.79	*0.72*
c-means	0.84	1.00	0.82	0.81	*0.72*
MixGau	0.87	0.82	1.00	0.77	*0.72*
fuzzyGK	0.79	0.81	0.77	1.00	*0.70*
random	*0.72*	*0.72*	*0.72*	*0.70*	1.00

MI (Mirkin 1970)

	k-means	c-means	MixGau	fuzzyGK	random
Kmeans	0.00	0.08	0.07	0.10	*0.14*
c-means	0.08	0.00	0.09	0.10	*0.14*
MixGau	0.07	0.09	0.00	0.12	*0.14*
fuzzyGK	0.10	0.10	0.12	0.00	*0.15*
random	*0.14*	*0.14*	*0.14*	*0.15*	0.00

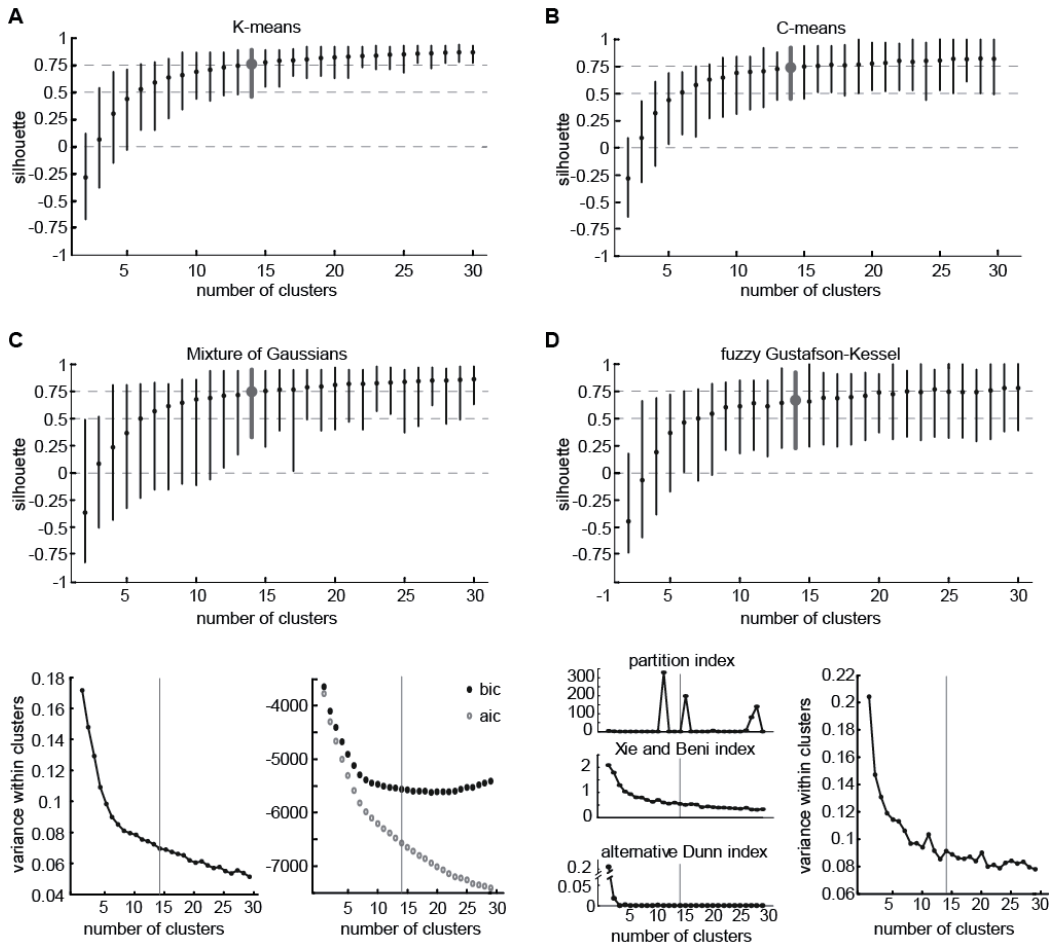

Supplementary Figure 1: Clustering of spatio-temporal response parameters. A) k-means clustering. *7 parameters (5 principal components and coordinates of the center of mass of a heat-map with Fourier transform amplitudes) were clustered by the Matlab routine for k-means clustering (1000 iterations, 10'000 replicates). The mean silhouette index for 2 to 29 clusters is given (circle) as well as the minimal and maximal silhouette (line). In gray the used results of 14 clusters.* ***B) c-means clustering.*** *c-means clustering is a fuzzy version of the k-means algorithm. The Matlab routine was applied (exponent = 2, maximum iterations = 10'000, minimum amount of improvement = 0.00001).* ***C) Mixture of Gaussians clustering.*** *Mixture of Gaussians assumes a Gaussian distribution of the data as a starting point for clustering. "Aic" (Akaike information criterion) and "bic" (Bayesan information criterion) both inform about the likelihood that clustering into more clusters would improve the result. Variance was defined as the sum of the squared Euclidean distance. According to within-cluster variance and bic, clustering into approximately 10 clusters could have been applied ("elbow" in the variance plot and stable bic values for higher numbers of clusters); however, the full range of silhouette values became only positive for at least 12 clusters. We used Matlab routines for clustering, aic and bic calculation.* ***D) Fuzzy Gustafson-Kessel clustering.*** *The GKclust Matlab routine was used (fuzziness parameter = 2, termination parameter = 0.00001). "Partition index" (ratio of compactness and separation), "Xie and*

Beni index" (ratio of total variation within clusters and separation of clusters), and "alternative Dunn index" (identification of compact and well-separated clusters) are all small for a result with 14 clusters, indicating a well-clustered dataset.

Publication 2

Katja Reinhard*, Marion Mutter*, Elisabeth Gustafsson, Leon Gustafsson, Martin Vaegler, Maximilian Schultheiss, Sebastian Müller, Efdal Yoeruek, Merle Schrader, Thomas A Münch (under review) Hypothermia promotes survival of ischemic retinal ganglion cells.
***equal contributions**

Framework: This original research paper describes the effect of ischemia on the retina and the beneficial impact of hypothermia.

My contribution: I established the collaboration with the Department for Experimental Surgery in Tübingen to obtain pig eyes. I originally planned the study as control experiments for human retina donations. I planned, performed, and analyzed experiments with pig and human retina. I worked on the manuscript after the first draft by MM.

Other contributions: MM was involved in performance and analysis of many of the pig experiments and all human retina experiments. She planned the experiments at 4°C and performed most of those recordings. MM cultured post-mortem human retinas and wrote the first draft. EG and LG helped with the organization of the pig experiments, assisted during pig eye enucleations, and helped with analysis of the cyclosporine data. MV provided pig eyes and helped during enucleations. MSchu gave experimental and clinical advice, and helped with the manuscript. SM and MSchr obtained consents from the donors' families. EY supervised post-mortem donations. TAM made the figures and helped with planning and analysis of experiments as well as with the manuscript.

Hypothermia promotes survival of ischemic retinal ganglion cells

*Katja **Reinhard** MSc[1,2,*], Marion **Mutter** MSc[1,2,*], Elisabeth **Gustafsson** vetMTA[1], Leon **Gustafsson** BSc[3],* Martin **Vaegler** Dr.rer.nat.[3], *Maximilian **Schultheiss** MD[4], Sebastian **Müller** MD[4], Efdal **Yoeruek** MD[4], Merle **Schrader** MD[4], Thomas A. **Münch** PhD[1]*

1 *Retinal Circuits and Optogenetics, Centre for Integrative Neuroscience and Bernstein Center for Computational Neuroscience, University Tübingen, Germany*
2 *Neuroscience Graduate School, University Tübingen, Germany*
3 *Department of Urology, University Tübingen, Germany*
4 *Centre for Ophthalmology, University Eye Hospital, University Tübingen, Germany*
5 *Institute for Ophthalmic Research, University Tübingen, Germany*
* *equal contribution*

Running title: Hypothermia protects retina during ischemia

Figures and Tables: 3 Figures

This article contains **additional supplementary material**:

Supplementary Methods
Supplementary Tables 1 – 4

Correspondence:

Thomas Münch, PhD
Centre for Integrative Neurosciences (CIN), University Tübingen
Otfried-Müller-Str. 25, 72076 Tübingen
Tel: +49 707129-89182
Fax: +49 707129-25006
thomas.muench@cin.uni-tuebingen.de

Grant information

Minipigs were funded by the Deutsche Forschungsgemeinschaft (DFG KFO 273). This study was supported by the Deutsche Forschungsgemeinschaft to the Centre for Integrative Neuroscience Tübingen (DFG EXC 307), and the German Ministry of Education, Science, Research and Technology to the Bernstein Center for Computational Neuroscience Tübingen (BMBF FKZ 01GQ1002), and a PhD stipend of the Pro-Retina Foundation, Germany, to KR.

The sponsor or funding organization had no role in the design or conduct of this research. The authors do not have any conflicting interests.

Word count: 3956

Abstract

Purpose – Ischemic stroke in the retinal arteries leads to death of neural tissue and ultimately to blindness. The retina is known to die within 4hrs after onset of ischemia. It is debated whether hypothermia might increase the time window for medical treatment and thereby the chance of recovering sight. In order to characterize the time course of cell death during ischemia and potential beneficial effects of hypothermia in more detail, we investigated the survival of ganglion cells in ischemic pig and human retina as a function of time and temperature.

Methods – Eyes were obtained from minipigs and from post-mortem human donors. Enucleated minipig eyes were stored for defined durations at three different temperatures (37°C, 21°C, and 4°C). In order to assess the viability of the tissue, we measured ganglion cell activity (spiking) with multi-electrode arrays.

Results – Minipig retinal ganglion cell function was severely compromised after 2hrs of ischemia at body temperature. After 4hrs, ganglion cells did not fire action potentials anymore. However, at 21°C, ganglion cell activity was maintained under ischemic conditions for up to 12hrs, and for at least 50hrs at 4°C. In post-mortem human retina, we recorded ganglion cell activity in retina received up to 27hrs after death.

Conclusion – Our results demonstrate that hypothermia greatly increases survival of retinal ganglion cells exposed to ischemia. These results might be relevant for the future treatment of retinal ischemia.

Key words: ischemia, hypothermia, pig retina, human retina, electrophysiology/function

Introduction

Circulatory disorders may cause a deficiency of oxygenation and nutrient supply to neural structures, ultimately leading to serious damage or even death of the nerve tissue[1]. Such ischemia is indicated as a critical factor also in a number of ophthalmic diseases, like diabetic retinopathy, glaucoma or central retinal artery occlusion[2-4]. Numerous studies examining ischemia in the brain have established that only a few minutes of ischemia can result in irreversible nerve damage[5]. The retina, however, appears to be considerably more resistant[6], as ganglion cells in rhesus monkeys survive up to 4hrs of ischemia[7,8].

Currently, there is no effective treatment to prevent ischemic damage[4]. However, temperature is known to have an important influence. Hypothermia is regarded as one of the oldest, yet most effective treatments for limiting cellular injury during ischemia[4]. Even a reduction of the temperature by 3-5°C leads to a clear improvement in survival rate of cortical neurons[9,10] and hypothermia is therefore rated as one of ''the most potent therapeutic approach for reducing experimental ischemic brain injury identified to date''[11,12]. In addition, the efficacy of hypothermia in stroke patients has been successfully investigated in early clinical trials[13]. Hypothermia might be particularly effective at extending retinal survival, as in the retina the time window for a promising treatment is considerably longer than in the rest of the brain. Positive effects of hypothermia on the survival of ischemic retina have been demonstrated by cooling the eye of rats to 33°C[4].

These results prompted us to investigate the influence of hypothermia systematically. This question has been addressed by several studies in rodents[14-16], but investigations with an animal model system closer to the human are still missing. Here, we used retinas of minipigs to investigate the time-course of retinal damage and the protective potential of hypothermia, and compared this with data from post-mortem human retina. As the inner retinal layers are supplied directly by the central retinal artery[17-18], ganglion cells are particularly affected by retinal artery occlusion. We used multielectrode-arrays (MEAs) to record spontaneous and light-evoked activity of ganglion cells in the isolated retina after various durations of ischemia at 37°C, 21°C and 4°C, thereby evaluating the influence of ischemia as well as the potentially protective effect of hypothermia on the functionality of the retina. Our results demonstrate a strong protective effect of hypothermia, prolonging ganglion cell survival to at least 50hrs, the longest time tested so far.

Material and Methods

Pieces from isolated retina of post-mortem human donors or of minipigs (Fig. 1A) were placed on flat 60-electrode multielectrode-arrays[19] and the spiking activity of ganglion cells was qualitatively assessed for each electrode (Fig. 1B). Before recording, minipig eyes were left intact and stored for a defined duration ("ischemia duration") at specific temperatures (37°C, 21°C, 4°C). In our experiments, we therefore induced global ischemia of the retina. Global ischemia is a more severe manipulation than the ischemia experienced by patients during central artery occlusion. In the clinical case, the outer retina (photoreceptors and bipolar-cells) is normally still supplied by an independent capillary system. The inner retina, in particular ganglion cells, is directly affected by the stroke. The capacity of ganglion cells to survive ischemic conditions is therefore of particular clinical

interest. Our experiments, which produce global ischemia in the retina, therefore probably overestimate the effects on the outer retina (e.g. light responses). Details on the experimental procedures are given in the Supplementary Methods.

Results

Human retinal ganglion cells can survive long periods of ischemia

We measured ganglion cell activity of 6 post-mortem human retinas (6 donors) on flat multi-electrode arrays. The eyes were obtained between 12 and 27 hrs post-mortem (Supplementary Table 1; in Fig. 2, the measurements from human tissue are represented by black circles). For each retina, the time spans between the death, enucleation of the eye and preparation of the retina are listed in Suppl. Table 1. Unfortunately, no information was available about the temperature conditions before enucleation of the eye, i.e. the temperature at which the body of the donor was stored, or the time at which the body was brought into a mortuary refrigerator. None of the post-mortem human retinas showed responses to light stimuli, and in retinas from two donations (12 and 15 hrs post-mortem) ganglion cell activity was completely absent. We were able to record ganglion cell spiking activity in the other 4 retinas, with ischemic durations of 12.5, 23.5 and 27 hrs. Ganglion cell activity was apparent on 52% to 83% of the recording electrodes. These results were surprising since previous reports showed that retinal activity ceased completely after 4 hrs of ischemia[7].

In order to investigate this phenomenon in more detail, we performed a series of experiments with minipig eyes to test the survival of ganglion cells under controlled conditions.

Ganglion cell activity ceases within 4 hrs of ischemia at 37°C

We first tested the survival of ganglion cells when ischemia was experienced at 37°C. 12 minipig eyes were exposed to ischemic conditions for 0.5 hrs to 5 hrs. Fig. 2 (orange disks) shows the fraction of electrodes of the multi-electrode array (MEA) on which ganglion cell spiking activity was detectable; Suppl. Table 2 lists these results together with the detailed experimental conditions. Spiking activity (Fig. 2A, orange disks) remained visible on most recording electrodes (93%) for up to 1.5 hrs of ischemia at 37°C and sharply dropped to 0 to 12% of electrodes after 2 hrs of ischemia. In a single retina, we had activity on 44% electrodes after 3.25 hrs of ischemia. After 4 hrs we found ganglion cell activity only on 1 electrode.

Next we counted only the electrodes on which ganglion cell spiking activity was modulated by light stimuli (Fig. 2B, orange disks, and Suppl. Table 2), which would be indicative of functional neural circuits from photoreceptors to bipolar cells to ganglion cells, including their synaptic machinery. Absence of light responses, on the other hand, would indicate that at least one step in this neural processing chain has been compromised. We found light-evoked activity in control conditions, i.e. when the retina was immersed into physiological solution immediately after enucleation (no ischemia), and after short ischemic durations of up to 1 hour on 49% to 83% of the electrodes. With ischemic duration of 1.5 hrs and more, light responses completely vanished, with the exception of responses on a single electrode (3%) after 3 hrs of ischemia.

Overall, we found a fast decay of ganglion cell activity with increasing duration

of ischemia at 37°C. Most light responses ceased after 1 hour and overall ganglion cell spiking activity strongly decreased within 1.5 hrs. These results are fully consistent with previous reports by Hayreh et al.[7,14], measured in monkeys. Our recordings from ischemic pig retina stored at 37°C could thus not explain why ganglion cells in post-mortem human retina survived almost 30 times longer.

Hypothermia (21°C) prolongs ganglion cell survival

Since the temperature of the post-mortem human retina quickly approaches room temperature, we hypothesized that hypothermia might be responsible for the long survival time observed in post-mortem human retina. Therefore, we repeated the experiments with minipig eyes while storing the enucleated bulbi at 21°C instead of 37°C. Otherwise, the experimental conditions were identical.

We tested ischemic durations between 0 and 24 hrs on 20 minipig eyes. Ganglion cell spiking activity (Fig. 2A, green triangles, and Suppl. Table 3) remained detectable after up to 12 hrs of ischemia at 21°C (activity on up to 61% of electrodes), with normal levels of activity remaining even after an ischemic time of 6 hrs (>85% of electrodes). Ganglion cell spiking activity was non-detectable only in later measurements after 16 to 24 hrs.

Abundant light-modulated ganglion cell activity could be detected for up to 2.5 hrs of ischemia (on 80-100% of electrodes, Fig. 2B, green triangles, and Suppl. Table 3). At 3 hrs, we found an abrupt cessation of light responses. Overall, the preservation of light responsiveness was 2.5-fold prolonged at 21°C compared to 37°C.

In summary, we found a slower decay of ganglion cell activity at 21°C compared to the 37°C condition. The longer survival time of ganglion cells at 21°C was statistically significant. We fitted a logistic model to the data recorded at 37°C and 21°C (see Supplementary Methods). The orange and green curves in Fig. 2A show the best fit, suggesting that ganglion cell activity would drop to be recorded on only half of the MEA electrodes after 1:48 hrs at 37°C, but only after around 9 hrs at 21°C. The corresponding horizontal bars in Fig. 2A show the 99% confidence interval for these time-estimates. However, despite the significantly longer survival time of minipig ganglion cells at 21°C, activity was present for more than twice as long in post-mortem human retina (up to 27hrs).

Long retinal ganglion cell survival by slow cooling to 4 ° C

The human donor's body might have been stored in the mortuary fridge for some time and the donor's bulbi were subsequently stored in the refrigerator between enucleation and preparation of the retina. We can therefore assume that the retina of post-mortem donors has been exposed to temperatures as low as 4°C. We performed a further experimental series aimed at mimicking these conditions.

Here, the minipig eyes were first kept for 2hrs at 21°C and then slowly cooled to 4°C. Fig. 2D shows the progression of the temperature measured inside one minipig eye by a temperature probe that we inserted into the vitreous. Otherwise, this bulbus was treated in the same way as the other eyes in this experimental series, and we expect that these retinas were exposed to a very similar temperature progression. Directly after enucleating of the eye, the vitreal temperature was at 25°C. During the 2 hrs at room temperature, temperature decreased to 22°C. Subsequently the eyes were stored in a 4°C degree coldroom, where the temperature

gradually decreased and reached a stable 4.3°C at all measured time points after 15:20 hrs.

The influence of such strong hypothermia was tested on eyes of 22 minipigs. We observed ganglion cell spiking activity for all ischemic durations between 5 and 50 hrs (in steps of 5 hrs, Fig. 2A, blue stars, and Suppl. Table 4). For ischemic durations of 10 to 30 hrs, activity was present on 25% to 98% of the electrodes and decreased to 4% to 13% for longer ischemic times (45 to 50 hrs). After 50 hrs, the longest ischemic duration measured so far, we found activity on 11% of electrodes, therefore the maximal ganglion cell tolerance for ischemia at 4°C might not have been reached yet. The logistic model suggests that on average ganglion cell activity is recordable on only 50% electrodes after around 20.5 hrs (blue curve in Fig. 2A), with the 99% confidence interval for this estimate spanning 13 to 28 hours of ischemia at 4°C. Therefore, the reduction of the temperature to as little as 4°C had a significant further beneficial effect on ganglion cells survival time.

When considering the relatively abrupt disappearance of light responses at 37°C and 21°C after less than 3 hours of ischemia, it was surprising to find clear light responses on 78% of the electrodes even after 5 hrs of ischemia at 4°C (Fig. 2B, blue stars). For longer ischemic durations than 5 hrs, only few light responses were found (on 3% of electrodes after 10 hrs, 7% after 20 hrs, 2% after 30 hrs). However, the number of electrodes with light responses for such long ischemic durations varied strongly from one retinal piece to another.

In a subset of experiments at 21°C and 4°C we added a high-contrast light stimulus. In response to such a strong contrast, abundant light responses could be recorded even after 3 hrs (21°C) and 35 hrs (4°C), respectively (Fig. 2C).

In summary, the number of electrodes on which we observed activity in human retina is comparable to the minipig data at 10 to 30 hrs of ischemia in the 4°C condition. Furthermore, loss of light responses was further delayed to more than 5 hrs (with low contrast stimulus) and 35 hrs of ischemia (with high contrast stimulus), suggesting that the whole neural circuit from photoreceptors to bipolar cells to ganglion cells, including their synaptic machinery, was still functional.

Schultheiss et al[20] demonstrated that cyclosporine-A has a dose-dependent neuroprotective effect that enhances the survival of rat ganglion cells in culture when cyclosporine-A concentrations exceed 1 µg/ml. The minipigs used for our study had been under cyclosporine-A treatment; however, we found that the spread of ganglion cell activity was equally large in the retinas of sham-treated pigs (no cyclosporine-A, data points to the left of the dashed vertical line in Fig. 3) as in treated pigs. There was no correlation between the number of electrodes with spiking activity and the level of cyclosporine-A in the blood samples ($p=0.74$, Spearman Rank Test, Fig. 3).

Discussion

In this study, we examined the survival of retinal ganglion cells during ischemia as a function of ischemia duration and temperature. Recordings with a multielectrode-array (MEA) allowed us to monitor the spiking activity and therefore vitality of ganglion cells directly. We also tested if spiking activity of ganglion cells was modulated by light stimuli. Preservation of light responses would indicate that the retina as a whole is still functional. Spontaneous

ganglion cell activity without light responses, on the other hand, demonstrates that at least some ganglion cells are still alive and able to produce action potentials, while the upstream retinal circuits are impaired at the level of the photoreceptors and/or bipolar-cells. In the clinically relevant case of a central retinal artery occlusion, the nutrient supply to the inner retina, in particular ganglion cells, is disrupted, while the upstream retinal structures (photoreceptors and bipolar-cells) are usually still supplied by an independent capillary system. Therefore, the survival of ganglion cells is of upmost importance in acute cases of a central retinal artery occlusion. However, in case of post-mortem human tissue used in our study, the ischemia is global. In our experimental conditions – in contrast to the clinical situation during central artery occlusion – not only the inner retinal circulation was ceased, but also the choroidal circulation.

For human retina, we defined the ischemia duration as the time between the death of the donor and the exposure of the retina to enriched medium. In general, for post-mortem retina, the temperature to which the retina is exposed after death will slowly decrease from body temperature to room temperature until the body is brought into a mortuary refrigerator. For the tissue samples that we obtained, we were unfortunately not able to recapitulate the exact times and temperature conditions at which the body had been stored. After enucleation, however, all eyes have been stored in a refrigerator (2 to 8°C) for 1 to 17 hrs before we obtained the retina for electrophysiological recordings. Under these conditions, human retinal ganglion cells survived for up to 27 hrs of ischemia, with ganglion cell activity observed on a large proportion of electrodes (52 to 84%). We found no ganglion cell activity in two human retinal donations with ischemia durations of 12:35 hrs and 15:10 hrs. In case of the donation 12:35 hrs after death this might be explained by the medical history of the donor, which included chemotherapy. For the second non-active retina, we have no further information about the donor's history. Nevertheless, we were able to detect spontaneous ganglion cell activity in 4 retinal donations with very long ischemic durations of 12 to 27 hrs. These results were in sharp contrast to published findings showing that the ganglion cells are dead after at most 4 hrs of ischemia[8]. To examine this phenomenon more closely, we developed a minipig eye model to study global retinal ischemia under controlled conditions.

We enucleated minipig eyes immediately after death and stored the intact bulbi for defined times at specific temperatures. In the first experimental condition we set the storage temperature to 37°C to mimic physiological conditions. In agreement with earlier results of Hayreh et al.[14], we found no detectable activity of ganglion cells after 4 hrs of ischemia, with ganglion cell spiking activity continuously decreasing with increasing duration of ischemia. Even though the tissue was supplied with nutrients during the preparation of the retina and during the MEA recording (which lasted 20 to 30 min) ganglion cell responses did not recover. This implies that the retina is irreversibly damaged by such long durations of nutrient deprivation. Hayreh et al.[7] used stereoscopic color fundus photography and fluorescein fundus angiography to characterize the degeneration of the retinal nerve fiber layer in rhesus monkeys. In those studies, the retinal central artery was occluded for 97 to 300 min. A retinal occlusion for less than 100 min led to no evidence for a morphological damage, while an occlusion of more than 240 min produced total or an almost total optic nerve atrophy and nerve fiber damage[7]. Intermediate ischemic durations between 100 and 240 min led to variable results. Taken

together, our data is fully consistent with these results.

At 37°C, we were able to record light responses on 78% of electrodes after 1 hour of ischemia. In all measurements with longer ischemic durations, no light responses could be found. Preserved light responses depend on intact light perception by the photoreceptors and on preserved synaptic transmission between photoreceptors, bipolar cells, and ganglion cells. If the nutrient supply (i.e. circulation) is restored within this time window of 1 hour, one can assume that the prospects for a restoration of visual function are still quite high. The retinal tolerance to short ischemic durations has also been shown by Zhao et al.[16] in the rat eye. There, the retinal arteries were occluded for 17 min, followed by reperfusion. Retinal activity measured by electroretinography (ERG) ceased during occlusion, but recovered within 48 hrs. Retinal ganglion cell death after acute retinal ischemia was also investigated by Lafuente et al.[17] in rat retina by ligature of the ophthalmic vessels. In response to 30 to 45 min of ischemia they observed a continuous decrease in the number of ganglion cells for up to 14 days, with about half of the cells surviving. Increasing the duration of ischemia to 60 to 120 min reduced the survival rate to 25% to 1% measured after up to 90 days. This supports our finding that short ischemic durations of less than 1 hour at 37°C are less harmful, while durations of more than 1 hour can cause severe damage.

Still, these findings could not explain why the post-mortem ganglion cells survived such long periods of ischemia. In further experimental conditions we lowered the temperature during ischemia to 21°C and even 4°C, as we expected that hypothermia might have a protective effect. Zilis et al.[21] reported that extreme cooling with 2°C fluid can lead to electroretinographic changes and retinal detachments. Therefore and for better comparison with post-mortem human retina, we ensured slow cooling during our 4°C experiments. Lowering the temperature indeed led to a pronounced increase in retinal cell survival times. While at 37°C light responses remained for only 1 hour, they were detectable after up to 2.5 hrs at 21°C (3 hrs for high-contrast stimuli), and after up to 5 hrs at 4°C (35 hrs for high-contrast stimuli). The ischemic duration after which spontaneous ganglion cell activity could still be measured increased to 12 hrs of ischemia at 21°C and 50 hrs at 4°C, the longest time we have tested so far. Together with our results from post-mortem human retina, this suggests that a reduction of temperature is highly beneficial. The overall level of spontaneous activity in the post-mortem human retinal tissue, recorded between 15 and 27 hrs post-mortem, was comparable to the activity in minipig retina measured after 2 to 3 hrs of ischemia at 21°C condition or after 20 to 40 hrs at 4°C. Our results at 21°C and 4°C thus confirm the positive effect of hypothermia on the retinal tolerance of ischemia. These results are in accordance with the study of Faberowsky et al.[22], who could show a clear decrease in cell damage in the rat retina (measured by counting non-pyknotic nuclei) after 2 hrs of ischemia while cooling with an ice pack.

Finally, we have kept some human retinal pieces of the donations obtained at 12 and 23 hrs post-mortem in organotypic tissue culture. Re-measurement after 72 to 96 hrs showed a comparable level of spontaneous activity as recorded directly after receiving the tissue (data not shown). This confirms that the ganglion cells were still viable after ischemia for at least several days. However, our data does not allow drawing conclusions about the long-term survival of ganglion cells, further studies will be necessary to investigate this in more detail.

Hypothermia appears to be a key factor for the survival of the retina under ischemic conditions and should be considered in clinically acute cases. In general, stronger cooling, if slowly applied[21], appears to increase chances of regeneration. It remains open how long hypothermia prolongs retinal survival under ischemic conditions in an in-vivo situation. Nevertheless, hypothermia is so far the only neuroprotective treatment which extends the ischemic tolerance and which would currently be applicable in a clinical case.

How could hypothermia be practically achieved? Once in the hospital, the retina can be cooled with neuroprotective irrigation solution[23]. Before reaching the hospital, however, non-invasive first-aid measures would be desirable, especially considering the narrow time window which is available until reperfusion of the retina has to be achieved. We suggest that it may be beneficial to cool the affected eye with an ice pack. Medical emergency personnel should be trained and made aware of the potential benefits of cooling. However, it remains to be investigated how well external cooling spreads to the retina.

Apart from the clinical implications, our study also shows that post-mortem human retina – because of its long survival times due to "naturally" occurring hypothermic conditions – is suited to be used for basic scientific questions dealing with retinal function, ranging from histological examinations to physiological studies, from viral expression studies to optogenetic treatment of blindness.

Acknowledgement

We thank Dr. Martin Spitzer (University Eye Hospital Tübingen) for helpful comments; the Cornea bank of the University Eye Hospital Tübingen for support and organization of human retina donations; Dr. Martin Schenk (Department of Experimental Surgery, Tübingen) for helpful support, Prof. Dr. Wilhelm Aicher, Dr. Bastian Amend, Dr. Alexandra Kelp (Department of Urology, Tübingen) for Göttingen minipig eyes.

References

1. Donnan GA, Fisher M, Macleod M, Davis SM. Stroke. *Lancet.* May 10 2008;371(9624):1612-1623.
2. Adachi M, Takahashi K, Nishikawa M, Miki H, Uyama M. High intraocular pressure-induced ischemia and reperfusion injury in the optic nerve and retina in rats. *Graefes Arch Clin Exp Ophthalmol.* Jul 1996;234(7):445-451.
3. Osborne NN, Ugarte M, Chao M, et al. Neuroprotection in relation to retinal ischemia and relevance to glaucoma. *Surv Ophthalmol.* Jun 1999;43 Suppl 1:S102-128.
4. Salido EM, Dorfman D, Bordone M, Chianelli M, Gonzalez Fleitas MF, Rosenstein RE. Global and ocular hypothermic preconditioning protect the rat retina from ischemic damage. *PLoS One.* 2013;8(4):e61656.
5. Astrup J, Siesjo BK, Symon L. Thresholds in cerebral ischemia - the ischemic penumbra. *Stroke; a journal of cerebral circulation.* Nov-Dec 1981;12(6):723-725.
6. Osborne NN, Casson RJ, Wood JP, Chidlow G, Graham M, Melena J. Retinal ischemia: mechanisms of damage and potential therapeutic strategies. *Prog Retin Eye Res.* Jan 2004;23(1):91-147.
7. Hayreh SS, Jonas JB. Optic disk and retinal nerve fiber layer damage after transient central retinal artery occlusion: an

experimental study in rhesus monkeys. *Am J Ophthalmol.* Jun 2000;129(6):786-795.

8. Hayreh SS, Zimmerman MB. Central retinal artery occlusion: visual outcome. *Am J Ophthalmol.* Sep 2005;140(3):376-391.
9. Antonic A, Dottori M, Leung J, et al. Hypothermia protects human neurons. *Int J Stroke.* Jan 3 2014;9:544-552.
10. Busto R, Dietrich WD, Globus MY, Valdes I, Scheinberg P, Ginsberg MD. Small differences in intraischemic brain temperature critically determine the extent of ischemic neuronal injury. *J Cereb Blood Flow Metab.* Dec 1987;7(6):729-738.
11. Barone FC, Feuerstein GZ, White RF. Brain cooling during transient focal ischemia provides complete neuroprotection. *Neurosci Biobehav Rev.* Jan 1997;21(1):31-44.
12. Yenari MA, Hemmen TM. Therapeutic hypothermia for brain ischemia: where have we come and where do we go? *Stroke; a journal of cerebral circulation.* Oct 2010;41(10 Suppl):S72-74.
13. Hong JM, Lee JS, Song HJ, Jeong HS, Choi HA, Lee K. Therapeutic hypothermia after recanalization in patients with acute ischemic stroke. *Stroke; a journal of cerebral circulation.* Jan 2014;45(1):134-140.
14. Hayreh SS, Weingeist TA. Experimental occlusion of the central artery of the retina. IV: Retinal tolerance time to acute ischaemia. *Br J Ophthalmol.* Nov 1980;64(11):818-825.
15. Steele EC, Jr., Guo Q, Namura S. Filamentous middle cerebral artery occlusion causes ischemic damage to the retina in mice. *Stroke; a journal of cerebral circulation.* Jul 2008;39(7):2099-2104.
16. Zhao Y, Yu B, Xiang YH, et al. Changes in retinal morphology, electroretinogram and visual behavior after transient global ischemia in adult rats. *PLoS One.* 2013;8(6):e65555.
17. Lafuente MP, Villegas-Perez MP, Selles-Navarro I, Mayor-Torroglosa S, Miralles de Imperial J, Vidal-Sanz M. Retinal ganglion cell death after acute retinal ischemia is an ongoing process whose severity and duration depends on the duration of the insult. *Neuroscience.* 2002;109(1):157-168.
18. Machida S, Gotoh Y, Tanaka M, Tazawa Y. Predominant loss of the photopic negative response in central retinal artery occlusion. *Am J Ophthalmol.* May 2004;137(5):938-940.
19. Reinhard K, Tikidji-Hamburyan A, Seitter H, et al. Step-by-step instructions for retina recordings with perforated multi electrode arrays. *PLoS One.* 2014;9(8):e106148.
20. Schultheiss M, Schnichels S, Mlynczak T, et al. Cyclosporine a protects RGC-5 cells from excitotoxic cell death. *Journal of glaucoma.* Apr-May 2014;23(4):219-224.
21. Zilis JD, Chandler D, Machemer R. Clinical and histologic effects of extreme intraocular hypothermia. *Am J Ophthalmol.* Apr 15 1990;109(4):469-473.
22. Faberowski N, Stefansson E, Davidson RC. Local hypothermia protects the retina from ischemia. A quantitative study in the rat. *Invest Ophthalmol Vis Sci.* Nov 1989;30(11):2309-2313.
23. Schultheiss M, Januschowski K, Ruschenburg H, et al. Dulbecco's Modified Eagle Medium is neuroprotective when compared to standard vitrectomy irrigation solution. *Graefes Arch Clin Exp Ophthalmol.* Jun 2013;251(6):1613-1619.

Figure Legends

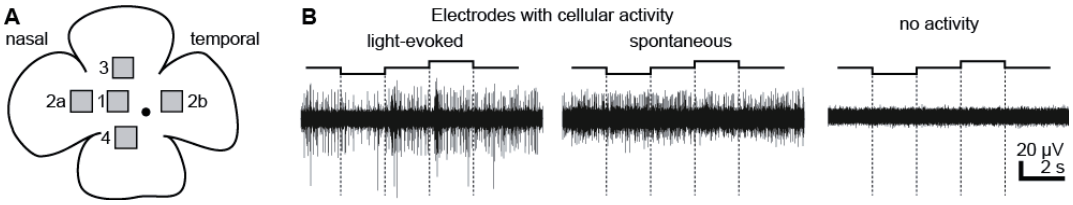

Figure 1: Retinal recordings and outcome measures.
A. Retinal regions used for recordings. Up to four regions have been tested in each retina to probe for ganglion cell activity after the retina had been exposed to ischemic conditions.
B. Outcome measures. Example Recordings of ganglion cell activity measured on individual electrodes (minipig retina). The corresponding full field light stimulus is shown on top. Left: Light responses are evident from the modulation of the spike density. Middle: In the case of spontaneous activity, the spiking activity is not modulated by the stimulus. Right: On this electrode, only electrical noise is visible, but no spiking activity.

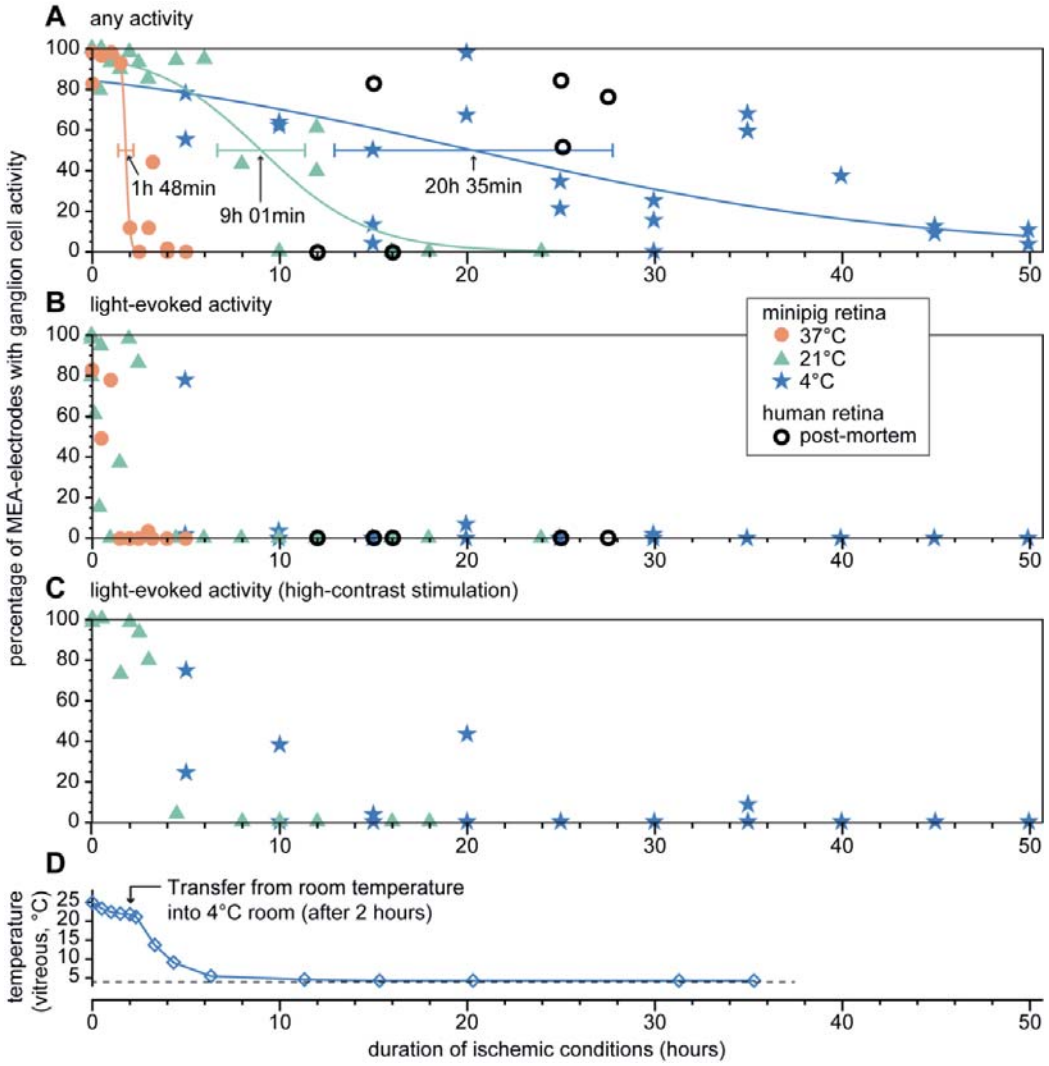

Figure 2: Ganglion cell activity in post-mortem human retina and in minipig retina after ischemia at various temperatures.

A) Ganglion cell spiking activity after ischemia at 37° (orange disks), 21° (green triangles), and 4° C (blue stars). Data from post-mortem human retina (black circles) shown for comparison. Values represent the fraction of MEA (multi-electrode array) electrodes with any activity (light-driven or spontaneous) for different ischemia durations. For each temperature, data was fitted by a logistic model (see Methods). Horizontal lines indicate the 99% confidence interval of the ischemic durations after which ganglion cell activity dropped to be recorded on only 50% of MEA electrodes. Note that the confidence intervals do not overlap, the difference between the temeperature conditions is therefore highly significant.

B) Fraction of electrodes with light-modulated ganglion cell spiking activity. Other conventions as in A.

C) Light responses of minipig ganglion cells to high-contrast light stimuli. After ischemia at 21°C and 4°C, minipig ganglion cells still exhibited substantial light responses after 3hrs (21°C) and 20hrs (4°C). Occasional responses were detectable after 35hrs (4°C) of ischemia.

D) Progression of vitreal temperature inside a minipig eye treated with the 4°C ischemia protocol.

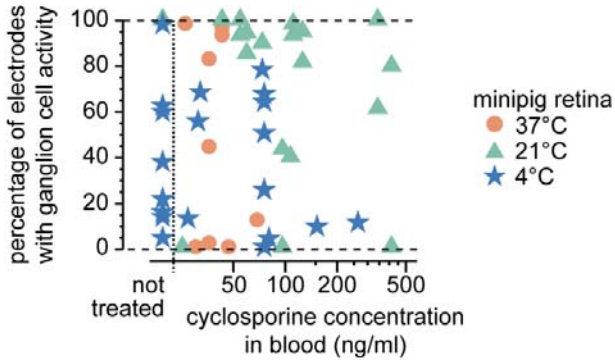

Figure 3: Retinal activity is not correlated with Cyclosporin-A concentration.
Spontaneous ganglion cell activity, as shown in Fig. 2A, as a function cyclosporin-A concentration (ng/ml) measured in blood samples. Values below 25 ng/ml are below the detection threshold; lower values are considered as 0 (sham-treated animals and one treated animal).

Supplementary Material for

Hypothermia promotes survival of ischemic retinal ganglion cells

*Katja **Reinhard** MSc[1,2,*], Marion **Mutter** MSc[1,2,*], Elisabeth **Gustafsson** vetMTA[1], Leon **Gustafsson** BSc[3],* Martin **Vaegler** Dr.rer.nat.[3], *Maximilian **Schultheiss** MD[4], Sebastian **Müller** MD[4], Efdal **Yoeruek** MD[4], Merle **Schrader** MD[4], Thomas A. **Münch** PhD[1,5]*

1 Retinal Circuits and Optogenetics, Centre for Integrative Neuroscience and Bernstein Center for Computational Neuroscience, University Tübingen, Germany
2 Neuroscience Graduate School, University Tübingen, Germany
3 Department of Urology, University Tübingen, Germany
4 Centre for Ophthalmology, University Eye Hospital, University Tübingen, Germany
5 Institute for Ophthalmic Research, University Tübingen, Germany
** equal contribution*

Content:

Supplementary Methods

Animals. The Göttingen Minipig (Ellegaard, Denmark) has been established as a standardized animal model system for biomedical research. Minipigs (4 - 16 months of age, weight 18 - 42 kg) were kept in the animal facility of the Department for Experimental Medicine (University Tübingen) under standardized conditions; food was portioned to 400g per animal per day. Ambient temperature was standardized to 21°C, at 55 - 60% relative humidity. Both males and females were housed in groups under a 12-hour light/dark schedule, and treated weekly with the immune-suppressant cyclosporine-A. Prior to the removal of organs, pigs were sedated and anesthetized by injection of Atropine, Azaperone, Benzodiazepine (Midazolam) and Ketamine. Blood samples were taken and analyzed for each animal. In addition, heparin was injected before the animals were euthanized with Embutramide (T61). Both eyes were enucleated immediately after sacrifice. In total, we obtained 55 minipig eyes. With the exception of the enucleation of the eyes after the death of the minipigs, all procedures were part of another unrelated pre-clinical study. The treatment of the animals used for this study was in accordance with the ARVO Statement for the Use of Animals in Ophthalmic and Vision Research.

Ischemic conditions and hypothermia induction. Ischemia is defined as a lack of blood circulation, and thereby by decreased oxygenation and nutrient supply. In this study, we defined the ischemic duration as the time span between death of the organism and the preparation of the retina. The nutrient and oxygen supply was restored at time of preparation, which was performed in in CO_2-independent medium (Gibco Catalog no. 18045-088). In our experiments, we induced ischemic conditions in the entire retina by storing the intact enucleated eyes in darkness inside a "climate chamber". The chamber consisted of a closed cup containing either a napkin soaked with CO_2-independent medium, or CO_2-independent medium. This chamber was stored for different durations (ischemic duration) either in an incubator (condition: 37°C) or in an air-conditioned room (condition: 21°C). For a third condition (4°C), we adapted the procedure to ensure that the tissue cooled down slowly. Here, the climate chamber was stored in a Styrofoam box (wall thickness 3 cm), and kept at room temperature for 2hrs. After 2hrs, the Styrofoam box was moved into a 4°C temperature controlled room. In order to establish the time course of the temperature experienced by the retina during the 4°C condition, we inserted a needle-shaped temperature probe into the vitreous of one otherwise intact eye. For each condition and test series, one eye was opened and supplied with nutrients immediately and the retinal responses were recorded subsequently (0hrs ischemia, control).

Human. To investigate the impact of ischemia on human retina, we obtained post-mortem human retinal tissue from six cornea donors at the age of 48 to 87 years and of both sexes (see Suppl. Table 1). All procedures were reviewed and approved by the Ethics Committee of the University Clinic Tübingen. The procedures were in accordance with the provisions for cornea donations for the removal and storage of eye donations. Ischemia duration was defined as the time span between death of the donor and the removal of the cornea, upon which the retina was exposed to CO_2-independent medium. Between death of the donor and enucleation of the eye, the bodies of the donors are usually situated either at room temperature or in a cooled mortuary. Unfortunately, it was not possible to trace back the exact storage temperature of the dead bodies for the pseudonymous donations used in this study. The enucleation of post-mortem human eyes was done by an ophthalmologist, at the earliest 6hrs and no longer than 24.5hrs post-mortem. The intact eyes were stored in saline at 2-6°C (refrigerator) until the preparation of the cornea. Prior to preparation the eye was disinfected for 5 minutes in iodide solution and afterwards washed in NaCl solution. In two cases the retina was isolated in NaCl solution by the cornea bank (duration ca. 5-10 minutes) and then transferred into CO_2-independent medium. In the other cases, the eye cup was transferred into CO_2-independent medium directly after removing the cornea and the retina was isolated in our laboratory. In each case, we defined the time-point when the retina was exposed to the CO_2-independent medium as the end of ischemia. Overall, it can be safely assumed that from the start of ischemic conditions (i.e., death of the donor), the temperature of the retina quickly deviated from body temperature, and reached values between room temperature and as low as 2°C until the time of our experiments.

Retina isolation. In the case of pig retina, the eye was opened at the edge of the cornea, and cornea and lens were removed. To remove the vitreous, two to three regularly spaced cuts were made into sclera and attached retina, and the vitreous was carefully wiped out with a pair of forceps. The eyeball was then cut open along the sides in a clover-leave pattern and the retina was exposed. The tissue was oriented based on the optic nerve and the retina was detached from the pigment epithelium. For both, pig and human tissue, retinal pieces of the size of about 0.5x0.5 cm² were cut out in central and mid-peripheral areas, avoiding the fovea in human retina (Fig. 1A). Retinal preparation was carried out in CO_2-independent medium (Gibco Catalog no. 18045-088) at room temperature. The whole preparation took around 5 minutes until the first piece was ready for recording on the multi-electrode array. The rest of the retina was kept in CO_2-independent medium. In case the first piece showed no spontaneous ganglion cell spiking activity, the next piece was recorded 30 to 45 minutes later. Up to 4 pieces were tested for each retina (Fig. 1A). The position of the second piece differed between the areas

marked as “2a” or “2b”. If we detected ganglion cell activity on approximately 15% or more of the electrodes, no further pieces were recorded for this retina. The regions “1” and “2” are located along the visual streak of the pig retina and are comparable in cell density in the ganglion cell layer (~5000 cells/mm²)[1]. Cell densities in regions “3” and “4” is about 5-fold lower. We never found that the retinal activity in areas “3” or “4” was better preserved than in areas “1” or “2” after any of the ischemic insults. Consequently, all data reported here is from the areas “1” or “2”.

Multi-electrode array (MEA) recordings. For electrophysiological recordings, the retina was transferred to the MEA recording chamber and experiments were performed as described in detail previously[2]. Briefly, the retina was oriented ganglion cell side down and centered on the electrode field of a perforated 60 electrode array (59 recording electrodes + 1 reference electrode, electrode grid 8x8, spacing 200µm, electrode diameter 30µm, pMEA200/30iR-Ti-gr, Multichannel Systems, Reutlingen, Germany). To enhance the contact between the electrodes and the ganglion cells, the tissue was gently sucked against the electrodes by applying slight negative pressure through the perforation between the electrodes. During the recordings, the tissue was continuously superfused at 3-4ml/min with Ringer solution (in mM: 110 NaCl, 2.5 KCl, 1 $CaCl_2$, 1.6 $MgCl_2$, 10 D-glucose, 22 $NaHCO_3$, bubbled with 5% CO_2/95% O_2, pH 7.4) at 35°C. The MEA was positioned under a microscope and connected to a data acquisition system (USB-MEA-system, Multichannel Systems or an MC-Card based MEA-system, Multichannel Systems) consisting of a computer with an integrated analog-digital converter board and a MEA1060 amplifier. Data was acquired at 25 kHz by the MC_Rack software (Multichannel Systems). Retinal light stimulation was performed by focusing a DLP projector (Sharp PG-F212X-L) onto the retina from below, through the microscope condenser. The projector intensity spanned a brightness of three log units between black (‘0’ RGB pixel intensity) and white (‘255’) stimulation. The absolute light intensity was reduced by insertion of neutral density filters. In our experiments we used only photopic (day light) stimulation, equivalent to mean brightness of 10^4 to 10^6 isomerization events per rod and second (R*/rod/s).

Visual stimulation. Some test stimuli were first applied at the dimmest light level (10^4 R*/rod/s). If clear light-evoked responses were visible, this light level was used for subsequent recordings. Otherwise, the light level was increased by at most 2 log units. All stimuli were presented around a mid-level gray background (RGB ‘128’). We used the following set of stimuli:

Full-field homogenous grey screen: a grey screen with a mid-level brightness of ‘128’ was presented for three minutes per trial to measure the basic level of spontaneous activity.
Full-field black and white stimulus: With an interval of two seconds, a homogenous illuminated screen with the following brightness sequence was presented: grey (128) – black (0) – grey (128) – white (255) – grey (128), i.e. Weber contrasts of -1 and 1.
Full-field chirp stimulus: Here, the grey-level of the screen was modulated in a sinusoidal fashion. In the first 8 seconds of the stimulus the frequency was modulated according to: intensity = $128 + 128 \sin(\pi (t^2 + t/10))$ at full contrast, t is given in seconds. The frequencies varied from 0.5 Hz to 8 Hz. In the second part (lasting 8.125s) the frequency was kept constant at 2 Hz and the contrast was increased linearly according to: intensity = $128 + 21.7\, t \cos(4 \pi t)$.
High contrast stimulus: in some experiments, high contrast stimuli where applied by closing a shutter and thereby preventing any light from reaching the retina, and subsequent opening of the shutter, leading to a stimulus with infinite Weber contrast.

Data Analysis and Statistics. For analysis of light responses, the data was high-pass filtered (500Hz, 10th-order Butterworth filter) and spikes for each electrode were extracted by thresholding. Each electrode was then analyzed in terms of its responses to the stimuli described above (Fig. 1B). All analysis was performed by in-house written Matlab scripts (written by Alexandra Tikidji-Hamburyan, K.R. and T.A.M.). To assess the viability of the recorded tissue quantitatively, we counted the number of recording electrodes on which any cellular activity (light-evoked or only spontaneous) could be detected. In addition, we counted the number of electrodes on which light-evoked modulation of the spiking activity was detectable.

To assess the significance of longer ganglion cell survival at lower temperatures, we fitted our data by a logistic model of the form

$$\text{remaining activity} = 100 / (1 + \exp[-k (t - t0)])$$

with t being the ischemic duration, and t0 and k being the fitted model parameters. k represents the steepness of the decline of ganglion cell activity, and t0 corresponds to the time when the number of electrodes with activity has dropped to 50%. We used the software package Mathematica 10.2 (Wolfram Research) to perform a least-square fit and to calculate the 99% confidence interval of the model parameters. Before fitting the model to the

4°C dataset, we supplemented the data with the datapoints from the 21°C datasets that were acquired before the timepoint of 5 hrs. The rational was that we did not have such early time points in our 4°C data set (those measurements started at 5 hours), and that the temperature experienced by the "4°C-retinas" was close to room temperature during this early time points anyway (see Fig. 2D). This approach of combining data would potentially make the two data sets more similar to each other, so that we would statistically underestimate the potential beneficial effects of the 4°C treatment.

References

1. **Hebel R. Distribution of retinal ganglion cells in five mammalian species (pig, sheep, ox, horse, dog). *Anatomy and embryology.* Dec 22 1976;150(1):45-51.**
2. **Reinhard K, Tikidji-Hamburyan A, Seitter H, et al. Step-by-step instructions for retina recordings with perforated multi electrode arrays. *PLoS One.* 2014;9(8):e106148.**

Supplementary Table 1: Influence of ischemia in post-mortem human retina

Total duration of ischemia	Time between death and enucleation	Minimal time at 4°C	Sex	Age	Result (activity of ganglion cells)	Fraction of electrodes with ganglion-cell activity [%]	Notes
12:35 hrs	10:35 hrs	2:00 hrs	f	48	No activity	0	Chemotherapy/ Mammary carcinoma
12:40 hrs	11:40 hrs	1:00 hrs	f	72	Spontaneous firing	83	
15:10 hrs	13:25 hrs	1:45 hrs	m	87	No activity	0	
23:30 hrs	22:30 hrs	1:00 hrs	f	87	Spontaneous firing	84	
23:40 hrs	6:10 hrs	17:30 hrs	m	63	Spontaneous firing	52	
27:08 hrs	24:38 hrs	2:30 hrs	m	74	Spontaneous firing	76	

Supplementary Table 2: Influence of ischemia duration at body temperature (37°C) in minipig eyes

Duration Ischemia	No. of eyes	Storage of enucleated bulbus	Fraction of electrodes with light resp. [%]	Fraction of electrodes with any cellular activity [%]
0:00 hrs	2	Solution, 37°C	83 83	98 83
0:30 hrs	1	Climate Chamber, 37°C	49	97
1:00 hrs	1	Climate Chamber, 37°C	78	98
1:30 hrs	1	Climate Chamber, 37°C	0	93
2:00 hrs	1	Solution, 37°C	0	12
2:30 hrs	1	Climate Chamber, 37°C	0	0
3:00 hrs	1	Solution, 37°C	3	12
3:15 hrs	1	Climate Chamber, 37°C	0	44
4:00 hrs	2	Climate Chamber, 37°C Solution, 37°C	0 0	2 0
5:00 hrs	1	Climate Chamber, 37°C	0	0

Supplementary Table 3: Influence of ischemia duration at room temperature (21°C) in minipig eyes

Duration Ischemia	No. of eyes	Storage of enucleated bulbus	Fraction of electrodes with light resp. [%]	Fraction of electrodes with any cellular activity [%]
0:00 hrs	3	Solution, 21°C	80 100 98	100 100 100
0:10 hrs	1	Solution, 21°C	61	81
0:25 hrs	1	Solution, 21°C	15	80
0:30 hrs	1	Solution, 21°C	95	100
1:00 hrs	1	Solution, 21°C	0	93
1:30 hrs	1	Climate Chamber, 21°C	37	90
2:00 hrs	1	Climate Chamber, 21°C	98	98
2:30 hrs	1	Climate Chamber, 21°C	86	93
3:00 hrs	1	Climate Chamber, 21°C	0	85
4:30 hrs	1	Climate Chamber, 21°C	0	94
6:00 hrs	1	Climate Chamber, 21°C	0	95
8:00 hrs	1	Climate Chamber, 21°C	0	43
10:00 hrs	1	Climate Chamber, 21°C	0	0
12:00 hrs	2	Climate Chamber, 21°C	0 0	61 40
16:00 hrs	1	Climate Chamber, 21°C	0	0
18:00 hrs	1	Climate Chamber, 21°C	0	0
24:00 hrs	1	Climate Chamber, 21°C	0	0

Supplementary Table 4: Influence of ischemia duration at 4°C in minipig eyes

Duration Ischemia	No. of eyes	Storage of enucleated bulbus	Fraction of electrodes with light resp. [%]	Fraction of electrodes with any cellular activity [%]
0:00 hrs	1	Solution, 21°C	100	100
5:00 hrs	2	Climate Chamber, 4°C	78 2	78 55
10:00 hrs	2	Climate Chamber, 4°C	3 0	62 64
15:00 hrs	3	Climate Chamber, 4°C	0 0 0	13 4 50
20:00 hrs	2	Climate Chamber, 4°C	0 7	98 67
25:00 hrs	2	Climate Chamber, 4°C	0 0	21 34
30:00 hrs	3	Climate Chamber, 4°C	0 0 2	15 0 25
35:00 hrs	2	Climate Chamber, 4°C	0 0	68 59
40:00 hrs	1	Climate Chamber, 4°C	0	37
45:00 hrs	2	Climate Chamber, 4°C	0 0	13 9
50:00 hrs	2	Climate Chamber, 4°C	0 0	4 11

Publication 3

Katja Reinhard*, Alexandra Tikidji-Hamburyan*, Hartwig Seitter*, Saad Idrees, Marion Mutter, Boris Benkner, Thomas A Münch (2014) Step-By-Step Instructions for Retina Recordings with Perforated Multi Electrode Arrays. *PLoS ONE* 9(8): e106148.
***equal contributions**

Framework: This is a method paper which explains how to perform multi-electrode array recordings with retina. It contains an extensive troubleshooting section and an additional section on in-vitro electroretinogram recordings.

My contribution: During my stay in the lab I improved our multi-electrode array setups, and collected potential issues and how to troubleshoot those. For this method paper, I formulated a step-by-step instruction to perform perforated multi-electrode array recordings with retina. Most of the troubleshooting section has been compiled by me. Further, I outlined the figures and produced many of them. Big parts of the mouse data as well as most of the pig and human data used for evaluation of the method have been acquired by me.

Other contributions: AHT initially implemented the multi-electrode array setup in our lab. HS developed and described the electroretinogram recordings, and helped with the rest of the manuscript. SI and TAM helped with the manuscript. MM and BB helped with the figures and proof-read the manuscript. Statistics on the number of extracted neurons per experiments are also based on independently collected data from HS, MM, and AHT as well as other people from the lab.

OPEN ACCESS Freely available online

PLOS ONE

Step-By-Step Instructions for Retina Recordings with Perforated Multi Electrode Arrays

Katja Reinhard[ϑ], Alexandra Tikidji-Hamburyan[ϑ¤], Hartwig Seitter[ϑ], Saad Idrees, Marion Mutter, Boris Benkner, Thomas A. Münch*

Werner Reichardt Centre for Integrative Neuroscience and Bernstein Center for Computational Neuroscience, University of Tübingen, Tübingen, Germany

Abstract

Multi-electrode arrays are a state-of-the-art tool in electrophysiology, also in retina research. The output cells of the retina, the retinal ganglion cells, form a monolayer in many species and are well accessible due to their proximity to the inner retinal surface. This structure has allowed the use of multi-electrode arrays for high-throughput, parallel recordings of retinal responses to presented visual stimuli, and has led to significant new insights into retinal organization and function. However, using conventional arrays where electrodes are embedded into a glass or ceramic plate can be associated with three main problems: (1) low signal-to-noise ratio due to poor contact between electrodes and tissue, especially in the case of strongly curved retinas from small animals, e.g. rodents; (2) insufficient oxygen and nutrient supply to cells located on the bottom of the recording chamber; and (3) displacement of the tissue during recordings. Perforated multi-electrode arrays (pMEAs) have been found to alleviate all three issues in brain slice recordings. Over the last years, we have been using such perforated arrays to study light evoked activity in the retinas of various species including mouse, pig, and human. In this article, we provide detailed step-by-step instructions for the use of perforated MEAs to record visual responses from the retina, including spike recordings from retinal ganglion cells and *in vitro* electroretinograms (ERG). In addition, we provide in-depth technical and methodological troubleshooting information, and show example recordings of good quality as well as examples for the various problems which might be encountered. While our description is based on the specific equipment we use in our own lab, it may also prove useful when establishing retinal MEA recordings with other equipment.

Citation: Reinhard K, Tikidji-Hamburyan A, Seitter H, Idrees S, Mutter M, et al. (2014) Step-By-Step Instructions for Retina Recordings with Perforated Multi Electrode Arrays. PLoS ONE 9(8): e106148. doi:10.1371/journal.pone.0106148

Editor: Steven Barnes, Dalhousie University, Canada

Received May 23, 2014; **Accepted** June 13, 2014; **Published** August 28, 2014

Data Availability: The authors confirm that all data underlying the findings are fully available without restriction. The methods are described in the paper.

Funding: This study was supported by funds from the Deutsche Forschungsgemeinschaft to the Werner Reichardt Centre for Integrative Neuroscience Tübingen (DFG EXC 307), and the German Ministry of Education, Science, Research and Technology to the Bernstein Center for Computational Neuroscience Tübingen (BMBF FKZ 01GQ1002), and a PhD stipend of the Pro-Retina Foundation, Germany, to KR. The authors acknowledge support by Deutsche Forschungsgemeinschaft and Open Access Publishing Fund of Tuebingen University. The funders had no role in study design, data collection and analysis, decision to publish, or preparation of the manuscript.

Competing Interests: The authors of this manuscript have read the journal's policy and have the following competing interests: One of the two pMEA setups in the lab of the authors was provided free of charge by MultiChannel Systems (Reutlingen, Germany). It is an older model demonstration system formerly used by their sales department. This does not alter the authors' adherence to all the PLOS ONE policies on sharing data and materials.

* Email: thomas.muench@cin.uni-tuebingen.de

ϑ These authors contributed equally to this work.

¤ Current address: Dept. of Neurosurgery and Hansen Experimental Physics Laboratory, Stanford University, Stanford, California, United States of America

Introduction

Multi-electrode arrays (MEAs) are a state-of-the-art tool in electrophysiological studies. Such arrays consist of dozens up to thousands of electrodes and allow measurements of many neurons in parallel. Especially in retina research, MEA recordings have proven to be a powerful technique [1–5]. The retina consists of many parallel yet interacting neural circuits which extract specific information about the visual input [6]. These circuits culminate at the output neurons of the retina, the retinal ganglion cells. The retina's layered structure with ganglion cells lying close to the proximal surface makes the retina particularly amenable for MEA recordings. Further, in many common laboratory species, including mouse, the ganglion cells form a monolayer with little or no three dimensional piling of cell bodies. This monolayer is covered only by the relatively thin inner limiting membrane, such that these neurons and the flat recording array can be brought into close proximity.

When performing in-vitro MEA recordings with retina, the retina is extracted from the eye and placed ganglion cell-side down on the electrodes of the MEA. Light stimulation is then applied either from the top or, if the MEA is transparent, through the MEA from the bottom. The photoreceptors capture the light and the visual information is processed by the retinal circuits, eventually leading to spike generation in the ganglion cells. These spikes can be measured as voltage changes by the electrodes of the MEA.

Retinal recordings with standard MEAs suffer from three main problems: (1) poor signal-to-noise ratio due to insufficient contact (physical proximity) between the tissue and the MEA (this problem is particularly pronounced when recording from small retinas, e.g. mouse, due to the strong curvature of the retina, and when recording from retinas with a thick inner limiting membrane, e.g.

human), (2) insufficient oxygenation and nutrient supply to the ganglion cells lying on the bottom of the recording chamber, and (3) movement of the retina due to insufficient fixation of the tissue on the array. Poor electrode contact and fixation of the tissue are usually dealt with by using some sort of "stamp", pushing the tissue against the MEA. This has obvious disadvantages, as one needs to find a fine balance between sufficiently holding the tissue in place on one hand, and not damaging the tissue by applying too much pressure on the other hand.

In our laboratory, we have implemented retinal recordings with perforated MEAs (pMEAs, from Multi Channel Systems MCS GmbH, Reutlingen, Germany). We found that pMEAs can alleviate all three issues encountered with standard MEAs. In pMEAs, the electrodes are not embedded into a ceramic or glass carrier, but instead in a fine membrane which also contains small holes of different sizes in-between the electrodes (Fig. 1). A slight vacuum can be applied through this perforation; this vacuum gently pulls the tissue towards the electrodes. This procedure enhances the contact between the tissue and the electrodes, and therefore increases the signal-to-noise ratio and decreases tissue movement during the experiment [7]. Additionally, it has been shown with brain slices that with pMEAs, more fresh solution reaches the bottom cell layers either through the tissue or through the small space between tissue and electrodes. Oxygenation of the bottom cell layer (i.e. ganglion cells in the case of retina) is thereby greatly enhanced when using pMEAs [8].

Several adjustments are necessary compared to the procedures applicable to brain slices [9–13]. The main reason is that the retina is relatively thin and fragile compared to brain slices, so that the vacuum needs to be very carefully controlled to prevent tearing of the retinal tissue. In this article we give a detailed description of our recording setup for perforated MEAs and step-by-step instructions for two different applications (spike recordings and *in vitro* electroretinogram recordings). We show example data demonstrating recording stability in long-term experiments, and provide an overview of the outcome which can be expected from such measurements. In addition, we discuss possible technical issues and provide troubleshooting suggestions.

Material

Perforated MEAs (60pMEA200/30iR by Multi Channel Systems MCS GmbH)

The 60pMEA200/30iR is a pMEA with 60 Titanium nitride electrodes. The electrodes are arranged in an 8×8 layout with 200 µm electrode distance and 30 µm electrode diameter. Electrodes are embedded in a perforated polyimide foil which allows perfusion and application of negative pressure to the retina (Fig. 1, further details can be found in the pMEA data sheet [14]). pMEAs are transparent and can therefore be used in upright and inverted setups. In this article we describe our experiments performed with a 60-electrode pMEA with glass ring and the MEA1060 amplifier. However, recordings with other pMEA systems should require only slight adaptations.

Figure 1. Layout of the 60-electrode pMEA. The electrodes are arranged in an 8×8 array with 200 µm electrode distance. Perforations of various size are visible in-between electrodes (source: 60pMEA200/30iR data sheet by Multi Channel Systems).
doi:10.1371/journal.pone.0106148.g001

Tissue

In previous studies we have used pMEAs in many experiments with retinas of several species. In the section "anticipated results" we discuss the quality of data to expect from retinas of various mouse strains, domestic pig retinas (sacrificed during independent studies at the Department of Experimental Surgery, Tübingen), Göttingen minipig retinas (Department of Urology) and human retinas (donated by patients of the University Eye Hospital in Tübingen). All recordings have been performed in the context of scientific studies in our laboratory. All studies were performed in accordance with German and European regulations. Use of human retinal tissue was approved by the Ethics Commission of the University Clinic Tübingen, approval number 531/2011. Written informed consent of the donors was obtained; the consent procedure was part of the Ethics Commission approval. Animal experiments were approved by the Regierungspräsidium Tübingen.

Setup components

The setup for pMEA recordings consists of two perfusion loops: An upper loop to supply the tissue with fresh solution (labeled "upper perfusion" and "suction" in Fig. 2), and a lower loop to adjust the proper negative pressure ("lower perfusion" and "vacuum system"). Here, we provide an overview of this dual perfusion system and a detailed list of the components we used to build our setup (excluding light stimulation and data acquisition). Details on how to use the system are described below in the section "experimental procedure". Except for the constant vacuum pump (D3), the amplifier baseplate that allows vacuum application, and some small components such as tubing, no additional material is needed compared to conventional MEA recordings. All numbers refer to Figure 2.

Upper perfusion. The upper perfusion system supplies the retina with fresh solution during the recordings. It can either be gravity driven (like in the scheme in Fig. 2, in which case the tubing can initially be filled with the help of a syringe, A1, v4), or it can be driven with a peristaltic pump. The solution is guided into the MEA chamber through a cannula or a stiff tube. A simple flow regulator (A2) can be used to adjust the speed of the solution flow in the gravity driven configuration. The components used for upper perfusion are listed below.

- Bottle with physiological solution
- 10–20 ml syringe (A1)
- Simple flow regulator (A2, e.g. Infudrop, Fresenius Kabi AG, Bad Homburg, Germany)
- Valve (v4)
- Cannula or similar
- Tubing (inner diameter)
  - 2×~1.6 mm to connect v4–A2 and A2–MEA
  - 2×~1.6 mm (or thicker) to connect v4–solution and v4–A1
  - Thinner tubes to connect to cannula (depending on cannula)
- Connectors for attaching the tubing to the other components

Suction. To prevent the MEA chamber from overflowing, a suction pump (B1) should be connected via a cannula to the MEA

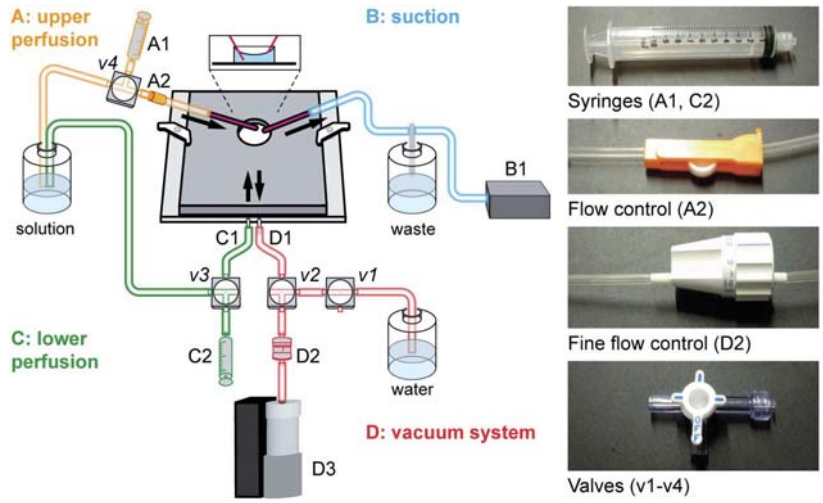

Figure 2. Setup for pMEA recordings. Our MEA setup consists of two perfusion loops. Solution is supplied to the MEA chamber from the top through the upper perfusion (A) and excessive solution is removed by the suction (B). The necessary negative pressure is supplied by the additional perfusion, consisting of the lower perfusion (C) and a vacuum (D). Details are given in the following text and figures.
doi:10.1371/journal.pone.0106148.g002

chamber. The solution can either be collected in an extra bottle and discarded after the experiment or, if the upper perfusion is performed with a peristaltic pump, it can be recycled and pumped back into the main solution bottle. The components for suction are listed below.

- Vacuum pump (B1)
- Bottle with gas washing bottle head
- Cannula or similar
- Tubing and connectors, appropriate to fit attachments for waste bottle and pump

Lower perfusion. The lower perfusion system is only used before the experiment and can be driven by gravity flow. Its purpose is to fill the MEA chamber with solution without introducing air bubbles into the vacuum system. The lower perfusion is connected to the shorter cannula of the pMEA amplifier baseplate (C1). To get the gravity-driven flow going, the tubing of the lower perfusion system can be filled with the help of a syringe (C2, v3). The components for lower perfusion are listed below.

- 10–20 ml syringe (C2, with screw connection for valve)
- Valve (v3)
- Tubing (inner diameter)
  - 1×0.8 mm to connect v3–C1
  - 1×~1.6 mm to connect v3–solution
- Connectors at v3

Vacuum system. The vacuum system provides negative pressure to pull the retina towards the electrodes. This negative pressure needs, first, to be constant to avoid fluctuations, and second, to be high enough to ensure good tissue-electrode contact, but low enough to not tear the tissue. Constant negative pressure is provided by a Constant Vacuum Pump (CVP, D3, Multi Channel Systems) and is further reduced by an additional fine flow control (D2) between the CVP (D3) and the MEA baseplate. The vacuum system is connected to the right (longer) cannula of the MEA baseplate (D1). The most important step for ensuring reliable negative pressure is the removal of air bubbles: any air bubble in the vacuum system will degrade the stable negative pressure. The additional valves (v1, v2) and the water bottle are needed for filling of the vacuum system and for removing air bubbles (see below). The components for the vacuum system are listed below.

- Constant vacuum pump (CVP, D3, Multi Channel Systems MCS GmbH, Reutlingen, Germany)
- Fine flow control (D2, Dosi-flow 10, P. J. Dahlhausen & Co. GmbH, Köln, Germany)
- Valves (v1, v2)

  Valve v1 can either be a 2-way valve, or a 3-way valve (like the other valves) with one connector closed with a plug
- Tubing (inner diameter)
  - 1×0.8 mm to connect v2–D1
  - 3×~1.6 mm to connect v2–D2, v2–v1, and v1–water bottle
- Connectors
- 1×18 ga blunt needle for 0.8 mm tubing at v2
- 1×plug for v1 if a 3-way valve is used
- Bottle with water

MEA Equipment. 60-electrode perforated MEA with glass ring (Multi Channel Systems MCS GmbH, Reutlingen, Germany).

- MEA1060 system (Multi Channel Systems MCS GmbH, Reutlingen, Germany)

Specific equipment for in vitro electroretinogram (in vitro ERG) recordings. Visual stimulation only possible from below

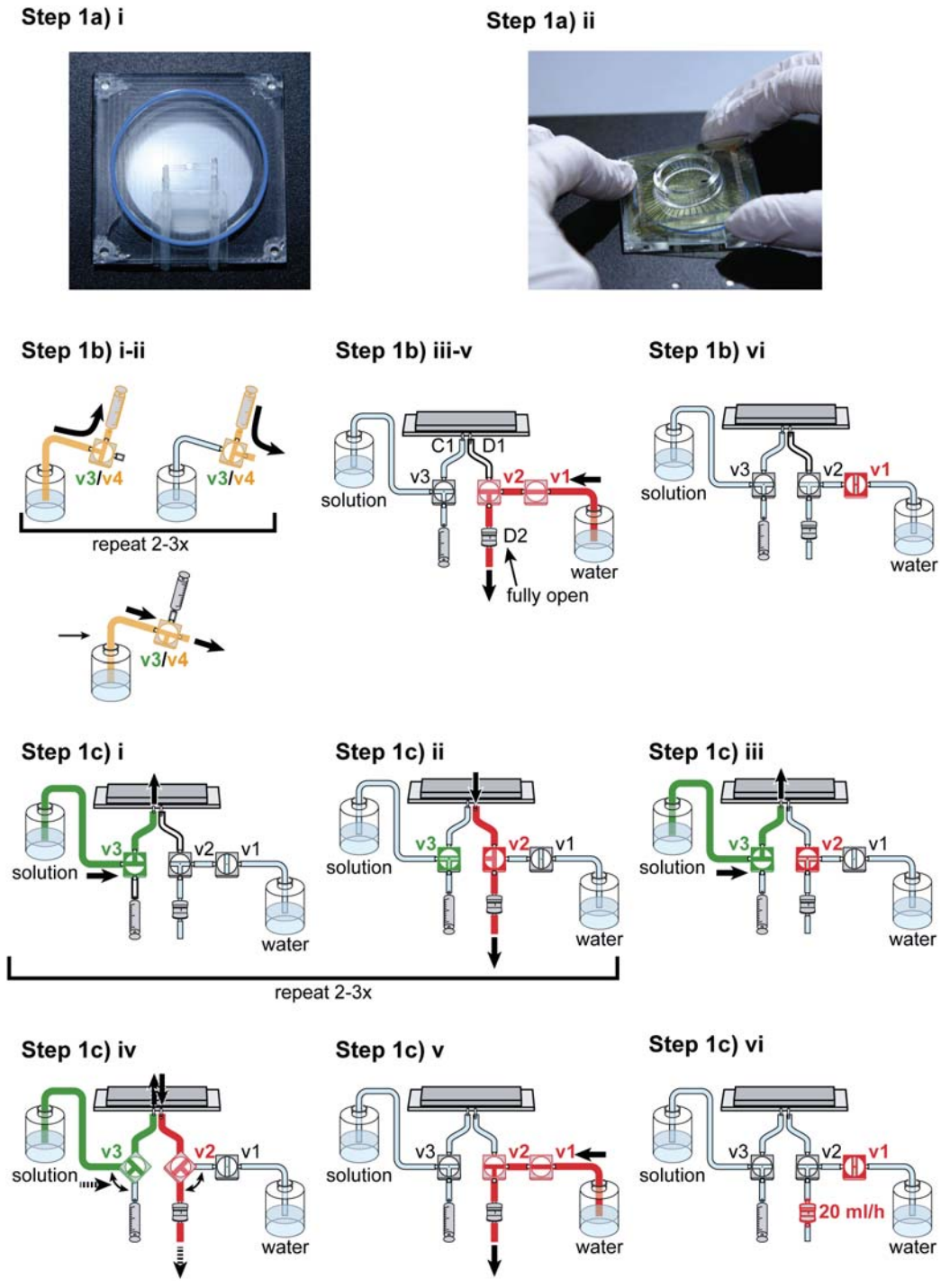
Step 1a) i
Step 1a) ii
Step 1b) i-ii
v3/v4
v3/v4
repeat 2-3x
v3/v4
Step 1b) iii-v
C1
D1
v3
v2
v1
solution
D2
water
fully open
Step 1b) vi
v3
v2
v1
solution
water
Step 1c) i
v3
v2
v1
solution
water
Step 1c) ii
v3
v2
v1
solution
water
repeat 2-3x
Step 1c) iii
v3
v2
v1
solution
water
Step 1c) iv
v3
v2
v1
solution
water
Step 1c) v
v3
v2
v1
solution
water
Step 1c) vi
v3
v2
v1
solution
20 ml/h
water

Figure 3. Experimental procedure Step 1: Filling of MEA chamber. Step 1a) Placing the MEA chamber on the baseplate. **Step 1b)** Preparation of perfusion and vacuum. **Step 1c)** Filling the MEA. Detailed description is given in the text.
doi:10.1371/journal.pone.0106148.g003

- Ag/AgCl pellet reference electrode (Science Products E-201ML)
- Insulated connector (e.g. wire ferrule with shrink-on tube) and optical shield (shrink-on tube) for reference electrode
- Holder for reference electrode
- Pharmacology: 50 µM L-AP4 (Sigma A7929 or Abcam ab120002), 10 µM NBQX (disodium salt, Tocris 1044), 10 µM RS-CPP (Tocris 0173) to block synaptic transmission to bipolar cells, 100 µM $BaCl_2$ (Sigma 342920) to block glial currents [15]

Other. Nitrocellulose filter papers (e.g. 13 mm diameter, 0.45 µm pore size, cat. no. HAWP01300, Merck Millipore, Billerica, USA).

Experimental Procedure

Step by step instructions

All specifications (e.g. flow control settings) are given for the equipment listed above and might have to be adjusted for different equipment. Although the procedure is explained for the 60-electrodes pMEA by Multi Channel Systems in combination with a MEA1060 amplifier, most steps could be transferred to experiments with other perforated MEA systems. For *in vitro* ERG recordings, most steps remain the same. Necessary adaptations and additional steps can be found in the section "Special considerations for *in vitro* electroretinogram recordings".

Setting up for pMEA recordings (including retina preparation and hardware preparation) takes approximately 40–60 minutes depending on the complexity of the setup and the visual stimulation. Except for the steps involving the vacuum system and preparation of the filter paper, all steps are very similar to conventional MEA recordings. Further, no coating of the MEA with substances such as poly L-Lysin (used to fix the retina on non-perforated MEAs) is necessary for pMEA recordings. Overall, pMEA recordings require about 10 minutes more preparation time than conventional MEAs.

IMPORTANT: Whenever negative pressure is applied to the MEA chamber, make sure that this is either for only a very short time or that you are perfusing with fresh solution in parallel. Due to the shape of the MEA chamber and the surface tension of the solution, the solution level in the middle of the chamber – directly above the perforated membrane – is significantly lower than at the edges of the chamber (see inset in Fig. 2). Therefore, the MEA chamber always needs to be almost full; otherwise air will enter the vacuum system which can harm the retina and impede the constant negative pressure necessary for stable recordings.

Step 1: Filling of MEA chamber. Illustrated in Figure 3. In this step, the MEA amplifier is prepared, the pMEA is filled with solution, and the vacuum is established. Two aspects are crucial in this step: first, that the MEA baseplate is tightly sealed, and second, that all air bubbles are removed from the perfusion-vacuum system.

a) Place pMEA on MEA baseplate

i. Place a rubber ring in the notch of the MEA baseplate.

IMPORTANT: Make sure that the ring is placed firmly in the notch

ii. Carefully place a clean and dry pMEA onto the ring. To do so, first place one edge of the MEA against the elevated edge of the MEA holder and then lower the MEA down onto the holder.

NOTE: By default, electrode number 15 is the reference electrode. Depending on the MEA amplifier this can be more or less easily changed. If you want to use the standard settings, make sure that the big reference electrode of the MEA is connected to recording pin 15 of the amplifier. This is achieved by placing the MEA with its reference electrode pointing to the right.

iii. Carefully touch the MEA chamber and try to move it: it should not move if it is placed correctly, otherwise it might wobble on the rubber ring.

iv. Close the amplifier.

b) Prepare perfusion and vacuum tubing

i. Upper perfusion: Wash and fill the tubing with physiological solution by the use of the syringe. Start gravity flow and then close the valve (v4). Do not yet connect it to the MEA chamber.

ii. Lower perfusion: Wash and fill the tubing of the lower perfusion in the same way. Close the valve

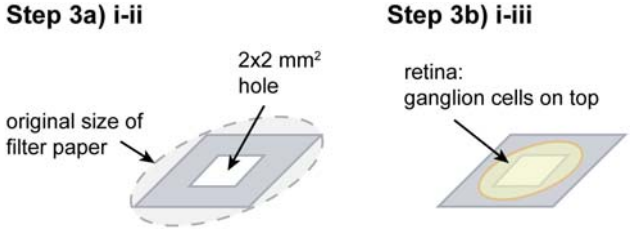

Figure 4. Experimental procedure Step 3: Fixation on filter paper. Step 3a) Preparation of filter paper. **Step 3b)** Fixation of retina on filter paper. Details are given in the text.
doi:10.1371/journal.pone.0106148.g004

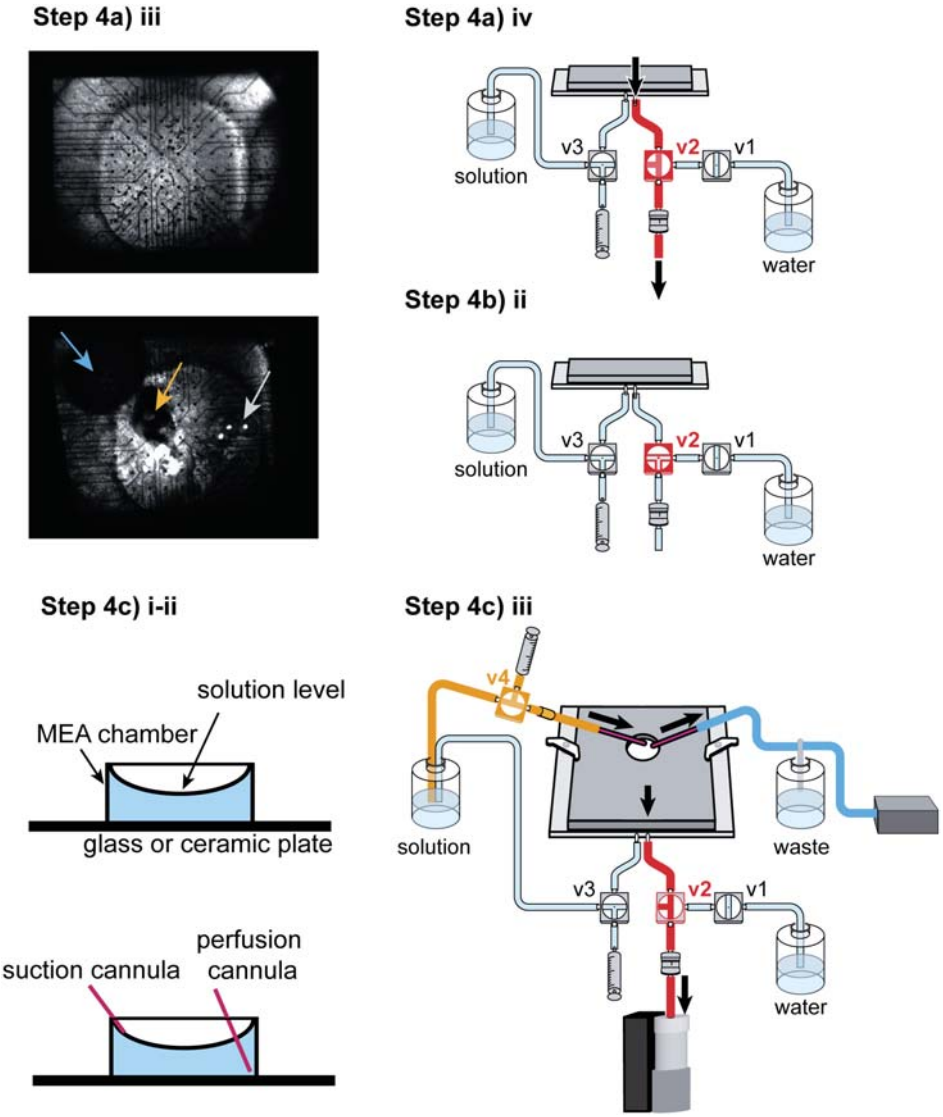

Figure 5. Experimental procedure Step 4: Transfer of retina to MEA chamber and setup. Step 4a) Placing the retina on the electrodes. **Step 4a) iii:** Top: Good MEA preparation. All electrodes are clearly visible; the retina looks homogeneous, flat, and without tears or holes. The retina and filter paper are nicely centered over the middle of the electrode array. Bottom: Bad MEA preparation with air bubble (blue arrow) and holes due to excessive negative pressure (gray arrow). Further, the filter paper is shifted towards the upper left corner. Orange arrow: optic nerve head. **Step 4b)** Transfer of MEA amplifier to setup. **Step 4c)** Installation of upper perfusion loop. Details are given in the text.
doi:10.1371/journal.pone.0106148.g005

(v3) so that no solution flows into the MEA chamber.

iii. Connect the lower perfusion to the left (shorter) cannula of the MEA baseplate and the vacuum tube to the right (longer) cannula.

iv. Set the valves so that the connection of the vacuum system to the MEA is closed (v2) but the connection to the water bottle is open (v1). Open the fine flow control (D2) to maximal flow.

v. Place the free end of the tubing into a bottle with water and switch on the constant vacuum pump

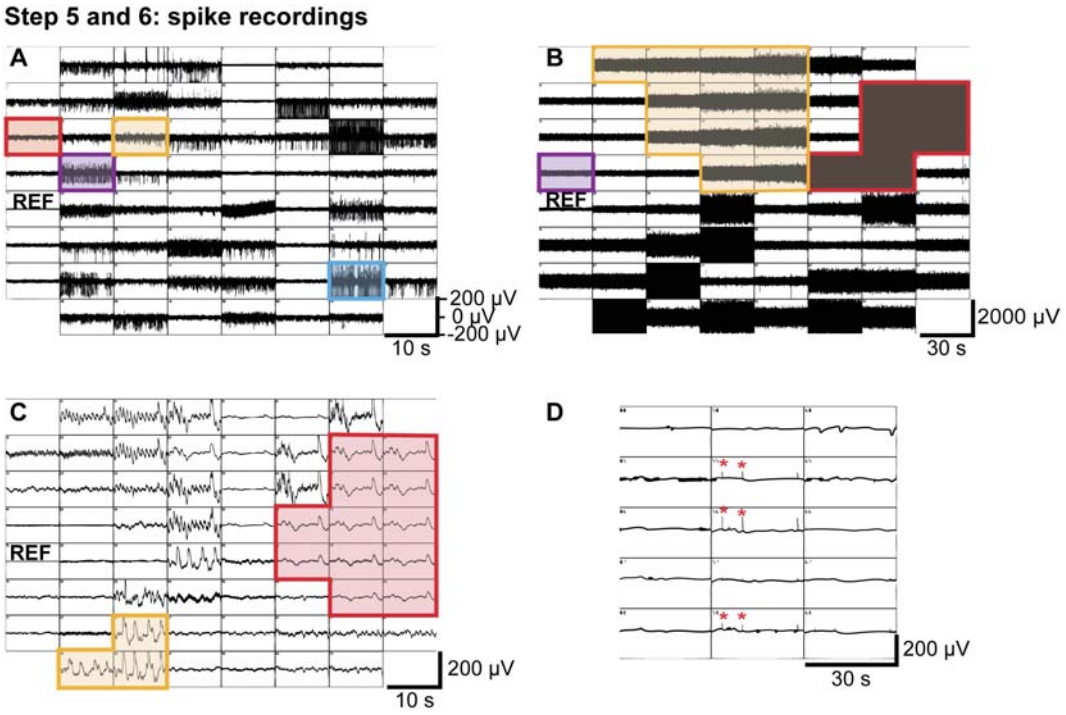

Figure 6. Experimental procedure Steps 5 and 6: Recording data (Spike recordings). A) Snapshot of a 500 Hz high-pass filtered MC_Rack display. Spiking activity with good signal-to-noise is visible on many electrodes. **B)** Snapshot of MC_Rack display after overflow. Noise with amplitudes of 200 to over 1000 µV due to wet electronics is visible on most electrodes. **C)** Snapshot of MC_Rack display several hours after strong overflow. Slow noise on many electrodes is visible either if the electronics is not fully dry yet or when the electronics has been irreversibly harmed. **D)** Snapshot with slow fluctuations and spike-like noise peaks (red asterisks). See text (Step 5 and 6, troubleshooting) for details.
doi:10.1371/journal.pone.0106148.g006

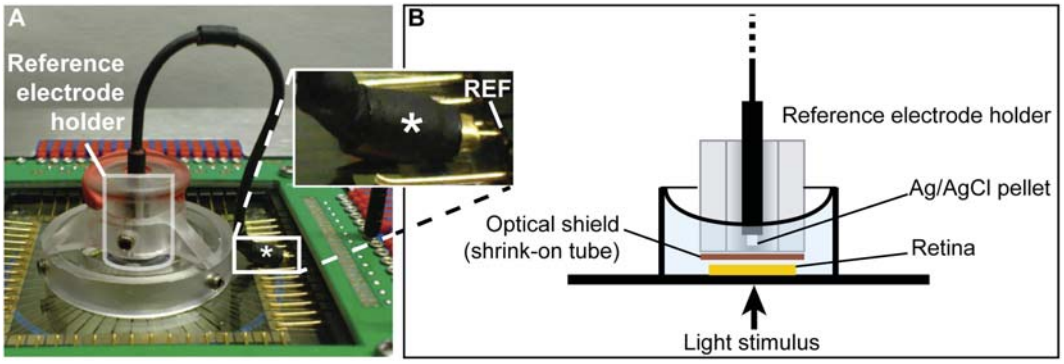

Figure 7. Additional steps for *in vitro* ERG recordings. A) Additions to Step 1: The AgCl reference is positioned over the MEA by a reference electrode holder and is attached to pin 15 (REF) by a wire ferrule insulated by shrink-on tubing (asterisk). **B) Additions to Step 5:** Schematic of the reference electrode and its holder as shown in A. Note the optical shield needed to avoid photoelectric artifacts resulting from light hitting the reference electrode.
doi:10.1371/journal.pone.0106148.g007

(set to ~80–100 mbar). Remove major air bubbles by flicking at connections that might trap air.

vi. When the tubing is filled with water, close the valve towards the water bottle (v1) so that all liquid flow is stopped.

c) Fill the MEA

In this step, the MEA and the cannulas of the MEA baseplate are washed, air bubbles are removed, and the MEA chamber is filled.

i. Fill the MEA by opening the valve of the lower perfusion (gravity flow, v3).

IMPORTANT: Solution should enter the MEA chamber within approximately 1–2 seconds; otherwise the system is most probably not tightly sealed. If it does fill slowly, stop gravity flow immediately, and open the amplifier to prevent the electrode contacts (top plate) from getting wet. See also troubleshooting section 1.

ii. When the MEA chamber is almost full, close the valve of the perfusion (v3). Then open the valve of the vacuum system towards the MEA (v2) and thereby suck out the solution from the MEA chamber. Repeat filling and emptying 2–3 times to wash the MEA chamber.

iii. Fill the MEA chamber again.

iv. Repeatedly open and close the lower perfusion and the vacuum system (alternating) to remove air bubbles from the MEA chamber as well as from the cannulas and the tube connected to the vacuum cannula. Make sure that the MEA chamber does not run empty during this procedure (this will introduce new bubbles) and that it is filled almost completely after having removed all air bubbles. Close the valves to the baseplate (v2, v3).

v. Remove again air bubbles from the tubing by washing through with water (open v1) and "flicking off" air bubbles.

IMPORTANT: Make sure that ALL air bubbles are removed from MEA baseplate cannulas, the MEA chamber, and the vacuum system.

vi. Close all valves and set the fine flow control to approximately 20 ml/h.

NOTE: The setting of the fine flow control determines the negative pressure that will eventually be applied to the retina. The retina will tear and be sucked through the perforation if that pressure is too high.

Step 2: Retina preparation. Prepare the retina as usually for physiology experiments. Pay special attention to removing the vitreous thoroughly in order to get good electrode contact. Further, do not introduce any holes or tears into the retina during preparation, especially when removing the optic nerve. Also do not cut the retina since any incisions or holes in the tissue might cause turbulences in the liquid flow through the perforation or might counteract the establishment of the necessary negative pressure.

Step 3: Fixation on filter paper. Illustrated in Figure 4. The filter paper is needed to flatten the retina without cutting the tissue.

NOTE: Using a filter paper is essential for small retinas with a strong curvature, such as mouse retina. In the case of big retinas (e.g. rabbit, pig, cow, human), a filter paper is often not necessary. Here, the retina is cut into small pieces, which have almost no curvature and which can be placed directly on the electrodes by the use of brushes. Sometimes, even large retinas can roll up after having been cut into small pieces. In this case, a filter paper can be used to flatten the retina.

a) Prepare filter paper

i. Use a piece of a razor blade to cut a ~2×2 mm hole into a filter paper.

ii. Cut the edges of the filter paper.

b) Place retina on filter paper

i. Center the retina with photoreceptors down over the hole in the filter paper.

ii. Carefully press the edges of the retina onto the filter paper with forceps. Start in one corner, and then fix the opposite corner while carefully flattening the retina. You may hold down on the already fixed part with one pair of forceps while fixing the opposite side with a second pair.

iii. Fix the rest of the retina while carefully flattening it.

Step 4: Transfer of retina to MEA chamber and setup. Illustrated in Figure 5.

a) Transfer retina to MEA chamber

i. Transfer the filter paper with the attached retina to the MEA chamber. This is best done with a spoon filled with solution so that the retina is always immersed in solution.

ii. The filter paper should be oriented such that the ganglion cells are facing the electrodes. Usually, this means that the filter paper has to be turned upside down.

iii. Center the retina over the electrodes. You can orient yourself using the layout of the wires connected to the electrodes.

IMPORTANT: Do not use forceps since you might destroy the electrodes or the perforated foil, instead use soft brushes to move the filter paper.

iv. Once the retina is centered, open the valve to the vacuum pump (v2). This will create negative pressure, pull the retina towards the electrodes, and hold it in place.

IMPORTANT: While applying negative pressure, the MEA chamber will slowly run dry. The next step has thus to be performed relatively swiftly.

b) Transfer MEA assembly to setup

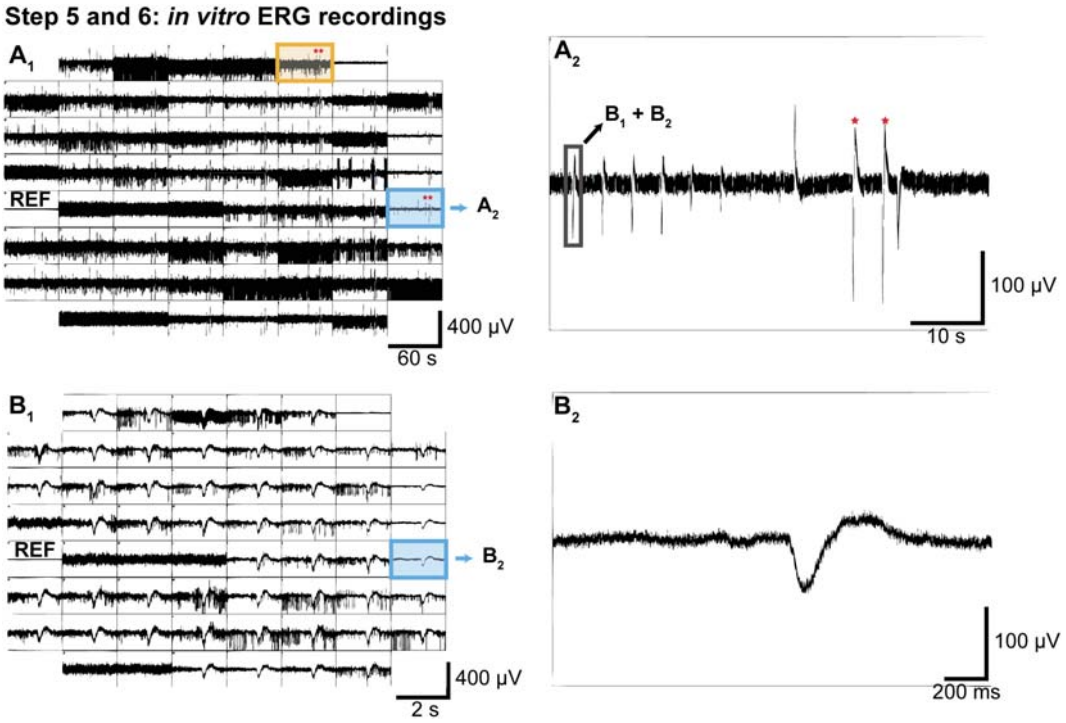

Figure 8. Experimental procedure Steps 5 and 6: Recording data (*in vitro* ERG recordings). A_1) Snapshot of the Longterm Data Display (raw data) from MC_Rack. Note that on most electrodes the ganglion cell spikes mask the *in vitro* ERG responses (e.g. the electrode marked in orange). Only the highest contrast flash elicits a response that is visible on most electrodes (red asterisks), while on some electrodes without ganglion cell spikes the *in vitro* ERG responses are clearly visible (electrode marked in blue). Reference electrode 15 (REF) is on the left. **A_2)** Zoomed view of the electrode marked in blue from panel A_1 showing the responses to flash stimuli of different contrast (highest two contrasts marked with red asterisks). The low-pass filtered data around the time highlighted by the box is shown in B_1+B_2. **B_1)** Data Display with 200 Hz low-pass filter applied. There is a clear response on almost all electrodes. Not all spikes get filtered out by the low-pass filter. Note the different time scale than in A_1. **B_2)** Zoomed view of the electrode marked in blue from panel B_1 that shows a very clear low frequency *in vitro* ERG response without contamination by ganglion cell spikes.
doi:10.1371/journal.pone.0106148.g008

i. If you performed the earlier steps outside of your recording setup, now move the MEA amplifier quickly into the setup and place it in the light path for visual stimulation.

ii. Once the MEA is in place, close the valve to the vacuum pump (v2). The retina is now sticking to the perforated membrane and will not easily move. Nevertheless, you should avoid moving the MEA amplifier while no negative pressure is applied. The vacuum can stay switched off (i.e. valve v2 can stay closed) for the next steps to prevent the MEA chamber from running dry.

c) Installation of upper perfusion loop

i. Add the top perfusion cannula into the MEA chamber. Make sure it is on the bottom and at the edge of the chamber. Placing it on the bottom of the chamber prevents dripping of solution into the bath, which would cause turbulence and noise in the recordings. Placing it into the edge of the chamber helps to prevent touching and damaging the retina.

ii. Add the suction cannula so that its opening is at the desired solution level (as high as possible without risking overflow).

iii. Switch on the top perfusion (v4) and the suction, and open the valve to the vacuum pump (v2).

NOTE: The lower perfusion is not used during the experiment. Flow through the perforation would cause turbulences and hence noise.

IMPORTANT: The flow speed of the upper perfusion has to be at least as fast as the suction speed of the (lower) vacuum pump, otherwise the MEA chamber will run dry. However, it is advisable to have the upper perfusion at a higher speed. The solution level in the MEA chamber will then rise up to the level at which solution is sucked away by the upper suction. Therefore, the cannula of the upper suction has to be placed low enough

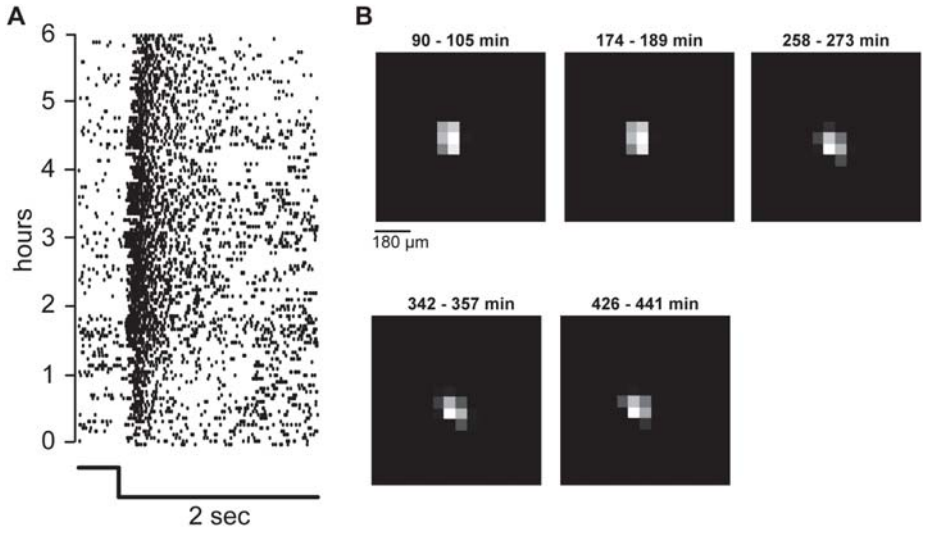

Figure 9. Recording stability. A) Responses of one ganglion cell to a step in contrast over 6 hours. A two second light decrement step has been shown >120 times over a period of 6 hours. Each dot in the raster plot represents one spike produced by the ganglion cell. The ganglion cell stably responded to the stimulus during the whole recording time. Changes in latency and number of spikes are due to different mean brightness levels used during the experiment. **B)** Receptive field of one ganglion cell calculated from checkerboard stimuli. 15×15 checkers out of 40×40 shown here. The stimulus has been repeated approximately every 90 minutes. Time above each receptive field map: presentation time of the checkerboard stimulus (0 min = beginning of experiment). The receptive field location and shape was stable during the whole 8 hours, indicating that the retina did not move significantly.
doi:10.1371/journal.pone.0106148.g009

to prevent overflow on one hand, and high enough to ensure sufficient liquid level.

Step 5: Check electrode contact. Illustrated in Figure 5 and 6. To check the contact of the retina with the electrodes, one can use visual inspection and check the signal-to-noise ratio.

a) Visual inspection

If the retina can be imaged in your setup (e.g., with an infrared camera system), visual inspection of the retina can be used to judge preparation and contact of retina with electrodes (photographs in Fig. 5). Contact with electrodes is usually good if the retina looks flat and if most or all electrodes can be seen through the retina. However, in the region of the optic nerve, the retina is often not totally flat. Now also the visual stimulus can be focused on the photoreceptors and centered on the middle of the electrode field.

b) Setting up MC_Rack software

Consult manuals provided by Multi Channel Systems for installation and setup of MC_Rack for recording of ganglion cell activity. In general, it is advisable to have a Longterm Data Display showing unfiltered activity for each electrode. In addition, it is useful to have a Data Display showing high-pass filtered data, i.e. spiking activity. To implement this, add a filter before the display with a 500 Hz high-pass Butterworth 2nd order filter. See also step 6 (spike recordings) and "Special considerations for *in vitro* electroretinogram recordings".

c) Signal-to-noise ratio

In addition to the *number* of electrodes with activity, the *amplitude* of this activity is crucial for the success of subsequent spike sorting. If the retina is flattened well, all electrodes should show activity (exceptions: those lying directly under the optic nerve, and the ground electrode). When inspecting the high-pass filtered data, the noise level should not exceed 20 µV and spiking activity should have an amplitude of 100–250 µV (signal-to-noise ratio of at least 5; see Fig. 6A). As a rule of thumb, the signal is strong if spiking activity is well visible or even filling the display window when the display y-axis is set to 200 µV; the spikes should be sortable for amplitudes of at least 100 µV. Raw data with smaller activity will most probably not be sortable.

NOTE: Spontaneous activity of ganglion cells can be very sparse in the beginning of the experiment. The retina should always be allowed to settle and adapt to the new environment (negative pressure, change in temperature, …) for at least 20 minutes before recording data. Usually, spontaneous activity appears during this time if it has not been present from the beginning. If there are very few spikes, the retina can be probed with some light stimuli and the elicited spikes can be used to check signal-to-noise ratios. If activity is still sparse and/or signal-to-noise ratio is low, increase the negative pressure slightly by changing the flow control to 30–50 ml/h. Also consult the troubleshooting section for possible counter-measures.

Step 6: Recording data. Illustrated in Figure 6. Spike recordings: In most cases, one uses MEAs to record spiking activity from ganglion cells. As mentioned above, when using the MC_Rack software, it is useful to show the data in two displays while recording: (1) Longterm Display with unfiltered data. Set the display y-axis to 500 µV for good overview. (2) Data Display with high-pass filtered data for better visualization of spiking activity. Add a 2nd order Butterworth 500 Hz high-pass filter before a Data Display and set the y-axis to 100 or 200 µV. Figure 6A shows such

filtered electrodes with the y-axis set to 200 μV. In optimal recordings, all electrodes would have activity with amplitudes such as the electrode marked in "blue". A signal-to-noise ratio and activity level like on the "purple" electrode is also sufficient for good spike sorting. Whether the spikes on the "orange" electrode are sortable will depend on how distinguishable the waveforms of various cells and of the noise are in each particular case. On the "red" electrode, the signal-to-noise ratio is clearly too small. The reference electrode 15 is on the left.

NOTE: Usually, the MEA is placed in the setup such that the vacuum and perfusion cannulas are at the "front" (i.e., facing the researcher). Note that in this configuration the physical reference electrode 15 is on the right side of the MEA chamber and electrodes 15–18, 25–28, 35–38 etc. will be in the upper half of the MEA (60-electrode pMEA, 8×8 layout). The orientation of electrodes in the MC_Rack displays is mirrored compared to that: the reference electrode 15 is on the left, electrodes 11–14, 21–24 etc. are displayed in the top half. Consequently, when showing a stimulus which moves from the top left to the bottom right corner of the MEA chamber, the retinal activity will move from the bottom right to the top left corner of the MC_Rack display.

Step 7: Removing the retina. The retina is a relatively thin tissue. It can thus rarely be removed entirely from the pMEA after the recording. In general, removing the retina works best when the vacuum system is off, the lower perfusion is switched on and the flow is slightly increased via the syringe. Use a very fine brush to help removing the retina from the recording chamber. Subsequent analysis of the tissue (e.g. histological stainings) is only possible if the negative pressure is kept as low as possible during the experiment and if the retina is removed very carefully from the perforated foil. This is easier for thicker (healthy) and bigger (species-dependent) retinas; however, we also performed experiments with very thin and vulnerable degenerated retinas (rd1 mouse model with quickly degenerating rods and cones). Even these retinas could be removed and stained after the recordings when only little negative pressure had been applied during the experiment (data not shown).

Special considerations for *in vitro* electroretinogram (ERG) recordings

Electroretinography (ERG) is the most common electrophysiological technique for recording retinal activity in both human patients and living animals. ERG signals reflect mainly the activity of cells oriented vertically in the retina, namely photoreceptors, bipolar cells and Mueller glia. The pMEA system can be configured to record an *in vitro* electroretinogram. For this, an additional reference electrode is added to achieve a recording configuration in which the retina is "sandwiched" between recording electrode(s) and reference electrode to record transretinal potential changes. Follow all procedures as outlined above for spike recordings and add the following steps:

Step 1a) iii. Place pMEA on MEA baseplate. Illustrated in Figure 7. An external reference electrode has to be attached to recording pin 15 of the amplifier before the next step. A wire ferrule soldered to an Ag/AgCl reference can be used to connect to pin 15. Shrink-on tube around the wire ferrule insulates from the MEA chamber's internal reference contact.

Step 5a) Visual inspection. After the stimulus is centered, the external reference electrode has to be put into the MEA chamber. Placing the reference electrode before this step would obscure the camera's view and make stimulus centering impossible (in configurations like in an upright microscope). It might be necessary to once again remove the upper perfusion/suction to place the reference electrode and reposition it after the external reference is in place. The Ag/AgCl pellet of the reference has to be positioned 2 to 3 mm above the center of the MEA electrode field and optically shielded from direct stimulus illumination to prevent photoelectric artifacts in the reference electrode. The upper suction has to be adjusted such that the solution level is high enough to completely immerse the Ag/AgCl pellet of the reference in the solution. Perforations in the optical shield that allow solution to pass but do not compromise the optical shielding, can help to achieve this. The suction has to be carefully adjusted so the solution level does not fluctuate; otherwise there will be periodic low frequency noise that can spoil the *in vitro* ERG data (see troubleshooting section).

Step 6) Recording data. Illustrated in Figure 8. For *in vitro* ERG recordings, the Data Displays in MC Rack are set up in a similar way as described above, except that the filter setting for the second Data Display is set to low-pass filter. This eliminates some of the ganglion cell spiking responses for clearer visualization of the slow *in vitro* ERG responses. Add a 2nd order Butterworth 300 Hz low-pass filter before the Data Display and set the y-axis to 100 or 200 μV.

In our experiments, synaptic transmission to bipolar cells and glial currents were pharmacologically blocked to isolate the field potentials generated by photoreceptor activity. Figure 8 shows example responses to several flashes with different contrasts (panels A) and a close-up view of a single flash response (panels B) from a good *in vitro* ERG recording.

Troubleshooting

Due to the two perfusion loops, solution leakage or overflow is encountered more often than with standard MEAs. Thus, most issues encountered during pMEA recordings will be linked to electronics which got in contact with solution, and will be recognizable in the noise level of the electrodes. In this troubleshooting section we discuss the 10 most frequent problems. The titles indicate the main aspect which will be noticed during MEA recordings. Each issue is then followed by a description of its possible causes, the detailed symptoms which can be observed, and the required actions.

1. MEA chamber fills very slowly during Step 1c) i. Possible cause (1): Leakage due to insufficient seal between MEA chamber and the baseplate (Step 1a) i). The solution from the lower perfusion can fill the space between the MEA chamber and the MEA baseplate, rather than being pushed quickly through the perforation.

Detailed symptoms (1): A long delay is observed between opening the lower perfusion and filling of MEA chamber.

Required actions (1): Immediately stop lower perfusion! Open the MEA amplifier immediately in order to prevent the solution from reaching the recording pins of the amplifier. MEA baseplate and the rubber ring should be dried completely and the MEA chamber should be placed again such that it does not move. Minor leakages are hard to detect while filling the MEA chamber and will reach the recording pins only later during the recording. These slow leakages are, however, very rare.

Possible cause (2): Mishandling of the MEA chamber (e.g. applying a relatively large force) can weaken the seal between MEA ring (forming the wall of the chamber) and MEA glass plate. This can introduce local gaps in the glue between wall and floor of the MEA chamber from where the solution can leak.

Detailed symptoms (2): A high latency is observed between opening the lower perfusion and filling of MEA chamber. Solution usually leaks from a specific region where the seal is weak.

Required actions (2): Immediately stop lower perfusion! Open the MEA amplifier immediately to avoid solution reaching

the recording pins. Experiment cannot be continued with this MEA chamber which should be sent to Multi Channel Systems for maintenance.

NOTE: Often the leak is not detected while filling the MEA but is reflected later in the signal as noise on a group of electrodes.

2. Noise observed on (almost) all electrodes. Possible cause: Overflow or leakage due to badly adjusted upper perfusion, negative pressure and suction. In this case the MEA chamber can either run dry, thereby damaging the tissue and introducing turbulences, or it can overflow and solution can reach the recording pins.

Detailed symptoms: Overflow or leakage lead to high amplitudes of noise in most of the recording electrodes, specifically the recording pins that are in contact with the solution. Figure 6B shows such a case. As visible in these traces, some electrodes are affected so strong (marked in red) that the noise is filling the whole display even when setting the y-axis to 1000 μV. But even on the electrode marked in purple the noise level is much higher than usual with amplitudes of around±200 μV. Often, distinct groups of electrodes have similar noise patterns (here one group in red and one in orange). This can be caused by "local" leakage/ overflow when only some of the pins have become wet. Alternatively, even when all pins are wet, the solution might seep into the electronic housing with different speeds and might thus affect the electronics of different channels with different delay.

Required actions: In the case of overflow, the recording should be stopped and the MEA amplifier should be removed immediately. If overflow was detected as soon as it started, the recording pins should be dried and carefully cleaned with a wet cotton swab (deionized water and/or alcohol). A tissue paper can be used to suck out solution from the small openings where the recording pins are connected to the MEA amplifier. If the overflow was detected at a later stage, a relatively large amount of solution could have entered the MEA amplifier. The whole amplifier should be placed in deionized water for several hours to wash out the salts, after which it requires 1–2 days to dry. The amplifier should then be tested using the model probe supplied with the amplifier. If the signal from the amplifier appears noise free (less than 20 μV amplitude) and does not show any slow fluctuations, it should be tested with a MEA chamber (filled with PBS or other physiological solution). If the electronics are not completely dry, localized slow noise waves, again affecting subgroups of electrodes (Fig. 6C: one group in red, one in orange), can be detected. However, if this noise persists after 2–3 days, most probably not all salts were washed out which possibly harmed the electronics. In such case, the MEA amplifier needs to be submitted to Multi Channel Systems for maintenance.

3. Stable high frequency noise on one or several electrodes. Possible cause: One or several electrodes are deteriorated either due to frequent and/or long-term use. Alternatively, they can also be harmed by use of forceps during placing or removing the retina.

Detailed symptoms: In contrast to noise caused by overflow, deteriorated electrodes often show very stable high frequency noise. Even if only one electrode is affected, the noise might spread to neighboring electrodes.

Required action: Refer to manuals provided by Multi Channel Systems for hardware or software based grounding of the affected electrodes.

4. Fluctuations/noise on a group of electrodes. Possible cause (1): Air bubbles under the retina, either above or below the perforated foil, can lead to significant noise levels. These bubbles usually arise either when air is trapped in the perfusion tubing or when the solution level in the MEA chamber becomes too low.

Detailed symptoms (1): Due to the continuous negative pressure, such air bubbles – once they are trapped in the MEA chamber – move around, change in size, and might disappear and reform constantly. They can easily be recognized when imaging the retina in the MEA chamber (Fig. 5, Step 4a) iii). These bubbles can often induce big voltage fluctuations on several electrodes, can cause large noise amplitudes or inhibit contact between solution/ tissue and electrodes (electrode traces are flat, as if connected without solution and retina).

Required Action (1): If air bubbles are caused by too little solution in the MEA chamber, the chamber should be filled immediately by increasing the flow speed of the upper perfusion and/or moving the suction cannula further up. If the bubbles do not disappear, the following two counter-measures can be applied:

i. *Increasing the negative pressure (short term)*

Increasing the negative pressure might "suck out" the air bubbles through the perforation. Make sure that your perfusion is fast enough so that the solution level does not drop again. Watch the retina closely to not increase the negative pressure too much, which might tear or destroy the retina. Try switching back to lower negative pressure once the air bubbles are removed.

ii. *Opening the lower perfusion*

Opening the lower perfusion can push out air bubbles from the space between retina and electrodes into the MEA chamber. This is often more effective when no negative pressure is applied; however, care should be taken not to wash away the retina.

Parallel application or quickly alternating the above mentioned measures can sometimes facilitate removal of the bubbles. It is advisable to image the retina and to observe noise levels and activity on the electrodes during this process.

NOTE: Air bubbles often cannot be removed and the experiment has to be stopped. The described measures are only advisable before recording data since the turbulences caused by the air bubbles as well as by the counter-measures will move the retina and might change the footprint of the recorded cells on the MEA electrodes.

Possible cause (2): Starting overflow or leakage due to incoherent upper perfusion, negative pressure and suction.

Detailed symptoms (2): As the overflow/leakage starts, only a group of electrodes is affected. In contrast to deteriorated electrodes, the noise is often a mixture of low and high frequencies and might show large fluctuations.

Required actions (2): Immediately stop the experiment and open the MEA amplifier. Check troubleshooting point 2 for further procedures.

5. High baseline noise on all electrodes. Possible cause: Poor grounding of the upper perfusion or suction system.

Detailed symptoms: Noise levels above 20 μV on all electrodes. Usually without big fluctuations.

Required actions: Refer to manuals provided by Multi Channel Systems for improving grounding.

6. Synchronous spike-like activity on all or a group of electrodes. Possible cause: Poor grounding of the upper perfusion can lead to spike-like activity (see Fig. 6D).

Detailed symptoms: Synchronous, regular, and sparse high frequency noise is observed on a group or all electrodes e.g. due to regular dripping of solution from the perfusion system.

Required actions: Check manuals provided by Multi Channel Systems for improving grounding.

7. Low signal-to-noise ratio. Possible cause: Poor retina preparation and placement or insufficient negative pressure can often lead to low signal-to-noise ratio.

Detailed symptoms: Spiking activity is visible, but very small.

Required actions: Once the retina is placed in the MEA chamber, contact can only be improved by increasing negative pressure. The flow control should not be set to values higher than 40–60 ml/h (depending on the species and retina condition). However, short term application of higher pressure (up to 100 ml/h flow) might increase signal-to-noise ratio. The negative pressure should not be changed during the recordings since it can move the retina and change the footprint of the recorded ganglion cells.

NOTE: During retina preparation, the vitreous should be completely removed from the retina and the retina should be properly flattened and carefully fixed on the filter paper.

8. Retina is suddenly out of focus (when imaging from top). Possible cause: The solution level is rising due to too fast upper perfusion or impaired suction.

Detailed symptoms: In the beginning of the experiment, while letting the retina settle down, the retina appears suddenly out of focus when imaged from top (sudden blurring of the camera image).

Required actions: Immediate adjustment of upper perfusion, suction, and/or negative pressure prevents overflow in this case. Noise levels have to be observed carefully to ensure that the solution does not reach the recording pins.

NOTE: The described procedures refer to very sudden blurring in the first 10–20 minutes after switching on the perfusion system. After many hours of recording, the solution level might have changed slightly so that the retina appears out of focus. In this case, usually no counter-measure is required.

9. Low frequency noise on some or all electrodes 1–2 days after overflow. Possible cause: Following an overflow, the electronics in the amplifier needs 1–2 days to dry completely. Low frequency noise indicates that either the electronics is not yet completely dry or that it has been harmed from salts.

Detailed symptoms: Slow noise waves, often affecting subgroups, are visible on most or all electrodes (Fig. 6C: one group in red, one in orange).

Required actions: The amplifier should be left to dry for an additional day. However, the noise can still persist after 2–3 days if not all salts were washed out which possibly harmed the recording pins or the electronics. In such case, the MEA amplifier needs to be submitted to Multi Channel Systems for maintenance.

10. Noise during ERG recordings. Possible cause: The external reference electrode is very sensitive to fluid level changes in the MEA chamber. Periodic fluctuations of the fluid level can be caused by use of a peristaltic pump for perfusion or, more importantly, by intermittent interruptions in the suction stream. This is usually caused by periods of rapid suction of solution until the fluid level drops below the suction cannula opening, followed by no solution being sucked out until the fluid level gets high again.

Detailed symptoms: Simultaneous high amplitude signals on most electrodes that often appear in regular intervals of up to tens of seconds. The noise signals can resemble ERG responses or look like spikes but can also have less stereotypical shape. Sometimes the noise signals look similar to sinusoidal 50 Hz noise.

Required actions: Adjust the depth and angle of the suction cannula. Ideally, an uninterrupted suction stream should be achieved that sets the fluid level in the MEA chamber such that the external reference electrode is fully immersed in solution at all times. This might require several adjusting steps and longer waiting times until the solution level stabilizes, and changes to the suction cannula might be necessary.

Anticipated results

pMEAs provide good signal-to-noise ratios

The vacuum applied through the perforation of pMEAs greatly enhances the contact between the tissue and the electrodes. In our experience, on good recording electrodes, we can detect and properly spike-sort one to three cells per electrode. On some electrodes, no spikes might be visible because blood vessels or the optic nerve lie on these electrodes. Our pMEAs have 59 recording electrodes. After multiple experiments, some electrodes might deteriorate and might not be usable anymore due to increased electrical noise. Good signal-to-noise ratios are crucial for most spike sorting algorithms since they usually depend on amplitude and principal component analysis of the recorded spikes. To get an estimate of the number of recorded cells that one might expect in such experiments, we counted the number of extractable cells in 153 recordings from mouse retina (without pre-selecting "good" and "bad" experiments), and found on average 38 ± 18 cells (median $\pm$ standard deviation) with 6 sorted cells in the worst and 110 cells in the best case. Pig (domestic and minipig) and human retina recordings often had even better signal-to-noise ratios and therefore lead to more sortable cells. In pig retina, we found on average 48 ± 31 cells (range: 13–109, $n = 20$ retinal pieces), and in human retina 51 ± 32 cells (range: 6–154, $n = 35$ retinal pieces).

pMEAs allow stable long-term recordings

Nutrient and oxygen supply is crucial for the survival of ganglion cells. If ganglion cells do not receive enough oxygen and nutrients, their responsiveness might change and/or decrease over time which leads to instability of light responses in long-term recordings. During conventional MEA experiments, the supply to the ganglion cell might be insufficient. It has been shown by Egert et al. that with pMEAs, the oxygenation of the bottom layer cells is greatly enhanced, and it can be assumed that the same is true for nutrient supply to these cells [8]. We additionally show the viability of the ganglion cells by example data from a long-term recording. We showed various light stimuli to a mouse retina on a pMEA during 6 hours and recorded ganglion cell responses. A very simple stimulus – namely a full-field step in contrast – was part of the stimulus set and has been presented over 120 times during these 6 hours. Fig. 9A shows the responses of one ganglion cell to all these repetitions. As visible in the raster plot (every dot represents one spike), the cell responded to every repetition of the stimulus, also after 6 hours of continuous recording. The differences in response latencies are due to switches in absolute brightness which have been part of the stimulus protocol.

pMEAs prevent movement of retina

The third advantage of applying negative pressure to the retina is that movement of the tissue is prevented. We recorded ganglion cell responses to binary checkerboard stimuli to calculate receptive fields and to visualize tissue movement. The checkerboard stimulus consisted of 40×40 checkers with 60 µm edge length. Fig. 9B shows the spatial receptive field of a single ganglion cell, repeatedly calculated from 15 min of checkerboard stimulus, presented every 90 minutes during this 8 hour recording. Location and shape of the calculated receptive fields are very stable. Note that slight changes in shape are also due to different absolute brightness levels used at each presentation (from scotopic to photopic).

Conclusions

In this article we provide a step-by-step procedure for retina recordings with perforated MEAs. Although the preparation and adjustment of the additionally required perfusion and vacuum system might seem complicated at a first glance, the additional time required for perforated compared to conventional MEA recordings amounts to only around 10 minutes. Further, little additional material is needed when switching from standard to perforated MEA recordings. Finally, pMEAs provide better oxygenation of ganglion cells which allows for long-term recordings, and the applied negative pressure facilitates flattening and placement of small retinas with strong curvature. Especially when isolating single cell responses from MEA recordings, the user will appreciate the resulting high signal-to-noise ratio in pMEA recordings.

Acknowledgments

We thank the University Eye Hospital Tübingen, Germany for support and organization of human retina donations; the Department of Experimental Surgery, Tübingen, Germany (Dr. Martin Schenk) for providing us with domestic pig eyes, and the Department of Urology, Tübingen, Germany (Dr. Martin Vaegler) for Göttingen minipig eyes. Further, we thank Prof. Vladimir Kefalov (Washington University, St. Louis, MI, USA) for his advice while establishing in-vitro ERG recordings.

Author Contributions

Conceived and designed the experiments: KR AT HS TAM. Performed the experiments: KR AT HS MM. Analyzed the data: KR AT HS MM BB TAM. Contributed reagents/materials/analysis tools: KR AT HS MM BB TAM. Contributed to the writing of the manuscript: KR AT HS SI MM BB TAM.

References

1. Meister M, Pine J, Baylor DA (1994) Multi-neuronal signals from the retina: acquisition and analysis. Journal of neuroscience methods 51: 95–106.
2. Zeck GM, Masland RH (2007) Spike train signatures of retinal ganglion cell types. The European journal of neuroscience 26: 367–380.
3. Frey U, Egert U, Heer F, Hafizovic S, Hierlemann A (2009) Microelectronic system for high-resolution mapping of extracellular electric fields applied to brain slices. Biosensors & bioelectronics 24: 2191–2198.
4. Chichilnisky EJ, Kalmar RS (2002) Functional asymmetries in ON and OFF ganglion cells of primate retina. The Journal of neuroscience: the official journal of the Society for Neuroscience 22: 2737–2747.
5. Segev R, Goodhouse J, Puchalla J, Berry MJ 2nd (2004) Recording spikes from a large fraction of the ganglion cells in a retinal patch. Nature neuroscience 7: 1154–1161.
6. Masland RH (2001) The fundamental plan of the retina. Nature neuroscience 4: 877–886.
7. Feitl M, Stett A, Nisch W, Boven KH, Möller A (2006) On Micro-Electrode Array Revival: Its Development, Sophistication of Recording, and Stimulation. In: Taketani M, Baudry M, editors. Advances in Network Electrophysiology: Using Multi-Electrode Arrays.
8. Egert U, Okujeni S, Nisch W, Boven KH, Rudorf R, et al. (2005) Perforated Microelectrode Arrays Optimize Oxygen Availability and Signal-to-Noise Ratio in Brain Slice Recordings. Mikrosystemtechnologie Kongress. Freiburg.
9. Gonzalez-Sulser A, Wang J, Motamedi GK, Avoli M, Vicini S, et al. (2011) The 4-aminopyridine in vitro epilepsy model analyzed with a perforated multi-electrode array. Neuropharmacology 60: 1142–1153.
10. Gonzalez-Sulser A, Wang J, Queenan BN, Avoli M, Vicini S, et al. (2012) Hippocampal neuron firing and local field potentials in the in vitro 4-aminopyridine epilepsy model. J Neurophysiol 108: 2568–2580.
11. Grosser S, Queenan BN, Lalchandani RR, Vicini S (2014) Hilar somatostatin interneurons contribute to synchronized GABA activity in an in vitro epilepsy model. PLoS One 9: e86250.
12. Motamedi GK, Gonzalez-Sulser A, Dzakpasu R, Vicini S (2012) Cellular mechanisms of desynchronizing effects of hypothermia in an in vitro epilepsy model. Neurotherapeutics 9: 199–209.
13. Schmidt SL, Chew EY, Bennett DV, Hammad MA, Frohlich F (2013) Differential effects of cholinergic and noradrenergic neuromodulation on spontaneous cortical network dynamics. Neuropharmacology 72: 259–273.
14. Multi Channel Systems MCS GmbH (2013) 60pMEA200/30iR-Ti.
15. Bolnick DA, Walter AE, Sillman AJ (1979) Barium suppresses slow PIII in perfused bullfrog retina. Vision Res 19: 1117–1119.

Publication 4

Alexandra Tikidji-Hamburyan*, Katja Reinhard*, Hartwig Seitter, Anahit Hovhannisyan, Christopher A Procyk, Annette E Allen, Martin Schenk, Robert J Lucas, Thomas A Münch (2015) Retinal output changes qualitatively with every change in ambient illuminance. ***Nature Neuroscience*** **18(1):66-74.**
***equal contributions**

Framework: Here we studied how ambient brightness affects the output of the retina. It is an original research paper in collaboration with the lab of Rob Lucas (University of Manchester) for in-vivo LGN recordings and with Martin Schenk (Experimental Surgery Department, Tübingen) for pig retina recordings.

My contributions: I took this project over from ATH after she finished her PhD. I tested several aspects to confirm and further characterize the basic finding. For this I planned and performed many of the multi-electrode array recordings, and established and performed the related data analysis (in some cases together with ATH and/or TAM). These aspects include stability of the phenomenon (Fig. 5, experiments and analysis), center-surround effects (Fig. 8, experiments and analysis), photoreceptor influence (Suppl. Fig. 4, experiments and analysis), species specificity (pig data in Suppl. Fig. 5, experiments and analysis), behavior in response to complex stimuli (Suppl. Fig. 3, some experiments), and inhibitory effects (Suppl. Fig. 2, experiments and analysis). Further I helped with analysis of the in-vivo data and wrote the manuscript together with TAM and ATH.

Other contributions: ATH started the project and described the basic findings in her doctoral thesis. She performed the wild-type experiments (Fig. 2-4) and was involved in data analysis of my follow-up experiments. HS performed multi-electrode array recordings and helped with data processing. HS and TAM performed and analyzed single-cell recordings and immunohistochemistry (Fig. 6). In-vivo recordings (Fig. 7) were designed by CAP, AEA, and RJL, conducted by CAP and AEA, and analyzed by CAP and AEA together with me. AH performed some multi-electrode array recordings; MS provided pig eyes. ATH, TAM, and I wrote the manuscript with the help of HS, CAP, AEA, and RJL.

ARTICLES

nature neuroscience

Retinal output changes qualitatively with every change in ambient illuminance

Alexandra Tikidji-Hamburyan[1,4,5], Katja Reinhard[1,5], Hartwig Seitter[1], Anahit Hovhannisyan[1], Christopher A Procyk[2], Annette E Allen[2], Martin Schenk[3], Robert J Lucas[2] & Thomas A Münch[1]

The collective activity pattern of retinal ganglion cells, the retinal code, underlies higher visual processing. How does the ambient illuminance of the visual scene influence this retinal output? We recorded from isolated mouse and pig retina and from mouse dorsal lateral geniculate nucleus *in vivo* at up to seven ambient light levels covering the scotopic to photopic regimes. Across each luminance transition, most ganglion cells exhibited qualitative response changes, whereas they maintained stable responses within each luminance. We commonly observed the appearance and disappearance of ON responses in OFF cells and vice versa. Such qualitative response changes occurred for a variety of stimuli, including full-field and localized contrast steps and naturalistic movies. Our results suggest that the retinal code is not fixed but varies with every change of ambient luminance. This finding raises questions about signal processing within the retina and has implications for visual processing in higher brain areas.

The mammalian visual system functions over a wide range of light intensities, spanning roughly a dozen orders of brightness magnitude. Specialized photoreceptors, the rods and cones, are active at low and high light intensities, respectively. At low light intensities, only rods are active (scotopic vision). With increasing luminance, cones become active (mesopic vision), while at high luminance, rods saturate but cones remain active (photopic vision). In the outer retina, signals from the photoreceptors are both combined within and distributed across more than ten different bipolar cell types. In the inner retina, the bipolar cell terminals interact with amacrine cell interneurons to bring about sophisticated responses in the output neurons of the retina, the ganglion cells. The diversity of ganglion cells is characterized by physiological parameters[1], as well as by functional specifications such as directional selectivity, approach sensitivity, object motion sensitivity and many more[2]. On a simpler level, all ganglion cells can be classified by their response polarity to step-like changes in brightness: ON cells increase spiking activity to light increments, OFF cells to light decrements, and ON-OFF cells to both. This property is often called "polarity" and is one of the most basic features for further classification of ganglion cells in the vertebrate retina.

It is not well understood how the properties of ganglion cell responses (that is, the retinal output) vary with changes in ambient luminance. On one hand, it is conceivable that adaptation in retinal circuitry counteracts the changes in ambient luminance to maintain a stable representation of the incoming visual scene. On the other hand, several reports suggest that the retinal output changes with changing ambient luminance. Some of these changes are linked to the switch from scotopic to mesopic vision; that is, from purely rod-mediated to mixed rod- and cone-mediated signaling. Examples include color vision[3], changing responses due to surround activation[4–6], changes in temporal and spatial frequency processing[7,8], 2-amino-4-phosphorobutanoic acid (APB)- and strychnine-resistant OFF responses appearing in response to dim high-contrast stimuli[9], or luminance-dependent inhibitory modulation of rod signals[10]. In addition, the coexistence of several parallel rod pathways[11] might allow different retinal processing within the scotopic range as well: for example, the primary rod pathway shifts from encoding of single photons to encoding of contrast modulations[12]. Furthermore, light adaptation switching from circuit-based to photoreceptor-based mechanisms has been found within both scotopic[13] and photopic regimes[14]. Finally, melanopsin-driven changes in retinal responses have been described within the photopic range[15]. Most of these reports concentrate on individual building blocks of the retinal circuit, and each describes luminance-dependent changes over a limited range of light intensities. What is missing is a systematic description of the retinal output and its modulation across a wide range of light intensities, from scotopic to photopic light levels.

We asked whether luminance-dependent changes of the responses of ganglion cells are a widespread phenomenon or whether they are restricted to few cell types or specific luminance transitions. Using multielectrode array (MEA) recordings from isolated mouse retina, we systematically surveyed ganglion cell responses across many orders of ambient luminance, in discrete steps separated by 1 log unit. We found that the output of the retina was qualitatively different at each tested light level. For example, we found OFF cells gaining or losing ON responses, and vice versa. Such response changes occurred

[1]Retinal Circuits and Optogenetics, Centre for Integrative Neuroscience and Bernstein Center for Computational Neuroscience, University of Tübingen, Tübingen, Germany. [2]Faculty of Life Science, University of Manchester, Manchester, UK. [3]Department for General, Visceral and Transplant Surgery, Institute for Experimental Surgery, University Hospital Tübingen, Tübingen, Germany. [4]Present address: Department of Neurosurgery and Hansen Experimental Physics Laboratory, Stanford University, Stanford, California, USA. [5]These authors contributed equally to this work. Correspondence should be addressed to T.A.M. (thomas.muench@cin.uni-tuebingen.de).

Received 25 August; accepted 28 October; published online 8 December 2014; doi:10.1038/nn.3891

to both simple stimuli and complex natural movies. Sometimes, but not always, these changes depended on modifications of the center-surround receptive field structure or on GABA-mediated inhibition. Consequently, diverse mechanisms seem to underlie the response changes in different ganglion cell types. In addition, we show that such alterations of the retinal output are not restricted to the isolated mouse retina but can also be observed *in vivo*, where the changing output of the retina is reflected by changing activity of dorsal lateral geniculate nucleus (dLGN) neurons, and in the retina of another species, the pig. It thus appears that luminance-dependent changes of retinal output are a phenomenon that is preserved across species and that higher visual centers are exposed to these changes.

RESULTS

Experimental procedure

We presented our visual stimuli, grayscale images, to isolated mouse retinas using a digital projector (**Supplementary Fig. 1**). The ambient light level was set by placing neutral density (ND) filters into the light-path, such that the intensity of the stimulus could be attenuated without changing the computer-controlled images presented by the projector. Consequently, the contrast of the stimuli remained constant during the experiment (**Fig. 1a**), independent of the ambient light level. The actual physical intensity of the stimuli associated with each ND-filter is shown in **Figure 1b**. We estimate (see Online Methods) that ND8 and ND7 correspond to scotopic conditions, ND6 weakly activates cones, ND5 is fully mesopic, and ND4 is photopic. Unless otherwise noted, we started our experiments from low intensity (ND8) and increased it in the course of the experiment (that is, from ND8 to ND4 in 1-log-unit steps). The retina was kept at each ambient luminance for 20 to 70 min, and we showed the same set of stimuli at each light level.

With this experimental procedure, we recorded from ganglion cells using MEAs and compared their responses across different ambient light levels, initially using spatially homogeneous contrast steps ('full-field steps') of positive and negative contrast ('white step' and 'black step', ± 66% Weber contrast; **Fig. 1a**). We will refer to increases of a cell's spike rate to light increments (both after the white step onset and black step termination) as ON responses and to increases of a cell's spike rate to light decrements (both after the black step onset and white step termination) as OFF responses.

Luminance-dependent changes of retinal output

To our surprise, most ganglion cells changed their response type (ON, OFF or ON-OFF) at different ambient luminance. The example cell in **Figure 2a** had OFF responses to all light decrements, but its ON responses were not consistent across light levels. First, they were absent at ND8 but present at ND7 to ND4. Second, when present, they occurred with either short or long latency ('early' or 'delayed',

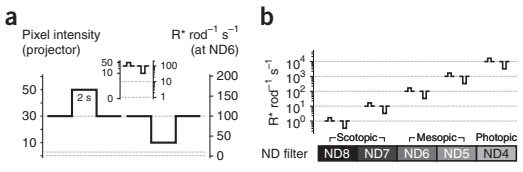

Figure 1 Overview of experimental procedure. (**a**) Light stimuli were grayscale images on a gray background. The full-field step stimulus had a Weber contrast of ± 66%. Inset, stimulus depicted at logarithmic scale. (**b**) Absolute intensity of stimuli, converted to R* rod^{-1} s^{-1}, as a function of the ambient luminance set by neutral density (ND) filters.

respectively), measured as time to peak of the firing rate. Third, at any given light level, the ON responses to the two stimuli (white and black steps) were either the same—that is they were absent (ND8) or had the same latency (ND4)—or they had different latencies (ND7, ND6 and ND5). We will refer to the latter as 'asymmetry' of the response at a given luminance. In summary, the OFF responses of this cell at the different light levels (ND8 to ND4) differed from each other only quantitatively (amplitude, duration and moderate latency changes), whereas the ON responses were affected qualitatively.

We take a 'qualitative change' of a response across light levels to mean not only its presence versus absence, but also alternations between early and delayed responses. Indeed, early and delayed responses, as seen in **Figure 2a**, seem to be two distinct response categories, and not merely separate realizations of a continuous latency distribution. The distributions of the response latencies (**Fig. 2b**), measured separately in ON cells and OFF cells and separately for ON and OFF responses, was unimodal for the preferred contrast—that is, for ON responses in ON cells and for OFF responses in OFF cells—with a median time to peak between 130 and 140 ms. In contrast, the distributions of latencies for responses to the anti-preferred contrast had an additional mode peaking between 600 and 800 ms, in both ON cells and OFF cells. In other words, delayed ON responses occurred only in OFF cells, whereas delayed OFF responses occurred only in ON cells. The bimodality of the distribution indicated two categories of responses and let us treat early and delayed responses as qualitatively different. In our analysis below, we concentrate only on the qualitative response changes. Quantitative aspects were not considered.

The response patterns of ganglion cells usually remained stable while probed at the same luminance level, tested up to 70 min (luminance levels with unreliable responses were excluded from the analysis; see Online Methods). When the response pattern of a cell changed at luminance transitions, the new pattern was observed from the very first stimulus presentation. The earliest time point we tested was 10 s after the luminance transition because a luminance increase by 1 log unit itself evoked a strong response in all cells.

The cell in **Figure 2a** could be classified as OFF at some light levels and as ON-OFF at other light levels on the basis of its full-field step responses. Since such luminance-dependent response changes were common in many ganglion cells, we used an ON/OFF classification based on properties of the cells' linear filters. We calculated the linear filters from responses to Gaussian white noise full-field flicker (see Online Methods). Cells with a downward deflected linear filter were marked as OFF and cells with an upward deflected filter as ON. In contrast to full-field step responses, almost all cells had consistent linear filter polarities over all luminance levels. The cell in **Figure 2a** fell into the OFF category at each light level, despite its changing ON responses. Note that with such a classification scheme, ON-OFF cells will not be categorized as such, but would fall into either the ON or OFF category, depending on which input was predominant; similarly, cells with an exceptionally strong surround might be mistaken for a cell of opposite polarity. Furthermore, if ON and OFF inputs were very well balanced, the cell would have a noisy linear filter. However, such cases were rare, and we excluded from the analysis all cells with noisy or changing linear filters across light levels (34 out of 517 recorded units were excluded).

We obtained 219 OFF and 264 ON cells (as based on their linear filter properties) from 15 wild-type retinas. The validity of this ON/OFF classification approach was supported by the observations that >97.5% of ganglion cells from the ON group consistently responded to light increments (that is, their preferred stimulus) at all light levels and >97.4% of cells from the OFF group consistently

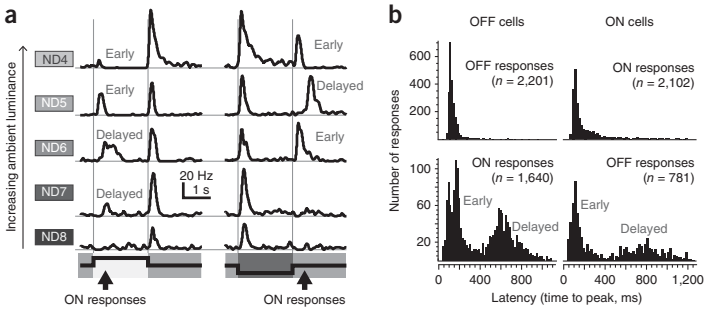

Figure 2 Early and delayed anti-preferred responses. (**a**) Responses (firing rate) of a single OFF ganglion cell to white and black full-field contrast steps (average firing rate to 45 repetitions at each of five different light levels, ND8 to ND4). (**b**) Histogram of response latencies (time to peak) in OFF cells (left column) and ON cells (right column), measured from responses of all units at all light levels, to both black and white full-field steps.

responded to light decrements. It follows that luminance-dependent changes mostly occurred in response to the anti-preferred contrast. In the following analysis, we concentrated on the responses to anti-preferred contrast steps (**Fig. 3**), and we describe the ON responses in OFF cells first.

ON responses in OFF ganglion cells

Across all light levels tested, only 9% of our OFF cells never had an ON response. The number of cells displaying early or delayed ON responses changed at different ambient light levels (**Fig. 3a**). Almost 100% of OFF cells had no ON responses at ND8, whereas at ND5, this number fell below 20%. Notably, the early and delayed responses could also occur together (most often at ND5). They were still easily separable in most cases because of the considerable difference in their latencies (for examples, see **Fig. 4** and **Supplementary Fig. 2**).

At every transition of ambient luminance, the ON responses of a considerable fraction of OFF cells changed (**Fig. 3b**), ranging from 38% at the ND8–ND7 transition (within the scotopic regime) to 83% at the ND6–ND5 and ND5–ND4 transitions. Overall, 89% of the OFF cells changed their responses at least once between ND8 and ND4. The response changes were diverse. At any given light level, some cells would lose a certain response type, others would gain it, and some cells would not change. Furthermore, the responses to white steps and black steps changed asymmetrically (**Fig. 3a**). For example, at ND6 there was a predominance of delayed responses to the white step and early responses to the black step, whereas at ND5 the ratio was opposite.

In summary, the presence of ON responses and their variability across light levels were two prominent features in OFF cells: we found that early and delayed ON responses in OFF cells could appear or disappear with changing ambient light levels, that they could occur independently or together during a response and that they could differ for white and black contrast steps. These findings suggest that these early and delayed ON responses in OFF cells may have independent origins and be heterogeneously affected in different OFF cell types by the immediate stimulus history (that is, white or black step) and by ambient luminance.

OFF responses in ON ganglion cells

Occurrences of OFF responses in ON cells (**Fig. 3c**,**d** for summary, **Fig. 4a**,**b** for examples) were less common than occurrences of ON responses in OFF cells. In fact, most ON cells were strongly suppressed by light decrements, such that their spiking activity fell below their spontaneous firing rates, often to zero. Black steps often suppressed spiking for the entire stimulus duration (2 s); white step termination, for about 500 ms (**Fig. 4a**). Strong pre- or postsynaptic inhibition may have counteracted excitation and decreased the occurrence of the OFF responses. Indeed, there were almost no OFF responses to black steps (**Fig. 3c**), with the exception of the photopic ND4 light level, at which 11% of ON cells had early OFF responses. Delayed OFF responses were observed quite frequently after white step termination, especially in scotopic and mesopic light levels (ND7 to ND5).

In our experiments, the luminance-dependent qualitative change of response patterns was such a surprising and yet prominent feature of most ganglion cells that this raises concerns about how trustable and stable these observations are. We tested the following: (1) How strongly are the different response types bound to a particular ambient luminance? (2) Do these response changes occur in morphologically identified ON and OFF cells? (3) Is this finding restricted to *in vitro*

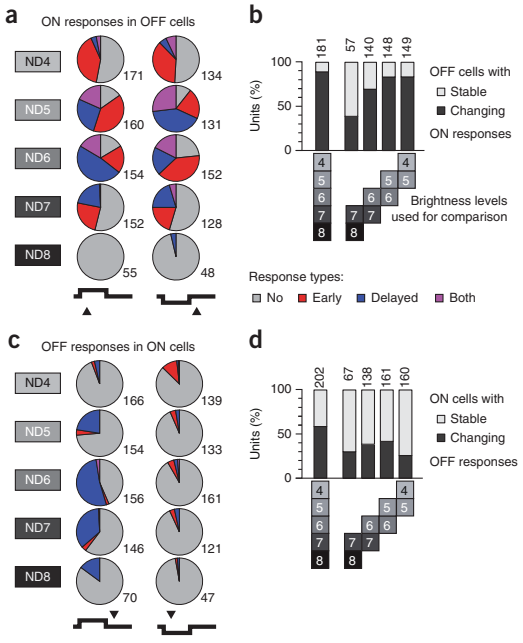

Figure 3 Summary of luminance-dependent response types. (**a**) Fraction of OFF cells displaying no, early and delayed ON responses at each luminance level to white and black full-field step stimuli. (**b**) Fraction of units with stable and changing responses. Cells were defined as stable if they had the same response type (no, early, delayed or both) at all compared light levels, both to the black step and to the white step. All other cells were defined as changing. (**c**,**d**) Same statistics as in **a** and **b** for OFF responses in ON cells. Numbers indicate units included in the analysis, selected on the basis of their reliable responses at these light levels (see Online Methods).

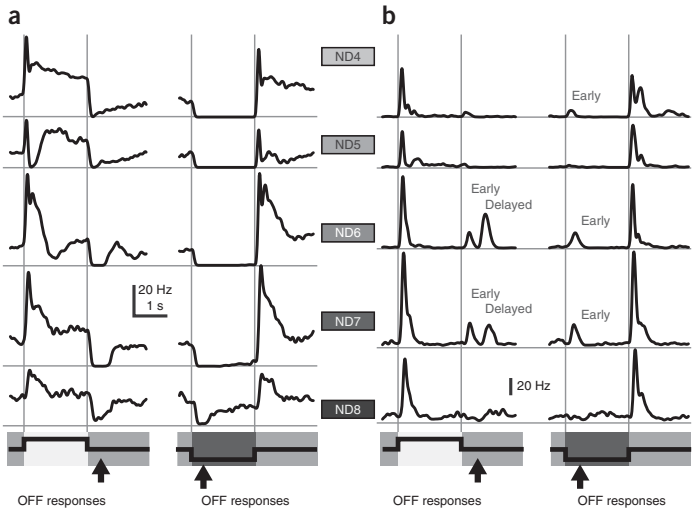

Figure 4 Responses (firing rate) of two ON ganglion cells. Stimulus was a 2-s white or black full-field step, presented at different ambient light levels. (**a**) Many ON ganglion cells were strongly suppressed by OFF stimuli. (**b**) ON ganglion cell with asymmetric and changing OFF responses.

conditions, or may it also be observed *in vivo*? (4) How much of the responses variability is due to the unnatural stimulus properties of full-field contrast steps? Furthermore, we investigated the contribution of center-surround receptive field interactions, GABAergic inhibition and rod-cone interactions to the mechanism of qualitative luminance-dependent response changes.

Response patterns are bound to individual light levels

As described above, the response patterns of ganglion cells were stable at each individual light level but could change after a luminance increase. We next tested whether ganglion cell responses would revert when the luminance returns to the previous level (**Fig. 5a**). Indeed, in the ND8 to ND5 luminance ranges, all recorded cells that changed their responses at a luminance transition ($n = 16$ from 2 retinas) immediately reverted to the previous pattern after an intermittent exposure to either lower or higher luminance levels (**Fig. 5b**,**c**). However, once exposed to ND4 (photopic level), cells did not immediately return to the response they had at ND5 earlier. This may be due to stronger bleaching caused by this light level (~10^4 R* rod^{-1} s^{-1}) or to some light adaptation triggered by this light level that reverses only slowly. In further experiments discussed below (**Supplementary Fig. 2**), 2 of the 15 cells studied did not revert to their previous response pattern at the ND7 light level after they had a different pattern during an interleaved exposure to ND6, while 13 of 15 cells did revert to their previous response pattern. Taken together, these results suggest that specific response patterns of ganglion cells are strongly associated with distinct luminance levels rather than with the history of luminance or with a luminance-independent drift.

Confirmation using single-cell recordings

Most cells in our data set had ON-OFF responses at least at one light level. Our cell type classification based on linear filter polarity cannot identify 'classical' ON-OFF cells (that is, cells stratifying in both ON and OFF sublaminae of the inner plexiform layer and having short-latency responses to both light increments and decrements) and distinguish them from 'real' ON cells or OFF cells (that is, cells with dendrites stratifying exclusively in the ON or OFF sublamina). To confirm that the latter can indeed have responses to anti-preferred contrast steps at some light level(s), we recorded action potentials from individual ganglion cells using patch electrodes. Most cells were filled with neurobiotin and imaged with confocal microscopy to assess whether they had typical ON or OFF morphology (**Fig. 6a–c**).

We recorded from three PV-5 ganglion cells, the well-studied[16,17] mouse homolog of the transient OFF-alpha cell (monostratified in the OFF sublamina of the inner plexiform layer; $n = 2$ of 3 cells confirmed with the neurobiotin marker). All three cells had delayed ON responses up to ND5 that disappeared at the photopic light level ND4. For one cell, we repeatedly switched between ND4 and ND5, and the responses reliably reverted (**Fig. 6d**). Consistent with the related MEA experiments (**Fig. 5**), switching from ND4 back to ND5 did not lead to an immediate reappearance of the delayed ON responses; here they reemerged about 1 min after the luminance switch. Four out of 5 more cells of unknown types, stratifying exclusively in the OFF ($n = 3$) or ON ($n = 2$) sublamina (**Fig. 6e**), had luminance-dependent response changes, confirming our findings based on MEA recordings.

Luminance-dependent response changes *in vivo*

One caveat of the results described so far is that they have been recorded from the isolated retina, and that these experiments can last several hours. Do luminance-dependent response changes also happen *in vivo*? To test this, we recorded from the dLGN of anesthetized mice (**Fig. 7a**) and projected step stimuli into their eyes that were comparable in absolute intensity and contrast to the stimuli we used for the *in vitro* recordings (**Fig. 7b**). Consistent with our findings in the *in vitro* retina preparation, in the dLGN 18 out of 28 units ($n =$ 5 mice) changed their responses qualitatively with changing ambient luminance (**Fig. 7c**). We could also test higher light levels (ND3 and ND2) *in vivo* than *in vitro* (see also Discussion). More than one-third of the recorded neurons changed their responses within the photopic regime as well (ND4–ND3 and ND3–ND2), including the example shown in **Figure 7d**. These observations suggest that luminance-dependent qualitative changes of retinal ganglion cell responses also occur *in vivo* and that these changes are reflected in the thalamus. This confirms scattered reports of this phenomenon in the literature[3].

Luminance-dependent changes to naturalistic movies

Full-field contrast steps are easy to analyze and interpret. However, they are not a natural stimulus for the retina and visual system in general. The retina might employ specific mechanisms to stabilize the output to a more natural stimulus when it is presented under varying luminance conditions. We tested this by stimulating the retina with a naturalistic movie repeatedly shown at different light levels.

Ganglion cells ($n = 172$ units from 8 retinas) responded to the natural movie with interleaved sequences of spike bursts ('events') and silence, as described previously[18]. Such bursting events presumably correspond to features in the movie that are relevant to this ganglion

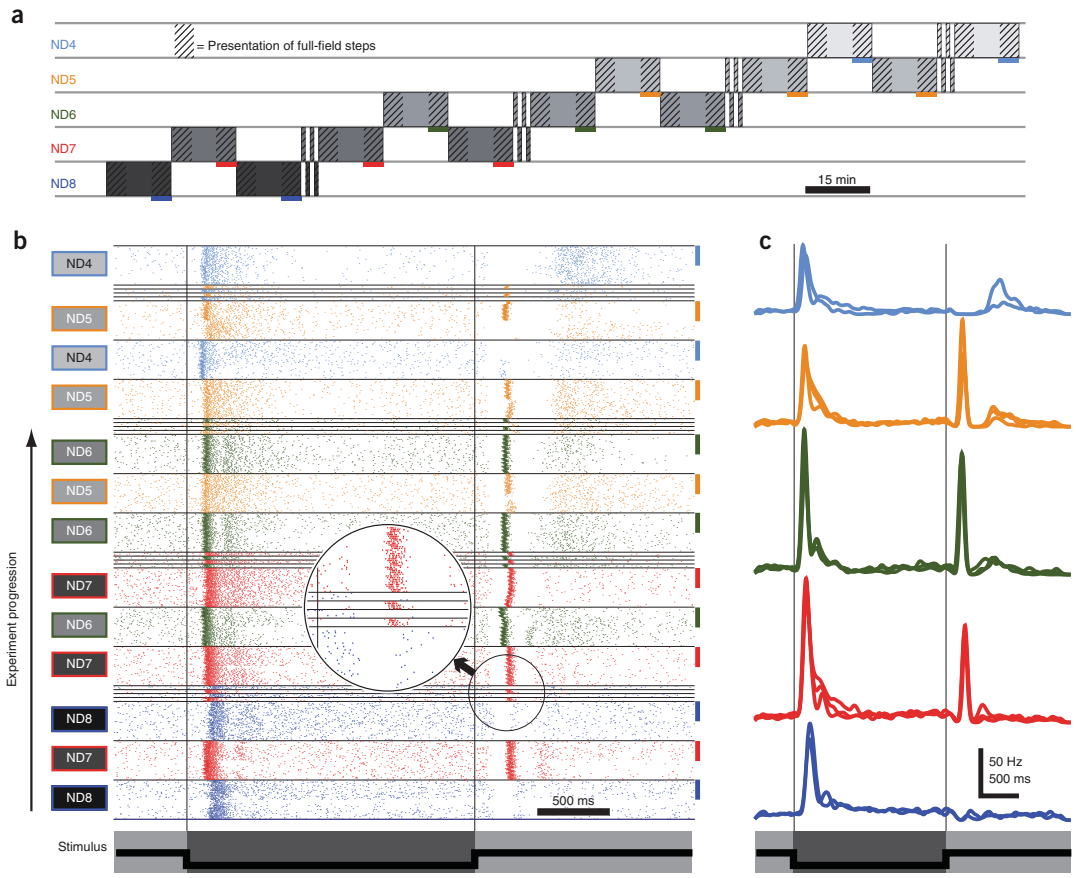

Figure 5 Stability of responses at individual light levels. (**a**) Experimental protocol. Colored bars label the last 5 min at each light level. (**b**) Raster plot of the responses of a single unit to all 730 presentations of the black full-field step (50 repetitions during each 15-min sequence, 5 repetitions during each 1-min sequence). Even quick luminance changes are immediately reflected in a different response pattern (see magnification). Colored bars mark the same experimental sections as in **a**. (**c**) Average spike rates of the responses marked by colored bars in **a** and **b**.

cell. If a cell had a robust bursting event at some light levels but not at others, we classified this as a qualitative response change (see Online Methods for details).

We observed such qualitative changes in 57% of the units (n = 98 of 172). For each of these units, some features (scenes of the movie) evoked a response at all light levels tested, and other features evoked a response only at certain light levels (**Supplementary Fig. 3a**,**b**). Some units (n = 55) were also tested with our full-field step stimulus. Response changes to the movie stimulus and to the full-field step stimulus could occur independently from each other (**Supplementary Fig. 3c**). This suggests that ambient luminance can alter different receptive field properties of ganglion cells, some of which are triggered by a homogeneous full-field step and some by a stimulus with more complex temporal and spatial properties.

Cells' peripheries involved in only some response changes

Most ganglion cells' receptive fields consist of a spatially distinct center and periphery. Stimulation of the center and periphery can evoke responses of opposite polarities in some ganglion cells[19]. Furthermore, it is known that the receptive field structure of some cells changes during light adaptation[5]. Thus, the changing response patterns that we observed in our experiments might have been caused by luminance-dependent changes in the balance of the receptive field center and periphery. To test this, we stimulated the retina with disks of 150 µm diameter with identical contrast properties to the full-field steps (n = 107 units in 4 retinas).

We observed the same variety of response types to the localized disk stimulus as for the full-field stimulation. 80% of the units changed the response type to the disk stimulus at least at one luminance transition, while 20% had stable responses at all light levels (**Fig. 8a**). At any individual luminance transition, between 44% and 61% of the units changed their responses. We also mapped the receptive fields of all units using a binary noise checkerboard flicker stimulus and measured how much of the disk stimulus lay within the receptive field center (**Fig. 8b**). For more than half the units, both with changing or stable responses, 80% or more of the disk stimulus was contained

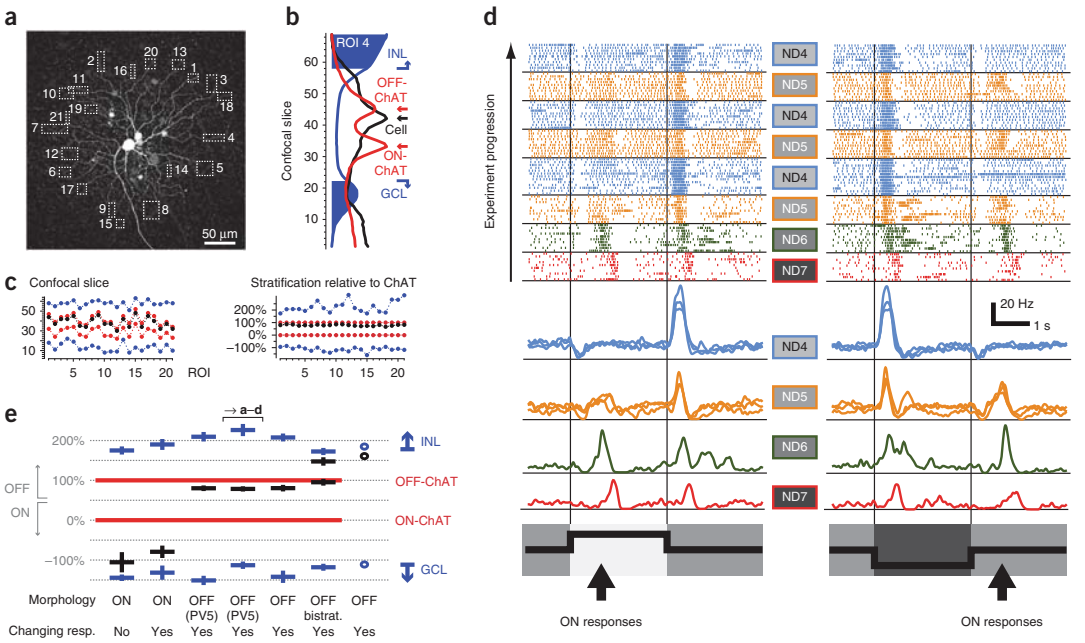

Figure 6 Responses recorded from individual ganglion cells. (**a**–**d**) Results from one PV5 ganglion cell. (**a**) Maximum-intensity projection of a confocal microscopy stack, showing the neurobiotin-filled PV5 ganglion cell and the regions of interests (ROIs) used for analyzing stratification level. (**b**) Fluorescence intensity profile along the *z* axis of ROI 4. Blue, DAPI nuclear label; red, choline acetyltransferase (ChAT) label; black, neurobiotin label. Stratification levels of cell and ChAT bands represent peaks of their intensity profiles. Borders of inner nuclear layer (INL) and ganglion cell layer (GCL) are drawn where the intensity profile dropped below 67% of its peak. (**c**) Left, stratification measurements for each ROI, as in **b**. Right, conversion of stratification relative to ChAT bands. (**d**) This OFF-stratifying cell had pronounced delayed ON responses from ND7 to ND5. (**e**) Dendritic stratification level (black, mean ± s.e.m. relative to the ChAT bands, red) of individually recorded cells. Bistrat., bistratified. For rightmost cell, ChAT staining was not successful. Most cells had luminance-dependent response changes.

within the receptive field center, suggesting that the stimulus had little influence on the periphery. The cell shown in **Figure 8c**, for example, was an OFF ganglion cell that acquired a delayed ON response to the white disk at ND7 and also to the black disk at ND6. The disk stimulus was 100% contained within the receptive field center. In this case, stimulation of the receptive field center alone elicited luminance-dependent response changes. In this and similar cases, luminance-induced reorganization of the center-surround receptive field structure cannot account for changing response patterns.

Nevertheless, the receptive field periphery did influence the responses of many units: the responses to the local disk and full-field stimuli differed from each other at least at one light level in 67 of the 107 units. Distinct responses to localized and full-field stimulation could be observed at all light levels, from ND8 (scotopic) to ND4 (photopic), suggesting that at least some ganglion cells possess a receptive field surround in scotopic conditions.

Notably, we observed several units that stably maintained their response type to disks with changing luminance but that qualitatively changed their responses to full-field steps (**Fig. 8d**). In these units, it is likely that a reorganization of the overall receptive field structure (for example, of center-surround interactions) is responsible for the changes of the responses, and not a reorganization of the central receptive field alone. Taken together, our results suggest that most units can change their responses to local stimulation but that a dynamic reorganization of the overall receptive field structure can be responsible for some qualitative luminance-dependent response changes as well.

GABAergic inhibition involved in some response changes

GABA-mediated inhibition can mask responses of ganglion cells[20,21]; release from GABAergic inhibition at some light levels might therefore be a valid mechanism for luminance-dependent response changes. To test this, we compared the responses of ganglion cells to full-field contrast steps at ND7 and ND6 with and without blockade of ionotropic GABA receptors (5 µM SR-95531 and 100 µM picrotoxin; **Supplementary Fig. 2a**). From two retinas, we extracted 37 units with stable responses during the two repeats of ND7 in control conditions.

The drugs had diverse effects on the ganglion cell responses (**Supplementary Fig. 2b**–**e**): in some cells, GABA blockers prevented luminance-dependent response changes, whereas in other cells they enabled such changes. In yet other cells, responses were not influenced by GABA blockade. In summary, we found that the mechanism of GABAergic response regulation was highly diverse and that it influenced some but not all luminance-dependent qualitative response changes.

Response changes do not require rod-cone interactions

Many ganglion cells changed their response pattern at transitions within the scotopic regime (ND8–ND7). This suggests that rod-cone circuit interactions are not required for all response changes.

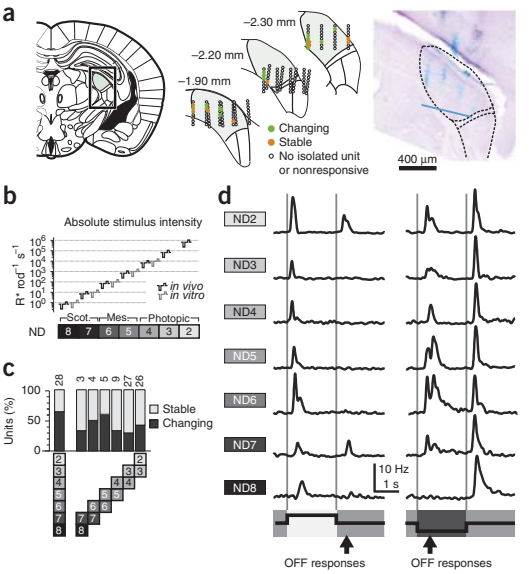

Figure 7 Luminance-dependent qualitative response changes in the dLGN. (**a**) Recording locations in the dLGN, outlined on the left. Middle, reconstructed positions (colored dots) of recording sites in three rostro-caudal positions relative to the bregma. Reconstruction was based on DiI labeling of electrode shanks (right); blue line, maximum depth of recording electrode. Brain schematics based on Paxinos and Franklin[50]. (**b**) Absolute stimulus intensities used for the *in vivo* experiments (black) in comparison to the intensities used during *in vitro* experiments (gray; see **Fig. 1b**). Note that the stimulus range is extended to higher intensities. Scot., scotopic; mes., mesopic. (**c**) Fraction of light-responsive units in the dLGN with changing or stable responses. Conventions as in **Figure 3b**. (**d**) A single ON unit from the dLGN that has both changing and asymmetric OFF responses at different ambient light levels.

To further explore how much of the response variability is brought about by the rod pathways, we used three different mouse models with nonfunctional cone photoreceptors ('rod-only retinas'): *Gnat2*^{cpfl3}, *Pde6c*^{cpfl1} (*Cpfl1*) and *Cnga3*$^{-/-}$ mice, which carry mutations in cone-specific members of the phototransduction cascade: a transducin, phosphodiesterase and cyclic nucleotide–gated channel, respectively.

In retinas from all three cone-deficient mouse lines, we found a similar prevalence of luminance-dependent response changes as in wild-type retinas (**Supplementary Fig. 4**). Together, these results confirm that not all luminance-dependent response changes rely on rod-cone interactions, as such changes can be observed in retinas with nonfunctional cones. Instead, some response changes might reflect more subtle changes in processing due to engaging different rod-mediated pathways[11] at low and high scotopic light levels.

Generalization to other species

To exclude the possibility that luminance-dependent response changes are a feature restricted to the mouse retina, we recorded from the isolated pig retina, using the same procedure as for the mouse retina. Luminance-dependent response changes were also commonly observed in pig ganglion cells (n = 98 cells, three retinal pieces from two different animals; **Supplementary Fig. 5**). While the pig and mouse data differed in some details (for example, hardly any delayed ON responses in pig OFF cells), the phenomenon of luminance-dependent qualitative response changes was observed in both species with comparable frequencies.

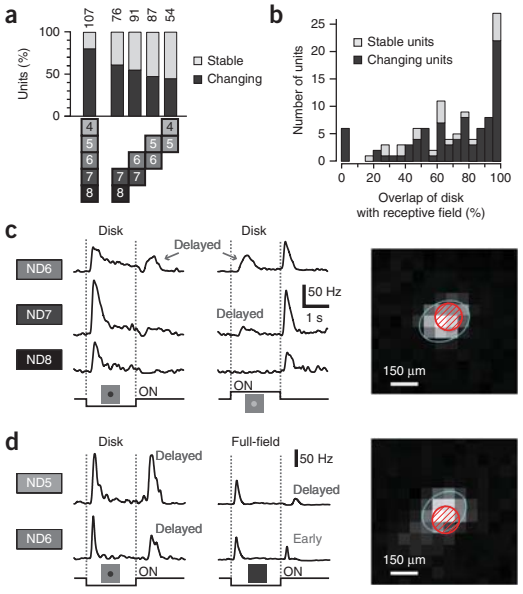

Figure 8 Luminance-dependent response changes to small localized disk stimuli. (**a**) Percentage of units with stable or changing responses across different luminance levels. Conventions as in **Figure 3b**, but combining both ON and OFF cells. (**b**) Histogram showing how much of the disk stimulus was contained within the receptive field center, as determined by a binary checkerboard flicker stimulus. (**c**) Example unit changing its responses to localized stimulation of the receptive field center. Right, overlap of the disk stimulus (red) with the receptive field (blue ellipse shows 2.5 σ of Gaussian fit). (**d**) Example unit that had stable responses to the disk stimulus but changing responses to the full-field step at the ND6–ND5 luminance transition.

DISCUSSION

We studied the responses of retinal ganglion cells to full-field contrast steps over 5 log units of background light intensities. We classified ganglion cells into ON and OFF groups based on their linear filter and found that most OFF ganglion cells and a large fraction of ON cells behave as ON-OFF at least at some luminance levels. In both groups, the responses to the anti-preferred stimulus contrast could have short latency (early responses) or long latency (delayed responses). Early and delayed responses, which may occur together in many cells (**Fig. 3a**,**c**), appeared to be distinct response categories (**Fig. 2b**) that can be regulated independently (**Supplementary Fig. 2**). Most intriguingly, over 80% of cells displayed different response types to the anti-preferred contrast at different background luminance (**Fig. 3b**,**d**). It is noteworthy that the linear filter polarity, obtained as spike-triggered average to full-field Gaussian white noise flicker, was stable at all light intensities despite changing responses to step stimuli.

Despite such a high degree of variability in the responses of ganglion cells, we found them to be reliably bound to the specific luminance: most cells would always respond in a similar way at a particular light

level, even if such trials were interleaved with exposure to higher or lower light levels (**Fig. 5**). Moreover, luminance-dependent qualitative changes of the responses were also demonstrated in recordings from dLGN neurons *in vivo* (**Fig. 7**) and to spatially heterogeneous stimuli, such as small disks (**Fig. 8**) and a naturalistic movie, which is a more ecologically relevant visual stimulus for the retina and the visual system in general. In several single-cell recordings from ganglion cells identified to be morphologically ON or OFF, we observed similar light-dependent response changes (**Fig. 6**), further corroborating the conclusions drawn from the MEA recordings. Finally, we found that luminance-dependent response changes were not restricted to the mouse retina but existed in pig retina as well (**Supplementary Fig. 5**).

In the isolated retina, stimulation at light levels higher than ND4 (corresponding to 10^4 R* rod^{-1} s^{-1}) led to subtle changes in response properties that are likely associated with excessive bleaching of photopigment (data not shown). While the retina continued to respond well to visual stimulation, the results obtained at those high intensities probably do not reflect normal retinal processing as it would happen in the intact eye (data not shown), and hence we excluded these higher light levels from our analysis. The recordings from the dLGN therefore not only confirm that luminance-dependent response variability occurs *in vivo*, but they also expand the range of light intensities at which that phenomenon was observed. Overall, we found luminance-dependent response changes over all intensity ranges and at each luminance transition we tested, from scotopic to photopic light levels.

The collective activity (firing pattern) of all retinal ganglion cells in response to a visual stimulus is sometimes referred to as the retinal code, which is, simply put, "what the eye tells the brain" about the stimulus[22]. Common research questions related to the retinal code often revolve around two topics: first, how does the retina encode the visual stimulus, and second, how might the visual brain decode the action potential pattern generated by the retinal ganglion cells? Our results have intriguing implications for both of these questions.

The first topic, encoding of visual stimuli, boils down to a mechanistic understanding of retinal circuits: how do cellular and circuit properties combine to produce certain ganglion cell responses? Decades of research have revealed fundamental aspects of this issue, ranging from the workings of the phototransduction cascade[23], to the identity of retinal cell types[24], to complex receptive and projective field organizations[2,25–27], to adaptation to first and higher order statistics of the visual stimulus[28–30]. Our results suggest that it may be worth revisiting many of these functional findings and comparing them in detail at different light levels.

Recent reports on the connectome of the inner retina can form a framework for understanding the mechanisms for the response variability we describe here. Three-dimensional electron microscopy reconstruction of the inner mouse[31] and rabbit[32] retina has shown that many bipolar cell types connect to many different ganglion cell types, including ON bipolar cells to OFF ganglion cells and vice versa. Such promiscuous connectivity was confirmed by physiological recordings in salamander retina[25]. Additionally, some ganglion cells receive excitatory drive during anti-preferred contrast steps through gap-junction coupling with amacrine cells[20]. These diverse connectivity patterns, in combination with amacrine cell–mediated feedback inhibition to veto synaptic release from bipolar cell terminals[21,25,33], provide all necessary building blocks for turning on or off certain inputs to ganglion cells under different (luminance) conditions. However, we have shown that the particular mechanism underlying luminance-dependent response variability may differ in different ganglion cell types. For example, two ganglion cells might change their responses during the same luminance transition for different reasons: while one cell gains a surround, the other cell remodels its central receptive field (**Fig. 8**). While one cell's response variability is regulated by GABAergic inhibition, the other cell changes its responses independently of GABA (**Supplementary Fig. 2**). Furthermore, we found many cells to change their responses at several luminance transitions, so that even a single ganglion cell might employ diverse mechanisms at different luminance transitions. This variety of observed effects suggests that the detailed mechanisms underlying luminance-dependent response changes likely need to be investigated on the level of individual ganglion cells and their circuits.

Related to the topic of encoding is the problem of functional classification of ganglion cell types. This question has been approached by describing ganglion cell responses with several parameters, such as polarity, latency, transiency, direction selectivity and so forth, usually in response to simple stimuli such as full-field flashes and moving bars[34–36]. However, as we show here, response properties of ganglion cells depend on the ambient luminance, including properties that serve as parameters used for cell classification. For example, a cell identified as an OFF cell at one luminance might behave as an ON-OFF cell at another luminance, even within the same coarse brightness range (scotopic, mesopic and photopic). Thus, two cells of the same cell type might be artificially separated into different groups if measurements were done under different luminance conditions. Consequently, using controlled and comparable luminance conditions, as well as similar stimuli, is crucial not only for proper comparison of response patterns between research groups, but also between several experiments within a single study. In the future, it will be important to rigorously test whether all ganglion cells of the same (morphological) type change their responses coherently during luminance transitions.

The recent advances in retinal prosthetic technology, including electrical retinal implants[37–39] and optogenetic approaches[40–43], have raised the bar on the stated goals in vision restoration: the goal is no longer to simply confer light perception on the blind patient, but to try to fully restore normal function. Ideally, an implant would encode the light stimulus such that the induced retinal output would be as natural as possible. Our work suggests that the 'natural' retinal output is a moving target. This may, in fact, be advantageous for prosthetics that lack cellular specificity, such as electrical retinal implants. They have always suffered from the problem of not being able to specifically stimulate ON or OFF cells (but see ref. 44). According to our results, ON responses are a common feature in OFF cells. Nonspecific electrical stimulation at light onset might therefore not confuse the brain as much as has been feared. Whether or not this really is the case, however, depends on how the retinal output is decoded.

The second topic, decoding of the retinal output, views the retina as a black box and asks questions about how the output of the retina is treated by receiving neurons. Is the exact spike timing important[45,46], or is the firing rate the relevant unit[47,48]? How is the correlation structure of multineuron firing patterns taken into account[49]? When we started this research project, we expected to see only a moderate influence of illuminance on the retinal output, maybe with more pronounced effects at certain brightness thresholds (namely, cone activation threshold and rod saturation threshold). Overall, however, we assumed that adaptation in the retina largely would compensate for illuminance differences, so that the retinal black box delivers a rather stable input to the visual brain. Since this does not seem to be the case, there is a whole new dimension that is added to the already existing questions on decoding. How does the brain deal with the changes of the retinal output? Are they successfully filtered out and discarded, or do they indeed carry important information, maybe even used to identify viewing conditions?

The data we present are probably insufficient to even start tackling these questions. Furthermore, in the current work we have only focused on qualitative response changes. In addition, there are widespread quantitative changes in response to both preferred and anti-preferred contrast steps (for example, response amplitude, transiency), as can be seen in many of the example responses depicted in our figures. Various aspects of quantitative luminance-induced changes have also been described by others[5,7]. In the future, it will be desirable to monitor the luminance-dependent changes of the retinal output on a better spatial scale. In particular, it will be important to test whether the information transmitted to the brain by a population of ganglion cells is, in aggregate, luminance independent despite the luminance-dependent changes of single cells. It is also possible that the phenomenon of changing output described in this paper allows the retina to encode the visual stimulus more efficiently in the ever-changing and dynamic luminance conditions of natural viewing[15].

METHODS

Methods and any associated references are available in the online version of the paper.

Note: Any Supplementary Information and Source Data files are available in the online version of the paper.

ACKNOWLEDGMENTS

We thank J. Wynne for technical assistance and M. Biel (LMU München) for supplying *Cnga3*$^{-/-}$ mice. This research was supported by funds of the Deutsche Forschungsgemeinschaft (DFG) to the Werner Reichardt Centre for Integrative Neuroscience (DFG EXC 307), by the Bundesministerium für Bildung and Forschung (BMBF) to the Bernstein Center for Computational Neuroscience (FKZ 01GQ1002), by funds of the Biotechnology and Biological Sciences Research Council (BBSRC BB/1007296/1) and the European Commission (ERC Advanced Grant MeloVision) to R.J.L., a Christiane-Nüsslein-Volhard Stipend to A.T.-H., and a Pro-Retina Stipend to K.R.

AUTHOR CONTRIBUTIONS

A.T.-H., K.R. and T.A.M. designed the study. MEA recordings and spike sorting were performed by A.T.-H., K.R., H.S. and A.H., and analyzed by A.T.-H., K.R. and T.A.M. Patch-clamp experiments and immunohistochemistry were conducted and analyzed by H.S. and T.A.M. *In vivo* experiments were designed by C.A.P., A.E.A. and R.J.L., performed by C.A.P. and A.E.A., and analyzed by C.A.P., A.E.A. and K.R. Pig eyes were provided by M.S. The manuscript was prepared by A.T.-H., K.R. and T.A.M. with the help of H.S., C.A.P., A.E.A. and R.J.L.

COMPETING FINANCIAL INTERESTS

The authors declare no competing financial interests.

1. O'Brien, B.J., Isayama, T., Richardson, R. & Berson, D.M. Intrinsic physiological properties of cat retinal ganglion cells. *J. Physiol.* (*Lond.*) **538**, 787–802 (2002).
2. Gollisch, T. & Meister, M. Eye smarter than scientists believed: neural computations in circuits of the retina. *Neuron* **65**, 150–164 (2010).
3. Reitner, A., Sharpe, L.T. & Zrenner, E. Is colour vision possible with only rods and blue-sensitive cones? *Nature* **352**, 798–800 (1991).
4. Enroth-Cugell, C. & Lennie, P. The control of retinal ganglion cell discharge by receptive field surrounds. *J. Physiol.* (*Lond.*) **247**, 551–578 (1975).
5. Farrow, K. *et al.* Ambient illumination toggles a neuronal circuit switch in the retina and visual perception at cone threshold. *Neuron* **78**, 325–338 (2013).
6. Sagdullaev, B.T. & McCall, M.A. Stimulus size and intensity alter fundamental receptive-field properties of mouse retinal ganglion cells in vivo. *Vis. Neurosci.* **22**, 649–659 (2005).
7. Grimes, W.N., Schwartz, G.W. & Rieke, F. The synaptic and circuit mechanisms underlying a change in spatial encoding in the retina. *Neuron* **82**, 460–473 (2014).
8. Umino, Y., Solessio, E. & Barlow, R.B. Speed, spatial, and temporal tuning of rod and cone vision in mouse. *J. Neurosci.* **28**, 189–198 (2008).
9. Protti, D.A., Flores-Herr, N., Li, W., Massey, S.C. & Wassle, H. Light signaling in scotopic conditions in the rabbit, mouse and rat retina: a physiological and anatomical study. *J. Neurophysiol.* **93**, 3479–3488 (2005).
10. Eggers, E.D., Mazade, R.E. & Klein, J.S. Inhibition to retinal rod bipolar cells is regulated by light levels. *J. Neurophysiol.* **110**, 153–161 (2013).
11. Bloomfield, S.A. & Dacheux, R.F. Rod vision: pathways and processing in the mammalian retina. *Prog. Retin. Eye Res.* **20**, 351–384 (2001).
12. Ke, J.B. *et al.* Adaptation to background light enables contrast coding at rod bipolar cell synapses. *Neuron* **81**, 388–401 (2014).
13. Dunn, F.A., Doan, T., Sampath, A.P. & Rieke, F. Controlling the gain of rod-mediated signals in the mammalian retina. *J. Neurosci.* **26**, 3959–3970 (2006).
14. Dunn, F.A., Lankheet, M.J. & Rieke, F. Light adaptation in cone vision involves switching between receptor and post-receptor sites. *Nature* **449**, 603–606 (2007).
15. Allen, A.E. *et al.* Melanopsin-driven light adaptation in mouse vision. *Curr. Biol.* published online, doi:10.1016/j.cub.2014.09.015 (7 October 2014).
16. Manookin, M.B., Beaudoin, D.L., Ernst, Z.R., Flagel, L.J. & Demb, J.B. Disinhibition combines with excitation to extend the operating range of the OFF visual pathway in daylight. *J. Neurosci.* **28**, 4136–4150 (2008).
17. Münch, T.A. *et al.* Approach sensitivity in the retina processed by a multifunctional neural circuit. *Nat. Neurosci.* **12**, 1308–1316 (2009).
18. Pitkow, X. & Meister, M. Decorrelation and efficient coding by retinal ganglion cells. *Nat. Neurosci.* **15**, 628–635 (2012).
19. Kuffler, S.W. Discharge patterns and functional organization of mammalian retina. *J. Neurophysiol.* **16**, 37–68 (1953).
20. Farajian, R., Pan, F., Akopian, A., Volgyi, B. & Bloomfield, S.A. Masked excitatory crosstalk between the ON and OFF visual pathways in the mammalian retina. *J. Physiol.* (*Lond.*) **589**, 4473–4489 (2011).
21. Roska, B. & Werblin, F. Vertical interactions across ten parallel, stacked representations in the mammalian retina. *Nature* **410**, 583–587 (2001).
22. Meister, M. & Berry, M.J. II. The neural code of the retina. *Neuron* **22**, 435–450 (1999).
23. Lamb, T.D. & Pugh, E.N. Jr. Phototransduction, dark adaptation, and rhodopsin regeneration: the Proctor lecture. *Invest. Ophthalmol. Vis. Sci.* **47**, 5137–5152 (2006).
24. Werblin, F.S. & Dowling, J.E. Organization of the retina of the mudpuppy, *Necturus maculosus.* II. Intracellular recording. *J. Neurophysiol.* **32**, 339–355 (1969).
25. Asari, H. & Meister, M. The projective field of retinal bipolar cells and its modulation by visual context. *Neuron* **81**, 641–652 (2014).
26. Lukasiewicz, P.D. Synaptic mechanisms that shape visual signaling at the inner retina. *Prog. Brain Res.* **147**, 205–218 (2005).
27. Thoreson, W.B. & Mangel, S.C. Lateral interactions in the outer retina. *Prog. Retin. Eye Res.* **31**, 407–441 (2012).
28. Baccus, S.A. & Meister, M. Fast and slow contrast adaptation in retinal circuitry. *Neuron* **36**, 909–919 (2002).
29. Smirnakis, S.M., Berry, M.J., Warland, D.K., Bialek, W. & Meister, M. Adaptation of retinal processing to image contrast and spatial scale. *Nature* **386**, 69–73 (1997).
30. Tkačik, G., Ghosh, A., Schneidman, E. & Segev, R. Adaptation to changes in higher-order stimulus statistics in the salamander retina. *PLoS ONE* **9**, e85841 (2014).
31. Helmstaedter, M. *et al.* Connectomic reconstruction of the inner plexiform layer in the mouse retina. *Nature* **500**, 168–174 (2013).
32. Lauritzen, J.S. *et al.* ON cone bipolar cell axonal synapses in the OFF inner plexiform layer of the rabbit retina. *J. Comp. Neurol.* **521**, 977–1000 (2013).
33. Geffen, M.N., de Vries, S.E. & Meister, M. Retinal ganglion cells can rapidly change polarity from Off to On. *PLoS Biol.* **5**, e65 (2007).
34. Farrow, K. & Masland, R.H. Physiological clustering of visual channels in the mouse retina. *J. Neurophysiol.* **105**, 1516–1530 (2011).
35. Rockhill, R.L., Daly, F.J., MacNeil, M.A., Brown, S.P. & Masland, R.H. The diversity of ganglion cells in a mammalian retina. *J. Neurosci.* **22**, 3831–3843 (2002).
36. Zeck, G.M. & Masland, R.H. Spike train signatures of retinal ganglion cell types. *Eur. J. Neurosci.* **26**, 367–380 (2007).
37. Dorn, J.D. *et al.* The detection of motion by blind subjects with the Epiretinal 60-Electrode (Argus II) retinal prosthesis. *JAMA Ophthalmol.* **131**, 183–189 (2013).
38. Wang, L. *et al.* Photovoltaic retinal prosthesis: implant fabrication and performance. *J. Neural Eng.* **9**, 046014 (2012).
39. Zrenner, E. *et al.* Subretinal electronic chips allow blind patients to read letters and combine them to words. *Proc. Biol. Sci.* **278**, 1489–1497 (2011).
40. Bi, A. *et al.* Ectopic expression of a microbial-type rhodopsin restores visual responses in mice with photoreceptor degeneration. *Neuron* **50**, 23–33 (2006).
41. Busskamp, V., Picaud, S., Sahel, J.A. & Roska, B. Optogenetic therapy for retinitis pigmentosa. *Gene Ther.* **19**, 169–175 (2012).
42. Lagali, P.S. *et al.* Light-activated channels targeted to ON bipolar cells restore visual function in retinal degeneration. *Nat. Neurosci.* **11**, 667–675 (2008).
43. Nirenberg, S. & Pandarinath, C. Retinal prosthetic strategy with the capacity to restore normal vision. *Proc. Natl. Acad. Sci. USA* **109**, 15012–15017 (2012).
44. Cai, C., Twyford, P. & Fried, S. The response of retinal neurons to high-frequency stimulation. *J. Neural Eng.* **10**, 036009 (2013).
45. Jacobs, A.L. *et al.* Ruling out and ruling in neural codes. *Proc. Natl. Acad. Sci. USA* **106**, 5936–5941 (2009).
46. Rathbun, D.L., Alitto, H.J., Weyand, T.G. & Usrey, W.M. Interspike interval analysis of retinal ganglion cell receptive fields. *J. Neurophysiol.* **98**, 911–919 (2007).
47. Berry, M.J., Warland, D.K. & Meister, M. The structure and precision of retinal spike trains. *Proc. Natl. Acad. Sci. USA* **94**, 5411–5416 (1997).
48. Funke, K. & Worgotter, F. On the significance of temporally structured activity in the dorsal lateral geniculate nucleus (LGN). *Prog. Neurobiol.* **53**, 67–119 (1997).
49. Schnitzer, M.J. & Meister, M. Multineuronal firing patterns in the signal from eye to brain. *Neuron* **37**, 499–511 (2003).
50. Paxinos, G. & Franklin, K. *The Mouse Brain in Stereotaxic Coordinates* (Academic Press, 2001).

ONLINE METHODS

Animals. As wild-type animals, we used PV-Cre × Thy-S-Y mice[17] (B6;129P2-*Pvalb*$^{tm1(cre)Arbr}$/J × C57BL/6-tg(ThystopYFPJS) and C57Bl/6J mice. For cone-deficient mice, we used *Cnga3*$^{-/-}$ (ref. 51, kindly provided by M. Biel, LMU München), *Cpfl1* (B6.CXB1-*Pde6c*^{cpfl1}, Jackson strain 3678), kindly provided by B. Chang (The Jackson Laboratory, Bar Harbor, ME), and *Gnat2*^{cpfl3} mice (B6.Cg-*Gnat2*^{cpfl3}/Boc, Jackson strain 6795). Wild-type animals were 5 weeks to 6 months old at the time of the experiments, *Cnga3*$^{-/-}$ animals 4.5–6 weeks old, *Cpfl1* animals 11–13 weeks old and *Gnat2*^{cpfl3} animals 12 months old. We used both male and female mice for all experiments. Mice were kept in groups of one to five animals. Animal use was in accordance with German, UK and European regulations and approved by the Regierungspräsidium Tübingen (*in vitro* experiments).

Pig retinas were obtained from two female domestic pigs sacrificed during independent scientific studies at the Department of Experimental Surgery, University of Tübingen. Pigs were sedated and anesthetized by injection of atropine, azaperone, benzodiazepine (midazolam), and ketamine, and sacrificed with embutramide (T61). Before administration of embutramide, heparin was injected. During sedation and anesthesia, the pigs were dark-adapted for 15–20 min. After death, the eyes were enucleated immediately under dim red light conditions, the cornea, lens and vitreous removed, and the eyecup kept in CO_2-independent culture medium (Gibco) and protected from light. After transportation to the laboratory, pieces ~4 × 4 mm^2 were cut from the mid-peripheral retina. Recordings were performed identically to those in experiments with mouse retina.

***In vitro* MEA recordings.** Mice were kept on a 12/12 h light/dark cycle, dark-adapted for 4–16 h before the experiment, and sacrificed under dim red light by cervical dislocation. The eyecups were removed, put in Ringer solution (in mM: 110 NaCl, 2.5 KCl, 1 $CaCl_2$, 1.6 $MgCl_2$, 10 D-glucose and 22 $NaHCO_3$) bubbled with 5% CO_2/95% O_2. The retina was isolated and attached to a nitrocellulose filter (Millipore) with a central 2 × 2 mm hole, with the optic nerve head centered. Experiments were performed at different circadian times with no noticeable effects on the outcome.

All recordings were performed with a perforated 60-electrode MEA (60pMEA200/30iR-Ti-gr, Multichannel Systems, Reutlingen) with square grid arrangement and 200 µm electrode distance. The mounted retina was placed ganglion cell–side down in the recording chamber, and good electrode contact was achieved by negative pressure through the perforated MEA. The tissue was superfused with Ringer solution at 34 °C. Data were recorded at 25 kHz with a USB-MEA-system (USB-MEA1060, Multichannel Systems) or a MC-Card based MEA-system (MEA1060, Multichannel Systems). The detailed experimental procedure has been published before[51].

Pharmacology. To block ionotropic GABA receptors, 5 µM SR-95531 (gabazine, an antagonist of $GABA_A$ receptors; Sigma) and 100 µM picrotoxin (an antagonist of $GABA_A$ and $GABA_C$ receptors; Sigma) were added to the Ringer solution. SR-95531 was dissolved in water at a concentration of 5 mM; picrotoxin was dissolved in DMSO at a concentration of 100 mM. Wash-in was performed during 10 min at a speed of approximately 1 ml/min.

Single-cell recordings, immunostaining and confocal microscopy. Retina preparation was carried out in Ringer solution, as described for MEA recordings. The isolated retina mounted on the nitrocellulose filter was attached in the recording chamber by vacuum grease. The same setup as for the MEA recordings, including visual stimulation hardware and software, was used. Patch electrodes pulled from borosilicate glass capillaries (Science Products, GB150F-8P) were filled with an internal solution (in mM: 115 potassium gluconate, 2 KCl, 0.5 $CaCl_2$, 1 $MgCl_2$, 1.5 EGTA, 10 HEPES, 4 ATP-Na_2, 0.5 GTP-Na_3, 7.75 neurobiotin chloride, <1 Alexa 568) and had resistances between 4 and 8 MΩ. Recordings were made from ganglion cells of PV-Cre × Thy-S-Y mice in loose cell-attached mode or whole-cell mode using current clamp (0 pA). Ganglion cells were targeted by two-photon imaging (920–950 nm) or chosen randomly. At the end of the recording, cells were filled with neurobiotin-containing internal solution and retinas were immersion-fixed in 4% PFA for 10 min at room temperature, washed in PBS, cryoprotected in 30% sucrose, frozen (at −150 °C) and thawed three times and washed again in PBS. After blocking 1 h in 10% normal donkey serum (NDS), 1% bovine serum albumin (BSA), 0.5% Triton X-100, 0.02% sodium azide in PBS, retinas were incubated 4–6 d with primary antibody goat anti-ChAT (Millipore, AB144P, 1:200)[52], diluted in 3% NDS, 1% BSA, 0.5% Triton X-100, 0.02% sodium azide in PBS. Retinas were washed in PBS and incubated overnight with secondary antibody donkey anti-goat Cy5 (Jackson ImmunoResearch, 705-175-147, 1:200)[53] and streptavidin-Cy3 (Jackson ImmunoResearch, 016-160-084, 1:200–1:400) or donkey anti-goat Alexa 555 (Invitrogen, A-21432, 1:200)[54] and streptavidin Cy5 (Rockland, S000-06, 1:200), diluted in 0.5% Triton X-100 in PBS. Retinas were washed in PBS, incubated with DAPI (2.5 µg/ml in PBS) for 20 min, washed again and mounted in Vectashield (Vector Laboratories). All steps were carried out at room temperature. Confocal image stacks of the filled ganglion cells were taken on a Zeiss LSM710, using a 40X NA1.3 oil immersion objective. *xy* image and *z*-stack size were chosen such that they covered the complete ganglion cell, including its entire dendritic arbor, and encompassed the full thickness of the inner plexiform layer. Dendritic stratification depths relative to ChAT bands and DAPI-stained nuclei of inner nuclear layer and ganglion cell layer were determined on several dendritic locations of each cell using a custom-written Mathematica script.

Light stimuli during *in vitro* experiments. *Intensities.* Light stimulation was performed with a digital light processing (DLP) projector (PG-F212X-L, Sharp) and focused onto the photoreceptors through the condenser of the microscope (**Supplementary Fig. 1**). The light path contained a shutter and two motorized filter wheels with a set of neutral density (ND) filters (Thorlabs NE10B-A to NE50B-A), having optical densities from 1 ('ND1') to 5 ('ND5'). To achieve light attenuation stronger than 5 log units, we serially combined an ND5 filter in one filter wheel with another ND filter in the second filter wheel. We refer to the filter settings as ND4 (brightest setting used, 10^4-fold light attenuation) to ND8 (darkest setting used, 10^8-fold light attenuation). While changing the ND filters during the experiment, we closed the shutter to prevent intermittent exposure to bright light. We usually started the experiments at ND8, and step by step increased the ambient stimulation luminance by changing the ND filters by 1 unit. Unless otherwise noted, we presented the same set of visual stimuli at each ND level during an experiment.

The stimulus projector output spanned 3 log units of light intensities (that is, a 1,000-fold difference between black (0) and white (255) pixels). We linearized the projector output, and limited our visual stimuli to the range of 0 to 60, with the background set to 30 (**Fig. 1a**). As a consequence, the brightest pixels at any given ND-filter setting were fivefold dimmer than the background illumination at the next brighter ND-setting (**Fig. 1b**).

Light intensity measurements. We measured the spectral intensity profile (in µW cm^{-2} nm^{-1}) of our light stimuli with a calibrated USB2000+ spectrophotometer (Ocean Optics). We transformed the stimulus intensity into equivalents of photoisomerizations per rod and per second, assuming dark-adapted rods[42]. Briefly, the spectrum was converted to photons cm^{-2} s^{-1} nm^{-1}, convolved with the normalized spectrum of rod sensitivity[5], and multiplied with the effective collection area of rods (0.5 µm^2)[55]. The results for a stimulus intensity of 30 ranged from 1 R* s^{-1} per rod (ND8) to 10^4 R* s^{-1} per rod (ND4) (**Fig. 1b**). These calculations, as well as recordings from mice lacking functional rods and functional cones (data not shown), suggest that ND8 and ND7 correspond to scotopic conditions, ND6 weakly activates cones, ND5 is fully mesopic and ND4 is photopic. Note that our characterization of ND7 as scotopic may partly be owed to our use of low-contrast stimuli. We cannot exclude the possibility that stimuli with stronger contrast might activate cones even at ND7 (see, for example, refs. 5,56).

Light stimuli. All stimuli were grayscale images with pixel values between 0 (black) and 60 (white). The background was kept at 30 (gray), and the stimuli were balanced to keep the mean intensity over time at 30.

Our stimulus set for MEA recordings contained the following: (1) Full-field steps (**Fig. 1a,b**). ON step: stepping to an intensity of 50 for 2 s from the background of 30 (66% Weber contrast); OFF step: stepping to 10 for 2s (−66%). (2) Full-field Gaussian flicker, 30 s or 1 min. Screen brightness was updated every frame (60 Hz) or every other frame (30 Hz) and was drawn from a Gaussian distribution with mean 30 and s.d. 9. This stimulus was used to calculate the linear filters of ganglion cells[57]. (3) Disk stimulus. Disks (diameter, 150 µm on the retina) were presented on a gray (30) background for 2s and had the same contrast as the full-field step stimulus (10 for black disks, 50 for white disks). They were centered over the recording electrodes. The sequence of disk locations was chosen such that the next disk was always at least 600 µm away from the previous disk, and at least 7 white and 7 black disks were presented at each location at

each ND level. (4) Binary checkerboard flicker, 15 min. The screen was divided into a 40 × 40 checkerboard pattern; each checker covered 60 × 60 μm^2 on the retina. The intensity of each checker was updated independently from the other checkers and randomly switched between 10 and 50. This stimulus was used to calculate the spatial receptive field of ganglion cells. (5) Natural movie, 22 s. It consisted of sequences taken from the music video "Rip It Up" by Bill Haley (https://www.youtube.com/watch?v=HdlfZ4213zM). The contrast of the movie was compressed so that it spanned brightness values between 0 and 60.

We used different combinations or subsets of these stimuli in different experiments, repeated several times at each ND filter. The complete experimental stimulus set lasted at least 20 min at each ND. See results for details.

Our stimulus set for single cell recordings contained the following: (1) Full-field steps (see above). (2) Full-field Gaussian flicker (see above). (3) Disk stimulus (see above). Disks were centered over the patched cell's soma. (4) Annulus stimulus. Full-field contrast step (see above) with an inner hole (diameter, 500 µm on the retina) staying at gray (30) background, centered on the patched cell's soma. The same set of stimuli was presented at each ND from ND8 to ND4, taking a total of 35 min. Only one cell was recorded from each retina.

Data analysis. *Spike sorting.* Data were high-pass filtered (500 Hz, tenth-order Butterworth filter), and spike waveforms and spike times were extracted from the raw data using Matlab (The MathWorks Inc., MA, USA). Spike sorting (assignment of spikes to individual units, presumably ganglion cells) was performed semimanually with custom written software (Matlab). The quality of each unit was individually and manually assessed by inter-spike interval and spike shape variation. Data analysis was based on the spiking responses of individual units.

Calculation of cell polarities and receptive fields. We calculated linear filters in response to full-field Gaussian flicker and to binary checkerboard flicker by summing the 500-ms stimulus history before each spike. Linear filters calculated in response to the full-field flicker were used to determine cell polarity. Latency and amplitude of the first peak of the filter were determined. If the peak was positively deflected, the cell was categorized as an ON cell. If negatively deflected, the cell was categorized as an OFF cell. Linear filters calculated in response to the binary checkerboard flicker were used to determine the spatial receptive field. For each checker, we determined the s.d. along the 500-ms temporal kernel. From the resulting 40 × 40 matrix entries, we calculated the mean and s.d., set all checkers lying below mean + 4 s.d. to zero, fit a two-dimensional Gaussian, and took the 2.5-σ ellipse as a representation for the receptive field (**Fig. 8c**,**d**).

Firing rate calculation. We estimated the instantaneous firing rate by convolving the spike train (time series of 0's and 1's) with a Gaussian with σ = 40 ms and amplitude = 0.25 σ^{-1} $e^{1/2}$ (≈10 Hz for σ = 40 ms), unless otherwise noted.

Algorithm to detect and classify early and delayed responses. For the step-stimuli (full-field and disks), we applied an algorithm to automatically detect ON responses in OFF cells or OFF responses in ON cells and to classify them as early or delayed (see Results for definitions). Responses were rejected as unreliable for specific light levels if less than 50% of them were strongly correlated with each other ("strong correlation" was defined here as pairwise Pearson correlation coefficient of at least 0.4; 0.2 for experiments where automated classification was only taken as a suggestion and manually corrected). Then we applied an automatic algorithm to detect and classify early and delayed responses at each reliable light level. Briefly, we compared the maximal firing rates during spontaneous activity on the one hand and the relevant time windows for early (50–350 ms after the stimulus) and delayed (350–1,000 ms) responses on the other hand. If the peak firing rate in the response windows was higher than during spontaneous activity and also more correlated from trial to trial, we categorized the response as present, regardless of its absolute amplitude (that is, binary classification 'absent/present'). Additional checks were implemented to distinguish these responses from 'tails' of sustained responses to the preferred contrast and to distinguish a delayed response from a slowly declining early response (in both cases, we checked for 'valleys', or firing rate decreases, before the response peak). Mostly, the specific parameters used by the algorithm were based on heuristics and we made extensive checks to confirm that the automatic classification was valid. The responses to the small disk and in *Gnat2* retinas had smaller signal-to noise ratio; for those responses we treated the result of the automated algorithm only as a suggestion and confirmed each individual response by hand. Responses during GABA blocker application had different shapes in some cells (sharp peaks, thus slightly different latency distribution). Responses obtained during these experiments were checked manually and corrected where necessary. Responses of the LGN neurons were classified by hand.

We next compared the responses across light levels. Overall, a cell was classified as stable if, at all light levels being compared, it always had the same response type to the black step (that is, no response, early response, delayed response, or both early and delayed response) and always the same response type to the white step. Otherwise the unit was classified as changing. If a cell had unreliable responses at some light level (see above), this light level was not considered for the analysis. For example, if a cell had unreliable responses at ND6, we did not compare this cell's responses for the ND7/6 or the ND6/5 transition, but we still compared its responses between all other light levels, for example, between ND7 and ND5. This is the reason for the different numbers of cells for each luminance transition in the plots showing the fraction of changing and stable units (for example, **Fig. 3b**,**d**). As a consequence, a cell may be classified as stable even if it had unreliable responses at one or more light levels. The fraction of changing cells can therefore be viewed as a conservative estimate.

Analysis of movie responses. Responses to the movie typically consisted of interleaved sequences of spike bursts ('events') and silence. To test whether the response to the movie would change across light levels, we analyzed whether a cell would have an event during some light level(s), but not other(s). This analysis proceeded in several steps: (1) Alignment. We calculated the average spike rate for each light level (see above) with a σ of 10 ms, and calculated the pairwise cross-correlation to estimate the relative temporal shift of the spike trains (spiking always gets faster at higher intensities). We then aligned the spike trains across light levels. (2) Event detection. (a) From the aligned spikes, we calculated the average firing rate across the whole experiment with a σ of 30 ms. Events were preliminarily defined as periods where the spike rate exceeded the mean firing rate of the 2 s before movie onset + 3 STD. (b) If spike bursts occur close to each other, they are fused into 1 event because the calculated firing rate does not drop below the threshold between the bursts. We therefore identified local minima in the spike rate and split events at those minima. (c) Of the resulting events we discarded those that were shorter than 20 ms and those that had a peak firing rate smaller than 5% of the second-largest event. (3) Response strength. We counted the spikes in each event at each light level, and converted that count into an average spike rate (number of spikes/s per movie presentation). We refer to this as the activity of the cell during an event and at each light level. (4) Light levels with very low activity. Events are inherently defined by high activity. To look for qualitative response changes across light levels, we therefore identified light levels during which there was low activity during an event. We applied 2 criteria to identify such 'silent' light levels: (a) Comparison across light levels within an event: the activity during a silent light level had to be lower than 10% of the maximal activity during this event. (b) Comparison across events within a light level: The activity during a silent event had to be less than 10% of the mean activity across all events at that light level. For analysis we counted only such events as silent that fulfilled both criteria (dark gray in **Supplementary Fig. 3**).

Statistical analysis. No statistical methods were used to predetermine sample sizes, but our sample sizes are similar to those generally employed in the field. No statistical tests were required for analysis of the data presented.

***In vivo* recordings.** Five adult female C57 wild-type mice (6–8 weeks, housed in a 12-h light-dark cycle with 6 animals per cage) were used for experiments between 8 a.m. and 6 p.m. Mice were anaesthetized by i.p. injection of 30% (w/v) urethane (1.5 g/kg; Sigma, UK) and placed in a stereotaxic apparatus (SR-15 M; Narishige International Ltd., UK). Additional top up doses of anesthetic (0.2 g/kg) were applied as required and body temperature maintained at 37 °C with a homoeothermic blanket (Harvard Apparatus, Kent, UK).

An incision to expose the skull surface was made and a small hole (~1 mm diameter) drilled 2.5 mm posterior and 2.3 mm lateral to the bregma, targeting the dorsal LGN. The pupil, contralateral to the craniotomy, was dilated with topical 1% (w/v) atropine sulfate (Sigma) and the cornea kept moist with mineral oil. A recording probe (A4X8-5 mm-50-200-413; Neuronexus, MI, USA) consisting of four shanks (spaced 200 µm apart), each with eight recordings sites (spaced 50 µm apart) was then positioned centrally on the exposed surface in the coronal plane, and lowered to a depth of 2.5–3.3 mm using a fluid-filled micromanipulator (MO-10; Narishige).

Once the recording probe was in position and light responses confirmed, mice were dark adapted for 1 h, which also allowed neuronal activity to stabilize after

probe insertion. Neural signals were acquired using a Recorder64 system (Plexon, TX, USA). Signals were amplified ×3,000, high-pass filtered at 300 Hz and digitized at 40 kHz. Multiunit activity (spikes with amplitudes >50 µV) were saved as time-stamped waveforms and analyzed offline (see below).

Light stimuli (λ_{max}, 460 nm; half peak width, ± 10 nm) were generated by a custom-built LED-based light source (Cairn Research Ltd.), passed through a filter wheel with various ND filters and focused onto a 5-mm-diameter piece of opal diffusing glass (Edmund Optics Inc., York, UK) positioned 3 mm from the eye contralateral to the recording probe. LED intensity and filter wheel position were controlled by a PC running LabView 8.6 (National instruments). At each intensity, starting from the lowest (6.1×10^{-1} R* rod^{-1} s^{-1}), a 2-s light increment from background (+66% contrast) was followed by a 5-s inter-stimulus interval of background light, after which a 2-s light decrement (−66% contrast) was presented. This was repeated 120 times at each background level before being increased by a factor of ten, spanning a 6-log-unit range in total. Mice were otherwise kept in complete darkness.

At the end of the experiment mice were transcardially perfused with 0.1 M PBS followed by 4% PFA. The brain was removed, postfixed overnight, cryoprotected with 30% sucrose and sectioned at 50 µm on a freezing sledge microtome. Sections were mounted with DPX (Sigma), coverslipped and electrode placement in the dLGN confirmed by visualization of a fluorescence dye (Cell Tracker CM-DiI; Invitrogen Ltd. Paisley, UK) applied to the probe before recording.

Multichannel, multiunit recordings were analyzed in Offline Sorter (Plexon). Following removal of cross-channel artifacts, principal component–based sorting was used to discriminate single units, identifiable as a distinct cluster of spikes in principal component space with a clear refractory period in their inter-spike interval distribution. Following spike sorting, data were exported to Neuroexplorer (Nex technologies, MA, USA) and Matlab R2013a for construction of peristimulus histograms and further analysis. Light-responsive units were identified as those for which the peristimulus average showed a clear peak (or trough) that exceeded the 99% confidence limits estimated from a Poisson distribution derived from the prestimulus spike counts.

Corneal irradiance was measured using a calibrated spectroradiometer (Bentham Instruments, Reading, UK; Ocean Optics, FL, USA). Retinal irradiance was calculated by multiplying these values by pupil area/retinal area, based on calculations by Lyubarsky *et al.*[58], where a pupil size of 3.2 mm^2 and retinal area of 17.8 mm^2 were used to generate a correction factor of 0.18. Effective photon flux was calculated by multiplying retinal irradiance by spectral transmission through the mouse lens[59]. Photoisomerizations were calculated as described for MEA recordings. All procedures conformed to requirements of the UK Animals (Scientific Procedures) Act, 1986.

A **Supplementary Methods** checklist is available.

51. Reinhard, K. *et al.* Step-by-step instructions for retina recordings with perforated multi electrode arrays. *PLoS ONE* **9**, e106148 (2014).
52. Yonehara, K. *et al.* Spatially asymmetric reorganization of inhibition establishes a motion-sensitive circuit. *Nature* **469**, 407–410 (2011).
53. Gavrikov, K.E., Nilson, J.E., Dmitriev, A.V., Zucker, C.L. & Mangel, S.C. Dendritic compartmentalization of chloride cotransporters underlies directional responses of starburst amacrine cells in retina. *Proc. Natl. Acad. Sci. USA* **103**, 18793–18798 (2006).
54. Hoover, J.L., Bond, C.E., Hoover, D.B. & Defoe, D.M. Effect of neurturin deficiency on cholinergic and catecholaminergic innervation of the murine eye. *Exp. Eye Res.* **122**, 32–39 (2014).
55. Nikonov, S.S., Kholodenko, R., Lem, J. & Pugh, E.N. Jr. Physiological features of the S- and M-cone photoreceptors of wild-type mice from single-cell recordings. *J. Gen. Physiol.* **127**, 359–374 (2006).
56. Szikra, T. *et al.* Rods in daylight act as relay cells for cone-driven horizontal cell–mediated surround inhibition. *Nat. Neurosci.* doi:10.1038/nn.3852 (26 October 2014).
57. Chichilnisky, E.J. A simple white noise analysis of neuronal light responses. *Network* **12**, 199–213 (2001).
58. Lyubarsky, A.L., Daniele, L.L. & Pugh, E.N. Jr. From candelas to photoisomerizations in the mouse eye by rhodopsin bleaching in situ and the light-rearing dependence of the major components of the mouse ERG. *Vision Res.* **44**, 3235–3251 (2004).
59. Jacobs, G.H. & Williams, G.A. Contributions of the mouse UV photopigment to the ERG and to vision. *Doc. Ophthalmol.* **115**, 137–144 (2007).

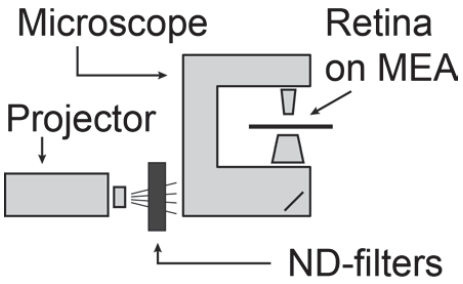

Supplementary Figure 1
Experimental setup for multi-electrode array recordings.

The retina was placed on a multi-electrode array and visual stimulation was achieved with a projector through the condenser of the microscope. Neutral density (ND) filters were used to decrease the mean luminance of the visual stimulation in 1-log-unit steps.

Nature Neuroscience: doi:10.1038/nn.3891

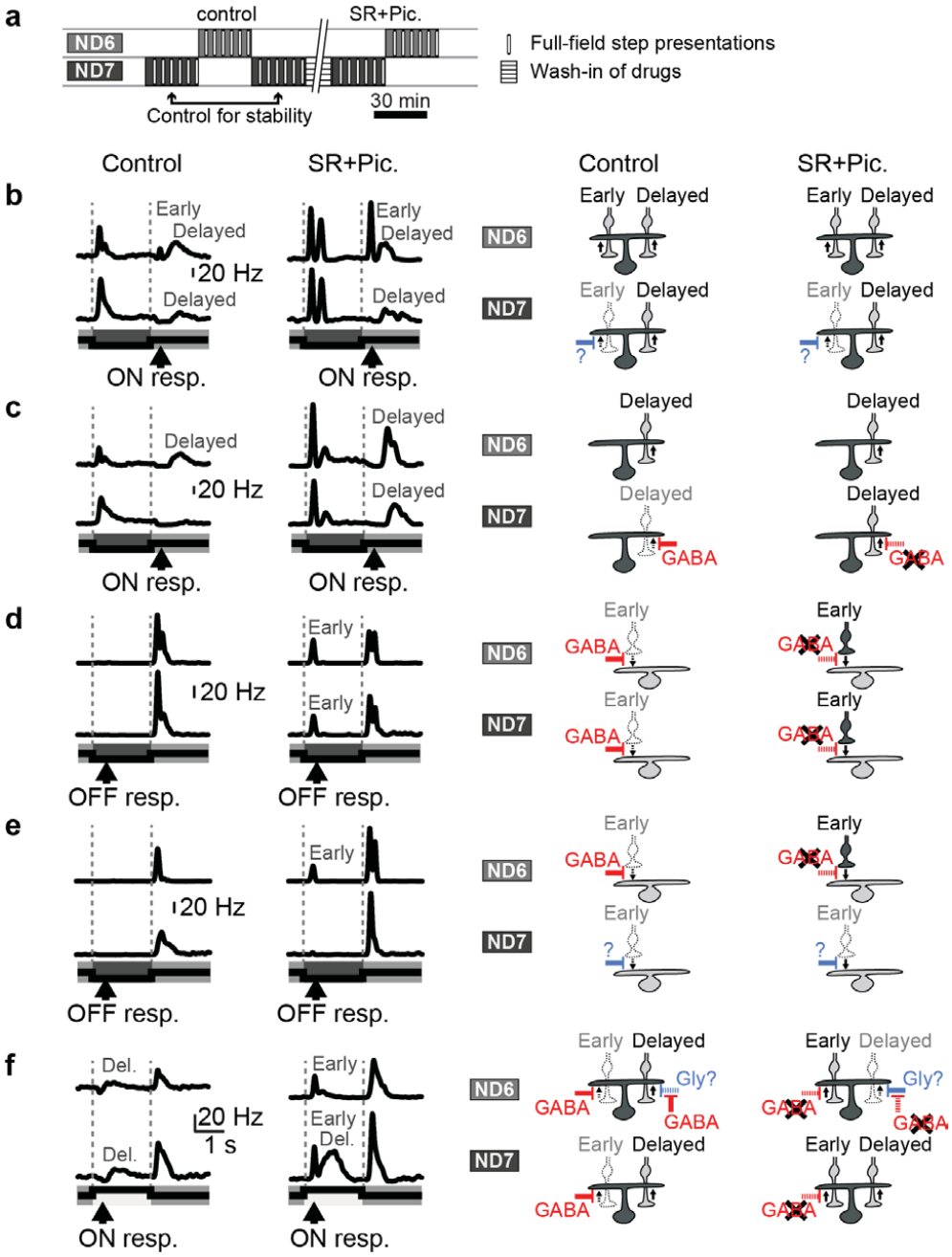

Nature Neuroscience: doi:10.1038/nn.3891

Supplementary Figure 2
Luminance-dependent response changes with and without GABA blockers.

(**a**) Stimulus protocol. SR: SR-95531 (gabazine), Pic.: picrotoxin. (**b–e**) Examples of luminance- and GABA-blocker-dependent response patterns in three OFF cells (**b**,**d**,**f**) and two ON cell (**c**,**e**). Left: Spike rates at ND7 and ND6 luminance levels with and without GABA blockers. Right: One possible circuit scheme each which is consistent with the observed responses. The five examples represent the following categories of observations: (**b**) *Luminance-dependent response changes not influenced by GABA* (observed in n = 3 units; the example shows appearing early ON response at ND6 under both control and drug condition). Such cells changed their response properties identically under control and drug conditions between ND7 and ND6. Thus, these luminance-dependent response changes were independent of GABAergic regulation. (**c**) *Luminance-dependent GABAergic masking of responses* (n=3; example cell has a delayed ON response masked at ND7). In such cells, light responses differed at ND7 and ND6 under control conditions, but not in the presence of GABA blockers. This suggests that GABAergic inhibition masked a response at one light level. (**d**) *Luminance-independent GABAergic masking of responses* (n=12; example: unmasked early response at ND7 and ND6). Such cells did not show any luminance-dependent changes, neither in control nor with GABA blockers, but their responses were different between control and drug conditions within each light level. This suggests that GABAergic inhibition regulated responses at both luminance levels. Potentially, these masked responses might be revealed at other brightness levels. Note that the same phenomenon applies to the early ON responses in **f**. (**e**) *GABA-dependent stabilization of responses* (n=13; the example illustrates this effect for early OFF responses). Such cells with stable responses under control conditions had changing responses under drug conditions. Thus, those changing response themselves were GABA-independent, while at the same time GABA stabilized the responses during the luminance-switch under control conditions. Note that the same phenomenon applies to the delayed ON responses in **f**. (**f**) *GABA-dependent disinhibition* (n=6, the example shows disappearance of delayed ON response with GABA blockers at ND6). While in all examples above GABA blockers revealed additional responses, in few cells responses disappeared in GABA blockers (n=2 at ND7, n=5 at ND6, of which 1 unit was affected at both NDs). This suggests luminance-dependent disinhibitory GABAergic mechanisms.

The phenomena described by these examples occurred in both ON and OFF cells. In some cells, we observed one phenomenon to the white step, and another phenomenon to the black step, highlighting the response asymmetry already observed in control conditions (**Fig. 3**). In summary, we found that the mechanism of GABAergic response regulation is highly diverse, and that it underlies some but not all luminance-dependent qualitative response changes.

Nature Neuroscience: doi:10.1038/nn.3891

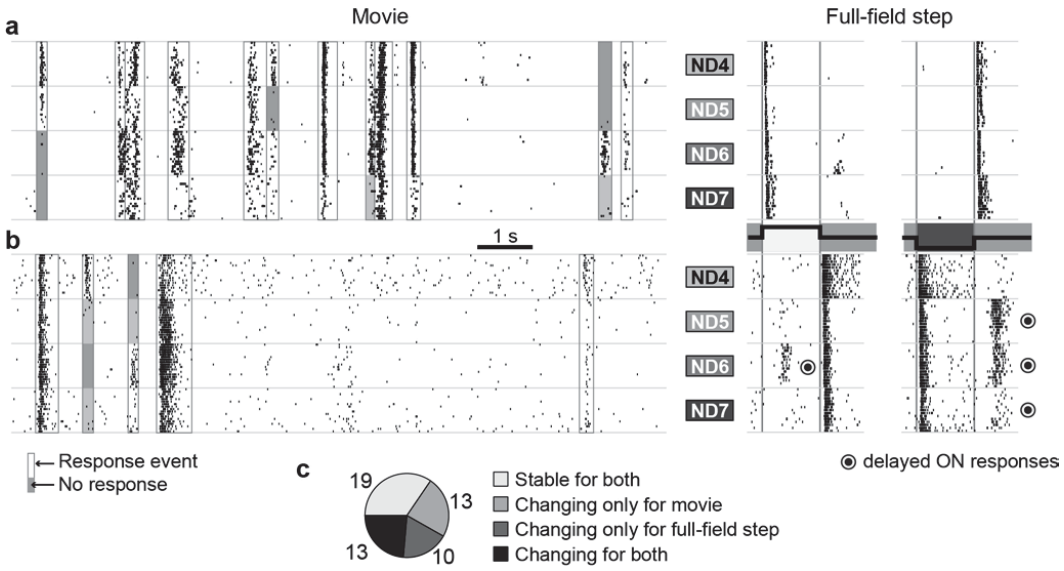

Supplementary Figure 3
Luminance-dependent changes in ganglion cell responses to a naturalistic movie.

Raster plots: responses of individual ganglion cells to the movie stimulus (left) and to the full-field step stimulus (right). Shaded regions indicate events where the neuron was silent, even though it responded at other light levels. (**a**) ON ganglion cell with stable responses to the full-field step, but qualitative changes in its movie response. (**b**) OFF ganglion cell with changing responses to both movie and full-field step stimulus. (**c**) Response changes to full-field steps do not always occur together with response changes to movies, and vice versa. Numbers indicate the number of units in each group.

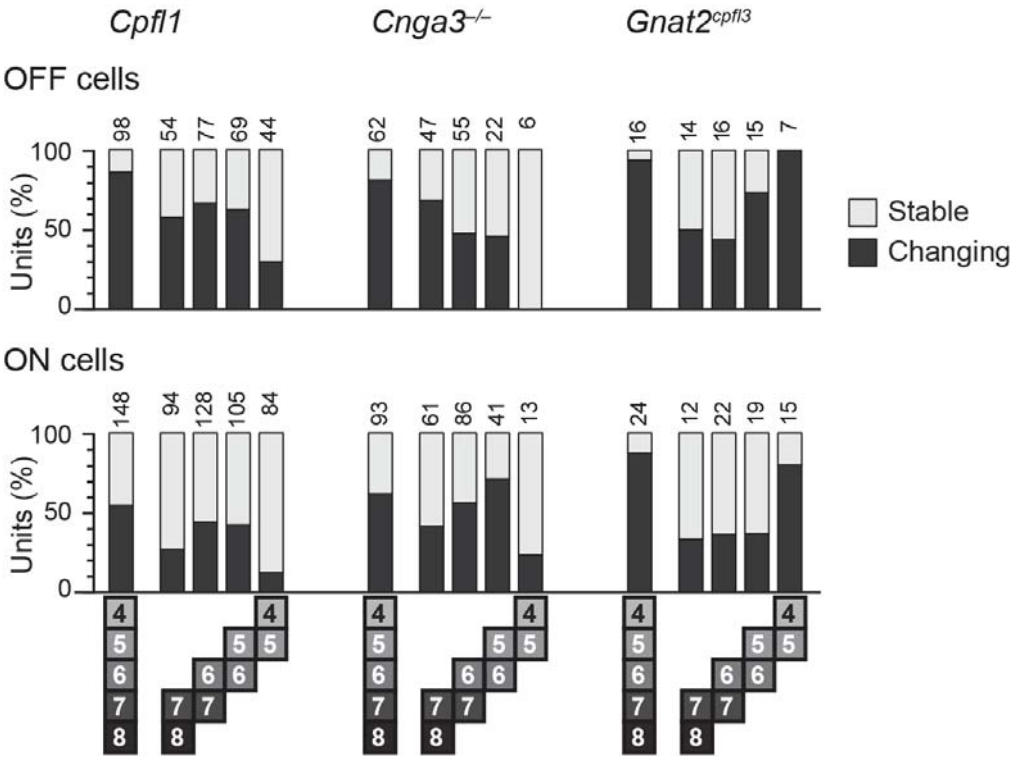

Supplementary Figure 4
Luminance-dependent qualitative response changes in different mouse lines lacking functional cones.

Cpfl1: 98 OFF cells and 148 ON cells from 6 retinas. *Cnga3*$^{-/-}$: 62 OFF cells and 93 ON cells from 6 retinas. *Gnat2*^{cpfl3}: 16 OFF cells and 24 ON cells from 5 retinas. Conventions as in **Fig. 3b**.

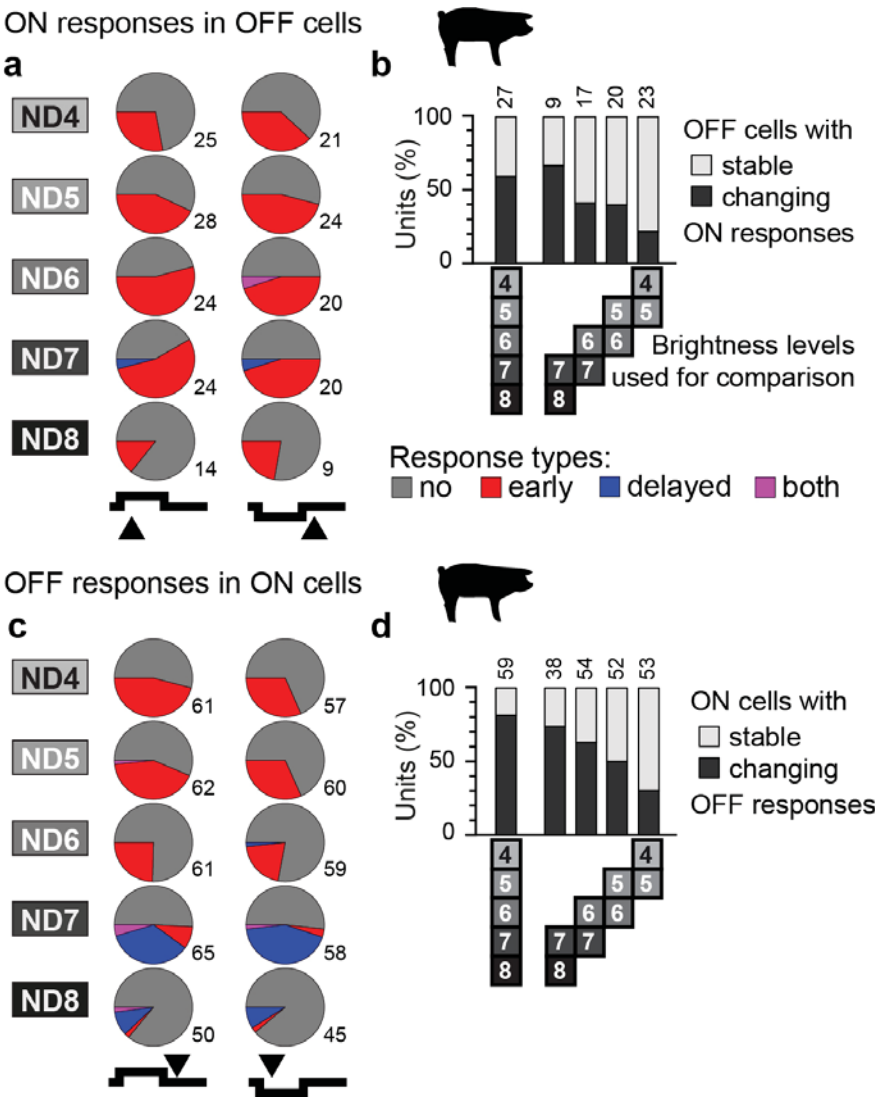

Supplementary Figure 5
Summary of luminance-dependent response types in pig retina.

Data is based on recordings from 27 ON cells and 59 OFF cells from 3 retinal pieces from 2 animals. Conventions as in **Fig. 3**.

Publication 5

Irene González-Menéndez*, Katja Reinhard*, Jorge Tolivia, Bernd Wissinger, Thomas A Münch (2015) Influence of Opa1 mutation on survival and function of retinal ganglion cells. ***Invest Ophthalmol Vis Sci.*** **DOI:10.1167/iovs.15-16743**

*** equal contributions**

Framework: In this original research paper, we characterized the effect of retinal degeneration in a mouse model for optic atrophy ($Opa1^{+/-}$). The study contains morphological and physiological analysis in mice of different ages.

My contributions: I performed all multi-electrode array recordings, and analyzed and interpreted the data with the help of TAM. Processing of the data is a time-intensive task and involved manual inspection of several hundred recorded cells. Analysis of this data required extensive implementation of various complex algorithms for cell type clustering and evaluation of their performance. I wrote the physiological part of the manuscript, helped with introduction and discussion, and prepared the figures for the physiological data.

Other contributions: IGM performed all morphological and histological experiments and analyzed the thereby gained data. She wrote the corresponding parts of the manuscript as well as the first draft of the introduction. Experimental design and analysis of the morphological part was supported by BW, and of the physiological part by TAM. TAM helped with the figures. TAM and BW helped with the manuscript. JT helped with analysis of optic nerve sections.

Retina

Influence of *Opa1* Mutation on Survival and Function of Retinal Ganglion Cells

Irene González-Menéndez,[1] Katja Reinhard,[2,3] Jorge Tolivia,[4] Bernd Wissinger,[1] and Thomas A. Münch[2]

[1]Molecular Genetics Laboratory, Institute for Ophthalmic Research, University of Tübingen, Tübingen, Germany
[2]Retinal Circuits and Optogenetics, Centre for Integrative Neuroscience and Bernstein Center for Computational Neuroscience, University of Tübingen, Tübingen, Germany
[3]International Max Planck Research School, University of Tübingen, Tübingen, Germany
[4]Morphology and Cell Biology Department, University of Oviedo, Oviedo, Spain

Correspondence: Thomas A. Münch, Centre for Integrative Neurosciences (CIN), University of Tübingen, Otfried-Müller-Str. 25, 72076 Tübingen, Germany;
thomas.muench@cin.uni-tuebingen.de.
Bernd Wissinger, Molecular Genetics Laboratory, Institute for Ophthalmic Research, University of Tübingen, Röntgenweg 11, 72076 Tübingen, Germany;
wissinger@uni-tuebingen.de.

IG-M and KR contributed equally to the work presented here and should therefore be regarded as equivalent authors.

Submitted: February 24, 2015
Accepted: June 12, 2015

Citation: Gonzalez-Menendez I, Reinhard K, Tolivia J, Wissinger B, Münch TA. Influence of *Opa1* mutation on survival and function of retinal ganglion cells. *Invest Ophthalmol Vis Sci*. 2015;56:4835–4845. DOI:10.1167/iovs.15-16743

Purpose. Mutations in the *OPA1* gene cause autosomal dominant optic atrophy (ADOA), a visual disorder associated with degeneration of retinal ganglion cells (RGCs). Here, we characterized the disease progression in a homologous mouse model B6;C3-*Opa1*$^{329\text{-}355del}$ and asked whether the pronounced cell death affects certain RGC types more than others.

Methods. The influence of the *Opa1* mutation was assessed by morphologic (retina and optic nerve histology) and functional (multielectrode array) methods.

Results. The RGC loss of approximately 50% within 18 months was significantly more pronounced in RGCs with small-caliber axons. Small-caliber axon RGCs comprise a variety of functional RGC types. Accordingly, electrophysiological analyses of RGCs did not show a dropout of distinct functional RGC subgroups. However, the response properties of RGCs were affected significantly by the mutation. Surprisingly, these functional changes were different under different luminance conditions (scotopic, mesopic, and photopic). Finally, melanopsin cells are known to be less susceptible to retinal insults. We found that these cells are also spared in the *Opa1* mouse model, and demonstrated for the first time that this resistance persisted even when the melanopsin gene had been knocked-out.

Conclusions. Small-caliber axons show a higher vulnerability to the *Opa1* mutation in our mouse model for ADOA. Luminance-dependent functional changes suggest an influence of the *Opa1* mutation on the retinal circuitry upstream of RGCs. Photoresponsive RGCs are protected against cell death due to the *Opa1* mutation, but not by melanopsin expression itself.

Keywords: optic neuropathy, retinal ganglion cells, optic nerve, MEA recordings, melanopsin

Autosomal dominant optic atrophy (ADOA) is the most frequent hereditary neuropathy, besides Leber's hereditary optic neuropathy, with an estimated prevalence of 1:30,000 worldwide.[1] Autosomal dominant optic atrophy patients suffer from a slow but progressive bilateral vision loss characterized by caecocentral scotoma, pallor of the optic disk together with reduced thickness of the nerve fiber layer, and specific color vision disturbances in the blue-yellow axis. Further, extensive cell death has been observed in retinal ganglion cells (RGCs), but no other retinal cell type.[2,3] However, there is high variability in onset, visual impairment, and penetrance, indicating that the phenotype might be influenced by the genetic background, genetic modifiers or the environment.[1] The Optic Atrophy 1 gene (*OPA1*) is by far the most common gene mutated in ADOA and accounts for 65% to 90% of cases in well-defined patient cohorts.[4,5] The nuclear *OPA1* gene encodes a ubiquitously expressed mitochondria-targeted, dynamin-related GTPase, which is a key factor in the mitochondrial fusion dynamics.[6] OPA1 also participates in the formation of protein complexes that bridge and tighten the cristae junction leading to retention of cytochrome C in the lumen of the cristae,[7,8] and it interacts with the oxidative phosphorylation complexes I, II, and III.[9–11]

Two mouse models for nonsyndromic ADOA with mutation in the *OPA1* gene have been developed: B6;C3-*Opa1*^{Q285STOP} and B6;C3-*Opa1*$^{329\text{-}355del}$.[12,13] Both models reflect the phenotype (optic nerve atrophy, altered mitochondria organization) observed in patients with similar mutations. However, the RGC loss in the B6;C3-*Opa1*^{Q285STOP} mouse is limited, while the B6;C3-*Opa1*$^{329\text{-}355del}$ model shows a significant reduction in RGC counts.[14] Retinal ganglion cells are a heterogeneous cell class, which can be divided into several clusters depending on their morphologic[15] or functional[16] properties. The various subpopulations might be affected differently by pathophysiological events. In fact, Williams et al.[17] identified in the B6;C3-*Opa1*^{Q285STOP} mouse model an altered dendritic morphology together with changes in the synaptic profile in the On-center RGCs. The Off-center RGCs remained unaffected. So far, there has been no detailed study on how the *Opa1* mutations affect the function of different RGC subpopulations. Here, we aimed

Investigative Ophthalmology & Visual Science

at identifying RGC types that might be specifically affected in the B6;C3-*Opa1*$^{329\text{-}355del}$ model, by morphologic analysis of the optic nerve and functional evaluation of light responses of RGCs.

Further, we studied the melanopsin system and the potential protective role of melanopsin in the B6;C3-*Opa1*$^{329\text{-}355del}$ mouse model. It has been shown that melanopsin-expressing RGCs[18] might be preserved in ADOA patients as well as in the B6;C3-*Opa1*^{Q285STOP} mouse model.[3,19] This led to the hypothesis that melanopsin expression per se may protect these cells from light damage,[3] whereas similar light exposure might be harmful to nonmelanopsin RGCs, especially in the presence of abnormal cellular function.[20]

Materials and Methods

Animals and Experimental Design

Male and female B6;C3-*Opa1*$^{329\text{-}355del}$ and Opn4^{tauLacZ} mice were used in this study. Animals were fed with standard food and tap water ad libitum, and maintained under constant temperature conditions (22°C ± 2°C) and daily cycles of 12-hour light/darkness. All experiments were performed in accordance to the ARVO Statement for the Use of Animals in Ophthalmic and Vision Research as well as the Tübingen Institutional Animal Care and Use Committee (Tübingen, Germany), and have been approved by the local authorities.

Opa1 Mouse Line

The B6;C3-*Opa1*$^{329\text{-}355del}$ mouse strain was used in this study. In the homozygous state this mutation is lethal. We used heterozygous mutants (Opa1$^{enu/+}$) and their wild-type littermates (Opa1$^{+/+}$, in the following text called WT) to determine the effects of the *Opa1* mutation on the number and functionality of the RGCs and the melanopsin system. Animals were killed at 1, 6, 12, and 18 months of age. The day prior to the experiments, mice were kept in darkness (necessary to perform multielectrode array [MEA] recording under scotopic conditions) and killed under dim red light. All animals are listed in Supplementary Table S1.

Opn4$^{tau\text{-}Lacz}$ Mouse Line

The Opn4$^{tau\text{-}lacZ}$ mouse (kindly provided by King-Wai Yau, Johns Hopkins School of Medicine, Baltimore, MD, USA), has the *Opn4* gene (encoding melanopsin) replaced with sequences encoding for a tau-lacZ fusion protein. This mouse model has no expression of melanopsin, but "naturally" melanopsin-expressing RGCs can be labeled by β-galactosidase staining. This allows the identification of these cells when melanopsin is removed, and to determine the potentially protective role of the melanopsin protein itself. Therefore, we crossbred the B6;C3-*Opa1*$^{329\text{-}355del}$ with the Opn4$^{tau\text{-}lacZ}$ mice and analyzed 18- to 23-month-old animals. These animals are listed in Supplementary Table S2.

Optic Nerve Analysis

Tissue Sampling. Optic nerve samples were placed for 2 hours in 2% glutaraldehyde/2% paraformaldehyde in 0.1 M cacodylate (CACO) buffer (pH 7.4), then washed three times in 0.1 M CACO buffer and postfixed in 1% osmium tetroxide (OsO_4) in 0.1 M phosphate buffer (PB) for 80 minutes. After washing three times in 0.1 M CACO buffer, samples were dehydrated in ethanol: 50%, 70%, 70% ethanol with uranyl acetate overnight at 4°, 80%, 90%, 95%, 100%, 100% ethanol with molecular sieve and finished by immersing the samples twice in propylene oxide (Sigma-Aldrich Corp., St. Louis, MO, USA). The samples were placed in EPON resin (Sigma-Aldrich Corp.) with propylene oxide (ratio 1:1) for 1 hour and then embedded in EPON resin overnight. The resin was polymerized after placing the samples into a flat mold, covered with fresh 100% EPON resin with 1.5% Starter (N-Benzyldimethylamin 98%; Sigma-Aldrich Corp.) and incubated at 55°C for 96 hours. All steps were performed at room temperature (RT) and for 10 minutes, unless otherwise noted.

Sectioning. Using a glass knife on an ultramicrotome (Leica, Solms, Germany), 0.5-μm thick sections were cut and placed on distilled water on a poly-L-lysine coated slide, flattened by heating (40°C for ~30 minutes), and stained with Richardson solution.[21] The slides were then coverslipped and sealed with DPX mounting medium (Sigma-Aldrich Corp.).

Acquisition and Processing of the Images. Three random nonoverlapping 5809-μm^2 squares including peripheral and central regions were imaged with a digital camera (Olympus V-CMAC3; Olympus, Tokyo, Japan) mounted on an Olympus AX70 microscope. Images were processed with a modification of the method described by Tolivia et al.[22,23] (example images shown in Fig. 1A were contrast enhanced in Adobe Photoshop [Adobe Systems, Inc., San Jose, CA, USA] for clarity). Briefly, in Adobe Photoshop the specific outlines of axons were selected (mask). Being based on light-microscopic images, this analysis misses nonmyelinated axons, which however represent only 1% to 2% of the total number of axons.[24] Nevertheless, even small-caliber axons, if myelinated, are reliably detected, and consequently our results are fully consistent with previous observations based on electron microscopy analysis.[13] The nonneural elements were then removed from the mask by hand, and this "clean" mask was analyzed with the "Analyze particles" routine (ImageJ 1.37c[25]). By this process, we generated an image in which each axon is labeled with a number allowing its identification as well as its morphometric characteristics (area, perimeter; Fig. 1A). Additionally, the whole section of the optic nerve was imaged in order to measure the cross-sectional area. Data is represented as estimated number of axons per optic nerve, which was calculated based on the overall cross-sectional area of each optic nerve and the number of axons observed in the three studied areas.

Multielectrode Array Recordings

Eye cups were placed in Ringer solution (in mM: 110 NaCl, 2.5 KCl, 1 $CaCl_2$, 1.6 $MgCl_2$, 10 D-Glucose, and 22 $NaHCO_3$ bubbled with 5% CO_2/95% O_2). All recordings were performed with a perforated 60-electrode MEA (60pMEA200/30iR-Ti-gr; Multichannel Systems, Reutlingen, Germany) as described previously.[26] Briefly, the retina was placed ganglion cell-side down in the recording chamber and perfused with Ringer solution at 34°C. Stimulation was performed from the bottom with a Digital Light Processing projector (Sharp PG-F212X-L; Sharp Corporation, Osaka, Japan). Data was recorded at 25 kHz with a USB or MC-Card based MEA-system (USB-MEA1060 or MEA1060; Multichannel Systems).

Visual Stimulation. The same set of stimuli (see below) was focused through the condenser onto the retina at scotopic (mean intensity: 8 rhodopsin isomerizations ($R^*{\cdot}s^{-1}$ per rod), mesopic ($8{\cdot}10^2$ $R^*{\cdot}s^{-1}$), and photopic light levels ($8{\cdot}10^4$ $R^*{\cdot}s^{-1}$) for 1 to 1.5 hours each. Each stimulus was repeated 4 to 15 times at each light level.

Spike Sorting and Correlation of Stimuli and Responses. Spike waveforms and spike-times were extracted from raw data with Matlab (MathWorks, Natick, MA, USA). Different features of the action potentials (amplitude, width, principal components) were calculated and projected onto 2-dimensional space either with Offline Sorter (Plexon, Inc.,

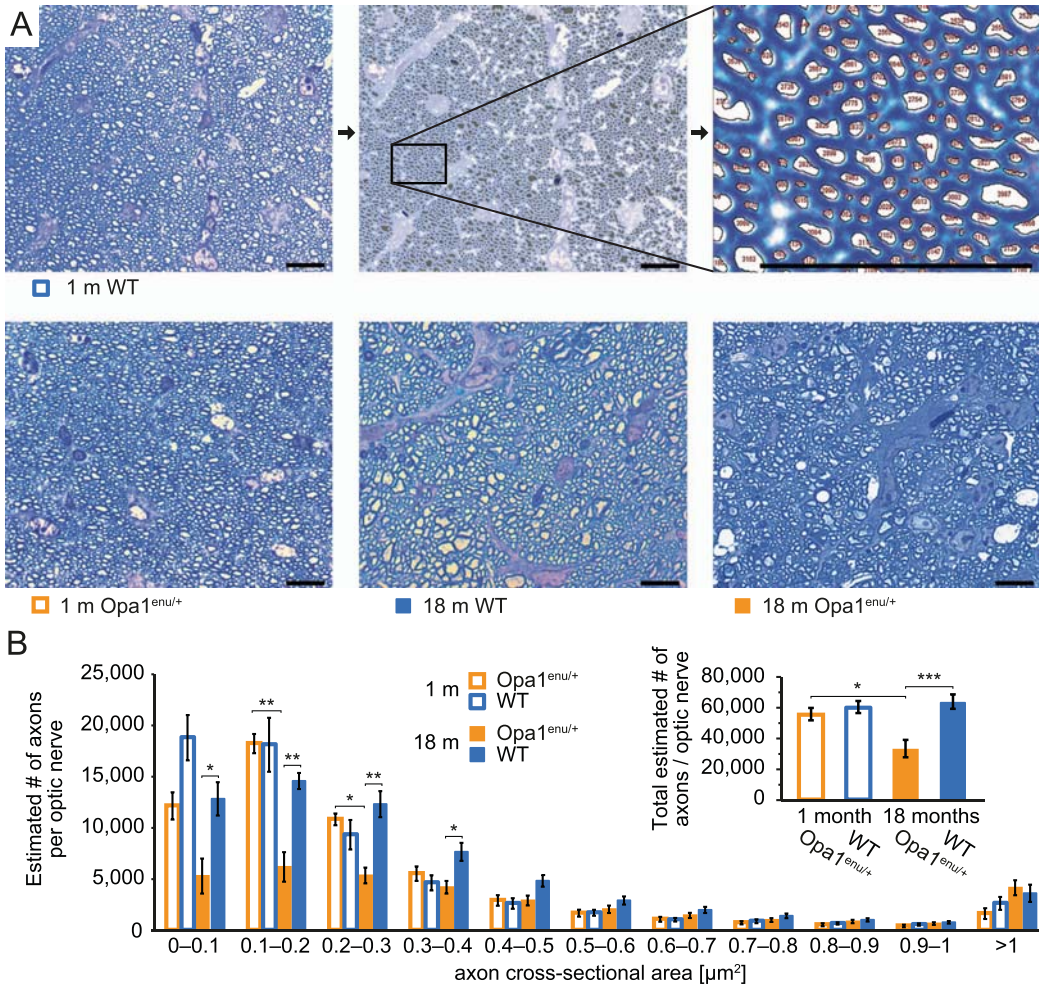

FIGURE 1. The number of small caliber axons is decreased in aged Opa1$^{enu/+}$ mice. (**A**) Representative light-microscopic images of Richardson-stained optic nerve cross sections. *Top row*: For axonal counting, a mask was automatically calculated and manually cleaned up to remove nonaxonal parts such as blood vessels (*top middle*); the resulting axon layouts were analyzed with respect to their number, area, and perimeter (*top right*, magnified view of the area indicated in the *middle*). In each optic nerve cross-section, three areas were analyzed (one central, two peripheral). Representative areas are shown for 1-month-old WT (*top left*) and Opa1$^{enu/+}$ mice (*bottom left*), and for 18-month-old WT (*bottom middle*) and Opa1$^{enu/+}$ mice (*bottom right*). *Scale bar*: 10 µm. (**B**) Axon numbers across age and genotype. The overall axonal number is significantly decreased in the Opa1$^{enu/+}$ 18-month group (~50% decrease when compared with the WT littermates) with an influence of the variables "age" and "genotype" (ANOVA test, $P < 0.0001$). No influence of the age was detected within the WT group (ANOVA test, $P > 0.05$) or of the genotype at the age of 1 month (ANOVA test, $P > 0.05$; *inset*). The number of small axons (<0.4 µm²) is significantly higher than that of the big ones, without influence of the age or genotype (ANOVA test, $P > 0.05$). The estimated number of the small axons (<0.4 µm²) is significantly reduced in the Opa1$^{enu/+}$18-month group when compared with WT 18 month or Opa1$^{enu/+}$ 1 month. Scheffe post hoc test revealed a decrease in the number of axons that belong to the 0.1 to 0.2 µm² bin in the Opa1$^{enu/+}$ 18-month animals compared with WT 18 month and with Opa1$^{enu/+}$ 1 month ($P < 0.01$). Similar result was obtained related to the 0.2- to 0.3-µm² bin (Opa1$^{enu/+}$ 18 month versus WT 18 month, $P < 0.01$; Opa1$^{enu/+}$ 18 month versus Opa1$^{enu/+}$ 1 month, $P < 0.05$). Axonal loss was also observed in the 0.01- to 0.1- and 0.3- to 0.4-µm² bin in the Opa1$^{enu/+}$ 18-month group when compared with the WT 18 month ($P < 0.05$ for both comparisons). No significant changes were detected in bins with areas > 0.4 µm² (ANOVA test, $P > 0.05$). Opa1$^{enu/+}$ 18 month: $n = 7$, WT 18 month: $n = 5$; Opa1$^{enu/+}$ 1 month: $n = 3$, WT 1 month: $n = 4$). $^{*}P < 0.05$, $^{**}P < 0.01$, $^{***}P < 0.001$, Scheffe post hoc test.

Dallas, TX, USA) or with an in-house written Matlab routine in order to semimanually assign spikes to individual units (presumably RGCs). We extracted 654 cells (Opa1$^{enu/+}$: $n = 85$ from 3 retinas (18 months), $n = 119$ from 4 retinas (12 months), $n = 108$ from 4 retinas (6 months), $n = 62$ from 4 retinas (1 month); WT: $n = 80$ from 5 retinas (18 months), $n = 74$ from 3 retinas (12 months), $n = 52$ from 4 retinas (6 months), $n = 74$ from 3 retinas (1 month), see also

Supplementary Table S1. To calculate the firing rate, the spike train of each cell was convolved with a Gaussian (sigma 40 ms), and the resulting firing rate trace was plotted against the time course of the presented stimuli. For each brightness level (scotopic, mesopic, photopic), we analyzed the parameters described below.

1. Spatial tuning: Responses to 24 different drifting sine-wave gratings (combination of different temporal frequencies: 1, 2, 4, 8 Hz; and spatial periods: 100, 200, 500, 1000, 2000, 4000 μm) were used for spatial tuning calculations. For each stimulus we calculated the Fourier transform of the response. The amplitude of the Fourier transform at the frequency of the grating stimulus was taken as the response strength of the cell. To estimate the spatial tuning, we calculated the median response to all grating stimuli with the same spatial period (Figs. 2A, 2B);
2. Temporal frequency tuning: The same analysis as for the spatial tuning was performed, but response median to the same temporal frequency were calculated (Figs. 2A, 2B);
3. Sustainedness: Peak responses to full-field contrast steps (gray → black → gray → white → gray, step duration: 2 seconds) were extracted. For the step which caused the maximal response, the fraction of this maximal response and the remaining average response strength 1700 to 2000 ms after stimulus onset was defined as "sustainedness" (Fig. $3A_1$). Cells whose firing rate dropped back to or below their background firing rate within these 2 seconds (i.e., transient cells) were assigned a sustainedness parameter of 0;
4. Latency: The same full-field contrast step as above was taken for latency measurements. Latency was defined as the time between stimulus onset and the peak response (Fig. $3A_1$); and
5. Speed tuning: Speed tuning was calculated from a single bar moving with various speeds (bar width: 1000 μm; speeds: 0.2, 1, 2, 4, 8, 16 mm/s; black and white bars used). The peak firing rate to each speed was measured and summed starting from the slowest speed (cumulative sum). Further parameter calculations were restricted to the stimulus to which the cell responded better (black or white bar) based on the summed peak firing rates. As speed tuning parameter we defined the speed at which the cumulative sum exceeded 50% (Fig. $3A_2$).

Parameters described above were calculated automatically. Cells that did not respond at all to a certain stimulus were removed manually (for single parameters) after inspection of the raw response as well as of the analyzed parameters where applicable (e.g., Fourier transforms).

Immunohistochemistry Analysis

Eye cups were fixed in 4% paraformaldehyde either for 24 hours at 4°C (melanopsin immunohistochemistry [IHC]) or for 2 hours at RT (β-galactosidase IHC). Fluorescence IHC was performed on whole-mounted retinae using an anti-mouse melanopsin antibody (UF006; Advanced Targeting Systems, San Diego, CA, USA) 1:5000 diluted in PBS with 0.4% Triton X-100 (PBS-T) for 72 hours at 4°C, and an anti-mouse β-galactosidase antibody (ab9361; Abcam, Cambridge, UK) 1:1500 diluted in PBS-T for 72 hours at 4°C as described previously.[27] Whole-mounted retinas were imaged with a fluorescence microscope (Olympus AX70; Olympus). The somata of the immunopositive cells were counted across the whole retina.

Statistical Analysis

Optic Nerves Analysis and Immunohistochemistry. SPSS 15 software (SPSS, Chicago, IL, USA) was used for statistical analysis. Kolmogorov-Smirnov and Levene's test were used to assess the normal distribution and homocedasticity of the data. One-way ANOVA tests were performed to analyze the effect of the genotype and age on the number of axons, number of melanopsin- and β-galactosidase-immunopositive cells. Scheffe post hoc tests were performed to detect differences between specific genotypes or ages. All data are presented as mean ± SEM. P less than 0.05 was considered statistically significant. Data was plotted in Matlab.

MEA Recordings. For each age group, brightness level, and response parameter, we performed a Wilcoxon rank sum test on the measurements of $Opa1^{enu/+}$ and WT RGC response parameters, as described in the results section. Where applicable, data is presented as median ± SD and ±95% confidence interval. Data was plotted in Matlab.

RESULTS

Optic Nerve Analysis

A large variability in visual impairment and corresponding RGC loss has been reported both in ADOA patients[28] and in the B6;C3-*Opa1*$^{329\text{-}355del}$ mouse model.[13,29] In order to assess the progression of RGC degeneration over time, we have quantified the number of axons in the optic nerve in 1- and 18-month-old WT and $Opa1^{enu/+}$ animals (Fig. 1A). No significant differences in the cross-sectional area of the optic nerve was observed between the different groups (ANOVA test, $P > 0.05$; data not shown). However, one-way ANOVA test showed an influence of the variables genotype and age on the estimated number of axons ($P < 0.0001$). Scheffe post hoc test revealed significant reduction in axon number in $Opa1^{enu/+}$ 18 months when compared both with WT 18 months ($P < 0.001$) and with $Opa1^{enu/+}$ 1 month ($P < 0.05$; inset Fig. 1B), with similar axonal loss in the central and peripheral optic nerve (ANOVA test, $P > 0.05$; data not shown). However, the phenotype was quite variable: the axonal loss ranged from 23% to 77% (average: 47%; $Opa1^{enu/+}$ 18 versus WT 18 months). We detected no differences between WT and $Opa1^{enu/+}$ at the age of 1 month (Scheffe post hoc test, $P > 0.05$), indicating that no axonal loss occurred at earlier ages. Moreover, no significant influence of age was detected in the WT (Scheffe post hoc test, $P > 0.05$). These results suggest that the decrease in the number of axons observed in the $Opa1^{enu/+}$ 18-month animals is time- and mutation-dependent.

We classified the axons into different groups depending on their morphometric parameters (area, perimeter). The axons were classified into 11 bins depending on their cross-sectional area (with 0.1-μm^2 step size up to 1 μm^2, and one additional bin with axons >1 μm^2, Fig. 1B). Small axons (smaller than 0.4 μm^2) were more abundant than big ones (ANOVA test, $P <$ 0.0001 in all groups, Fig. 1B). We observed a significant effect of the variables genotype and age on the number of axons with an area up to 0.4 μm^2 (ANOVA test, bins 0–0.1 μm^2 and 0.1–0.2 μm^2: $P < 0.001$; bin 0.2–0.3 μm^2: $P < 0.01$; bin 0.3–0.4 μm^2: $P < 0.05$, Fig. 1B). No significant changes were detected for the other bins (ANOVA test, $P > 0.05$ in all bins with areas > 0.4 μm^2). Similar results were observed when the axons were classified depending on their perimeter (data not shown). It is noteworthy that approximately 95% of the axons lost in the $Opa1^{enu/+}$ 18-month animals are smaller than 0.4 μm^2. We observed no influence of the age within the WT group or of the genotype at the age of 1 month (ANOVA test, $P > 0.05$).

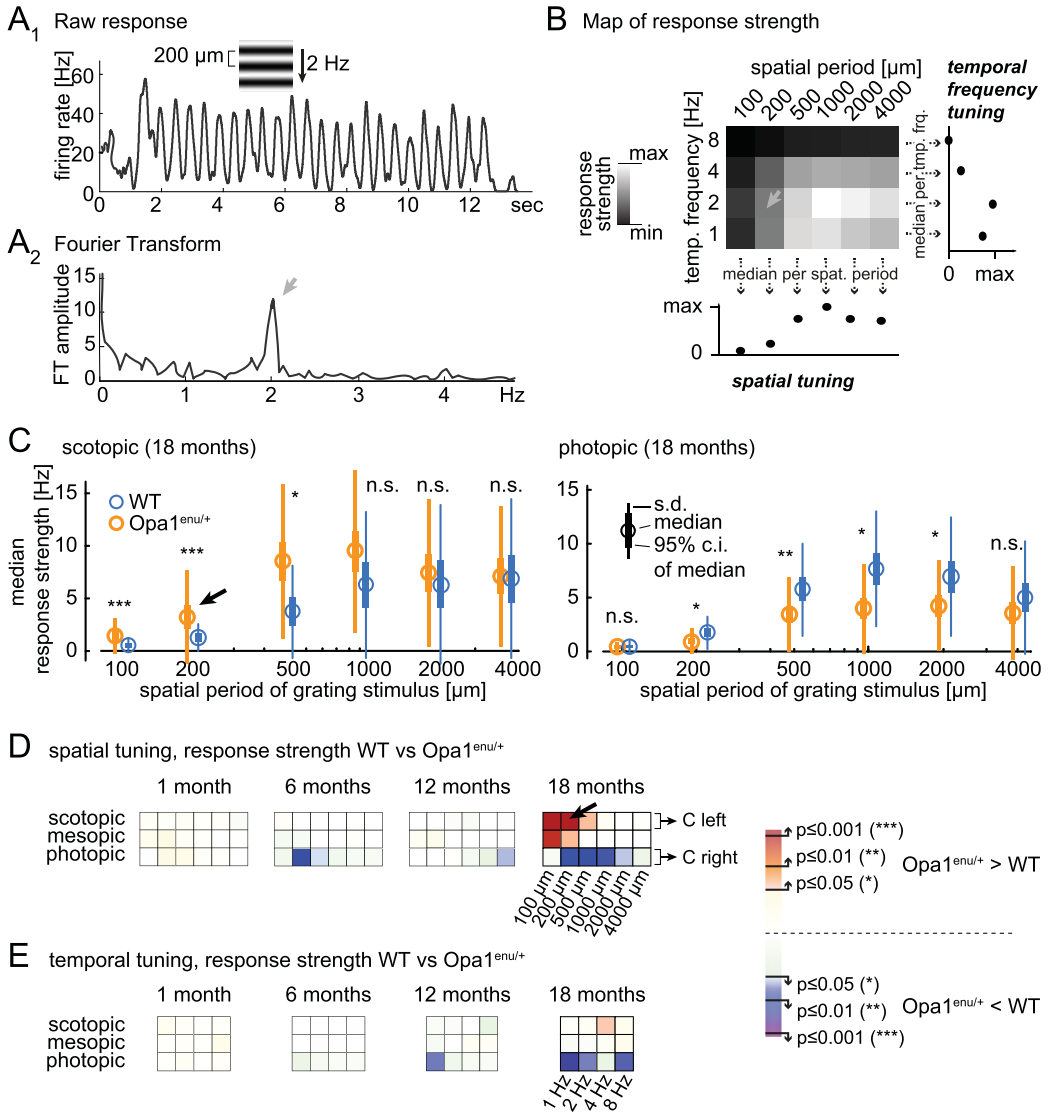

FIGURE 2. Spatial and temporal tuning parameter calculations and results. (**A$_1$**) Response of a single RGCs to a drifting sine wave grating. The cell responded throughout the presentation of a sine wave grating with a period of 200 µm moving with 2 Hz. (**A$_2$**) Fourier transformation of response in (**A$_1$**). The peak value around the stimulus frequency was taken as the response strength of the cell for further analysis (*gray arrow*). (**B**) Calculation of temporal frequency tuning and spatial tuning. Peaks from Fourier transforms (**A$_2$**) are *color-coded* with *white* being the maximal peak measured for a single cell. For spatial tuning parameters, the median for each spatial period over various temporal frequencies was calculated (*below*). Similarly, temporal frequency tuning parameters were calculated by averaging over various spatial periods (*right*). *Gray arrow*: data point from (**A$_1$**) and (**A$_2$**). (**C**) Distribution of spatial tuning parameters from 18-month-old animals. *Left*: median (*circle*), 95% confidence interval of median (*thick line*), and SD (*thin line*), for data obtained under scotopic conditions. *Black arrow*: data recorded in response to sine wave gratings with 200-µm periods, also indicated in (**D**). *Right*: bar-whisker plots for data recorded under photopic conditions. (**D**) Statistical differences between spatial tuning in WT and Opa1$^{enu/+}$ mutants. Wilcoxon rank sum tests were applied to detect significant differences between the spatial tuning parameter distribution of WT and Opa1$^{enu/+}$ RGCs at all ages and luminance conditions. Each *square* represents one *P* value which is color-coded according to the legend on the *right*. *Black arrow* indicates the same data as in (**C**). Underlying raw data is given in Supplementary Figures S1 through S4. (**E**) Statistical comparison of temporal frequency tuning in Opa1$^{enu/+}$ and WT retinas. Wilcoxon rank sum tests were applied to detect statistical differences between WT and Opa1$^{enu/+}$ RGCs as described for spatial tuning in (**D**). Underlying raw data is given in Supplementary Figures S5 through S8. $^{*}P < 0.05$, $^{**}P < 0.01$, $^{***}P < 0.001$, Wilcoxon rank sum test.

Investigative Ophthalmology & Visual Science

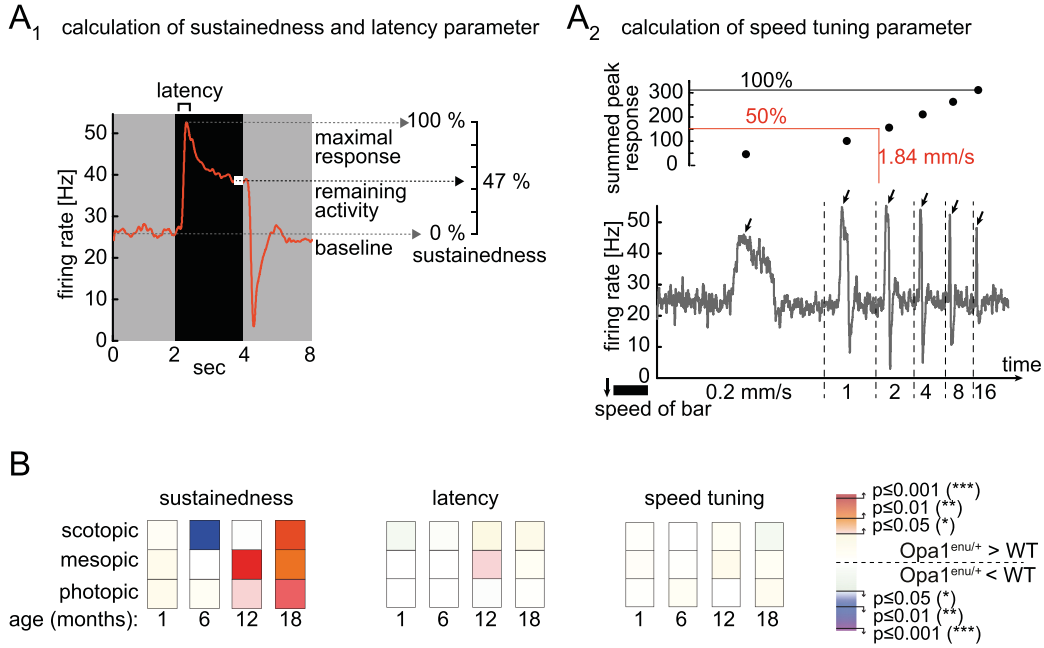

FIGURE 3. Response sustainedness and latency, and speed tuning in WT and Opa1$^{enu/+}$ RGCs. (**A$_1$**) Calculation of sustainedness and latency. Sustainedness was calculated from responses to full-field contrast steps. The remaining activity 1700 to 2000 ms after onset of the stimulus that elicited the maximal response was considered. Sustainedness was expressed as the fraction of this remaining activity from the maximal response (both baseline-subtracted). Latency was defined as the time from stimulus onset to the peak response. (**A$_2$**) Calculation of speed tuning parameter. Speed tuning was calculated from peak responses to a bar moving with six different speeds. Peak responses were summed starting from the slowest speed (cumulative sum), and speed tuning was defined as the speed for which 50% of the summed responses was reached. (**B**) Statistical differences between sustainedness, latency, and speed tuning of Opa1$^{enu/+}$ and WT RGCs calculated by Wilcoxon rank sum tests. *P* value of the difference is color-coded as described in Figure 2. Transient cells were excluded before applying statistical tests for the sustainedness parameter. Sustainedness differed between Opa1$^{enu/+}$ and WT retinas mostly at old age, but also under scotopic conditions at the age of 6 months (*left*). Retinal ganglion cells response latency to full-field flashes is similar in both genotypes under all conditions and at all ages (*middle*). Only under mesopic conditions, WT RGCs have a borderline significantly lower latency at the age of 12 months. Speed tuning is similar in both genotypes under all conditions (*right*). Raw data is depicted in Supplementary Figures S9 through S11.

Ganglion Cell Responses Differ Between Old WT and Old Opa1$^{enu/+}$ Retinas

Our morphologic data suggest that ganglion cells with small-caliber axons are especially vulnerable in Opa1$^{enu/+}$ retinas. We wondered if this would be reflected in a selective loss of functional subtypes of RGCs. We thus recorded visual responses from RGCs in isolated whole-mount retina at three different luminance levels (scotopic, mesopic, photopic) using MEAs. We characterized each recorded RGC with several functional parameters (see Methods).

Spatial and Temporal Tuning Differs Between Opa1$^{enu/+}$ and WT RGCs. Spatial and temporal response properties of individual RGCs were calculated from 24 different drifting sine-wave grating stimuli (6 different spatial scales × 4 different temporal frequencies, see Methods and Figs. 2A, 2B; population data are presented in Supplementary Figs. S1–S8). We measured the response strength of individual RGCs for each of the 24 different grating stimuli. For example, Figure 2A$_1$ shows the raw response of a single RGC (from an 18-month Opa1$^{enu/+}$ retina recorded in scotopic conditions) to the 200-µm grating drifting at 2 Hz. Figure 2A$_2$ shows the corresponding Fourier transform, from which we extracted the response strength to this stimulus (arrow). The raster in Figure 2B shows the color-coded response strengths of the same cell to all 24-grating stimuli. Spatial and temporal tuning for this cell was then calculated by taking the median of the response strengths along the space and time dimensions of this response raster, as indicated in Figure 2B. Such measurements were performed for all RGCs and the results were grouped separately for the four age groups, three brightness levels, and two genotypes. Examples of the resulting distributions of spatial tuning are shown in Figure 2C where we compare the response strengths of 18-month-old WT (blue) and Opa1$^{enu/+}$ (orange) RGCs measured in scotopic (left) and photopic (right) conditions. We applied Wilcoxon rank sum tests to these distributions to assess if they differed between Opa1$^{enu/+}$ and WT retinas. A summary of these tests for each age group and brightness condition is shown in Figure 2D as color-coded *P* values (red if a parameter was enhanced in Opa1$^{enu/+}$ compared with WT retinas, blue if it was decreased in Opa1$^{enu/+}$). Similarly, Figure 2E shows the summary for the temporal tuning differences between Opa1$^{enu/+}$ and WT RGCs. The underlying raw data for the *P* values depicted in Figures 2D and 2E are shown in Supplementary Figures S1 through S8. It is striking that most differences between WT and Opa1$^{enu/+}$ response

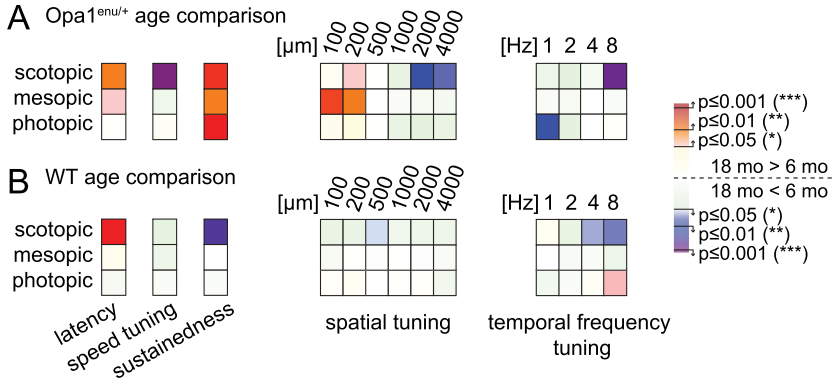

FIGURE 4. Aging effects in WT and Opa1$^{enu/+}$ retinas. **(A)** Aging effects in Opa1$^{enu/+}$ retinas. *P* values obtained with Wilcoxon rank sum tests on parameters obtained at the age of 6 and 18 months. Latency increased with age under scotopic and mesopic conditions. Old Opa1$^{enu/+}$ RGCs were tuned to slower speeds under scotopic conditions. Further, in Opa1$^{enu/+}$ retinas, aging lead to increased activity modulation in response to sine wave gratings with small periods under scotopic and mesopic conditions, while responsiveness was decreased to large periods. Temporal frequency tuning decreased with age under scotopic (8 Hz) and photopic (1 Hz) conditions, and sustainedness increased in old Opa1$^{enu/+}$ retinas under all conditions. **(B)** Aging effects in WT retinas. Response latency increased and sustainedness decreased in old WT RGCs under scotopic conditions. Moreover, in old WT retinas, modulation of RGCs activity tended to decrease for all spatial periods under scotopic conditions (significant for 500 µm). Similarly to Opa1$^{enu/+}$ RGCs, responsiveness to higher frequency stimuli was decreased in old WT retinas under scotopic conditions, while at photopic luminance levels responsiveness to 8-Hz stimuli was increased.

properties only emerge in the oldest age group (18 months). Secondly, the specific difference in spatial and temporal tuning was not fixed, but depended on the stimulus conditions. Under scotopic conditions, responses to gratings with small spatial periods were enhanced in old Opa1$^{enu/+}$ retinas compared with WT (Fig. 2C left, red squares in Fig. 2D), while the responses did not differ at the other spatial scales. Under photopic conditions, on the other hand, the responses of WT RGCs were stronger than in Opa1$^{enu/+}$ retinas at medium spatial scales (Fig. 2C right, blue squares in Fig. 2D). Similarly to spatial tuning, we found opposite effects under scotopic and photopic stimulus conditions for temporal frequency tuning: While old Opa1$^{enu/+}$ RGCs tended to respond more strongly to 4-Hz stimuli under scotopic luminance conditions, RGCs in WT retinas had stronger responses under photopic conditions (Fig. 2E).

Sustainedness Is Increased in Old Opa1$^{enu/+}$ RGCs. We next measured the sustainedness of RGC responses during full-field contrast steps stimuli (Fig. 3A$_1$). In general, 12- and 18-month Opa1$^{enu/+}$ RGCs had more sustained responses than WT cells, independent of the luminance level (Fig. 3B, left). Under scotopic conditions, we found differences already at the age of 6 months and with opposing tendency: There, WT RGCs displayed more sustained responses (population raw data in Supplementary Fig. S9).

Latency and Speed Tuning Are the Same in WT and Opa1$^{enu/+}$ RGCs. Latency and speed tuning did not differ between WT and Opa1$^{enu/+}$ RGCs, independently of age and luminance (Fig. 3B middle and right; population raw data in Supplementary Figs. S10, S11). As an exception we found a slightly higher latency in Opa1$^{enu/+}$ RGCs at the age of 12 months under mesopic conditions ($P = 0.049$).

Aging Affects Responses of WT and Opa1$^{enu/+}$ Retinas Differently

In the previous section, we focused on differences between the two genotypes. In the following, we address the age-dependent development of RGC responses within each genotype. Synaptic input measurements in mouse RGCs suggest that 1-month retinas might not yet be fully developed functionally.[30] We thus decided to compare data from 6- ("young") and 18-month ("old") animals within each genotype group.

Latency and Speed Tuning Are Only Affected by Age, But Not by the *Opa1* Mutation. In accordance with the finding that latency and speed tuning did not differ significantly between WT and Opa1$^{enu/+}$ retinas, we found similar aging effects in both genotypes for these parameters. Latency increased in old animals under scotopic conditions and, in Opa1$^{enu/+}$ retinas, also under mesopic conditions ($P = 0.045$). Speed tuning tended to drop in old retinas under scotopic conditions, significantly in old Opa1$^{enu/+}$ retinas (WT: $P = 0.072$; Fig. 4).

Spatial and Temporal Tuning Is Affected by Age in Opa1$^{enu/+}$ Retinas. Under scotopic conditions, the responses of Opa1$^{enu/+}$ RGCs became weaker with age when exposed to drifting gratings with large spatial periods, but response strength increased for gratings with small spatial periods (Fig. 4A). This increase was more pronounced under mesopic conditions. On the other hand, age had very little effect on WT RGCs (Fig. 4B). These different age-dependent response characters can explain the differences between the genotypes observed at 18 months (Fig. 2D). Temporal frequency was affected similarly by age in Opa1$^{enu/+}$ and WT retinas under scotopic conditions. However, at photopic levels, aging induced a drop in response strength to 1-Hz stimuli in Opa1$^{enu/+}$ retinas (Fig. 4A), while response strength for 8-Hz stimuli increased in WT retinas (Fig. 4B).

Sustainedness Increases With Age in Opa1$^{Enu/+}$ Retinas. Sustainedness of RGC responses increased with age in Opa1$^{enu/+}$ retinas under all luminance conditions (Fig. 4A). In WT retinas we detected a drop in sustainedness under scotopic conditions (Fig. 4B).

Melanopsin Is Not Per Se Neuroprotective

Melanopsin-expressing RGCs were found to be spared from degeneration provoked by different insults,[31–33] including

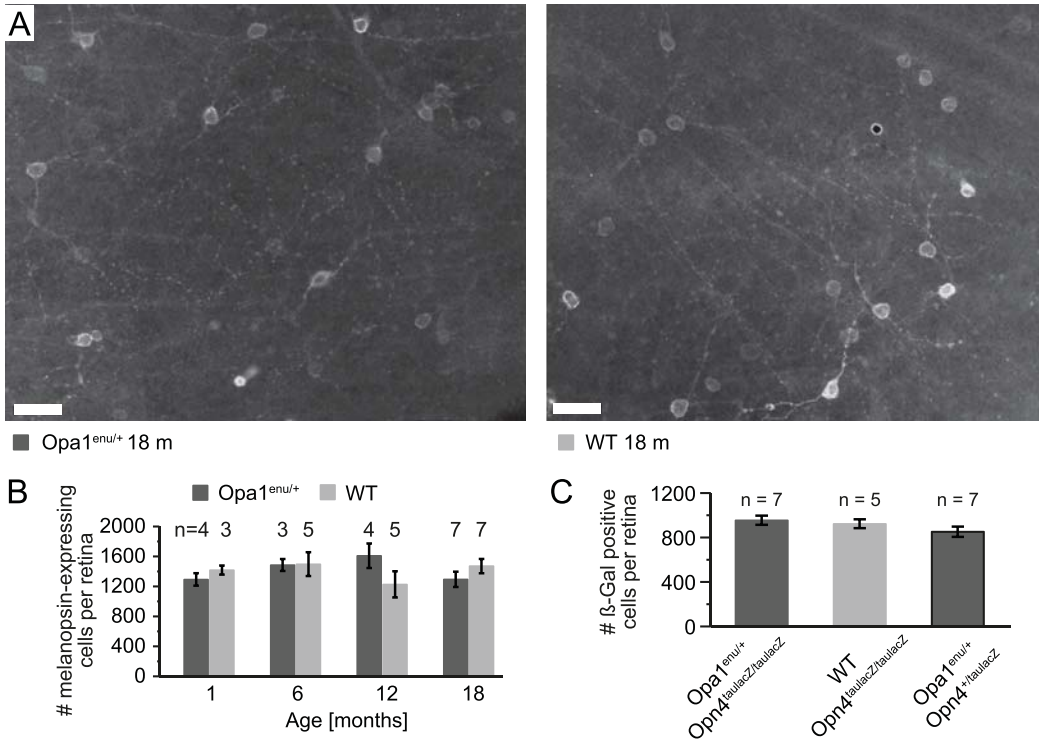

FIGURE 5. Stable number of melanopsin-expressing and β-galactosidase reporter expressing cells per retina in Opa1$^{enu/+}$ mutants. (**A**) Melanopsin immunofluorescence in whole-mount retinas. Representative examples (contrast-enhanced in Adobe Photoshop for clarity) are shown for 18-month Opa1$^{enu/+}$ (*left*) and WT retinas (*right*). *Scale bar*: 20 μm. (**B**) Melanopsin-expressing cells. The number of immunopositive cells does not change with the variable "age" or "genotype" with an average of 1427 ± 16 immunopositive cells per retina (ANOVA test, $P > 0.05$). (**C**) β-galactosidase positive cells. The number of β-galactosidase–positive cells per retina does not change within the different genotypes (ANOVA test, $P > 0.05$). Scheffe post hoc test does not show significant differences between Opa1$^{enu/+}$ × Opn4$^{taulacZ/taulacZ}$ and WT × Opn4$^{taulacZ/taulacZ}$ groups (Scheffe post hoc test, $P > 0.05$). Additionally, no differences were identified when Opa1$^{enu/+}$ × Opn4$^{+/taulacZ}$ was compared with the previous groups (Scheffe post hoc test, $P > 0.05$).

ADOA.[3,19] We therefore examined if melanopsin-expressing RGCs are also spared in our *Opa1* mouse model and investigated a potential neuroprotective role of the melanopsin protein (representative immunohistochemistry for melanopsin is shown in Fig. 5A).

As shown in Figure 1, there is a significant decrease in the number of axons in the 18-month Opa1$^{enu/+}$ mice. However, we found the number of melanopsin-expressing cells in retinal whole-mounts to remain stable (Fig. 5B). One-way ANOVA test demonstrated no influence of the genotype or age on the number of immunopositive cells ($P > 0.05$). To determine whether the melanopsin-expressing cells are protected against *Opa1* mutation–induced degeneration due to the presence of the melanopsin protein per se, we compared the number of β-galactosidase immunopositive cells in retinal whole-mounts. No significant difference in the number of immunolabelled cells was observed between the different genotypes, including the double heterozygote in which both melanopsin and β-galactosidase are expressed (ANOVA test, $P > 0.5$; Fig. 5C). Thus, these results suggest that the resistance to neurodegenerative insults of these cells is not dependent on the presence of melanopsin.

DISCUSSION

Loss of Optic Nerve Axons in the B6;C3-*Opa1*$^{329\text{-}355del}$ Model for ADOA

In the present work we have used the B6;C3-*Opa1*$^{329\text{-}355del}$ mouse model, which has a comparable phenotype with that observed in patients with *OPA1*-associated nonsyndromic ADOA.[13,29] By counting axons in the optic nerve, we observed an approximately 50% age-related axonal loss in the Opa1$^{enu/+}$ 18-month animals when compared with WT 18 month, which is in agreement with previous studies.[13,34] However, the axonal loss was quite variable from mouse to mouse, ranging from 20% to 75%. This finding corresponds with the pronounced clinical variability observed in ADOA patients.[4,35]

Optic nerve axons can be classified depending on their morphometric characteristics. We have observed that axonal loss tends to be biased to axons with small cross-sectional areas (up to 0.4 μm^2) in the aged Opa1$^{enu/+}$ animals, representing 95% of the total axonal loss. Such loss of small caliber fibers has also been observed previously in this mouse model, using electron microscopy to classify and count axons in optic nerve cross sections,[13] and in other optic neuropathies,[36] indicating

that the axon size may be highly correlated with its vulnerability.

No differences between Opa1$^{enu/+}$ and WT animals were observed at 1 month of age, indicating that no early onset of axonal loss occurs in this mouse model; however, this does not exclude potential subcellular changes. Additionally, we have not observed any significant changes in the number or morphology of optic nerve axons between 1- and 18-month-old WT animals. This is in agreement with previous studies,[13] while other publications have shown an age-related decrease in the number of RGCs.[37,38] These differences might be due to a background effect as well as environmental factors.

Aging Affects Functional Properties of RGCs

Based on MEA-recordings, we found two major functional changes in aging retinas, which were similar in WT and Opa1$^{enu/+}$ retinas. First, old RGCs seem to react more slowly (i.e., they had a longer latency), most pronounced under scotopic conditions. Further, in both genotypes we could detect a tendency to slower speed tunings. On the other hand, spatial and temporal frequency tuning as well as sustainedness were affected differently in ganglion cells of Opa1$^{enu/+}$ and WT retinas.

Opa1 Mutation Changes Ganglion Cell Output: Are Upstream Neurons Affected?

We wondered whether the pronounced loss of RGC axons in older Opa1$^{enu/+}$ mice represents a general loss of all RGC types, or if we could find a hint for specific loss of certain functional cell types. If certain RGC types were more affected than others by the *Opa1* mutation, this may be reflected in a disappearance of cells in a certain region in the functional parameter space (e.g., no or few transient cells in old Opa1$^{enu/+}$ retinas). It has been shown that cells with small axon diameter comprise a variety of morphologically, and presumably functionally, different RGC types.[15] Consequently, we could not detect a clear drop-out of a specific functional cell type although we found differences in spatial and temporal frequency tuning, and sustainedness between the two genotypes, mostly in old (12- and 18-month) animals. This does not come into conflict with our histologic findings of a specific loss of small-axon RGCs.

Instead of a clear drop-out of a functional type, we detected various shifts in the measured physiological parameters. This may be explained by two mechanisms, which are not mutually exclusive. First, although cell death is not limited to a specific cell type, it might still affect certain functional types more than others. Second, the output of the surviving RGCs might be altered by the *Opa1* mutation and/or secondary to the loss of RGCs. While we can neither confirm nor refute these possibilities, our data actually hints at yet a third explanation, namely that there are alterations not only of the surviving RGCs but also of the remaining upstream retinal circuitry. If differences were only due to RGC death or changes in their properties, we would expect the differences to be similar under different luminance conditions. However, we found very different tendencies under scotopic, mesopic, and photopic conditions (e.g., spatial tuning of 18-month-old RGCs under scotopic versus photopic conditions, Fig. 2D). Such luminance-dependent changes suggest additional alterations in the retinal processing (e.g., in homeostasis, synaptic connections, neurotransmitter release, etc. of upstream neurons [bipolar cells, amacrine cells, photoreceptors]). So far, RGCs have been thought to be the only retinal cells affected in OPA1 deficiency.[39] However, previous publications support possible involvement of the outer retina: Heiduschka and colleagues[29] found that the amplitudes of scotopic but not of photopic visually evoked potentials in old Opa1$^{enu/+}$ mice were reduced significantly, which may indicate functional impairment of the rod driven signaling circuitry. Moreover, Reis and colleagues[40] recently reported significantly reduced multifocal ERG amplitudes in a cohort of ADOA patients with defined *OPA1* mutation.

Effect of *Opa1* Deficiency on the Melanopsin System and Melanopsin's Potential Protective Role

Within the population of RGCs there is an outstanding cell subtype, the intrinsically photoresponsive RGCs (ipRGCs). These cells express the photopigment melanopsin and are responsible for nonimage forming vision.[18] In the last years, melanopsin cells have been shown to be resistant to different retinal insults such as axotomy[32] and glaucoma,[33] while the nonmelanopsin cells are massively affected. Furthermore, previous publications pointed out that melanopsin-expressing RGCs are also spared in ADOA in human and in the B6;C3-*Opa1*^{Q285STOP} mouse model.[3,19] However, just one patient was available for the study in humans, and the B6;C3-*Opa1*^{Q285STOP} mouse model presents with a limited loss of RGCs.[12] With our B6;C3-*Opa1*$^{329\text{-}355del}$ mouse model, in which there is an extensive loss of RGCs (~50% reduced number of RGC at 18 months), we could confirm that no loss of melanopsin-expressing RGCs occurs, indicating that they are resistant. Additionally, no influence of age was observed on the survival of melanopsin-expressing RGCs consistent with previous reports.[41,42] Why are melanopsin-expressing cells more resistant than other RGCs? A main difference between the melanopsin-expressing cells and the other RGCs is the presence of the melanopsin protein per se. It has been suggested that blue light might be damaging to RGCs due to the generation of reactive oxidative species, especially in case of mitochondria dysfunction, as in ADOA.[20] Since melanopsin absorbs blue light this might exert a protective effect against this light insult.[43] To test this hypothesis we studied the Opn4^{tauLacZ} mouse mutant in which the melanopsin gene is replaced by sequences coding for a tau-lacZ fusion protein.[44] If melanopsin itself would have a protective effect one would expect a reduced number of β-galactosidase positive cells in Opa1$^{enu/+}$ × Opn4$^{taulacZ/taulacZ}$ mice. However, we found similar numbers of immunopositive cells in WT × Opn4$^{taulacZ/taulacZ}$ and Opa1$^{enu/+}$ × Opn4$^{taulacZ/taulacZ}$ animals, indicating that melanopsin does not have a protective role at least in the context of Opa1 deficiency. It should be noted that β-galactosidase expression can only be identified in the M1 cells.[45] Therefore, we cannot exclude a potentially protective role of melanopsin in the other melanopsin-expressing RGC subtypes (M2–M5).[45–47] Studies using the Opn4-EGFP mouse line,[48] in which the M1, M2, and M3 melanopsin-expressing cells can be identified, would allow a more detailed view of the potentially protective function of the melanopsin protein.

As a further difference, melanopsin-expressing cells, but no other RGC group, express pituitary adenylate cyclase-activating peptide (PACAP).[49] Pituitary adenylate cyclase-activating peptide has been shown to have neuroprotective potency.[50–52] Additionally, melanopsin-expressing cells may have different mitochondrial dynamics due to their intrinsic photosensitivity, which may protect them against cell stress. Furthermore, no details on the axonal morphology of the melanopsin-expressing cells are known, so that we cannot relate melanopsin-expressing cells to our axonal diameter measurements.

In conclusion, our study demonstrates that the axonal loss observed in the B6;C3-*Opa1*$^{329\text{-}355del}$ mouse model for human

ADOA is mutation- and age-dependent, with 50% of axons lost by 18 months. Moreover, we have shown that the RGC loss is biased toward RGCs with small axonal cross-sections. Our data reveal significant differences in the visual response properties between old Opa1$^{enu/+}$ and WT RGCs, but not a drop-out of a certain functionally defined RGC population. However, we found that differences between the two genotypes have different trends under scotopic and photopic conditions, suggesting that there are also alterations of the pre-RGC retinal circuitry. We thus suggest for future studies to more closely investigate presynaptic retinal neurons. Functional evaluation of RGCs can only be conclusive if changes in upstream neurons are either excluded or, if present, integrated with RGC measurements.

Our study also verified that the melanopsin system is neither affected by ageing nor in *Opa1*-induced RGC degeneration. Moreover, our results show that the melanopsin protein is not the factor that imposes the resistance of these intrinsically photoresponsive cells. Several other factors may be implicated in the survival of these cells and future studies are required to elucidate this question, which, if solved, may offer some therapeutic approaches.

Acknowledgments

Supported by grants from the Deutsche Forschungsgemeinschaft (DFG; Bonn, Germany) to the Werner Reichardt Centre for Integrative Neuroscience (DFG EXC 307), by the Bundesministerium für Bildung and Forschung ("Bernstein Center for Computational Neuroscience," FKZ 01GQ1002 [TAM], and E-Rare "ERMION," FZ 01GM1006 [BW], and a Stipend of the Pro Retina Foundation [KR]; Frankfurt, Germany).

Disclosure: **I. Gonzalez-Menendez**, None; **K. Reinhard**, None; **J. Tolivia**, None; **B. Wissinger**, None; **T.A. Münch**, None

References

1. Lenaers G, Hamel C, Delettre C, et al. Dominant optic atrophy. *Orphanet J Rare Dis*. 2012;7:46.
2. Kjer P, Jensen OA, Klinken L. Histopathology of eye, optic nerve and brain in a case of dominant optic atrophy. *Acta Ophthalmol (Copenh)*. 1983;61:300–312.
3. La Morgia C, Ross-Cisneros FN, Sadun AA, et al. Melanopsin retinal ganglion cells are resistant to neurodegeneration in mitochondrial optic neuropathies. *Brain*. 2010;133:2426–2438.
4. Cohn AC, Toomes C, Potter C, et al. Autosomal dominant optic atrophy: penetrance and expressivity in patients with OPA1 mutations. *Am J Ophthalmol*. 2007;143:656–662.
5. Almind GJ, Ek J, Rosenberg T, et al. Dominant optic atrophy in Denmark - report of 15 novel mutations in OPA1, using a strategy with a detection rate of 90%. *BMC Med Genet*. 2012; 13:65.
6. Cipolat S, Martins de Brito O, Dal Zilio B, Scorrano L. OPA1 requires mitofusin 1 to promote mitochondrial fusion. *Proc Natl Acad Sci U S A*. 2004;101:15927–15932.
7. Lee YJ, Jeong SY, Karbowski M, Smith CL, Youle RJ. Roles of the mammalian mitochondrial fission and fusion mediators Fis1, Drp1, and Opa1 in apoptosis. *Mol Biol Cell*. 2004;15: 5001–5011.
8. Frezza C, Cipolat S, Martins de Brito O, et al. OPA1 controls apoptotic cristae remodeling independently from mitochondrial fusion. *Cell*. 2006;126:177–189.
9. Lodi R, Tonon C, Valentino ML, et al. Deficit of in vivo mitochondrial ATP production in OPA1-related dominant optic atrophy. *Ann Neurol*. 2004;56:719–723.
10. Amati-Bonneau P, Guichet A, Olichon A, et al. OPA1 R445H mutation in optic atrophy associated with sensorineural deafness. *Ann Neurol*. 2005;58:958–963.
11. Zanna C, Ghelli A, Porcelli AM, et al. OPA1 mutations associated with dominant optic atrophy impair oxidative phosphorylation and mitochondrial fusion. *Brain*. 2008;131: 352–367.
12. Davies VJ, Hollins AJ, Piechota MJ, et al. Opa1 deficiency in a mouse model of autosomal dominant optic atrophy impairs mitochondrial morphology, optic nerve structure and visual function. *Hum Mol Genet*. 2007;16:1307–1318.
13. Alavi M, Bette S, Schimpf S, et al. A splice site mutation in the murine Opa1 gene features pathology of autosomal dominant optic atrophy. *Brain*. 2007;130:1029–1042.
14. Williams PA, Morgan JE, Votruba M. Mouse models of dominant optic atrophy: what do they tell us about the pathophysiology of visual loss? *Vision Res*. 2011;51:229–234.
15. Coombs J, van der List D, Wang GY, Chalupa LM. Morphological properties of mouse retinal ganglion cells. *Neuroscience*. 2006;140:123–136.
16. Farrow K, Masland RH. Physiological clustering of visual channels in the mouse retina. *J Neurophysiol*. 2011;105:1516–1530.
17. Williams PA, Morgan JE, Votruba M. Opa1 deficiency in a mouse model of dominant optic atrophy leads to retinal ganglion cell dendropathy. *Brain*. 2010;133:2942–2951.
18. Do MT, Yau KW. Intrinsically photosensitive retinal ganglion cells. *Physiol Rev*. 2010;90:1547–1581.
19. Perganta G, Barnard AR, Katti C, et al. Non-image-forming light driven functions are preserved in a mouse model of autosomal dominant optic atrophy. *PLoS One*. 2013;8:e56350.
20. Osborne NN, Núñez-Álvarez C, Del Olmo-Aguado S. The effect of visual blue light on mitochondrial function associated with retinal ganglions cells. *Exp Eye Res*. 2014;128:8–14.
21. Richardson KC, Jarrett L, Finke EH. Embedding in epoxy resins for ultrathin sectioning in electron microscopy. *Stain Technology*. 1960;35:313–323.
22. Tolivia J, Navarro A, del Valle E, Perez C, Ordoñez C, Martínez E. Application of Photoshop and Scion Image analysis to quantification of signals in histochemistry, immunocytochemistry and hybridocytochemistry. *Anal Quant Cytol Histol*. 2006;28:43–53.
23. Ganfornina MD, Do Carmo S, Martínez E, et al. ApoD, a glia-derived apolipoprotein, is required for peripheral nerve functional integrity and a timely response to injury. *Glia*. 2010;58:1320–1334.
24. Honjin R, Sakato S, Yamashita T. Electron microscopy of the mouse optic nerve: a quantitative study of the total optic nerve fibers. *Arch Histol Jpn*. 1977;40:321–332.
25. Rasband WS. *ImageJ*. Bethesda, Maryland: U.S. National Institutes of Health: 1997–2014. Available at: http://imagej.nih.gov/ij/.
26. Reinhard K, Tikidji-Hamburyan A, Seitter H, et al. Step-by-step instructions for retina recordings with perforated multi electrode arrays. *PLoS One*. 2014;9:e106148.
27. González-Menéndez I, Contreras F, Cernuda-Cernuda R, García-Fernández JM. No loss of melanopsin-expressing ganglion cells detected during postnatal development of the mouse retina. *Histol Histopathol*. 2010;25:73–82.
28. Pesch UE, Leo-Kottler B, Mayer S, et al. OPA1 mutations in patients with autosomal dominant optic atrophy and evidence for semi-dominant inheritance. *Hum Mol Genet*. 2001;10: 1359–1368.
29. Heiduschka P, Schnichels S, Fuhrmann N, et al. Electrophysiological and histologic assessment of retinal ganglion cell fate

in a mouse model for OPA1-associated autosomal dominant optic atrophy. *Invest Ophthalmol Vis Sci*. 2009;51:1424–1431.

30. Tian N, Copenhagen DR. Visual deprivation alters development of synaptic function in inner retina after eye opening. *Neuron*. 2001;32:439–449.
31. Hannibal J, Vrang N, Card JP, Fahrenkrug J. Light-dependent induction of cFos during subjective day and night in PACAP-containing ganglion cells of the retinohypothalamic tract. *J Biol Rhythms*. 2001;16:457–470.
32. Robinson GA, Madison RD. Axotomized mouse retinal ganglion cells containing melanopsin show enhanced survival, but not enhanced axon regrowth into a peripheral nerve graft. *Vision Res*. 2004;44:2667–2674.
33. Li RS, Chen BY, Tay DK, Chan HH, Pu ML, So KF. Melanopsin-expressing retinal ganglion cells are more injury-resistant in a chronic ocular hypertension model. *Invest Ophthalmol Vis Sci*. 2006;47:2951–2958.
34. Yu-Wai-Man P, Bailie M, Atawan A, Chinnery PF, Griffiths PG. Pattern of retinal ganglion cell loss in dominant optic atrophy due to OPA1 mutations. *Eye*. 2011;25:596–602.
35. Toomes C, Marchbank NJ, Mackey DA, et al. Spectrum, frequency and penetrance of OPA1 mutations in dominant optic atrophy. *Hum Mol Genet*. 2001;10:1369–1378.
36. Sadun AA, Win PH, Ross-Cisneros FN, Walker SO, Carelli V. Leber's hereditary optic neuropathy differentially affects smaller axons in the optic nerve. *Trans Am Ophthalmol Soc*. 2000;98:223–232.
37. Danias J, Lee KC, Zamora MF et al. Quantitative analysis of retinal ganglion cell (RGC) loss in aging DBA/2NNia glaucomatous mice: comparison with RGC loss in aging C57/BL6 mice. *Invest Ophthalmol Vis Sci*. 2003;44:5151–5162.
38. Neufeld AH, Gachie EN. The inherent, age-dependent loss of retinal ganglion cells is related to the lifespan of the species. *Neurobiol Aging*. 2003;24:167–172.
39. Schild AM, Ristau T, Fricke J, et al. SDOCT thickness measurements of various retinal layers in patients with autosomal dominant optic atrophy due to OPA1 mutations. *Biomed Res Int*. 2013;2013:121398.
40. Reis A, Mateus C, Viegas T, et al. Physiological evidence for impairment in autosomal dominant optic atrophy at the preganglion level. *Graefes Arch Clin Exp Ophthalmol*. 2013;251:221–234.
41. Semo M, Lupi D, Peirson SN, Butler JN, Foster RG. Light-induced c-fos in melanopsin retinal ganglion cells of young and aged rodless/coneless (rd/rd cl) mice. *Eur J Neurosci*. 2003;18:3007–3017.
42. Esquiva G, Lax P, Cuenca N. Impairment of intrinsically photosensitive retinal ganglion cells associated with late stages of retinal degeneration. *Invest Ophthalmol Vis Sci*. 2013;54:4605–4618.
43. Berson DM, Dunn FA, Takao M. Phototransduction by retinal ganglion cells that set the circadian clock. *Science*. 2002;295:1070–1073.
44. Hattar S, Liao HW, Takao M, Berson DM, Yau KW. Melanopsin-containing retinal ganglion cells: architecture, projections, and intrinsic photosensitivity. *Science*. 2002;295:1065–1070.
45. Hattar S, Kumar M, Park A, et al. Central projections of melanopsin-expressing retinal ganglion cells in the mouse. *J Comp Neurol*. 2006;497:326–349.
46. Ecker JL, Dumitrescu ON, Wong KY, et al. Melanopsin-expressing retinal ganglion-cell photoreceptors: cellular diversity and role in pattern vision. *Neuron*. 2010;67:49–60.
47. Brown TM, Tsujimura S, Allen A, et al. Melanopsin-based brightness discrimination in mice and humans. *Curr Biol*. 2012;22:1134–1141.
48. Schmidt TM, Taniguchi K, Kofuji P. Intrinsic and extrinsic light responses in melanopsin-expressing ganglion cells during mouse development. *J Neurophysiol*. 2008;100:371–384.
49. Hannibal J, Hindersson P, Ostergaard J, et al. Melanopsin is expressed in PACAP-containing retinal ganglion cells of the human retinohypothalamic tract. *Invest Ophthalmol Vis Sci*. 2004;45:4202–4209.
50. Tamas A, Gabriel R, Racz B, et al. Effects of pituitary adenylate cyclase activating polypeptide in retinal degeneration induced by monosodium-glutamate. *Neurosci Lett*. 2004;372:110–113.
51. Seki T, Nakatani M, Taki C, et al. Neuroprotective effect of PACAP against kainic acid-induced neurotoxicity in rat retina. *Ann N Y Acad Sci*. 2006;1070:531–534.
52. Seki T, Itoh H, Nakamachi T, et al. Suppression of rat retinal ganglion cell death by PACAP following transient ischemia induced by high intraocular pressure. *J Mol Neurosci*. 2011;43:30–34.

Investigative Ophthalmology & Visual Science

Supplementary Material

Supplementary Tables 1-2

Supplementary Table 1. List of used animals for the optic nerve analysis, MEA recordings and melanopsin study.

Supplementary Table 2. List of used animals for ß-galactosidase analysis.

Supplementary Figures 1-11

Supplementary Figure 1 - Distribution of median response strengths for spatial tuning (age of 1 month).

Supplementary Figure 2 - Distribution of median response strengths for spatial tuning (age of 6 month).

Supplementary Figure 3 - Distribution of median response strengths for spatial tuning (age of 12 month).

Supplementary Figure 4 - Distribution of median response strengths for spatial tuning (age of 18 month).

Supplementary Figure 5 - Distribution of median response strengths for temporal tuning (age of 1 month).

Supplementary Figure 6 - Distribution of median response strengths for temporal tuning (age of 6 month).

Supplementary Figure 7 - Distribution of median response strengths for temporal tuning (age of 12 month).

Supplementary Figure 8 - Distribution of median response strengths for temporal tuning (age of 18 month).

Supplementary Figure 9 - Distribution of the sustainedness parameter.

Supplementary Figure 10 - Distribution of the latency parameter.

Supplementary Figure 11 - Distribution of the speed tuning parameter.

Animal ID	Genotype	age (m)	Optic nerve	MEA	Melanopsin IHC
I3	Opa1$^{enu/+}$	18	√		√
I39	Opa1$^{enu/+}$	18	√		√
I41	Opa1$^{enu/+}$	18	√	√	√
I42	Opa1$^{enu/+}$	18	√		√
I44	Opa1$^{enu/+}$	18	√	√	√
II48	Opa1$^{enu/+}$	18	√	√	√
II49	Opa1$^{enu/+}$	18	√		
II50	Opa1$^{enu/+}$	18	√		√
I9	WT	18			√
I38	WT	18	/	/	/
I40	WT	18	√		√
I43	WT	18	√	√	
I45	WT	18	√	√	√
I49	WT	18		√	√
I50	WT	18	√	√	
I51	WT	18	√	√	√
I59	WT	18			√
I62	Opa1$^{enu/+}$	12		√	√
I63	Opa1$^{enu/+}$	12		√	√
I67	Opa1$^{enu/+}$	12		√	√
I71	Opa1$^{enu/+}$	12		√	
II7	Opa1$^{enu/+}$	12			√
I66	WT	12			√
I69	WT	12		√	√
I70	WT	12		√	√
I79	WT	12		√	
I84	WT	12			√
II8	WT	12			√
I88	Opa1$^{enu/+}$	6		√	√
I92	Opa1$^{enu/+}$	6		√	
II1	Opa1$^{enu/+}$	6		√	√
II4	Opa1$^{enu/+}$	6		√	√
I85	WT	6		√	
I87	WT	6		√	√
I89	WT	6			√
I97	WT	6		√	√
I98	WT	6		√	
II67	WT	6			√
II88	WT	6			√
II40	Opa1$^{enu/+}$	1	√	√	√
II42	Opa1$^{enu/+}$	1			√
II43	Opa1$^{enu/+}$	1	√	√	√
II45	Opa1$^{enu/+}$	1	√	√	√
II59	Opa1$^{enu/+}$	1	√	√	
II39	WT	1	√		√
II41	WT	1		√	√
II44	WT	1	√	√	√
II57	WT	1	√	√	

Supplementary Table 1. List of used animals for the optic nerve analysis, MEA recordings and melanopsin study. Optic nerves were harvested from the same animals that we have used for the melanopsin immunohistochemistry and MEA recordings. This experimental design has allowed us to correlate the results from the 3 different experiments, while at the same time reducing the number of animals needed for the experiments (3 R rule: reduce, refine and replace). Just one animal (WT 18m, I38, marked with "/") was not used for the subsequent experiments because of an abnormal histology of the optic nerve, which did not fit with the ADOA parameters.

Genotype designation	*Opa1*	melanopsin	ß-galactosidase	number of animals
$Opa1^{enu/+}$ x $Opn4^{taulacZ/taulacZ}$	enu/+	negative	positive	7
$Opa1^{enu/+}$ x $Opn4^{+/taulacZ}$	enu/+	positive	positive	7
WT x $Opn4^{taulacZ/taulacZ}$	+ / +	negative	positive	5

Supplementary Table 2. List of used animals for ß-galactosidase analysis.

The Opa1 mouse line has been crossed with the $Opn4^{tauLacZ}$ mouse mutant. Out of this breeding scheme 3 different genotypes were analyzed in our experiments:

$Opa1^{enu/+}$ x $Opn4^{taulacZ/taulacZ}$

$Opa1^{enu/+}$ x $Opn4^{+/taulacZ}$

WT x $Opn4^{taulacZ/taulacZ}$

The presence/absence of the Opa1 mutation, the melanopsin protein and the ß-galactosidase protein (encoded by the tauLacZ gene), as well as the number of animals used per genotype, are indicated in the table.

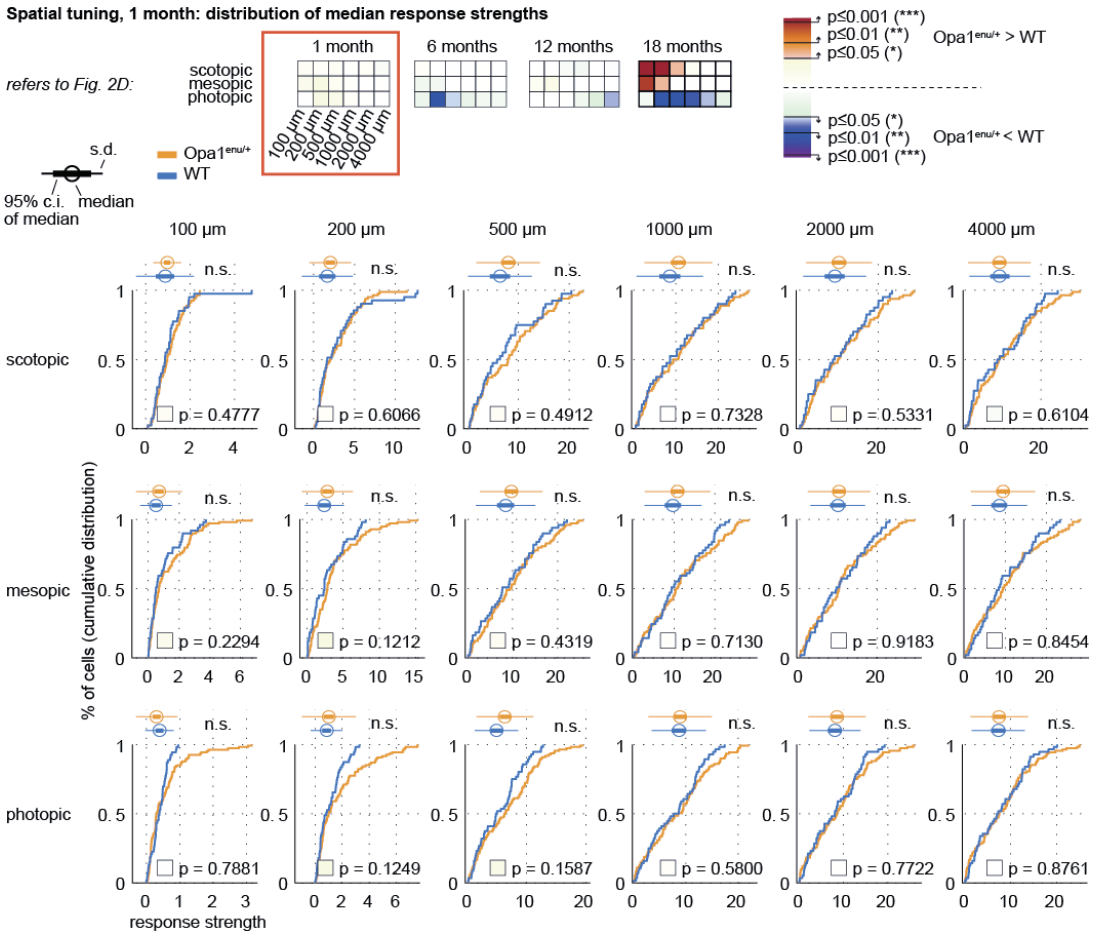

Supplementary Figure 1 - Distribution of median response strengths for spatial tuning (age of 1 month).

Raw data underlying the calculated p-Values depicted in Fig. 2D (repeated on top). Each subplot shows the cumulative distribution of response strengths measured in Opa1$^{enu/+}$ (orange, n = 64 units from 4 retinas) and WT (blue, n= 74 units from 3 retinas) ganglion cells in response to drifting gratings of different spatial periodicity (100 to 4000 µm spatial period, columns) measured at different light levels (scotopic, mesopic, photopic, rows). On top of each graph, we show the median response strength (circle), the 95% confidence interval for the median (thick line), and the standard deviation (thin lines). P-values are shown in each plot together with a color-coded swatch corresponding to the color-code used in Fig. 2D. P-values were obtained by Wilcoxon rank sum tests.

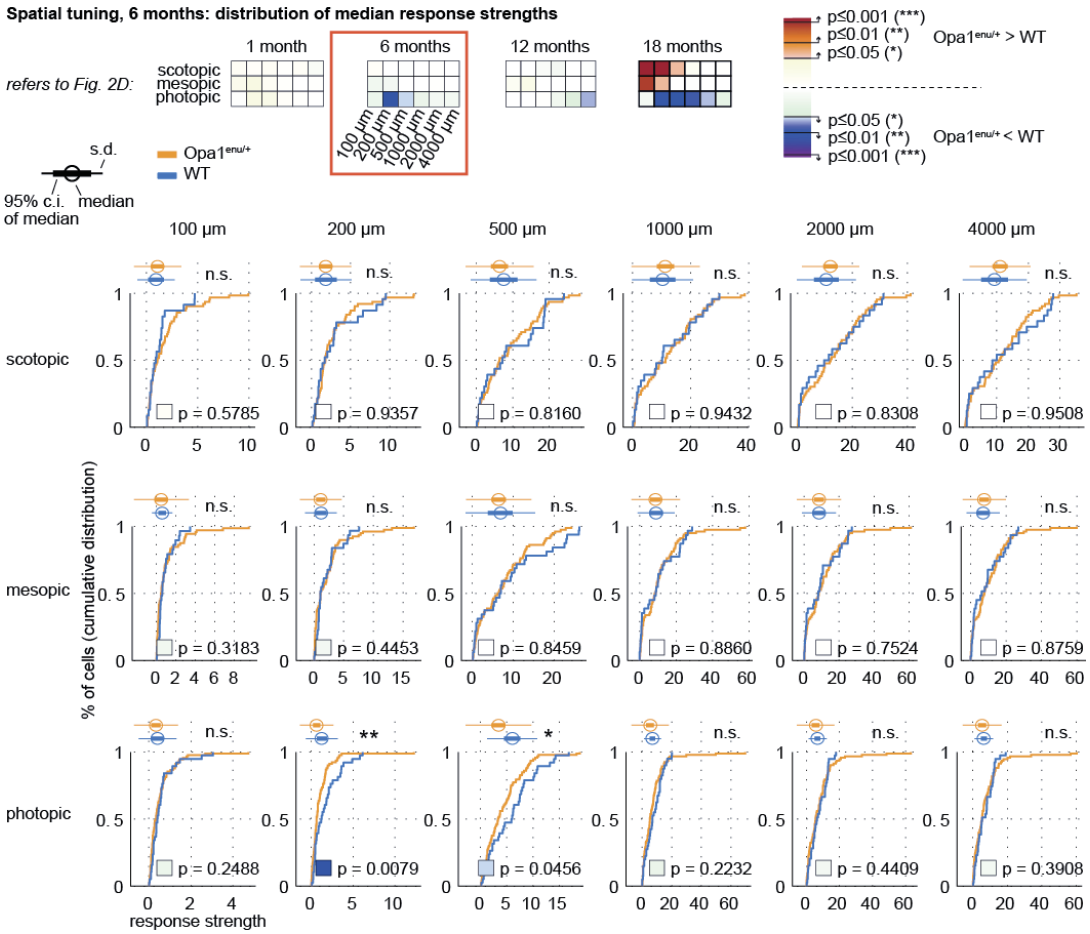

Supplementary Figure 2 - Distribution of median response strengths for spatial tuning (age of 6 month).

Raw data underlying the calculated p-Values depicted in Fig. 2D (repeated on top). Each subplot shows the cumulative distribution of response strengths measured in Opa1$^{enu/+}$ (orange, n = 108 units from 4 retinas) and WT (blue, n= 52 units from 4 retinas) ganglion cells. Conventions as in Supplementary Figure 1.

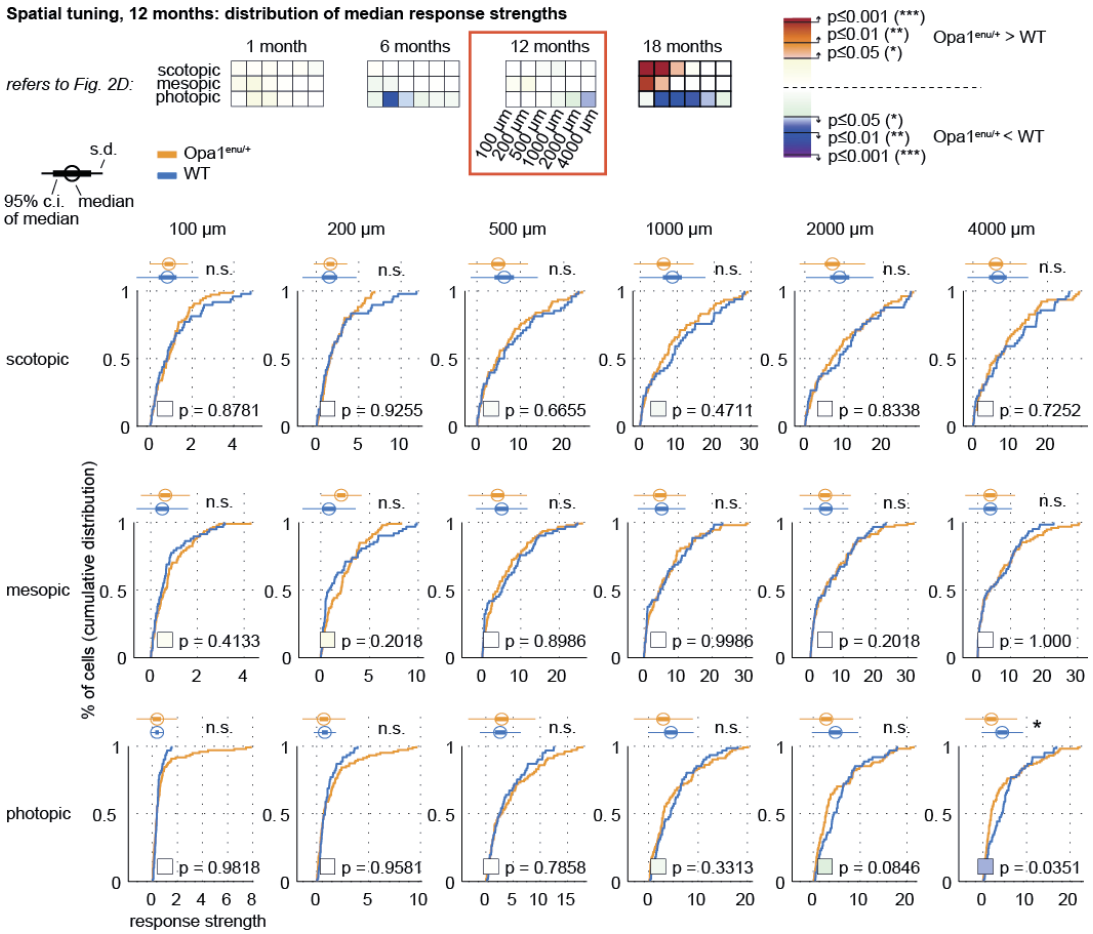

Supplementary Figure 3 - Distribution of median response strengths for spatial tuning (age of 12 month).

Raw data underlying the calculated p-Values depicted in Fig. 2D (repeated on top). Each subplot shows the cumulative distribution of response strengths measured in Opa1$^{enu/+}$ (orange, n = 119 units from 4 retinas) and WT (blue, n= 74 units from 3 retinas) ganglion cells. Conventions as in Supplementary Figure 1.

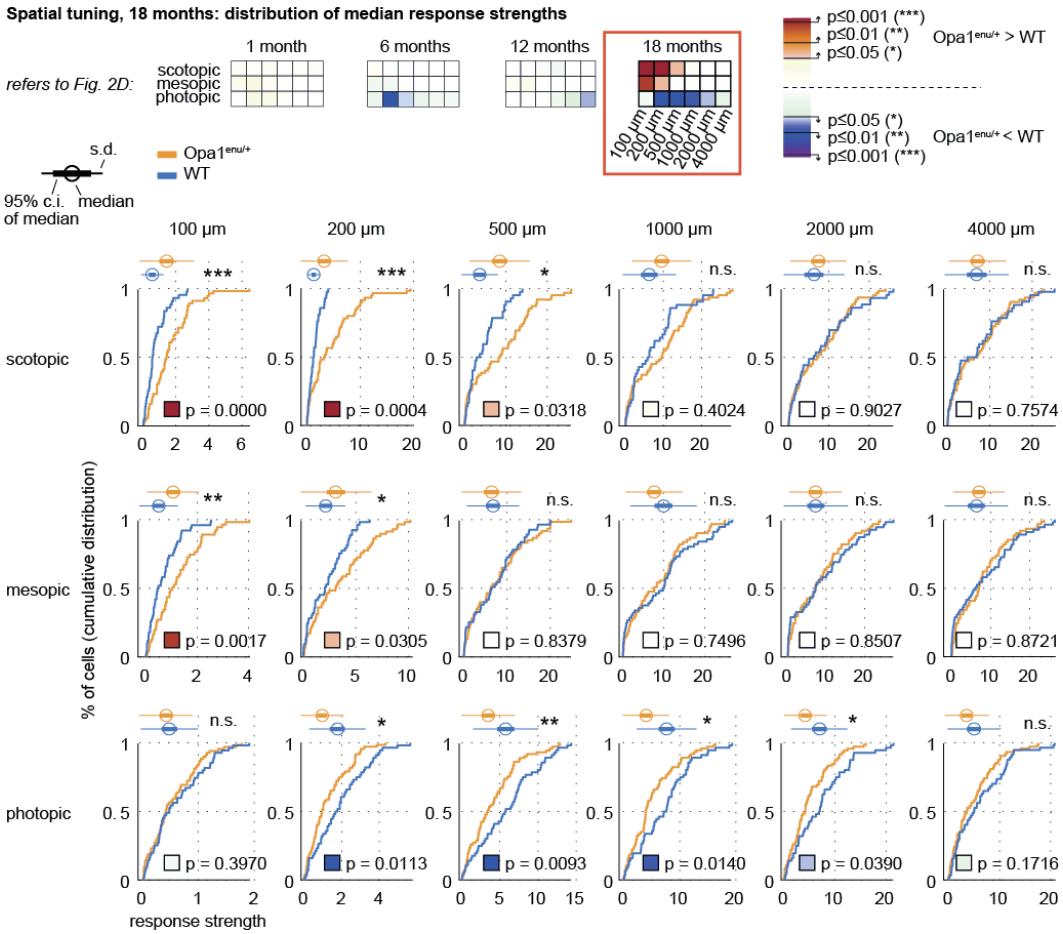

Supplementary Figure 4 - Distribution of median response strengths for spatial tuning (age of 18 month).

Raw data underlying the calculated p-Values depicted in Fig. 2D (repeated on top). Each subplot shows the cumulative distribution of response strengths measured in Opa1$^{enu/+}$ (orange, n = 85 units from 3 retinas) and WT (blue, n= 80 units from 5 retinas) ganglion cells. Conventions as in Supplementary Figure 1.

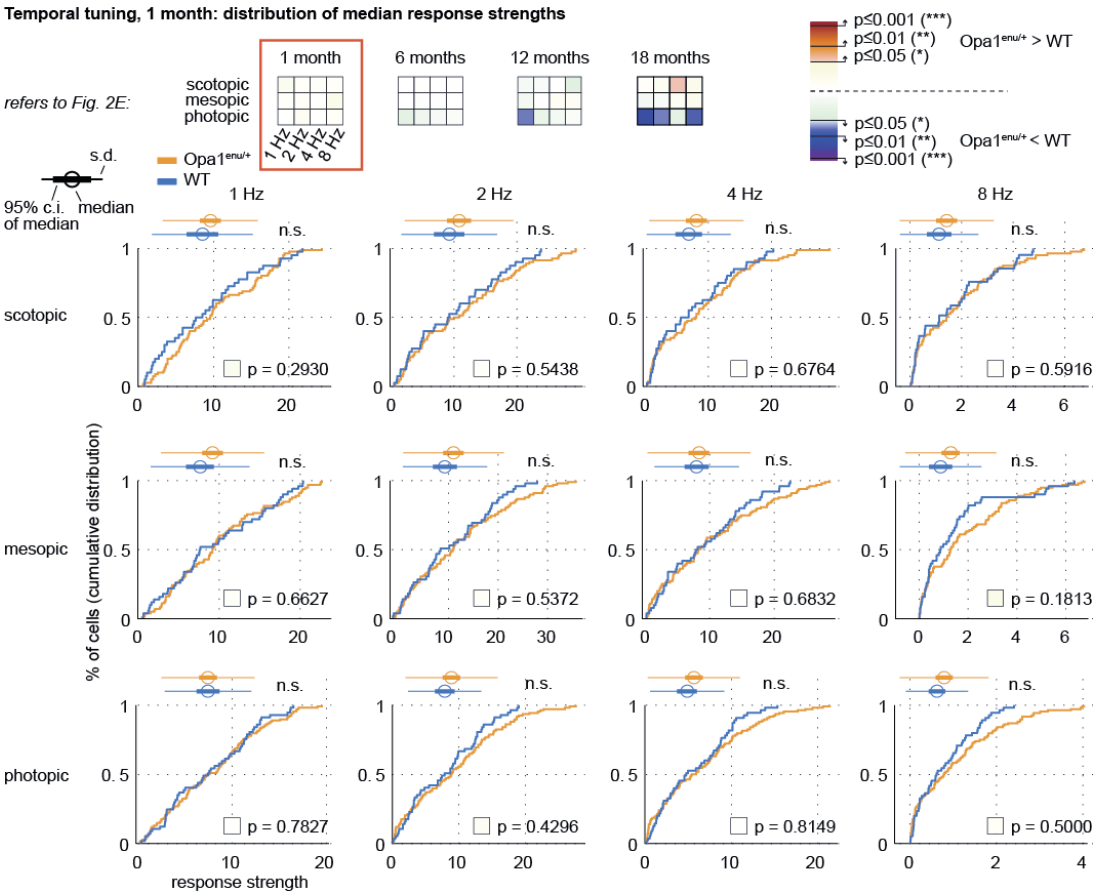

Supplementary Figure 5 - Distribution of median response strengths for temporal tuning (age of 1 month).

Raw data underlying the calculated p-Values depicted in Fig. 2E (repeated on top). Each subplot shows the cumulative distribution of response strengths measured in Opa1$^{enu/+}$ (orange, n = 62 units from 4 retinas) and WT (blue, n= 74 units from 3 retinas) ganglion cells in response to drifting gratings of different temporal frequency (1 to 8 Hz, columns) measured at different light levels (scotopic, mesopic, photopic, rows). Conventions as in Supplementary Figure 1.

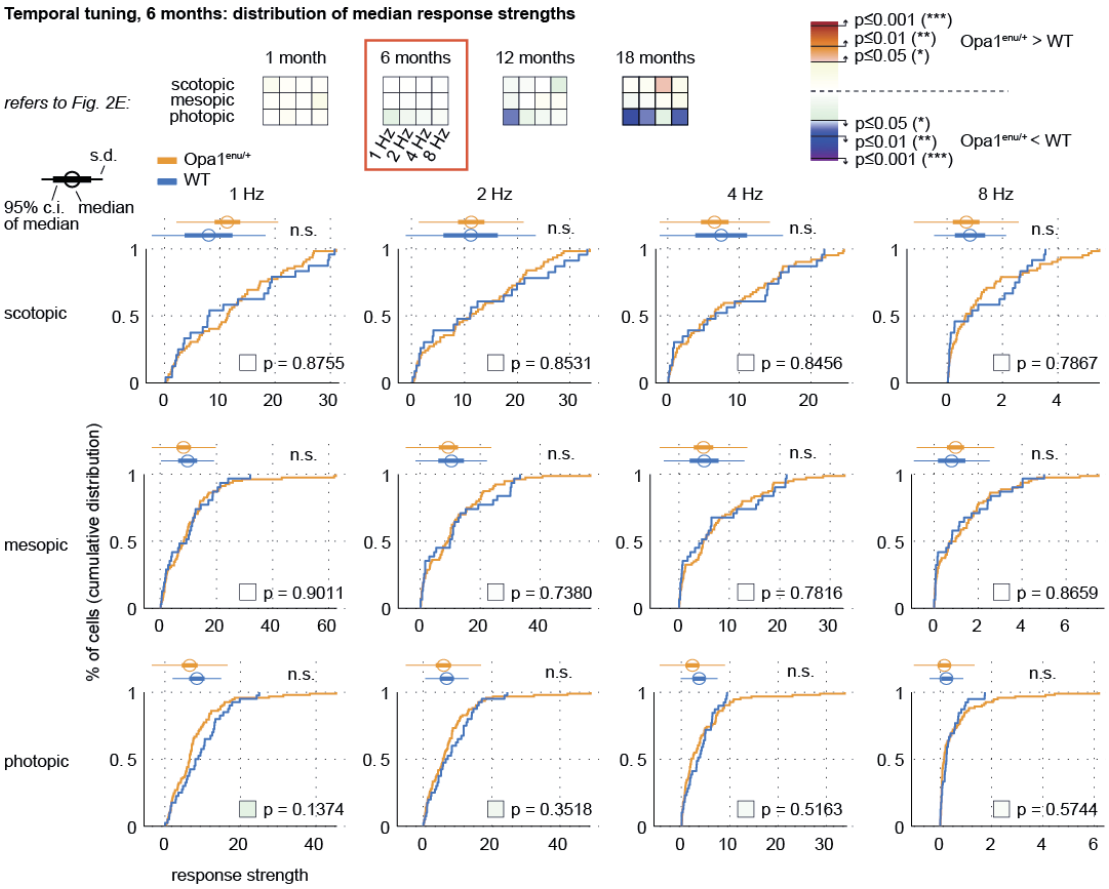

Supplementary Figure 6 - Distribution of median response strengths for temporal tuning (age of 6 month).

Raw data underlying the calculated p-Values depicted in Fig. 2E (repeated on top). Each subplot shows the cumulative distribution of response strengths measured in Opa1$^{enu/+}$ (orange, n = 108 units from 4 retinas) and WT (blue, n= 52 units from 4 retinas) ganglion cells. Conventions as in Supplementary Figure 5.

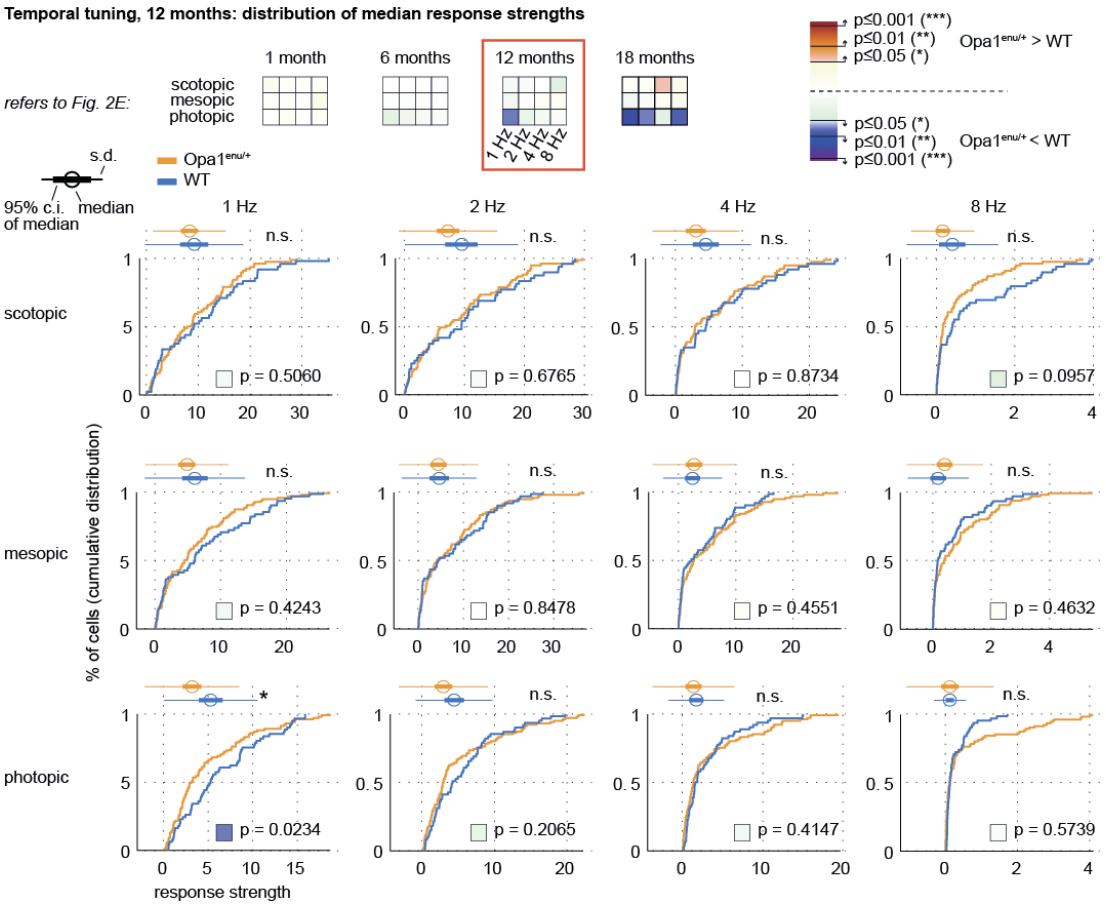

Supplementary Figure 7 - Distribution of median response strengths for temporal tuning (age of 12 month).

Raw data underlying the calculated p-Values depicted in Fig. 2E (repeated on top). Each subplot shows the cumulative distribution of response strengths measured in Opa1$^{enu/+}$ (orange, n = 119 units from 4 retinas) and WT (blue, n= 74 units from 3 retinas) ganglion cells. Conventions as in Supplementary Figure 5.

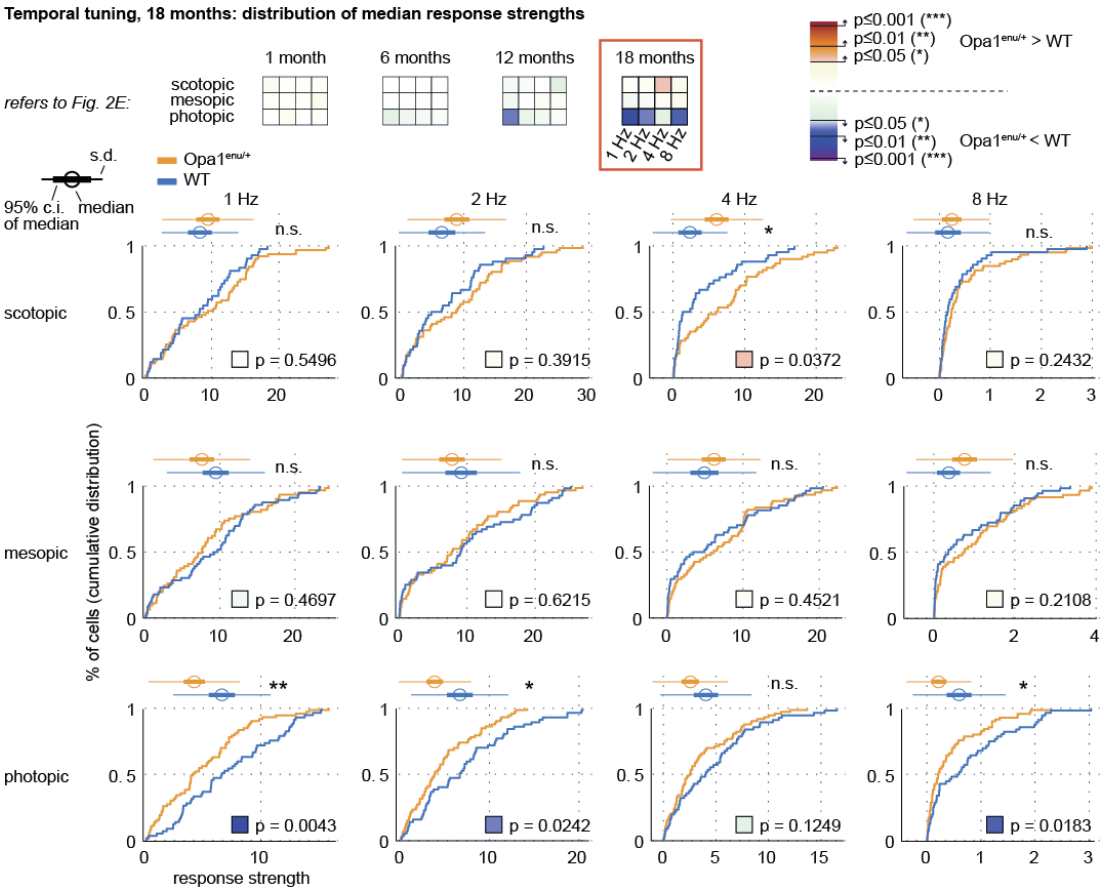

Supplementary Figure 8 - Distribution of median response strengths for temporal tuning (age of 18 month).

Raw data underlying the calculated p-Values depicted in Fig. 2E (repeated on top). Each subplot shows the cumulative distribution of response strengths measured in Opa1$^{enu/+}$ (orange, n = 85 units from 3 retinas) and WT (blue, n= 80 units from 5 retinas) ganglion cells. Conventions as in Supplementary Figure 5.

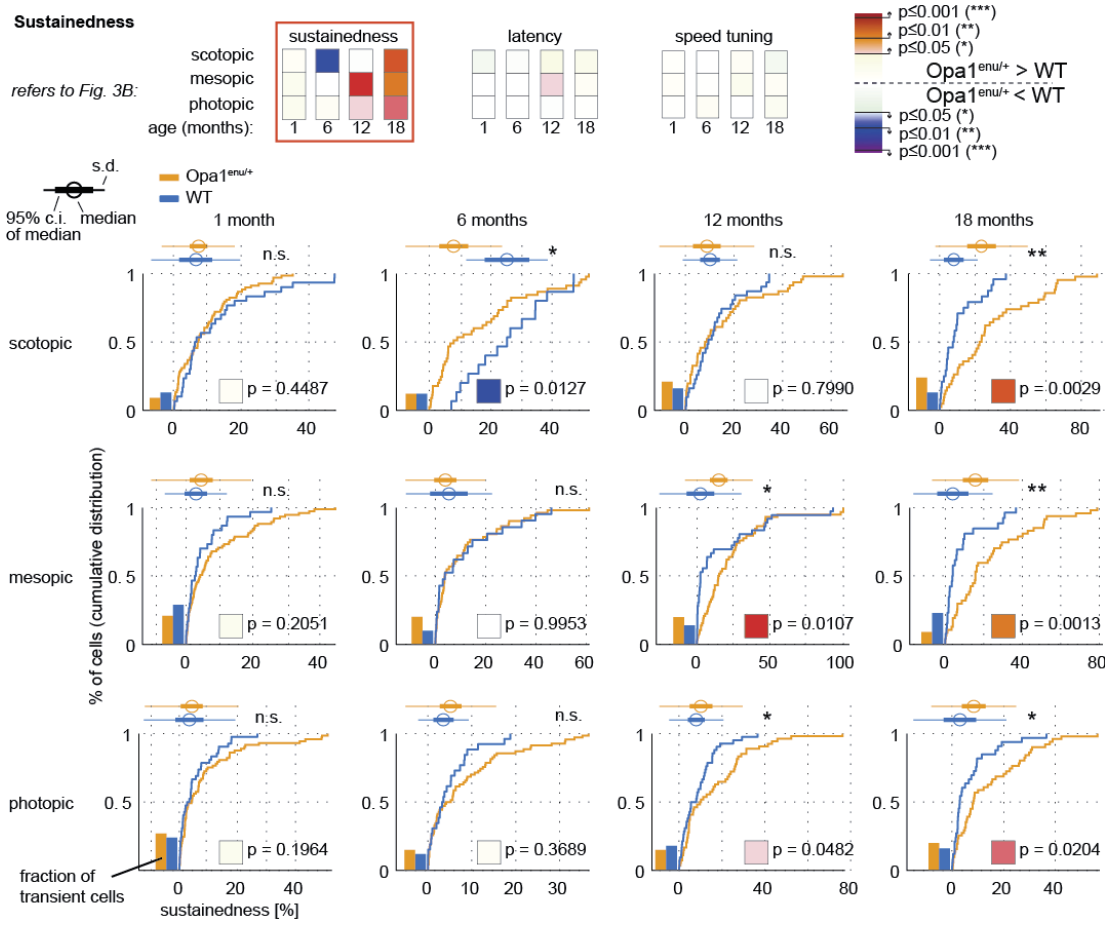

Supplementary Figure 9 - Distribution of the sustainedness parameter.

Raw data underlying the calculated p-Values depicted in Fig. 3B (repeated on top). Each subplot shows the cumulative distribution of the sustainedness parameter measured in different age groups in Opa1$^{enu/+}$ (orange, 1m: n = 62 units from 4 retinas, 6m: n = 108 units from 4 retinas, 12m: n = 119 units from 4 retinas, 18m: n = 85 units from 3 retinas) and WT (blue, 1m: n = 74 units from 3 retinas, 6m: n = 52 units from 4 retinas, 12m: n = 74 units from 3 retinas, 18m: n = 80 units from 5 retinas) ganglion cells. Number of transient cells (sustainedness parameter = 0) are given in % as bars on the left of each cumulative distribution. Conventions as in Supplementary Figure 1.

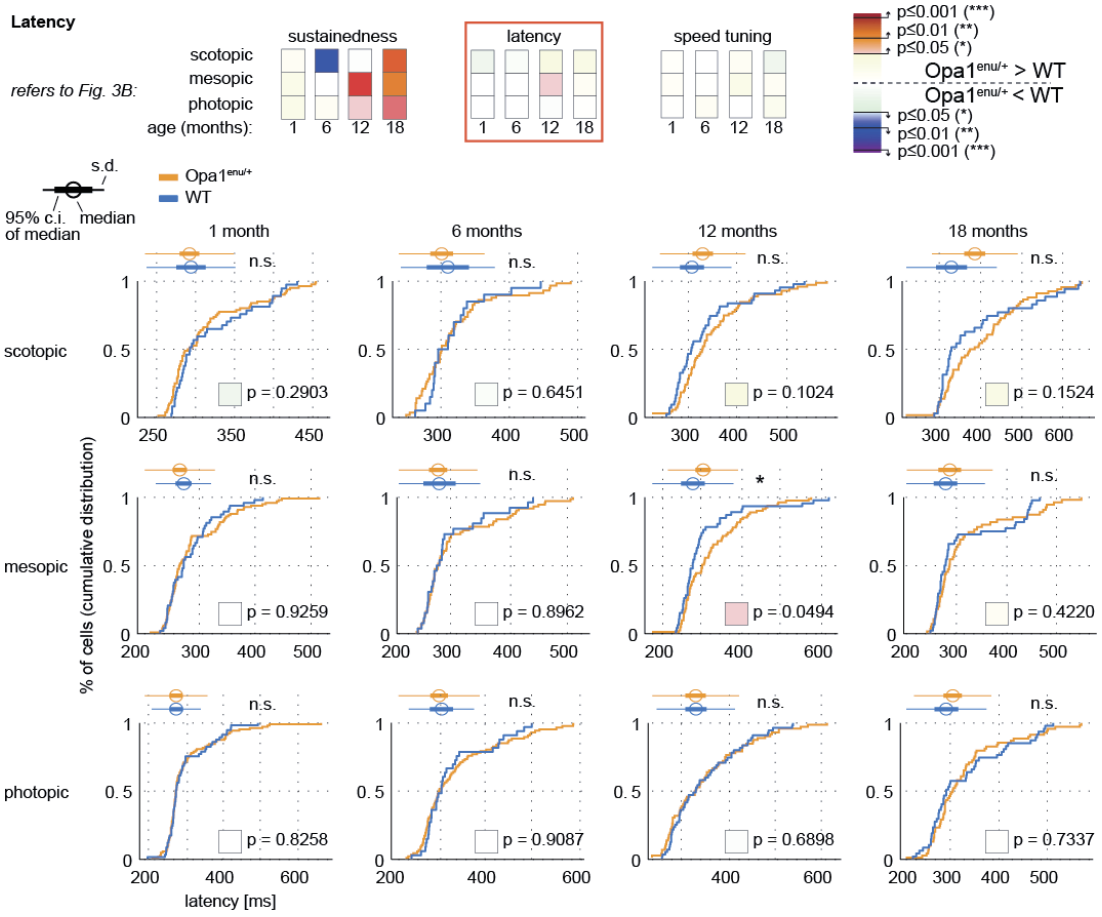

Supplementary Figure 10 - Distribution of the latency parameter.

Raw data underlying the calculated p-Values depicted in Fig. 3B (repeated on top). Each subplot shows the cumulative distribution of the latency parameter measured in different age groups in Opa1$^{enu/+}$ (orange, 1m: n = 62 units from 4 retinas, 6m: n = 108 units from 4 retinas, 12m: n = 119 units from 4 retinas, 18m: n = 85 units from 3 retinas) and WT (blue, 1m: n = 74 units from 3 retinas, 6m: n = 52 units from yy4y retinas, 12m: n = 74 units from 3 retinas, 18m: n = 80 units from 5 retinas) ganglion cells. Conventions as in Supplementary Figure 1.

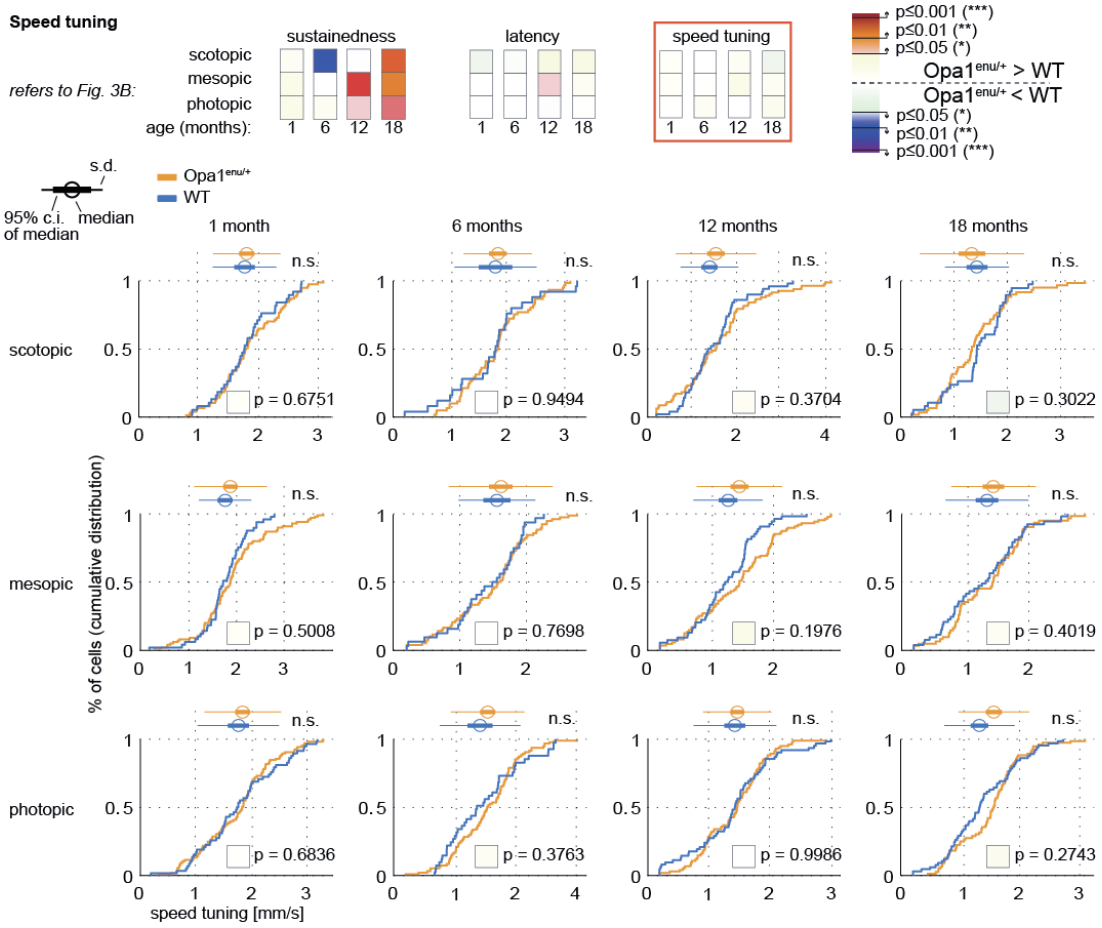

Supplementary Figure 11 - Distribution of the speed tuning parameter.

Raw data underlying the calculated p-Values depicted in Fig. 3B (repeated on top). Each subplot shows the cumulative distribution of the speed tuning parameter measured in different age groups in Opa1$^{enu/+}$ (orange, 1m: n = 62 units from 4 retinas, 6m: n = 108 units from 4 retinas, 12m: n = 119 units from 4 retinas, 18m: n = 85 units from 3 retinas) and WT (blue, 1m: n = 74 units from 3 retinas, 6m: n = 52 units from yy4y retinas, 12m: n = 74 units from 3 retinas, 18m: n = 80 units from 5 retinas) ganglion cells. Conventions as in Supplementary Figure 1.

Publication 6

Alexandra Tikidji-Hamburyan*, Katja Reinhard*, Riccardo Storchi*, Hartwig Seitter, Katherine E Davis, Johannes Dietter, Robert Bedford, Petri Ala-Laurila, Robert J Lucas, Thomas A Münch (under review) Rods escape saturation to drive visual responses in daylight conditions.
***equal contributions**

Framework: It has been unclear if and at which light levels rod photoreceptors saturate. In this study we systematically measured the contribution of rod photoreceptors to visual processing and found that rods can transmit information at any light level. This has been shown in-vitro and in-vivo in cone-deficient mice as well as in in-vivo studies of a wildtype-like mouse model.

My contributions: I took this study over from ATH. I planned and performed many of the multi-electrode array recordings in 3 different mouse models and few of the electroretinographic experiments. I analyzed the in-vitro ganglion cell as well as the in-vivo LGN recordings of cone-deficient mice. I was involved in writing the manuscript from the first draft on.

Other contributions: ATH measured and described the basic findings in her doctoral thesis. RS performed and analyzed in-vivo experiments with wildtype-like mice. HS performed most electroretinograms and part of the multi-electrode array recordings, and helped with processing of the data. KED performed and processed in vivo experiments in cone-deficient mice. RB helped with in-vivo recordings. JD and TAM implemented and adjusted the computational model with the help of PAL. RJL and TAM helped with the design and analysis of in-vivo and in-vitro experiments, respectively. ATH, TAM, RJL, and I wrote the manuscript with the help of all other authors.

Rods escape saturation to drive visual responses in daylight conditions

Alexandra Tikidji-Hamburyan[1,2,*], Katja Reinhard[1,2,*], Riccardo Storchi[3,*], Hartwig Seitter[1,2], Katherine E. Davis[3], Johannes Dietter[4], Robert Bedford[3], Petri Ala-Laurila[5], Robert J. Lucas[3], Thomas A. Münch[1,4]

*equal contribution

Correspondence:

RJS: robert.lucas@manchester.ac.uk

TAM: thomas.muench@cin.uni-tuebingen.de

Author affiliations

1 Retinal Circuits and Optogenetics, Centre for Integrative Neuroscience and Bernstein Center for Computational Neuroscience, University of Tübingen, Tübingen, Germany

2 International Max Planck Research School, University of Tübingen, Tübingen, Germany

3 Faculty of Life Science, University of Manchester, Manchester, UK

4 Institute for Ophthalmic Research, University of Tübingen, Tübingen, Germany

5 Department of Biosciences, University of Helsinki, Helsinki, Finland

Current address:

ATH: Department of Neurosurgery and Hansen Experimental Physics Laboratory, Stanford University, Stanford, California, USA

HS: Institute of Pharmacy, Department of Pharmacology and Toxicology, University of Innsbruck, Innsbruck, Austria

Abstract

The division of labor between specialized photoreceptor types, rods and cones, ensures that the mammalian retina can reliably signal across a range of light intensities that spans a dozen orders of brightness magnitude. Rod photoreceptors are exquisitely sensitive and mediate high-fidelity light detection at dim illumination, but are believed to saturate at higher light levels. At such high irradiance, solely cones are thought to transmit visual responses. Using electrophysiological recordings from the retina and dorsal lateral geniculate nucleus (dLGN) of cone-deficient and visually intact mice, we show here that rods can in fact contribute to vision at any physiological light level. Upon stepping to high irradiances their contrast sensitivity is initially strongly reduced. However, this recovers over time to allow rods to respond to moderate contrast stimuli. Surprisingly, they regain responsiveness faster at higher light levels. This recovery of rod responses is consistent with a mechanistic model that takes into account changes in phototransduction gain and bleaching adaptation. Overall, our data reveal not only that rods can respond to contrasts typical of those found in natural scenes across all irradiances, but that, paradoxically, raising irradiance across the photopic range increases the likelihood of eliciting such responses.

Introduction

Our visual system can function over a wide range of light intensities spanning about a dozen orders of magnitude(Land and Nilsson, 2002; Rodieck, 1998) . This remarkable dynamic range requires a precise set of neural mechanisms that allow visual processing under dim and bright light conditions. The main mechanism underlying this ability is the use of two different photoreceptor classes, namely the rods and the cones. Rods are specialized for high-fidelity signaling at low light levels, whereas cones mediate fast signaling at higher light levels. Based on the division of labor between rods and cones, light intensities are called scotopic (only rods are active, starlight vision), mesopic (both rods and cones are active), and photopic (rods are saturated, and only cones are active, daylight vision). This division of light intensities has become a dogma in vision.

The distinction between mesopic and photopic conditions is, by definition, determined by the irradiance at which rods saturate. However, the saturation point of rods has proved difficult to determine and depends upon experimental conditions such as the nature of the recording methodology, light history, stimulus contrast, and species studied (Adelson, 1982; Azevedo and Rieke, 2011; Govardovskii et al., 2000; Green, 1971; Nakatani et al., 1991; Nikonov et al., 2000) . Meanwhile, there is a body of literature suggesting that rods might not saturate at all and convey visual information at higher light levels (Altimus et al., 2010; Blakemore and Rushton, 1965; Jacobson et al., 2013; Naarendorp et al., 2001; Yin et al., 2006). Despite this lack of consensus, it is generally accepted that, under a given condition, increasing light intensity provides the best opportunity for minimizing rod responses.

We set out to explore the limits of rod vision by recording electrophysiological responses to light pulses presented over a wide range of background light intensities (up to 8 log units) in mice with non-functional cones. At each light level, we repeatedly measured light responses in the retina over 30 minutes to capture possible light adaptation effects. We find that rod responses are strongly reduced upon switching to backgrounds across the 'photopic' range, but that following a suitable period they become detectable under all light intensities tested, both *in-vitro* and *in-vivo*. Most surprisingly, we find that increasing the light intensities can even accelerate the recovery of rod responses, making it more likely that one would encounter rod activity at these irradiances. Recordings from mice with intact cone function suggest that these fundamental features are also apparent in rod contributions to the composite response of visually intact animals at high photopic levels. These data thus indicate that rods can contribute to visual responses at all physiological light intensities; and that contrary to conventional wisdom, raising the background light intensity under such 'photopic' conditions may even increase the likelihood of rod intrusion.

Results

Ganglion cells respond to contrast steps at all light levels in cone-deficient retinas

Using multi-electrode arrays, we recorded spiking activity of ganglion cells from isolated cone-deficient (*Cnga3*$^{-/-}$) retinas to determine the irradiance at which rod responses disappear (n=10 retinas). During each experiment, we increased the ambient light level at 10-fold increments every 30 min, from $2{\cdot}10^{8}$ rod-effective photons cm^{-2} s^{-1} (1 R*rod^{-1} s^{-1}, neutral density filter 8; ND8) to $2{\cdot}10^{15}$ rod-effective photons cm^{-2} s^{-1} (10^{7} R*rod^{-1} s^{-1},

ND1, Fig. 1A-C). The responses of a representative single ganglion cell to full-field steps of positive contrast (+0.25 Michelson, +0.66 Weber, see Methods for definition of contrast) or negative contrast (–0.49 Michelson, –0.66 Weber) are shown in Fig. 1D and E, respectively. We presented blocks of 5 repeats of this stimulus every 5 minutes (spike raster shown on the left, average spike rate shown on the right). After switching from ND5 to ND4 (from $2{\cdot}10^{11}$ to $2{\cdot}10^{12}$ rod-effective photons cm^{-2} s^{-1}), the cell shown in Fig. 1D,E did not respond to the stimulus during the first presentation consistent with the view that rods had become saturated. However, responses returned after continued exposure to this background. Surprisingly, rather than showing further evidence of saturation, responses actually became more apparent with subsequent increases in irradiance (even up to ND1, 1000-fold above the background at which we had first seen evidence of saturation).

This behavior was also apparent across the population of retinal ganglion cells (Fig. 2). The fraction of ganglion cells showing a significant response to positive or negative contrast steps was high through the lower irradiances and fell dramatically upon initially switching to ND4 ($2{\cdot}10^{12}$ rod-effective photons cm^{-2} s^{-1}, 10^4 R*rod^{-1} s^{-1}), only to recover over time (Fig. 2A). Responses collapsed again after switching to ND3 ($2{\cdot}10^{13}$ rod-effective photons cm^{-2} s^{-1}, 10^5 R*rod^{-1} s^{-1}), but once again recovered, and were then retained even at extremely high irradiances (ND2 and ND1, Fig. 2A). An analysis of mean response amplitude (averaging the amplitudes of only those units responding in any given epoch, Fig. 2B) painted a similar picture, with only transient loss of responsiveness upon switching to ND4 and ND3, but otherwise clear responses at all irradiances. Indeed, some units, like the one shown in Fig. 1, had their biggest responses at the brightest backgrounds.

The results shown in Fig. 2A indicated that the major difference between responses at ND4 and ND3 might be the rate at which they recovered following the irradiance increment. To explore this in more detail, we held a subset of retinas at these backgrounds for 2.5 hours. In both cases, the fraction of responding units fell close to zero immediately after the step to ND4 (Fig. 2C) or ND3 (Fig. 2D), but reached nearly 100% by the end of the recording. There was, however, a big difference in the rate of recovery, which occurred much faster at the brighter background (ND3, taking about 10 min for half of the ganglion cells to recover their responses) than at the dimmer background (ND4, taking between 30 and 60 min). We observed similar behavior as in Fig. 2A and B in two other cone-deficient mouse lines (*Pde3*$^{cpfl1/cpfl1}$ and *Gnat2*$^{cpfl3/cpfl3}$, see Suppl. Fig. S2).

Our ganglion cell recordings from isolated cone-deficient mice thus led to two surprising conclusions. First, rods can drive visual responses across all irradiances tested; and second, once within the 'photopic' range, rod-driven responses appeared to become more robust with increasing irradiance.

ERG recordings confirm rod responses at high light levels in cone-deficient retinas

We next set out to confirm these findings using a more direct recording of rod activity. To this end, we applied pharmacological agents (see Methods) to inhibit second-order responses in retinal explants of *Cnga3*$^{-/-}$ mice and recorded the isolated photoreceptor response using electroretinography (*in-vitro* ERG, Fig. 3). The stimulus shown in Fig. 3A, consisting of a variety of 50-ms light flashes of moderate to high contrasts, was shown 16 times at each light level (30 min) from ND8 to ND2. We quantified the strength of the elicited ERG signal as the mean amplitude of the negative voltage deflection during 300 ms

directly after the flash onset, while the 300 ms voltage signal preceding the flash was used as a baseline to test for significance of the flash-elicited responses (Wilcoxon rank sum test, resulting p-Values are color-coded in Fig. 3B).

In agreement with our conclusion that rods are functional across all backgrounds, we found clear ERG responses under all irradiances when employing a very high contrast flash (Michelson contrast of 0.99, Fig. 3B). Conversely, at the lowest contrasts (Michelson contrast 0.33 and 0.6) responses were not reliably detected across the higher irradiances (ND4 to ND2; Fig. 3B and Suppl. Fig. S3. In Fig. 3B, we omitted the responses to the lowest contrast for clarity.) However, since clear ganglion cell responses were elicited by stimuli of even lower contrast (Michelson contrast 0.25, Figs. 1, 2), our failure to detect ERG responses to these low-contrast stimuli seems to be a limitation of the *in-vitro* ERG recording technique. At the intermediate contrast (Michelson contrast 0.79, red curve in Fig. 3B, individual flash responses in Fig 3C), the ERG responses showed a characteristic pattern of recovery that was similar to the behavior of retinal ganglion cells described above (Fig. 2): ERG-responses were initially undetectable after switching to ND4 ($2{\cdot}10^{12}$ rod-effective photons cm^{-2} s^{-1}, 10^4 R^*rod^{-1} s^{-1}) but reemerged over time. The same occurred after switching to brighter light levels: responses first disappeared, but then reappeared with a time course that was faster for higher light levels. The time course of reemerging responses at the intermediate contrast of 0.79 was consistent across all tested retinas (n=4, mean ± s.e.m., Fig. 3D). This time course was also reflected in the increasing response amplitude to high-contrast flashes (Fig. 3B), and comparable to the temporal development of ganglion cell spiking responses (Fig. 2). It thus appears that rod activity that elicits only very small ERG signals at high irradiances (Fig. 3) is nevertheless sufficient to drive robust responses in ganglion cells (Figs. 1, 2).

We confirmed these findings with qualitatively identical and quantitatively similar results in two other cone-deficient mouse lines (*Pde3*$^{cpfl1/cpfl1}$ and *Gnat2*$^{cpfl3/cpfl3}$, Suppl. Fig. S3). These ERG recordings thus reveal that contrast sensitivity of rods is substantially reduced upon stepping to high irradiances, but that this recovers over time and that this recovery occurs faster at higher irradiances.

Rods drive light responses at high irradiances *in-vivo* in the *Cnga3*$^{-/-}$ thalamus

Having described rod responses in explanted retinas under even the brightest backgrounds, we next asked whether rod mediated light responses would also be apparent in the thalamus *in-vivo*. To this end, we recorded multiunit activity from the dLGN of anesthetized *Cnga3*$^{-/-}$ mice (Fig. 4, recording positions shown in Fig. 4D) in response to 50-ms flashes of positive contrast (0.75 Michelson Contrast). For these experiments we changed the sequence of irradiance presentations so that recordings at higher irradiance (ND4, ND3, and ND2) were interspersed with a moderate background (ND5, predicted to support strong rod responses), in order to confirm that the preparations retained good visual responses throughout the recording session.

Firing patterns of a representative multiunit recording are shown in Fig. 4A. As predicted, strong and stable flash responses were recorded at ND5 ($4.52{\cdot}10^{11}$ rod-effective photons cm^{-2} s^{-1}). In this example, responses became hard to discern at ND4 ($4.52{\cdot}10^{12}$ rod-effective photons cm^{-2} s^{-1}), while at the higher irradiances, responses disappeared immediately following the irradiance step, but returned during extended exposure to that background. Similar to the *in-vitro* recordings, the rate of response recovery was positively

correlated with irradiance. These general patterns were borne out by a more systematic analysis of these data (Fig. 4B), in which response amplitude (difference in spike rate in 200-ms windows before and after the flash) and reliability (p-Value for Rank Sum Test comparing these values) were plotted as a function of time.

Across the population of multi-unit traces there was more diversity in response characteristics. Of those that responded well at ND5, a minority (n=14/36) failed to show consistent responses at the highest irradiances ND3 and ND2 ($p>0.05$ for Rank Sum Test for at least half of trials at these irradiances). The majority (n=22/36), however, recovered sensitivity over time after an initial drop of responsiveness immediately after switching to these bright backgrounds (Fig. 4C). Once again, the rate of recovery was reliably fastest at the brightest background (ND2). Behavior at the intermediate irradiance (ND4) was variable, with some multiunit traces matching the very poor responses shown for the single example in Fig. 4A, B, while others responded reliably (Fig. 4C).

These experiments suggest that rods can drive visual responses at high light levels also *in-vivo*. The observed time course of response reemergence at high light levels (faster for brighter background) was consistent with the observations *in-vitro*.

Rods shape thalamic responses at high light levels in the presence of cones

The experiments with cone-deficient mice revealed that rods can function across all physiological background light intensities in this species. A reasonable question is whether this allows rods to contribute to visual responses in animals with an intact visual system, or whether the amplitude of rod signals at bright backgrounds is so weak that they are “drowned out” by cone activity. To answer this, we sought a method of identifying any putative rod contribution to the overall visual response in cone-sufficient mice. Our approach was to take advantage of a transgenic mouse line (*Opn1mw*^{R}) in which the mouse M-opsin coding sequence is replaced by the human long-wavelength sensitive (‘L‘ or ‘Red’) opsin sequence (Allen et al., 2014; Smallwood et al., 2003). In this animal, the wavelength sensitivity of rods and cones is very different, allowing us to ask if rods impact the spectral sensitivity of visual responses under bright backgrounds. To avoid the possibility of recording melanopsin-driven responses we crossed these *Opn1mw*^{R} animals with a melanopsin knockout (*Opn4*$^{-/-}$) line for use in our experiments.

Anaesthetised *Opn1mw*^{R}*:Opn4*$^{-/-}$ animals were adapted to a violet light (λ_{max}=400nm) to which rods, and cones containing L-opsin and S-opsin are approximately equally sensitive (Fig. 5A, B). Responses to blue (λ_{max}=430), cyan (λ_{max}=480) or red (λ_{max}=630) flashes, presented in pseudorandom order at 15 different intensities superimposed upon the background (Fig. 5B), were recorded in the contralateral dLGN (recording positions shown in Fig. 5F). Given the divergence in spectral sensitivity between rods and both S-opsin and L-opsin there is a big difference in the effective contrast of these flashes for rods and cones across the wavelengths. In particular, while flashes at all three wavelengths present significant contrast for L-opsin, rods should be much more responsive to the blue and cyan stimuli, while S-opsin contrast is much lower at all wavelengths (Fig. 5B). Under true photopic conditions, i.e. with rods truly saturated, we would expect equivalent responses to flashes at all wavelengths when expressed in L-cone contrast, while rod intrusion at mesopic irradiances should produce differential responses to blue and cyan vs red flashes.

When these flashes were presented at ND5 (1.38 10^{11} rod-effective photons cm^{-2} s^{-1}, at which rod responses were always strong in our recordings with cone-deficient mice, Fig. 4), we found clear evidence of rod intrusion in the composite flash responses. Thus, when flash intensities were expressed in L-opsin contrast, responses were consistently larger for blue and cyan flashes than for red flashes, as shown in Fig. 5C for a single unit and in Fig. 5D for the population of recorded units, see Supplementary Table S5A for statistical analysis. Stepping up to ND4, this difference disappeared, with response amplitude at all wavelengths being adequately predicted by L-opsin contrast. Responses at ND4 could thus be interpreted as being truly 'photopic'. In common with the other data presented here, however, a further increase in irradiance produced a surprising increase in rod intrusion. At ND3, flash response amplitude could no longer be predicted by L-opsin contrast. In this case, blue and cyan responses were consistently smaller than those elicited by red flashes of similar cone contrast. These data indicate an inhibitory influence of rods on the cone flash response at this high photopic level (such inhibitory rod-cone interactions have precedent in the psychophysics literature (Zele et al., 2014).) To confirm that the effect at ND3 was not attributable to some methodological error, we first tested how robust it was to errors in our estimate of *in-vivo* L-opsin spectral sensitivity. We varied the two parameters that could strongly influence this estimate (pigment optical density and pre-receptoral spectral filtering; see Methods), but found that the reduced responsiveness at blue and cyan was retained (Supplementary Table S5B). We next confirmed that responses to blue and cyan flashes in *Cnga3*$^{-/-}$ mice were equivalent when expressed as a function of our estimated rod contrast (Fig. 5E), suggesting that the difference to blue and cyan flashes at ND3 in *Opn1mw*^{R}*:Opn4*$^{-/-}$ mice could be attributable to a difference in relative excitation of rods and L-opsin (L-opsin to Rod-opsin ratio of excitation at brightest flash: 0.48 for blue and 0.44 for cyan). In summary, while our data are consistent with flash responses being wholly cone generated at ND4, they reveal a significant rod contribution at the brighter background (ND3).

Discussion

These experiments were motivated by a naïve desire to take advantage of transgenic cone-deficient mice to determine the irradiance at which mouse rods saturate. In fact, we have found both *in-vivo* and *in-vitro*, and in both cone-deficient and cone-sufficient mice, that no physiologically relevant background light intensity is able to completely saturate rods. This might have been expected for stimuli of very high contrast, but we recorded responses also to moderate contrasts, well within the contrast range experienced in natural scenes. Most surprisingly, we found that once within the realm of what would ordinarily be considered 'photopic' vision, increases in irradiance actually made it easier to record rod-driven responses. Thus, in all of our experiments rod responses were most inconsistent at a background light level of $2{\cdot}10^{12}$ rod-effective photons cm^{-2} s^{-1} (10^{4} $R^{*}rod^{-1}$ s^{-1}, ND4), but became more reliable with subsequent increases in irradiance. This latter finding is explained by our observation that rod contrast sensitivity was substantially reduced upon switching to high Irradiances (≥ ND4) but recovered under extended exposure to the bright background. In all cases in which this rod recovery was traced over time, we found that it occurred more rapidly at higher irradiances.

What physiological processes could explain the pattern of rod responses under bright

backgrounds that we observed? As a framework for thinking about this problem, we explored the most detailed available model of rod phototransduction (Invergo et al., 2014). We used the model to predict photocurrents induced by a sinusoidally modulated stimulus (0.25 Hz) of either high contrast (0.98 Michelson contrast, full amplitude: 2 log units) or moderate contrast (0.7 Michelson contrast, full amplitude: 0.75 log units, black traces in Fig. 6) against a range of irradiances mimicking our experiments: every 30 min the background increased by 1 log unit, spanning low (ND8) to high (ND1) intensities (Fig. 6).

The original model of Invergo et al, without any modifications, did not replicate our experimental findings, but it instead predicted rod saturation at high light levels (Fig. 6, panel 1; blue curves in Fig. 6 show the photocurrents predicted by the model). However, the model also predicted that the concentration of unbleached rhodopsin (red curves in Fig. 6) would keep being modulated at all irradiances through isomerization events triggered by the sinusoidal stimulus (see inset in panel 1). This indicates that a reduced gain of the phototransduction cascade might prevent saturation and allow rods to respond to this stimulus.

One feature of photoreceptor physiology that the original model does not include is the irradiance-dependent translocation of arrestin and transducin between inner and outer segments (Calvert et al., 2006; Slepak and Hurley, 2008). At higher light levels, arrestin moves into the outer segment, increasing its effective concentration; while transducin leaves the outer segment, reducing its concentration. Both translocations have the net effect of reducing the gain of the phototransduction cascade, thereby contributing a mechanism of light adaptation. We modified the model to include these events in a very simplified manner, namely as an instantaneous increase/decrease of their concentrations upon light-level transitions (Suppl. Fig. S4B). This modification resulted in modulated photocurrents to the high contrast stimulus at all light levels (Fig. 6, panel 2, blue curve). Moreover, the model replicated our observations that responses are initially weak after the light level increase, but gain strength with a time course that is faster at higher light levels (see also magnified view below panel 2). Note that this time course of the photocurrents needs to be shaped by other adaptive mechanisms beyond the translocation of transducin and arrestin, as the translocations were implemented as instantaneous changes. We found that the faster response reemergence at higher irradiances coincided with the increased rate of rhodopsin bleaching (red curve in panel 2). Rhodopsin bleaching reduces the rate of isomerization events and might thus be one of the mechanisms allowing for rod responses at high light levels, similar to the suggested role of bleaching adaptation in cones (Burkhardt, 1994).

We indeed found that the model behavior at high light levels (but not at low and moderate irradiances) was quite sensitive to parameter variations that influenced the rhodopsin concentration. The first model parameter we turned to was the rhodopsin regeneration rate (k_{recyc}). This parameter is highly relevant in the context of comparing our *in-vitro* and *in-vivo* experiments. We estimate that the regeneration rate is about 1000-fold lower in explanted retina because of the lack of pigment epithelium. The model predicts rod response reemergence at high irradiances in both cases (panels 2 and 3 in Fig. 6); however, while photocurrents *in-vivo* remained closer to saturated values (panel 2), they were more robust in isolated retina (panel 3). Indeed, the predicted properties of photoresponses *in-vitro* at bright backgrounds approached those

under “scotopic” conditions. This confirms that increased bleaching promotes escape from saturation, which may also explain our paradoxical experimental findings that rod responses reemerged more quickly and were more robust at the highest irradiances.

In fact, any variation of model parameters that resulted in a lower rhodopsin concentration promoted high-irradiance rod responses. Suppl. Fig. S4A gives an overview of the model behavior for all parameter combinations we tested. Only moderate reductions of either k_{recyc} (panel b in Suppl. Fig. S4A) or of the total number of rhodopsin molecules (R_{total}, panel g in Suppl. Fig. S4A) were necessary to rescue the responses to moderate-contrast stimuli, which were saturated with the original values for these model parameters (Fig. 6, panel 4). Reducing both parameters (k_{recyc}, R_{total}) in concert required even smaller adjustments that are well within physiologically reasonable values (Suppl. Fig. S4C). Taken together, we found that the model could reproduce all key features of our experimental data: the transient saturation when stepping to high backgrounds, the gradual recovery of responses at all backgrounds, and the irradiance-dependence of the rate of recovery. This could be achieved by physiologically plausible variations of the model parameters compared to the model devised by Invergo and colleagues (Invergo et al., 2014) (arrestin/transducin translocation and realistic changes in k_{recyc} and R_{total}).

The process of exploring these parameters also highlighted a couple of features of the rod response at high irradiance that are worthy of comment. Firstly, the gradual recovery of rod responses over extended exposure to bright backgrounds that we observed could have at least two plausible origins. The most parsimonious is that it simply reflects the kinetics of bleaching adaptation. In our model, bleaching can successfully recreate both the reappearance of rod signals over time and the observation that this occurs more rapidly at higher irradiance. However, time-dependent changes in transducin and arrestin location could also contribute to the time course of response reemergence. Secondly, because the amplitude of rod responses is so dependent upon k_{recyc}, it is very likely that rod activity at high light levels will be particularly strong in isolated retina in which native pigment regeneration mechanisms are impaired - a conclusion that may first seem counterintuitive. It follows that one cannot ensure suppression of rod responses experimentally by simply increasing the background irradiance; the opposite is true: such an approach is likely to even enhance rod responses, as reemergence of rod responses (mediated by bleaching, exchange of enzymes between inner and outer segment, and potentially additional adaptive processes) may require dozens of minutes at the dimmest high (photopic) light levels, but can be accelerated to a few minutes at brighter light levels.

What could explain the many reports in the literature of saturation of rod vision at high backgrounds? Although we observed rod activity at all backgrounds, our data certainly do not question the idea that saturation is a feature of their physiology. Transient saturation immediately after stepping to a bright background can last many minutes at the right background. Consistent with previous reports (Wang and Kefalov, 2009) we find rod signals to have low contrast sensitivity at high backgrounds, and low amplitude (at least in vivo). Rod responses could thus be invisible when using low contrasts or measurement systems with inherently low signal-to-noise ratio. Finally, the small rod signal may be hard to detect in visual pathways with low spatiotemporal

pooling. This could explain the wide spread of relative response amplitudes in individual ganglion cells we find (Fig. 2D); why rod responses at high backgrounds were not apparent in all visually responsive dLGN neurons; and a previous report that cone-deficient mice lose the optokinetic reflex at backgrounds (10 R^*rod^{-1} s^{-1}) well below established rod saturation thresholds (Umino et al., 2008).

Aside from this, our modeling suggests that the presence of rod responses at high light levels could be very sensitive to naturally occurring variations in the gain of the phototransduction cascade, in addition to variations of the total rhodopsin concentration (R_{total}) and the regeneration rate of rhodopsin (k_{recyc}). It is thus conceivable that slight variations in the properties of the rod phototransduction cascade and its regulation (e.g. differences in molecular concentrations, in kinetic properties, in translocation processes, in the volume of the outer segment) would result in a different preponderance of rods to support vision at high light levels. Such differences might exist between species, between individuals of the same species, between different rods in the same retina, or even within the same rod during the circadian cycle. The experience of human rod monochromats (achromatopsia patients) supports the idea of such diversity. These patients are commonly photophobic and blinded in a bright environment (Aboshiha et al., 2015), consistent with the idea that rods become saturated. However, for some individuals this is not the case (Jacobson et al., 2013) – their rod system does apparently not saturate. Deeper insight into the underlying mechanisms of this non-saturating phenotype in some individuals might even reveal new opportunities to treat rod monochromats by appropriately reducing the gain of the rod cascade. While such a reduced gain would be counterproductive for low-light vision, our daily lives, with electrical lighting all around us, happen mostly beyond the scotopic range, so that such treatment could indeed have a net positive benefit for the patients.

Methods

1. Animals

There are several transgenic mouse lines in which cone responses are abolished due to mutations disrupting the cone phototransduction cascade. In *Cnga3*$^{-/-}$ mice (Biel et al., 1999), kindly provided by M. Biel, the cone-specific alpha-subunit of the cyclic nucleotide gated channel is mutated, preventing voltage changes in cones upon light activation. *Cnga3*$^{-/-}$ mice were 4.5 to 6 weeks old for ganglion cell recordings, 8 weeks for ERG recordings, and approximately 6 to 8 weeks for in-vivo experiments. In *Pde3*$^{cpfl1/cpfl1}$ mice (Jackson strain #3678), kindly provided by Bo Chang (The Jackson Laboratory, Bar Harbor, ME), the cone-specific phosphodiesterase is non-functional. *Pde3*$^{cpfl1/cpfl1}$ mice were 11 to 13 weeks old. In *Gnat2*$^{cpfl3/cpfl3}$ mice (Jackson strain #6795), the cone-specific transducin is non-functional. *Gnat2*$^{cpfl3/cpfl3}$ mice were 5 to 13 months old. All in-vitro experiments were performed with explanted retinas, with retinal pigment epithelium removed. “Red opsin” mice (Opn1mwR; Opn4$^{-/-}$) of approximately 6 to 18 weeks were used for in vivo experiments and bred in-house at the University of Manchester, UK. Animal use was in accordance with German, UK and European regulations and approved by the Regierungspräsidium Tübingen (in vitro experiments) and the local Manchester Animal Welfare and Ethical Review Board (AWERB; Manchester, UK; in vivo experiments).

2. In vitro MEA recordings

MEA setup

Mice were kept on a 12/12 hour light/dark cycle, dark-adapted for 4-16h before the experiment, and sacrificed under dim red light by cervical dislocation, with or without preceding exposure to CO_2. Experiments were performed during daylight circadian times (experiment start in the morning or early afternoon). The eye cups were removed, put in Ringer solution (in mM: 110 NaCl, 2.5 KCl, 1 $CaCl_2$, 1.6 $MgCl_2$, 10 D-Glucose, and 22 $NaHCO_3$) bubbled with 5% CO_2 / 95% O_2. The retina was isolated and attached to a nitrocellulose filter (Millipore) with a central 2x2 mm hole, with the optic nerve head centred.

All recordings were performed with a perforated 60-electrode MEA (60pMEA200/30iR-Ti-gr, Multichannel Systems, Reutlingen). The electrodes are arranged on a square grid with a 200 µm distance between neighboring electrodes. Experiments were performed as described previously (Reinhard et al., 2014). Briefly, the mounted retina was placed ganglion cell-side down in the recording chamber, and good electrode contact was achieved by negative pressure through the perforated MEA. The tissue was superfused with Ringer solution at 34 °C. Data was recorded at 25 kHz with a USB-MEA-system (USB-MEA1060, Multichannel Systems, Reutlingen) or an MC-Card based MEA-system (MEA1060, Multichannel Systems).

Ganglion cell spike recordings

Data was high-pass filtered (500Hz, 10th-order butterworth filter), and spike waveforms and spike times were extracted from the raw data using Matlab (MathWorks). Spike sorting and thereby assignment of spikes to individual units (presumably ganglion cells) was performed semi-manually with custom written software (Matlab). Quality of each unit was individually/manually assessed by interspike interval and spike shape variation. Data analysis was based on the spiking responses of individual units. We estimated the instantaneous firing rate of ganglion cells by convolving the spike train (i.e. time series of 0's and 1's) with a Gaussian with sigma of 40 ms.

In-vitro ERG recordings

In vitro ERG recordings were performed as described previously utilizing the same 60-electrode MEA system as described above (Reinhard et al., 2014). An Ag/AgCl pellet reference electrode (Science Products E-201ML) was connected instead of the internal reference electrode of the MEA chamber. The AgCl reference was positioned 2 to 3 mm above the center of the MEA electrode field and was optically shielded from direct visual stimulation. Synaptic transmission from photoreceptors to bipolar cells was blocked with 50 µM L-AP4 (Sigma A7929 or Abcam ab120002), 10 µM NBQX (disodium salt, Tocris 1044) and 10 µM RS-CPP (Tocris 0173). Glial currents (slow PIII component) were inhibited with 100 µM $BaCl_2$ (Sigma 342920) (Kofuji et al. 2008). Data was low-pass filtered (300Hz, 4^{th}-order butterworth filter) and downsampled to 1 kHz. Noisy electrodes were discarded and all remaining electrodes were averaged for the analysis of in-vitro ERG responses.

3. Light stimulation and analysis: in vitro experiments

Experimental control of light intensities

The retina was stimulated with full-field gray scale visual stimuli with a computer-controlled digital light processing (DLP) projector (PG-F212X-L, Sharp or K11, Acer) and focused onto the photoreceptors through the condenser of the microscope (Fig. 1A). The stimulus projector produced output spanning 3 log units of light intensities (i.e. 1000-fold difference between black (‘0’) and white

('255') pixels). We linearized the gamma function of the projector output. The light path contained a shutter and two motorized filter wheels with a set of neutral density (ND) filters (Thorlabs NE10B-A to NE50B-A), having optical densities from 1 ("ND1", 10^1-fold light attenuation) to 5 ("ND5", 10^5-fold light attenuation). To achieve light attenuation stronger than 5 log units, we serially combined an ND5-filter in one filter wheel with another ND-filter in the second filter wheel, to achieve optical densities from 6 to 10. We refer to the filter settings as ND1 (brightest setting used) to ND8 (darkest setting used). While changing the ND filters, we closed the shutter to prevent intermittent exposure to bright light. We usually started the experiments at ND8 (i.e. combination of ND5 and ND3 filter), and step by step increased the ambient stimulation luminance by changing the ND filters by 1 unit. Unless otherwise noted, we presented the same set of visual stimuli at each ND-level during an experiment.

Light Intensity Measurements

We measured the spectral intensity profile (in µW cm^{-2} nm^{-1}) of our light stimuli with a calibrated USB2000+ spectrophotometer (Ocean Optics). We then transformed the stimulus intensity into rod-effective photon flux cm^{-2} s^{-1} by converting the spectrum to photons cm^{-2} s^{-1} nm^{-1}, and integrating it with the normalized spectrum of rod sensitivity (Umino et al., 2008). In addition, for comparison we report stimulus intensity in equivalents of photoisomerizations per rod and second, assuming dark-adapted rods, by multiplying the photon flux with the effective collection area of rods (0.5 µm²) (Nikonov et al., 2005). The results for a stimulus intensity of '30' range from $2{\cdot}10^7$ photons cm^{-2} s^{-1} (1 R* s^{-1} rod^{-1}, ND8) to $2{\cdot}10^{15}$ photons cm^{-2} s^{-1} (10^7 R* s^{-1} rod^{-1}, ND1), see Fig. 1B, C. Note that the intensity values given as "R* s^{-1} rod^{-1}" serves for only comparison. It truly reflects photoisomerizations only at low intensities; at high backgrounds, bleaching adaptation leads to a much lower effective rate of isomerizations.

Specific stimuli and response analysis

Contrast

We report stimulus contrast in "Michelson contrast" and, for comparison, also in "Weber contrast". For a flash stimulus of intensity I, presented on a background of intensity I_{back}, the definitions are as follows:

Michelson contrast = $(I - I_{back}) / (I + I_{back})$

Weber contrast = $(I - I_{back}) / I_{back}$

For the sinusoidal stimulus used in the model we calculated the Michelson contrast based on the minimum and maximum deflections of the sinusoid: Michelson contrast = $(I_{max} - I_{min}) / (I_{max} + I_{min})$

Ganglion cell spiking responses

Stimulus. Ganglion cell spiking responses were probed with full-field contrast steps (step duration: 2s) on a gray ('30' RGB pixel intensity) background (positive contrast: '30' → '50', Michelson: +0.25, Weber: +0.66; negative contrast: '30' → '10', Michelson: –0.49, Weber: –0.66, see Fig. 1B). Five positive and five negative steps were interleaved and presented as one block, and the firing rate to these 5 repetitions was averaged and taken as "one response". The firing rate curves on the right in Fig. 1D and E represent these "responses" which were used for further analysis; the rasters on the left show the underlying 5 individual responses.

Responsiveness. Whether or not a ganglion cell responded to a block (5 repetitions) of contrast steps was determined manually. For each unit and each stimulus block we manually inspected spike raster plots and firing rates. If a cell responded clearly and consistently to at least 3 out of 5 repetitions within one stimulus block, it was considered

as "responding" and was tagged with "1". Since the purpose of this analysis was to see if rods can drive light responses in ganglion cells, also purely "negative responses" (stimulus-evoked spike suppression) was counted as a response. Stimuli for which a cell responded to only 1 or 2 repetitions or for which the response was weak and/or sluggish were tagged with "0.5". If a cell did not respond during a stimulus block, it was tagged with "0". The average value of these assignments across all units was used as the value for "responsiveness" in Fig. 2A, C and D.

Amplitude. The amplitude of the response (used in Fig. 2B) was determined automatically as follows: first, the baseline firing rate was subtracted from the response (baseline firing rate was defined as the mean firing rate during 1300 ms before contrast step onset); second, we took the absolute value of the response (such that also negative deflections in the firing rate would be recognized as a response of the cell to stimulation); third, looking at all four brightness transitions (onsets and offsets of the positive and negative contrast steps) we took the maximal response value within 50 to 400 ms after the contrast step. This gave one "amplitude" value for each ganglion cell and for each stimulus block. For further analysis, we only considered amplitude values during stimulus blocks to which the cell actually responded (responsiveness tags "0.5" or "1", see above). These amplitudes were normalized for each ganglion cell separately to its maximal response across the experiment.

Averaging across experiments. In most experiments, full-field contrast steps were presented at the same time points after light-level transitions, with the earliest presentation about 4 min after the ND-filter switch and then regularly every 5 min (Protocol 1 in Suppl. Fig. S1; other stimuli, not discussed here, were presented in between. Note that the other stimuli were also presented on a background of '30' and their maximal intensity did not exceed '60', ensuring no excessive contribution to light adaptation compared to the full-field contrast step responses.) In the experiments depicted in Fig. 2B and C, we changed the order of stimuli and presented full-field contrast steps more closely after the light level switch (Protocol 2 in Suppl. Fig. S1). In those experiments, we probed the ND4 and ND3 light levels at even tighter intervals (Protocol 3) to follow the dynamic changes of ganglion cell responses with higher temporal precision. Suppl. Fig. S1 shows how the data points in Fig. 2 were averaged across experiments in which different stimulus protocols were used.

In-vitro ERG recordings

Stimulus. For in-vitro ERG recordings we used a series of 50 ms-flashes of different positive contrasts (Fig. 3A). One stimulus set consisted of 4 flashes with Michelson contrast +0.79 (Weber: +7.44, '30' → '255'), and 2 flashes each of Michelson contrast +0.6 (Weber: +2.97, '30' → '120'), +0.33 (Weber: +0.99, '30' → '60'), and +0.99 (Weber: +999, '0' → '255'). In order to achieve the high contrast (+0.99) it was necessary to intermittently reduce the gray background from '30' to '0'. 16 such stimulus sets were shown among other stimuli at each light level (30 min) from ND8 to ND2. The other stimuli, not discussed here, were limited to a brightness range between '0' and '60', presented on a background of '30'.

Analysis. We quantified the strength of the recorded ERG signal by measuring the mean amplitude of the negative voltage deflection during 300 ms directly after the onset of a 50-ms flash. The 300 ms voltage signal preceding the flash was used as a baseline to test for significance of the flash-elicited responses (Wilcoxon rank sum test). Significance testing was performed by using flashes of 3 consecutive stimulus sets, i.e. n=12 flashes for

contrast +0.79 and n=6 flashes for the other contrasts. Fig. 3B shows the moving average for this analysis (averaging 3 stimulus sets per data point, shifting by 1 stimulus set for the next data point; no averaging was done across light level transitions).

Response reliability. ERG responses at high light levels were usually very small, but nevertheless often clearly distinct from the voltage fluctuations of the background activity. As a measure of the reliability of such small signals, we devised a "response reliability index", which we calculated from the statistical measure of the presence of a response (namely p-value resulting from the Wilcoxon rank sum test, see above) according to the relationship depicted in the inset of Fig. 3D.

4. In vivo dLGN recordings

In vivo setup

Mice were anaesthetised using a single dose of urethane (30% w/v in dH2O, 1.6mg/kg, i.p) and placed in a stereotaxic frame (SR 5-M; Narishige, Japan) on a temperature-regulating 37°C heat mat (Harvard Apparatus, UK). A craniotomy was drilled above the coordinates for the dLGN (B–2.2mm to 2.6mm, ML 1.5-3mm) relative to the mouse stereotaxic atlas (Paxinos G, 2001). A 32 contact recording electrode (A4x8-5mm-50-200-177/413-A32; Neuronexus, USA) was lowered into the dLGN and extracellular spiking activity collected through a Recorder64 system (Plexon, USA). Light stimuli were delivered to the eye contralateral to the recorded brain hemisphere. Upon completion, animals were sacrificed by cervical dislocation and the brain fixed in 4% paraformaldehyde. Electrode placement (the electrode was dipped in fluorescent dye; CM-DiI, Life Technologies, UK) was verified in post-hoc histology.

Light stimuli

For *in-vivo* experiments, we delivered multi-spectral stimuli using a Spectra X light engine (Lumencor, USA). Stimuli were created by stepping four LEDs in combination from a low background to a high level (Blue, Cyan, Green and Yellow λ_{max} = 430nm, 480nm, 511nm and 575nm respectively). Light stimuli were presented through a light guide to the atropine-dilated eye as diffuse illumination of a Lambertian disc (10 mm in diameter, placed <5mm from corneal surface). A circular ND wedge (100FS04DV.4, Newport) in the light path between the exit point of the light engine and the end of the optical fiber, allowed light intensity to be modulated over a 4 log unit range. Spectral power densities for each LED were measured using a calibrated spectroradiometer (Bentham Instruments Ltd., UK). These were converted to retinal irradiance in rod-effective photon cm^{-2} s^{-1} to match the light levels used in *in-vitro* experiments by converting the corneal irradiance and correcting for the pre-receptoral filtering of the lens. For the light levels used *in-vivo*, we use as a short-hand the "ND5" to "ND2" nomenclature, as these are the closest corresponding intensities in the *in-vitro* experiments. Background intensity was $4.52*10^{14}$ rod-effective photon cm^{-2} s^{-1} at the brightest light level ("ND2"). 1200 flashes (duration: 50 ms) were shown at 1 Hz at each light level (+0.75 Michelson contrast for rods). These flashes were interleaved with a lower contrast (+0.5, data not shown here), thus protocol took 40 min per light level.

Data analysis Cnga3$^{-/-}$ mice

We measured 40 light responsive multi-units from 3 mice. 4 multi-units were excluded because they stopped responding completely after the first light level switch. In one mouse, recordings could only be performed up to ND2, but not for the last ND5 repetition. Firing rate has been calculated by convolving the spike train (i.e. time series of 0's and 1's) with a Gaussian with sigma of 5 ms. Then, responses to 10 flashes were averaged (= 1

group). For each group, we calculated the mean background firing rate for the 190 ms directly before stimulus onset. The background firing rates from 20 groups was then averaged and taken as the mean background firing rate for these 20 groups. The mean response rate 50 to 250 ms after the flash stimulus was considered as response. We applied a Wilcoxon rank sum test (1-sided) to test for significant differences between the 20 background and the 20 response values, i.e. we tested for significant light responses. These significance tests were performed on a running average with shifts of 2 groups for each data point. No averaging was performed across ND-borders. This resulted in approximately 350 p-values per recorded multiunit over the whole series of light levels. The measured p-values were then transformed into a response reliability measurement according to: p<0.01 = response strength 1, p>0.05 = response strength 0, and linear normalization of 0.01<=p<=0.05 to values between 0 and 1.

Detecting rod contributions to the visual response of Opnmw^{R};Opn4$^{-/-}$ mice.

Stimulus. We presented a series of blue, cyan and red flashes (50 ms duration) at 2Hz frequency on a light adapting violet background (λ_{max} = 400nm, Fig.5A). We used the same light engine and ND wedge described in section "Light Stimuli". Flashes followed a pseudorandom order for colours (λ_{max} = 430nm, 480nm and 630nm respectively for Blue, Cyan and Red LEDs) and intensities (15 different levels per colour) to prevent contrast adaptation in the response.

Stimulus intensity and contrast. Our estimate of S-, L-cone and rod Normalized Sensitivity for calculating flash contrasts was based upon Govardovskii nomograms (Govardovskii et al., 2000), using λ_{max} = 365nm for S-cones, λ_{max} = 556nm for L-cones (Smallwood et al., 2003) and λ_{max} = 498nm for rods (Naarendorp et al., 2010), adjusted for photopigment optical density (POD) (Thomas et al., 2011) and lens absorption, using a function adapted from (Lei and Yao, 2006):

Normalized Sensitivity = $10^{-\mu(\lambda)D}$ * Sensitivity / max(Sensitivity)

with Sensitivity = $(1 - 10^{-POD*S(\lambda)})$, $S(\lambda)$ is the pigment nomogram, D is the lens thickness (D = 2.07mm) (Lei and Yao, 2006), and $\mu(\lambda)$ is the attenuation coefficient calculated as

$\mu(\lambda) = c * (\lambda^{d} - \lambda_0^{d})$ for $\lambda < \lambda_0^{d}$; $\mu(\lambda) = 1$ otherwise;

The values for c and λ_0 (= wavelength of maximal lens transmission) were obtained by fitting tabulated data ($c = 5.33*10^{4}$; d = -2.27; λ_0 = 700nm) (Jacobs and Williams, 2007).

The absolute stimulus intensity of the violet background (effective photons cm^{-2} s^{-1} flux for the brightest background, ND3: rod-opsin $1.3758\ 10^{13}$, L-opsin: $1.3473\ 10^{13}$, S-opsin: $1.5833\ 10^{13}$) and contrast of the flashes (assuming POD=0.1 for cones, POD=0.01 for rods, and $c = 5.33*10^{4}$) are depicted in Fig. 5B.

Analysis. 45 PSTHs were estimated (15 intensities * 3 colours) for each light responsive unit and a PSTH matrix with mean firing rate responses (<fr>) was generated. In order to remove the high frequency noise due to the finite number of trials we computed the eigenvalue decomposition of the PSTH covariance matrix ($PSTH^{T}$*PSTH). Then we selected the smallest subset of eigenvectors whose associated eigenvalues accounted for >90% power of the PSTH covariance matrix. Finally we used the selected eigenvectors and their projections to reconstruct a "de-noised" version of the original PSTH matrix. The 45 responses were then calculated as the Euclidean norms of the "de-noised" PSTHs as follows:

Response = sqrt(Σ<fr>^{2})

with the summation taken across 20 time bins (time bin duration 15ms) in the first 300ms after the flash onset. We initially evaluated the possibility to measure flash responses as increments/decrements in firing rate in respect to the baseline. However we chose to use the Euclidean norm because we observed that a significant fraction of units exhibited multiphasic responses where those increments and decrements in firing rate tended to cancel each other out.

Statistical analysis of colored flash responses. The procedure for statistical analysis and their results are described in Supplementary Table S5.

5. Computational model

We have employed the model of Invergo and co-workers (Invergo et al., 2014) to simulate the phototransduction cascade within the rod outer segment. This model is an adaptation to mouse rods of previous models intended to simulate the phototransduction cascade in amphibians (Dell'Orco et al., 2009; Invergo et al., 2013). The current model of Invergo et al describes the phototransduction cascade on the system-level, i.e., based on a reaction network for the molecular species, a system of ordinary differential equations (ODE) is derived by simplifying assumptions like mass action kinetics. The numerical solution of this ODE-system yields the time dependence of each of the involved molecular species and as the main outcome the photo-response to a prescribed stimulus. We have implemented the model in the simulation software COPASI (Hoops et al., 2006). Compared to the original parameters of Invergo et al (2014), we have made the following adjustments: In all simulations, we have adjusted the total number of rhodopsin molecules (R_{total}). We used a maximum number of 7x10^7 (Lyubarsky et al., 2004) instead of 10^8, and reduced that number in some simulations to investigate the dependency of rod responses on that parameter (rows in Suppl. Fig. S4). We have varied the parameter for the rhodopsin regeneration rate (k_{recyc}) to mimic the different experimental conditions (*in-vitro*, *in-vivo*) and to investigate the dependency of rod responses on that parameter.

The original parameters of this model had been fit to biochemical and physiological data based on very different stimuli than the stimulus used in our study, namely to very brief and moderate-intensity flash stimuli on a dark-adapted rod (lasting tens of milliseconds of at most 2000 R* rod^{-1} $flash^{-1}$). Given the long duration and high intensity range of our stimulus, we took into account that arrestin and transducin are transported between the outer and inner segments (Calvert et al., 2006) and refs therein, resulting in a near-exchange of these molecular species between inner and outer segment. Under intense illumination, arrestin is transported from the inner segment to the outer segment, while transducin moves in the opposite direction. We have implemented this transport as a simplified step-wise change of concentration upon light-level transitions (Suppl. Fig. S4B). None of our parameter-adjustments changed the model behavior to the original stimuli used for parameter-fitting by Invergo et al (2014) (not shown).

Acknowledgements

We thank Martin Biel for supplying the *Cnga3*$^{-/-}$ mouse line for the in-vitro experiments. This research was supported by funds of the Deutsche Forschungsgemeinschaft (DFG) to the Werner Reichardt Centre for Integrative Neuroscience (DFG EXC 307), by the Bundesministerium für Bildung and Forschung (BMBF) to the Bernstein Center for Computational Neuroscience (FKZ 01GQ1002), by funds of the Biotechnology and Biological Sciences Research Council (BBSRC

BB/1007296/1) and the European Commission (ERC Advanced Grant 268970 MeloVision) to R.J.L., a Christiane-Nüsslein-Volhard Stipend to A.T.-H., and a Pro-Retina Stipend to K.R.

Author contribution

designed study: ATH, TAM, KR, RS, KED, RJL
performed experiments: ATH, KR, RS, HS, KED, RB
analyzed data: ATH, KR, RS, HS, KED, TAM
computational modeling: JD, PAL, TAM
wrote manuscript: ATH, KR, RJL, TAM

References

Aboshiha, J., Dubis, A.M., Carroll, J., Hardcastle, A.J., and Michaelides, M. (2015). The cone dysfunction syndromes. Br J Ophthalmol.

Adelson, E.H. (1982). Saturation and adaptation in the rod system. Vision Res 22, 1299-1312.

Allen, A.E., Storchi, R., Martial, F.P., Petersen, R.S., Montemurro, M.A., Brown, T.M., and Lucas, R.J. (2014). Melanopsin-driven light adaptation in mouse vision. Curr Biol 24, 2481-2490.

Altimus, C.M., Guler, A.D., Alam, N.M., Arman, A.C., Prusky, G.T., Sampath, A.P., and Hattar, S. (2010). Rod photoreceptors drive circadian photoentrainment across a wide range of light intensities. Nat Neurosci 13, 1107-1112.

Azevedo, A.W., and Rieke, F. (2011). Experimental protocols alter phototransduction: the implications for retinal processing at visual threshold. J Neurosci 31, 3670-3682.

Biel, M., Seeliger, M., Pfeifer, A., Kohler, K., Gerstner, A., Ludwig, A., Jaissle, G., Fauser, S., Zrenner, E., and Hofmann, F. (1999). Selective loss of cone function in mice lacking the cyclic nucleotide-gated channel CNG3. Proc Natl Acad Sci U S A 96, 7553-7557.

Blakemore, C.B., and Rushton, W.A. (1965). Dark adaptation and increment threshold in a rod monochromat. J Physiol 181, 612-628.

Burkhardt, D.A. (1994). Light adaptation and photopigment bleaching in cone photoreceptors in situ in the retina of the turtle. J Neurosci 14, 1091-1105.

Calvert, P.D., Strissel, K.J., Schiesser, W.E., Pugh, E.N., Jr., and Arshavsky, V.Y. (2006). Light-driven translocation of signaling proteins in vertebrate photoreceptors. Trends in cell biology 16, 560-568.

Dell'Orco, D., Schmidt, H., Mariani, S., and Fanelli, F. (2009). Network-level analysis of light adaptation in rod cells under normal and altered conditions. Molecular bioSystems 5, 1232-1246.

Govardovskii, V.I., Calvert, P.D., and Arshavsky, V.Y. (2000). Photoreceptor light adaptation. Untangling desensitization and sensitization. J Gen Physiol 116, 791-794.

Green, D.G. (1971). Light adaptation in the rat retina: evidence for two receptor mechanisms. Science 174, 598-600.

Hoops, S., Sahle, S., Gauges, R., Lee, C., Pahle, J., Simus, N., Singhal, M., Xu, L., Mendes, P., and Kummer, U. (2006). COPASI--a COmplex PAthway SImulator. Bioinformatics 22, 3067-3074.

Invergo, B.M., Dell'Orco, D., Montanucci, L., Koch, K.W., and Bertranpetit, J. (2014). A comprehensive model of the phototransduction cascade in mouse rod cells. Molecular bioSystems 10, 1481-1489.

Invergo, B.M., Montanucci, L., Koch, K.W., Bertranpetit, J., and Dell'orco, D. (2013). Exploring the rate-limiting steps in visual phototransduction recovery by bottom-up kinetic modeling. Cell communication and signaling : CCS 11, 36.

Jacobs, G.H., and Williams, G.A. (2007). Contributions of the mouse UV photopigment to the ERG and to vision. Doc Ophthalmol 115, 137-144.

Jacobson, S.G., Cideciyan, A.V., Peshenko, I.V., Sumaroka, A., Olshevskaya, E.V., Cao, L., Schwartz, S.B., Roman, A.J., Olivares, M.B., Sadigh, S*., et al.* (2013). Determining consequences of retinal membrane guanylyl cyclase (RetGC1) deficiency in human Leber congenital amaurosis en route to therapy: residual cone-photoreceptor vision correlates with biochemical properties of the mutants. Human molecular genetics 22, 168-183.

Land, M.F., and Nilsson, D.-E. (2002). Animal Eyes (Oxford University Press).

Lei, B., and Yao, G. (2006). Spectral attenuation of the mouse, rat, pig and human lenses from wavelengths 360 nm to 1020 nm. Exp Eye Res 83, 610-614.

Lyubarsky, A.L., Daniele, L.L., and Pugh, E.N., Jr. (2004). From candelas to photoisomerizations in the mouse eye by rhodopsin bleaching in situ and the light-rearing dependence of the major components of the mouse ERG. Vision Res 44, 3235-3251.

Montgomery D. C., R.G.C. (2010). Applied Statistics and Probability for Engineers, 5 Edition edn (Wiley).

Naarendorp, F., Esdaille, T.M., Banden, S.M., Andrews-Labenski, J., Gross, O.P., and Pugh, E.N., Jr. (2010). Dark light, rod saturation, and the absolute and incremental sensitivity of mouse cone vision. J Neurosci 30, 12495-12507.

Naarendorp, F., Sato, Y., Cajdric, A., and Hubbard, N.P. (2001). Absolute and relative sensitivity of the scotopic system of rat: electroretinography and behavior. Vis Neurosci 18, 641-656.

Nakagawa, S., and Cuthill, I.C. (2007). Effect size, confidence interval and statistical significance: a practical guide for biologists. Biological reviews of the Cambridge Philosophical Society 82, 591-605.

Nakatani, K., Tamura, T., and Yau, K.W. (1991). Light adaptation in retinal rods of the rabbit and two other nonprimate mammals. J Gen Physiol 97, 413-435.

Nikonov, S., Lamb, T.D., and Pugh, E.N., Jr. (2000). The role of steady phosphodiesterase activity in the kinetics and sensitivity of the light-adapted salamander rod photoresponse. J Gen Physiol 116, 795-824.

Nikonov, S.S., Daniele, L.L., Zhu, X., Craft, C.M., Swaroop, A., and Pugh, E.N., Jr. (2005). Photoreceptors of Nrl -/- mice coexpress functional S- and M-cone opsins having distinct inactivation mechanisms. J Gen Physiol 125, 287-304.

Paxinos G, F.K. (2001). The Mouse Brain in Stereotaxic Coordinates, Vol Second Edition (Academic Press).

Reinhard, K., Tikidji-Hamburyan, A., Seitter, H., Idrees, S., Mutter, M., Benkner, B., and Munch, T.A. (2014). Step-by-step instructions for retina recordings with perforated multi electrode arrays. PLoS One 9, e106148.

Rodieck, R.W. (1998). The First Steps in Seeing (Sinauer Assn).

Slepak, V.Z., and Hurley, J.B. (2008). Mechanism of light-induced translocation of arrestin and transducin in photoreceptors: interaction-restricted diffusion. IUBMB life 60, 2-9.

Smallwood, P.M., Olveczky, B.P., Williams, G.L., Jacobs, G.H., Reese, B.E., Meister, M., and Nathans, J. (2003). Genetically engineered mice with an additional class of cone photoreceptors: implications for the evolution of color vision. Proc Natl Acad Sci U S A 100, 11706-11711.

Thomas, P.B.M., Formankiewicz, M.A., and Mollon, J.D. (2011). The effect of photopigment optical density on the color vision of the anomalous trichromat. Vision Res 51, 2224-2233.

Umino, Y., Solessio, E., and Barlow, R.B. (2008). Speed, spatial, and temporal tuning of rod and cone vision in mouse. J Neurosci 28, 189-198.

Wang, J.S., and Kefalov, V.J. (2009). An alternative pathway mediates the mouse and human cone visual cycle. Curr Biol 19, 1665-1669.

Yin, L., Smith, R.G., Sterling, P., and Brainard, D.H. (2006). Chromatic properties of horizontal and ganglion cell responses follow a dual gradient in cone opsin expression. J Neurosci 26, 12351-12361.

Zele, A.J., Maynard, M.L., Joyce, D.S., and Cao, D. (2014). Effect of rod-cone interactions on mesopic visual performance mediated by chromatic and luminance pathways. Journal of the Optical Society of America A, Optics, image science, and vision 31, A7-A14.

Figures

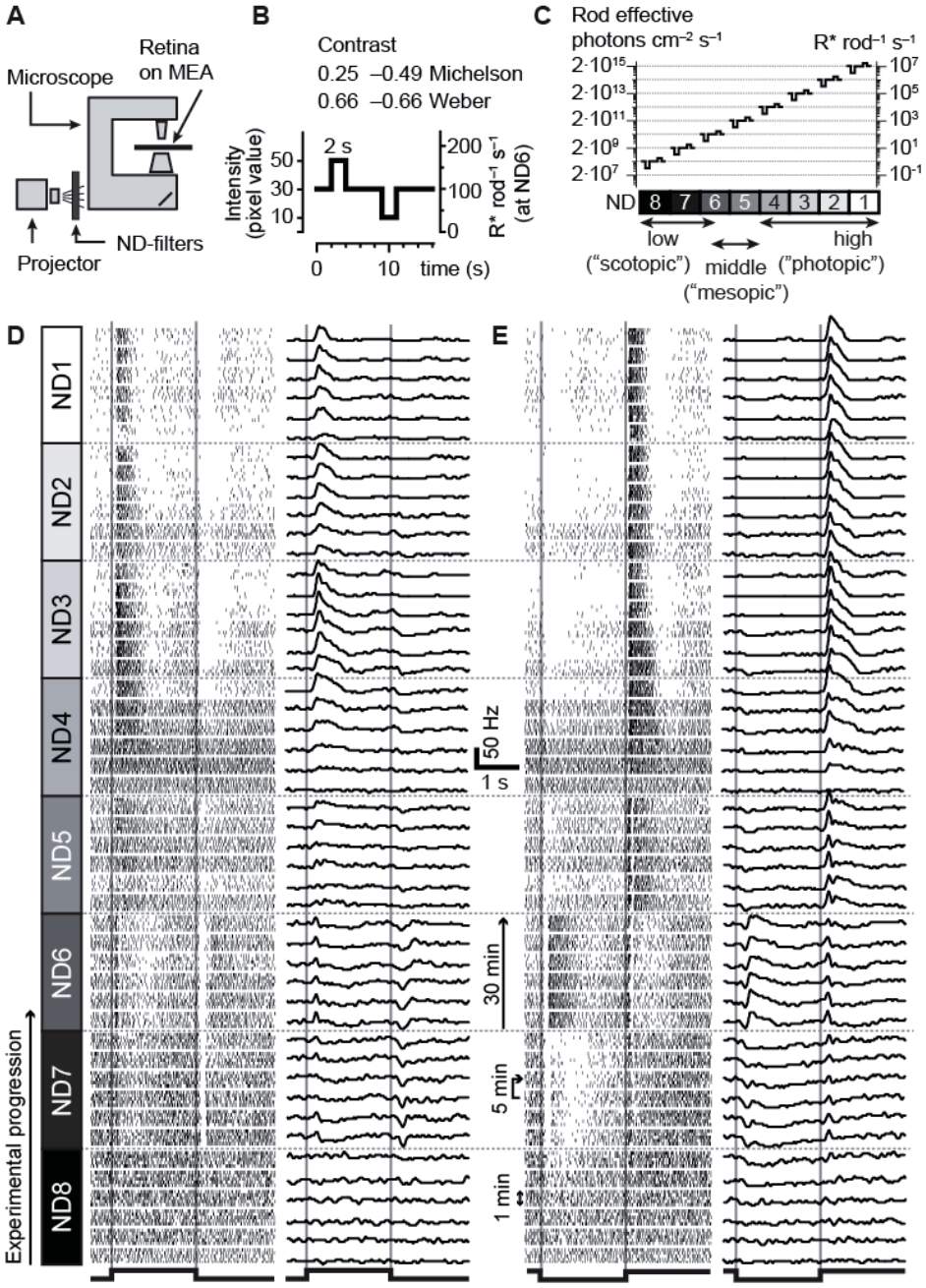

Figure 1: Example responses of a single *Cnga3*$^{-/-}$ ganglion cell across brightness levels.

A Different light levels were achieved experimentally by inserting neutral density (ND) filters in the stimulation light path.

B Full-field contrast step stimulus, consisting of positive and negative contrast steps. **C** Absolute intensities of the stimulus shown in **B** at different experimental light levels.

D, E Raster plots (left) and firing rates (right) for a single ganglion cell in response to the full-field positive (**D**) and negative (**E**) contrast steps. Blocks of 5 consecutive repetitions (left) are averaged in one trace on the right. This cell showed responses at all light levels (very weakly responding at ND8), with a short suppression of

responses in the beginning of ND4. Note that in this ganglion cell, the rod-mediated responses are even stronger at high (ND4 to ND1) than at lower (ND8 to ND5) light levels.

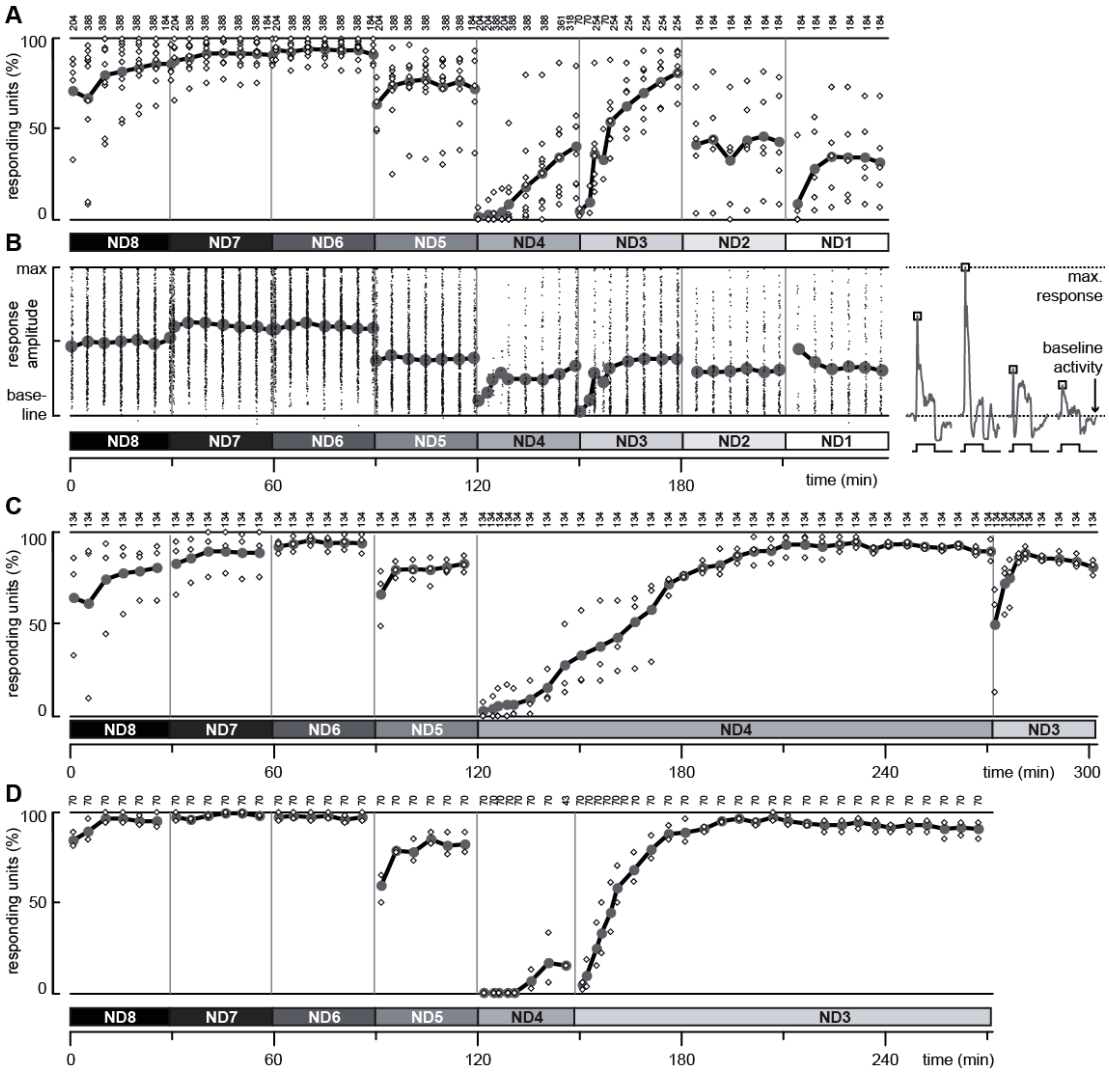

Figure 2 Responsiveness of ganglion cells in isolated *Cnga3*$^{-/-}$ retina

A Percentage of responsive ganglion cells in each retina (small white diamonds) and across all experiments (large gray disks and thick line) that responded to a full-field positive or negative contrast step. The numbers on top indicate the total number of ganglion cells recorded at each time point of the experimental paradigm. **B** Response amplitude (normalized peak spike rate) of all individual units that responded (small dots) and their mean response amplitude (large gray dots and thick line). Right panel: Schematic of how response amplitude was determined. Each ganglion cell was followed throughout the experiment, and response strength was taken as the relative peak spike rate (indicated by squares) between the baseline activity of the cell and the cell's maximal response. For simplicity, schematic shows only the positive contrast step.

C Percentage of responsive ganglion cells in a subset of experiments (n=3 retinas) in which we stayed at ND4 for 2.5 hours. Data from these retinas (up to 150 min) are also part of **A** and **B**.

D Percentage of responsive ganglion cells in a subset of experiments (n=2 retinas) in which we stayed at ND3 for 2 hours. Data from these retinas (up to 180 min) are also part of **A** and **B**.

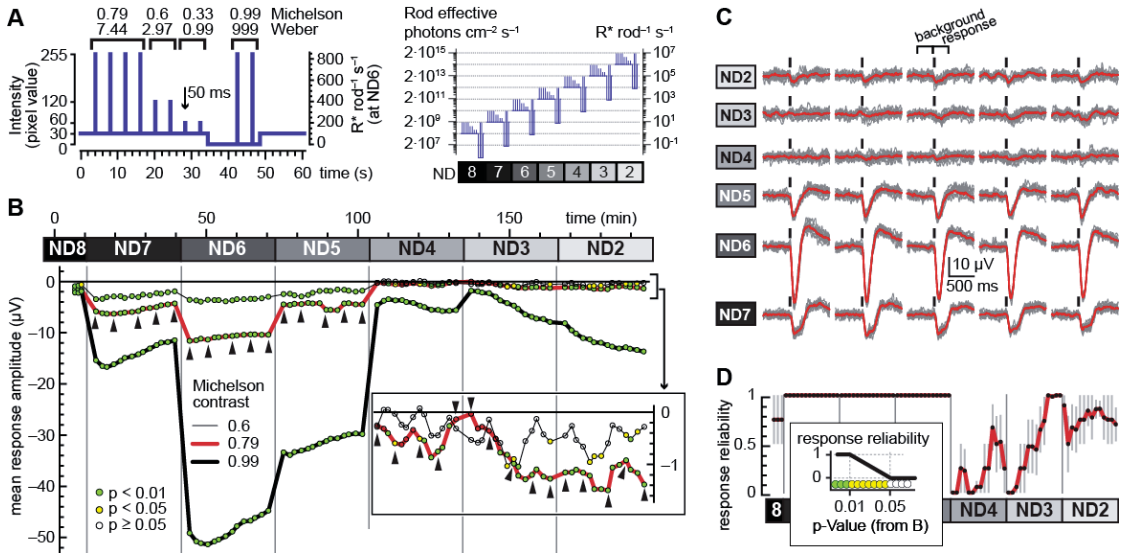

Figure 3 In-vitro ERG recordings from isolated *Cnga3*$^{-/-}$ retina

A Stimulus used for in-vitro ERG recordings consisted of 50-ms flashes ranging from 0.33 to 0.99 Michelson contrast. Right: absolute stimulus intensities with different ND filters.

B, C Data from one representative retina. **B** Running average of the mean negative voltage deflections in the 300 ms after flash onset (response minus background). Each data point shows mean from 3 consecutive stimuli (i.e. from 12 individual flashes for 0.79 Michelson contrast, and 6 flashes for the other contrasts; data for the lowest contrast is omitted for clarity). Neighboring data points are shifted by 1 stimulus. The color-coded disks indicate the level of significance of the response relative to the background activity (Wilcoxon rank sum test). Inset: magnification of the responses to the lower contrasts at ND4 to ND2. The raw traces underlying the data points indicated by the triangles are shown in **C** (gray: individual responses; red: average of 12 responses; black bars above traces: timing of flash).

D Response reliability of ERG responses to the flashes of 0.79 Michelson contrast (mean ± s.e.m. of n=4 retinas) calculated as indicated in the inset from the p-Values determined as in **B**. Even though ERG responses are small at high light levels, they can be reliably detected. Response reliability for flashes of other contrasts are shown in Supplementary Figure S3.

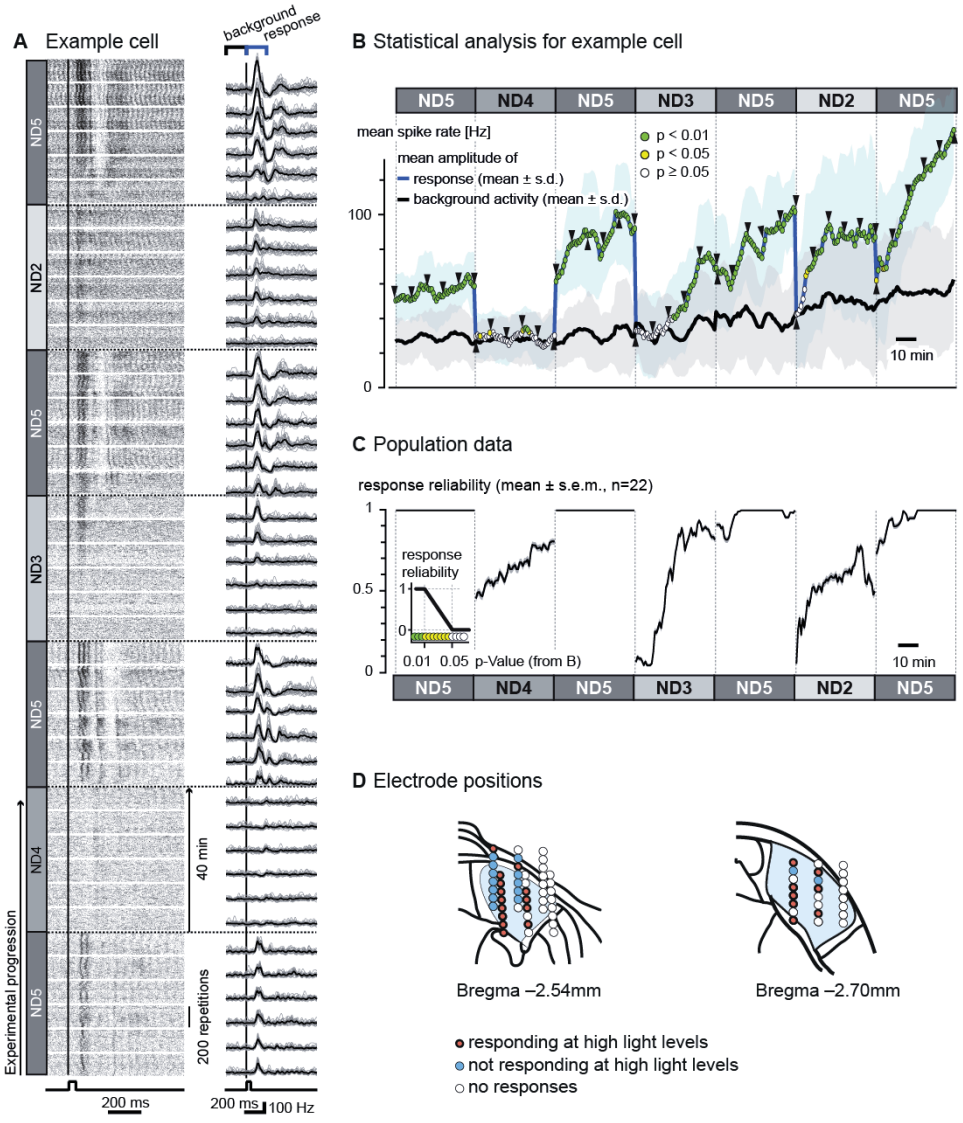

Figure 4: Rod responses in in-vivo dLGN recordings in *Cnga3*$^{-/-}$.

A Example response of one multiunit to a 50 ms flash at different light levels. Responses to each of the 8400 single repetitions are shown in the raster plot (left). For analysis, 10 consecutive repetitions were averaged (1 "group", gray lines on the right). In black, the averages over 20 such groups (200 flashes) are shown. **B** Response amplitude (blue curve) and background activity (black curve) of the unit shown in **A** (moving average over runs of 20 groups (=200 flashes), shifted by 1 group. Arrowheads mark values corresponding to the raw traces shown in the right column in A). Responses significantly above background are color-coded in green ($p<0.01$) and yellow ($p<0.05$, rank sum test). This example multiunit stops responding after switching to ND4. However, at ND3 and ND2 the responses reappear after several minutes.

C Population data for those multiunits responding at high light levels (n=22/36, mean ± s.e.m.). The color-coded p-values (as shown in **B**) were transformed into a response reliability value as shown in the inset. Responses at high light levels recovered with an intensity-dependent time course.

D Electrode positions during LGN recordings. Electrodes on which responses recovered at high light levels are color-coded in red, electrodes with responses only at moderate light levels are colored in blue.

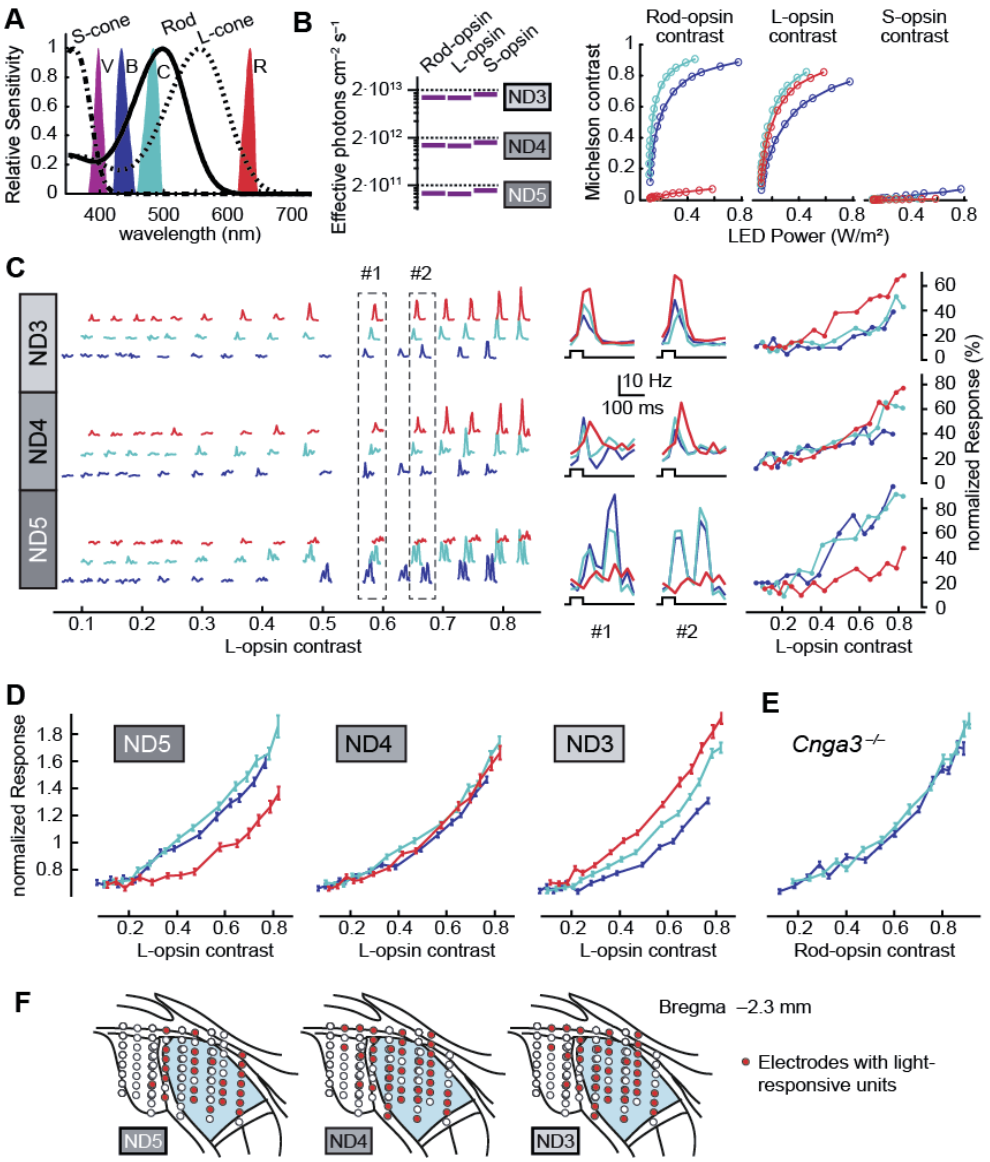

Figure 5: Rod responses in in-vivo LGN recordings in mice with rods and cones.

Across all panels, cyan symbols/lines represent data from cyan flashes, blue symbols/lines data from blue flashes and red symbols/lines data from red flashes.

A Spectral power of flash stimuli in relation to rod and cone spectral sensitivity. S-opsin, rods and L-opsin are roughly equally sensitive to the violet (V) background, but differ markedly in their sensitivity to blue (B), cyan (C) red (R) flash stimuli.

B Estimated absolute intensity of the violet background (retinal irradiance, left) and Michelson contrast of blue, cyan, and red flash stimuli for rod, L-opsin, and S-opsin (right). All flash colors are of similar contrast for L-opsin, while rods are only activated by blue and cyan stimuli, and all stimuli present very low contrast to S-opsin.

C Responses of an example unit at medium (ND5), high (ND4) and very high (ND3) irradiances. Left panel shows mean PSTH for stimuli of all presented contrasts; middle panel an expanded comparison of responses to blue, cyan and red stimuli of roughly equivalent L-opsin contrast; and right panel shows the relationship between normalized mean response amplitude (see methods) and L-opsin contrast across all flashes.

D Mean ± s.e.m. of normalized response amplitude (normalized by the mean response across contrasts and colors, see methods) to blue, cyan and red flashes as a function of L-opsin contrast for all light-responsive units at ND5 (n=131 units from n=6 out of 7 mice); ND4 (n=201 units from n=7 mice) and ND3 (n=213 units from n=7 mice). Responses at the three wavelengths could be adequately fit with a single function at ND4 (consistent with the view that they are driven by L-opsin), but not at either ND5 or ND3 (statistical analysis of curve fits for each wavelength are summarized in Supplementary Table S5).

E Mean ± s.e.m. of normalized response amplitude (see methods) for cyan and blue flashes presented to *Cnga3*$^{-/-}$ mice at ND6 plotted as a function of estimated rod contrast (n=229 responsive units from 3 mice; in mice 1 and 2 we collected data from two different electrode placements, in mouse 3 from three placements). The responses at the two colours were indistinguishable confirming the suitability of our methods for estimating photoreceptor spectral sensitivity *in vivo* (BC: $R^2_{BC} = 0.448$, $R^2_{BC,null} = 0.448$, $\Delta R^2_{BC} \approx 0$).

F: Histological confirmation for electrode placements in n = 3 *Opnmw*^{R}*:Opn4*$^{-/-}$ animals.

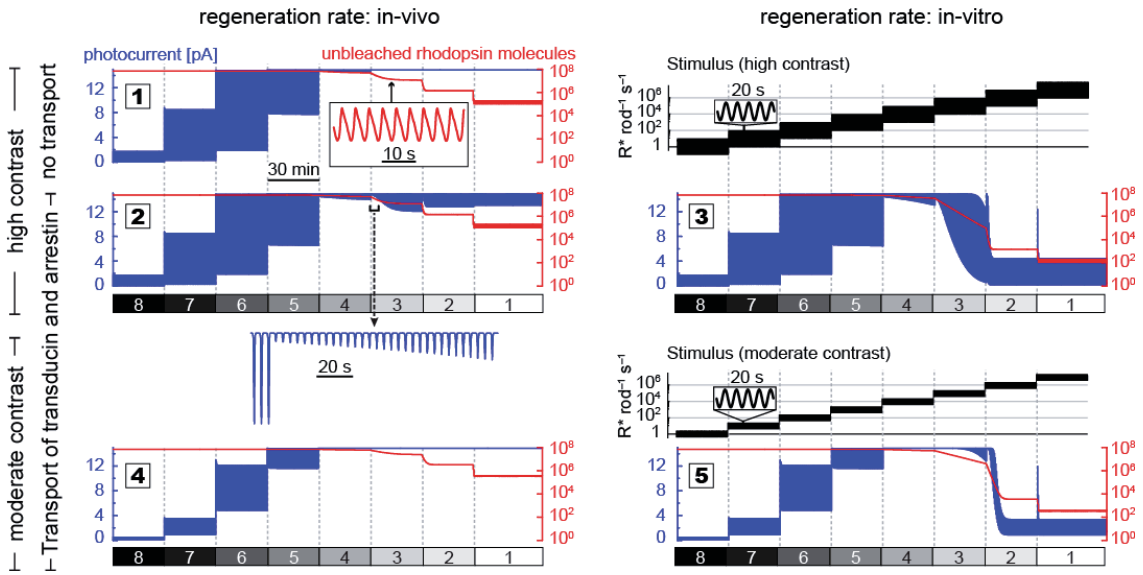

Figure 6: Computational model of rod behavior at different light levels for various parameter combinations.

The model was fed with a sinusoidal stimulus of high (upper panels) or moderate contrast (lower panels, stimulus shown in black). Mean brightness levels were changed every 30 minutes by 1 log unit as in our experiments. In-vivo and in-vitro experimental conditions (columns) were mimicked by adjusting the rhodopsin regeneration rate (parameter k_{recyc}). Without transducin and arrestin transport (panel 1), even the high-contrast stimulus did not elicit photocurrents (blue curves) at high light levels (ND4 and brighter). With transport, high-contrast responses were present at high light levels (panel 2), but not low-contrast responses (panel 4). Reducing the rhodopsin regeneration rate slightly (panel 6 in Suppl. Fig. S4) or strongly (panels 3 and 5) promoted photocurrents at high light levels. Rhodopsin bleaching (red curves) supports response re-emergence.

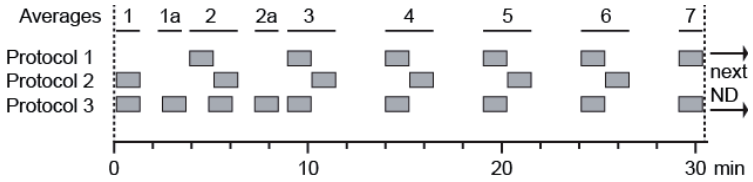

Suppl. Fig. S1: Supplementary information about methods.

Full-field contrast steps (see Fig. 1B) were always presented in blocks of 5 repetitions, lasting approximately 1 min (gray rectangles). In different experiments we presented these blocks at different times after transitioning to a new light level. In most experiments we used Protocol 1, in which the first presentation started at time 4 min. In some experiments we used Protocol 2 instead. We averaged across these different experiments as indicated on top, yielding 7 data points at each light level (see Fig. 2). At the ND4 and ND3 light levels, we used Protocol 3 instead of Protocol 2, yielding the additional data points 1a and 2a.

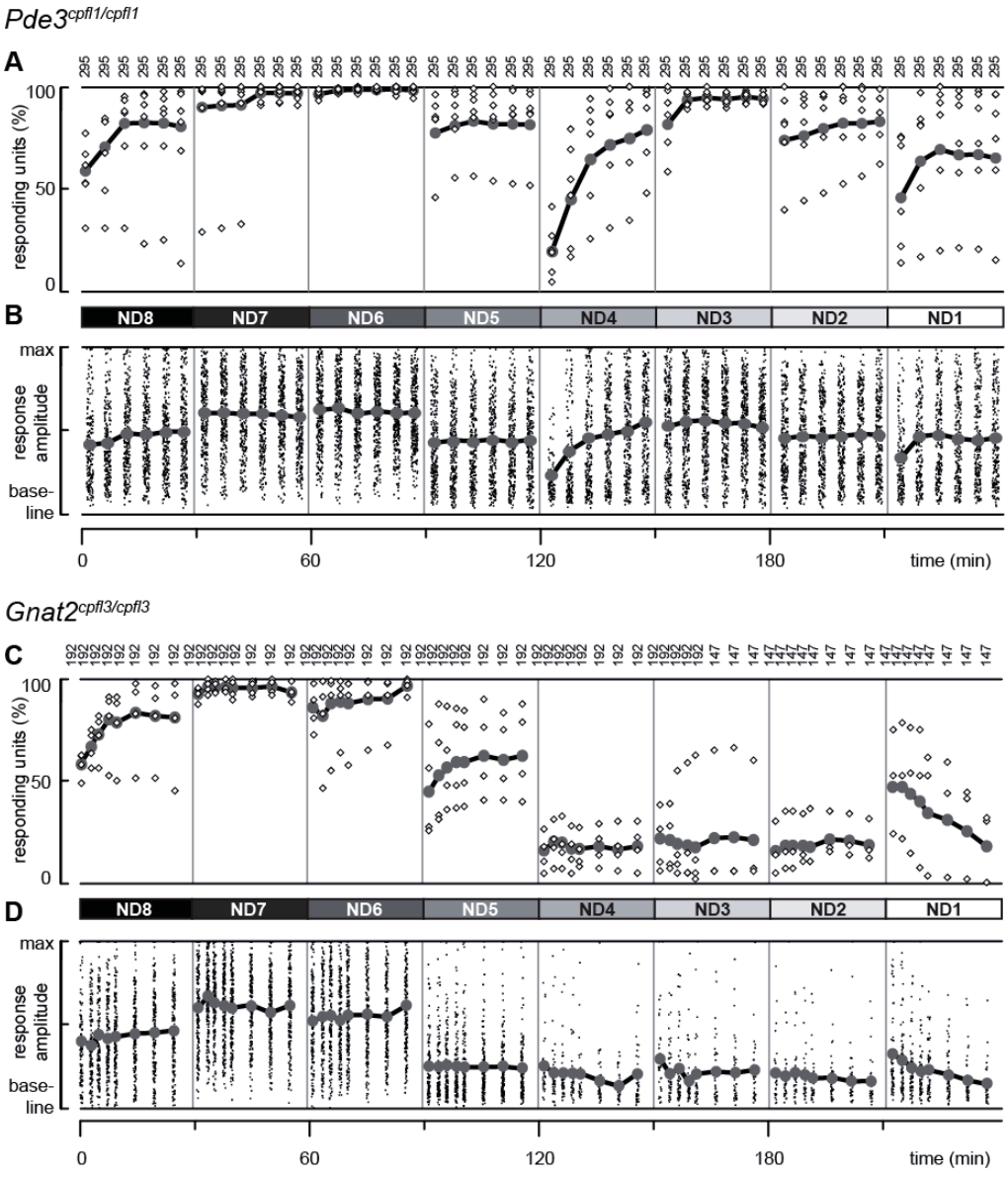

Suppl. Fig. S2: Responsiveness of ganglion cells in isolated *Pde3*$^{cpfl1/cpfl1}$ and *Gnat2*$^{cpfl3/cpfl3}$ retina.

A + B Percentages (A) and relative amplitudes (B) of responding units in *Pde3*$^{cpfl1/cpfl1}$ retinas (n=5). The percentage of responding units dropped in the beginning of high light levels, but recovered with a similar time course as found in *Cnga3*$^{-/-}$ retinas (Fig. RGC A). On a population level, the relative amplitude was stable across light levels, except for a small drop in the beginning of ND4 comparable to our findings in *Cnga3*$^{-/-}$ (Fig. RGC D). **C + D** Percentages (C) and relative amplitudes (D) of responding units in *Gnat2*$^{cpfl3/cpfl3}$ retinas (n=4). Consistent with our findings in *Pde3*$^{cpfl1/cpfl1}$ and *Cnga3*$^{-/-}$ retinas, rods drove visual responses at any light level also in *Gnat2*$^{cpfl3/cpfl3}$ retinas.

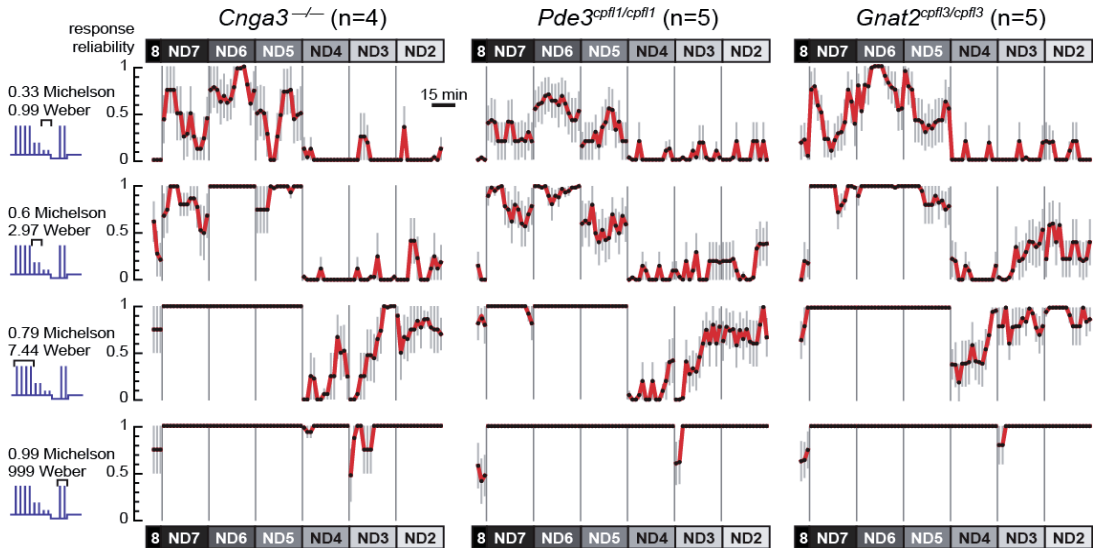

Suppl. Fig. S3: In-vitro ERG recordings from isolated *Cnga3*$^{-/-}$, *Pde3*$^{cpfl1/cpfl1}$, and *Gnat2*$^{cpfl3/cpfl3}$ retina.

Response reliability of ERG responses (mean ± s.e.m.) for *Cnga3*$^{-/-}$ (n=4 retinas), *Pde3*$^{cpfl1/cpfl1}$ (n=5), and *Gnat2*$^{cpfl3/cpfl3}$ (n=5) retinas to flashes of 0.33, 0.6, 0.79, and 0.99 Michelson contrast. Response reliability was calculated from the p-Values resulting from comparing background and response activity (as described in Fig. 3D and Methods). Similar contrast dependence of ERG responses was found for all three mouse strains. At high light levels (ND4 to ND2), responses could be detected reliably for stimuli with Michelson contrast of 0.79 and higher (for *Gnat2*$^{cpfl3/cpfl3}$ already for stimuli with contrast 0.6). For smaller contrast, only responses to low and medium light levels (ND8 to ND5) were reliably detectable. The time-dependent re-emergence of rod-driven light responses found for stimuli of contrast 0.79 in *Cnga3*$^{-/-}$retinas was also present in the two other mouse strains.

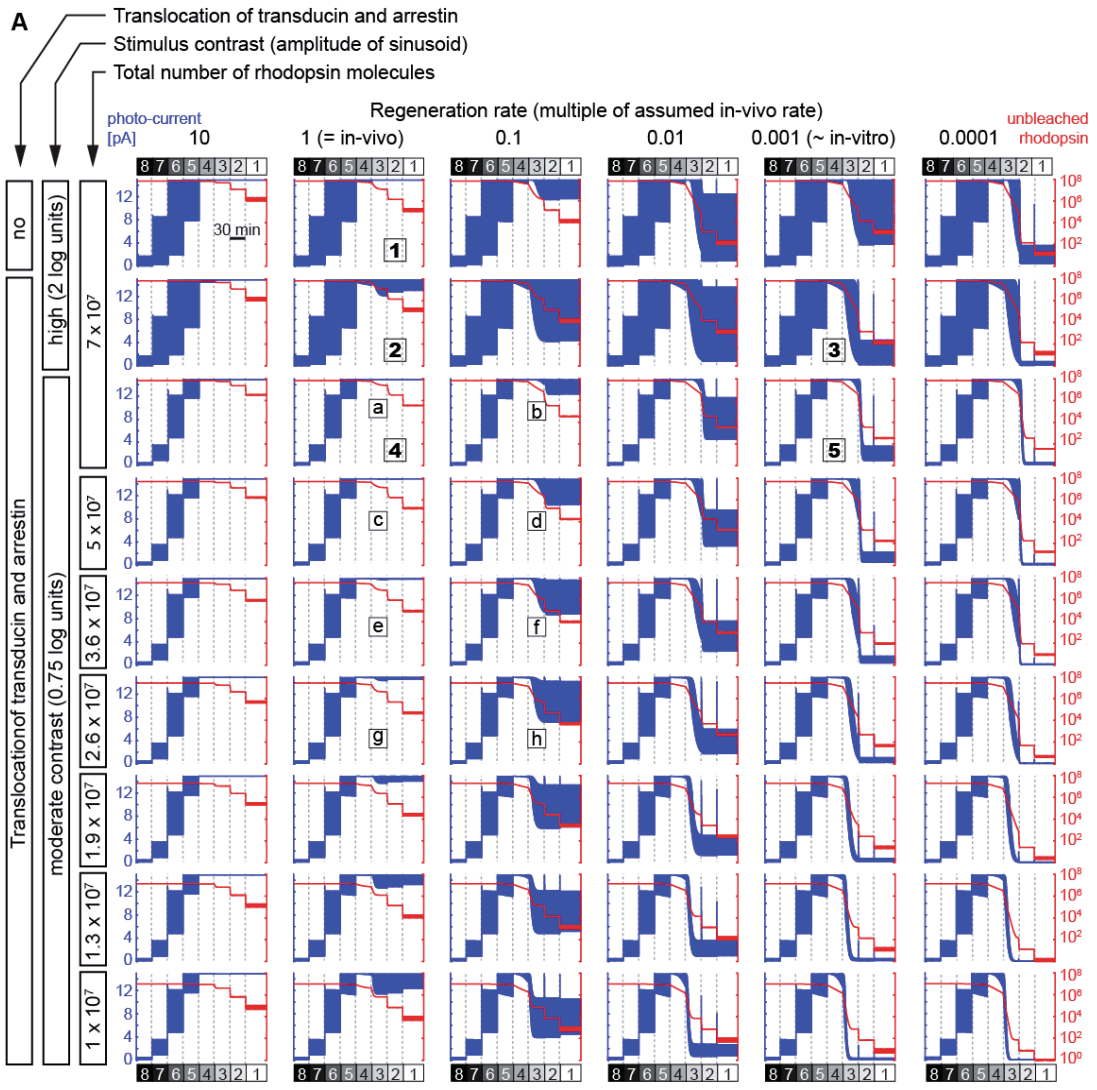
A
Translocation of transducin and arrestin
Stimulus contrast (amplitude of sinusoid)
Total number of rhodopsin molecules
photo-current [pA]
Regeneration rate (multiple of assumed in-vivo rate)
10
1 (= in-vivo)
0.1
0.01
0.001 (~ in-vitro)
0.0001
unbleached rhodopsin
no
high (2 log units)
moderate contrast (0.75 log units)
Translocationof transducin and arrestin
7 x 10⁷
5 x 10⁷
3.6 x 10⁷
2.6 x 10⁷
1.9 x 10⁷
1.3 x 10⁷
1 x 10⁷
30 min
B
Implementation of transducin and arrestin translocation
number of molecules
concentration (µM)
arrestin
transducin
C
Modulation amplitude of photocurrent (at end of ND3)
Total number of rhodopsin molecules
Regeneration rate (multiple of asumed in-vivo rate)
modulation amplitude
Modulation amplitude of photocurrents
during ND8: 0.38 pA
during ND7: 2.62 pA
during ND6: 7.27 pA
is independent of parameter combination

Suppl. Fig. S4: Model responses across the tested parameter space

A Model behavior for various rhodopsin concentrations (R_{total}, rows) and regeneration rates (k_{recyc}, columns). We simulated the photocurrent (blue) and the number of unbleached rhodopsin molecules (red) in response to a sinusoidal stimulus for rhodopsin concentrations varying between 7 x 10^7 (published upper bound (Lyubarsky et al., 2004), first three rows) down to 1 x 10^7 molecules (last row), and for multiples of the assumed *in-vivo* regeneration rate of rhodopsin varying between 0.0001 and 10 times the *in-vivo* value (columns).

[Note about the parameter k_{recyc}: We assume here that the value for k_{recyc} used in the original model (Invergo et al., 2014) (k_{recyc} = 0.007) corresponds to the *in-vivo* regeneration rate of rhodopsin. However, estimates for the "true" regeneration rate vary. In fact, for estimating rod responses at low and medium light levels, knowing the "true" value of k_{recyc} is of little importance. Across the full range of parameter variations presented here, responses at low light levels are hardly affected. For example, the stimuli used by Invergo et al for fitting the parameters of their original model produce the same output for all parameter combinations shown here.]

For low regeneration rates (0.0001 to 0.1 times in-vivo rates, last 4 columns), responses always reemerged at high light levels (ND4 and higher), independent of the other parameter values of the model. For the assumed *in-vivo* regeneration rate (column 2), responses reemerged only when transport of transducin and arrestin was implemented (rows 2 to 9), and only for high-contrast stimuli (panel 2), or for lower rhodopsin concentrations (starting with panel "e" downward). Panels 1 through 5 are also depicted in Fig. 6; panels "a" through "h" span the parameter range scrutinized more closely in **C**.

For the low-contrast stimuli (rows 3 to 9), the model showed similar behavior from ND8 to ND5 for all 42 parameter combinations shown. In other words, for low and medium light levels, the qualitative model behavior is robust even against these large variations of parameter values. Another consistent observation for all parameter combinations was that for this stimulus of moderate contrast (0.7 Michelson contrast) photocurrents initially vanished after switching to ND4 - the rod becomes saturated. However, the further qualitative development at ND4 and higher light levels depended strongly on the choice of parameters, especially on the choice of the regeneration rate k_{recyc}. Here, the assumed *in-vivo* regeneration rate of rhodopsin (second column) proved to be a turning point of the model behavior. For larger values of k_{recyc} (left-most column), rods always remained saturated. For smaller values of k_{recyc} (columns 3 to 6, including the estimated *in-vitro* regeneration rate, column 5), photocurrents always re-emerged independently of the absolute rhodopsin concentration. For the value of k_{recyc} used in the Invergo-model (the assumed *in-vivo* value), however, re-emergence of rod responses depended on the absolute rhodopsin concentration. Low rhodopsin concentration promoted responses at high light levels (lowest five rows, starting with panel "e"), while high rhodopsin concentration led to stable saturation (panels "a" and "c").

B Implementation of arrestin and transducin translocation in the computational model. Concentrations in the outer segment were adjusted in an instantaneous, step-like fashion upon light-level transitions.

C Detailed characterization of the modulation amplitude of the photocurrent, measured at the end of ND3, for variations of the parameters R_{total} and k_{recyc}. Parameter combinations corresponding to panels "a" through "h" in **A** are indicated. Note that the left-most contour line in the plot (corresponding to 0.5 pA) represents stronger modulation than the modulation observed under scotopic (ND8) conditions (0.38 pA).

Supplementary Table S5 : Statistical analysis of responses to blue, cyan and red flashes in the dLGN of *Opn1mw^{R}:Opn4$^{-/-}$* mice.

A: POD_{Lopsin} = 0.1; c = 5.33*10^4

	R^2_{BCR}	R^2_{null}	ΔR^2
ND5	47.5%	40.2%	7.3%
ND4	48.7%	48.3%	0.4%
ND3	57.3%	52.5%	4.8%

B: varying POD and c

ND5	R^2_{BCR}	R^2_{null}	ΔR^2
0.75*c	47.5%	40.6%	6.9%
1.25*c	47.4%	39.9%	7.6%
POD_{Lcone}=0.01	47.5%	40.4%	7.1%
POD_{Lcone}=1	47.5%	38.6%	8.9%

ND4	R^2_{BCR}	R^2_{null}	ΔR^2
0.75*c	48.7%	48.3%	0.4%
1.25*c	48.7%	48.3%	0.4%
POD_{Lcone}=0.01	48.7%	48.4%	0.3%
POD_{Lcone}=1	48.7%	47.4%	1.3%

ND3	R^2_{BCR}	R^2_{null}	ΔR^2
0.75*c	57.3%	52.0%	5.3%
1.25*c	57.3%	52.9%	4.4%
POD_{Lcone}=0.01	57.3%	52.5%	4.8%
POD_{Lcone}=1	57.3%	51.8%	5.5%

In order to analyze population responses, we first normalized single unit responses by their mean value across flashes and colours. This normalization was important to reduce the additional source of variability represented by the large differences in firing rates (both spontaneous and evoked) across units. Then, at each light level, we pooled normalized responses across units and flash intensities into three groups based in flash color (B: Blue, C: Cyan and R: Red). We observed that, separately, each group's response to flashes (as a function of L-opsin contrast) could be well fitted by using a quadratic polynomial model (i.e. two covariates and a constant term). We then asked whether responses to flashes of the three wavelengths, when expressed in L-opsin contrast, could be adequately described by a single function. Because of the large sample size (each group was constituted by more than 1000 responses) comparisons based on unstandardized p-values made little sense as even the slightest difference would result in highly significant comparisons (see e.g.(Nakagawa and Cuthill, 2007) for a review). Instead we focused on the explained variance that provided a meaningful measure of the effect size. Our null hypothesis was that L-opsin contrast could account for all the explainable variance. Therefore, if L-opsin contrast was the only drive for the observed responses, we would expect that, by pooling data from all three wavelengths, the explained variance would not be smaller than the one obtained by using a more complicated model that took into account the difference in flash colours (i.e. six covariates and a constant term). In order to compare the explained variance under the null and alternative hypothesis we used the R^2-adjusted as in (Montgomery D. C., 2010) so that the variance explained by null "pooled" model would be indicated as R^2_{null} and the variance explained by the alternative model would be indicated as R^2_{BCR}. The size of the effect was also evaluated as $\Delta R^2 = R^2_{BCR} - R^2_{null}$.

A Results of this analysis when cone contrast was calculated using our default estimates of pigment optical density (POD) and lens correction (parameter c, see methods). We observe that the Null hypothesis can explain the variance adequately only at ND4 (ΔR^2 < 1%), but not at ND5 or ND3.

B Impact of varying c and POD on these fits: results are stable in spite of large variations in these parameters and, again, the null hypothesis adequately describes our observations only at ND4.

IV. Acknowledgements

Ich bedanke mich bei meinem Doktorvater Thomas Münch, der mich durch die Höhen und Tiefen einer Doktorarbeit begleitet hat. Neben der wissenschaftlichen Unterstützung habe ich den familiären Umgang im Labor, die Freiheiten bei der Gestaltung meiner Arbeit und die vielen Konferenz-Besuche genossen.

The more than four years in Tübingen would have been only half as fun without my dear colleagues and friends at the institute. Hartwig, Natalia, Saad, Boris, Marion, Alex, Anahit, and our lab mothers Elli and Nadine – thank you for all the scientific discussions, coffee breaks, mental support, and help. It has always been very helpful to discuss data with Hartwig, and to improve codes and setups with Saad. To spend our rare free hours dancing or with the horses was a great diversion, Natalia. Thank you, Boris, for always helping me out on very short notice. Marion, human retina rocks! And special thanks to Elli for the first coffee in the morning.

Ich bedanke mich bei der ProRetina-Stiftung für die finanzielle Unterstützung und insbesondere bei Franz Badura für seine motivierende Einstellung. Mein Dank gilt auch meinem Advisory Board, Prof. Eberhart Zrenner und Dr. Günther Zeck, für Rat und Tat bezüglich meiner wissenschaftlichen Karriere. Die Arbeit mit menschlicher Netzhaut war nur möglich dank der Zusammenarbeit mit der Augenklinik Tübingen, insbesondere der Unterstützung von Prof. Karl Ulrich Bartz-Schmidt, Prof. Michael Partsch und Dr. Daniela Süsskind.

Un grand merci à Prof. Hugues Abriel pour son soutien continu.

Guo Da, thank you for believing in me, supporting me, and for being there for me.

Einen ganz besonderen Dank geht an meine Eltern, Elisabeth Lozar und Nik Reinhard. Seit ich denken kann, waren meine Ziele und Entscheidungen immer wichtig für euch. Ob mental, physisch oder finanziell, eure Unterstützung hat mir den Weg in die spannende und erfüllende Welt der Wissenschaft geebnet. Merci! Schön, dass mein Bruder Florian auch immer dabei war und ist. Auf viele weitere gemeinsame Reisen und Diskussionen.